

Faculty of Resource Science and Technology

Synthesis and Characterization of Molecularly Imprinted Polymer for the Removal of Triazine Herbicides from Water Samples

Rachel Marcella anak Roland

Doctor of Philosophy
2024

Synthesis and Characterization of Molecularly Imprinted Polymer for the Removal of Triazine Herbicides from Water Samples

Rachel Marcella anak Roland

A thesis submitted

In fulfillment of the requirements for the degree of Doctor of Philosophy

(Chemistry)

Faculty of Resource Science and Technology
UNIVERSITI MALAYSIA SARAWAK
2024

DECLARATION

I declare that the work in this thesis was carried out in accordance with the regulations of Universiti Malaysia Sarawak. Except where due acknowledgements have been made, the work is that of the author alone. The thesis has not been accepted for any degree and is not concurrently submitted in candidature of any other degree.



……

Signature

Name: Rachel Marcella anak Roland

Matric No.: 20010014

Faculty of Resource Science and Technology

Universiti Malaysia Sarawak

Date : 30th September 2023

ACKNOWLEDGEMENT

Firstly, I am very grateful for being given the golden opportunity to further my degree in Doctor of Philosophy at Universiti Malaysia Sarawak (UNIMAS) and now this journey has come to the finishing line. Thank you to the Zamalah UNIMAS scholarship for sponsoring years of PhD study in the Faculty of Resource Science and Technology (FRST).

I would like to offer my earnest gratitude towards my main research supervisor Associate Professor Dr Showkat Ahmad Bhawani, who has constantly supported me throughout my research and thesis writing with his diligence, encouragement, enthusiasm, and immense knowledge. Without his endless guidance and keen involvement in every process, my research thesis would have never been accomplished. To my co-supervisor, Associate Professor Dr Rafeah binti Wahi, thank you so much for your moral support and motivation throughout my PhD journey.

I would also like to thank the staff from the Faculty of Resource Science and Technology (FRST) and the Faculty of Engineering (FENG-Chemical Engineering Department) for their assistance in properly operating the instruments used in this research.

Finally, I must express my profound gratitude to my parents, Mr Roland Aji and Mdm Angela James for providing me with unfailing support, unending encouragement, and motivation throughout my years of PhD study and through the process of researching and writing this thesis. Thank you also to my relatives and great friends especially Ms Collyne who accompanied me whenever I had to do overtime in the lab until late at night. This accomplishment would be impossible without them.

ABSTRACT

Cyanazine (CYZ), Ametryn (AME) and Atrazine (ATZ) are mostly utilized 1, 3, 5-triazine herbicides to control the growth of broadleaf grasses and weeds, however, their extensive usage has adverse effects on the environment, non-target organisms, and human health. Therefore, molecularly imprinted polymers (MIPs) were applied to remove triazine herbicides in the environment. In this study, MIPs of triazine herbicides were synthesized by precipitation polymerization in the presence of template molecules (CYZ, AME and ATZ), functional monomers (methacrylic acid, acrylamide, 2-vinylpyirdine, and 4-vinylpyridine), cross-linker (ethylene glycol dimethacrylate), initiator (azo-bis-isobutyronitrile), and solvent (toluene and acetonitrile). For comparison study, the non-imprinted polymers (NIPs) were synthesized without the addition of template molecule. The Fourier Transform Infra-Red (FTIR) analysis of MIPs of triazine herbicides indicated the presence of CYZ, AME and ATZ were observed at ~756 cm^{-1}, ~1450 cm^{-1}, and ~1389 cm^{-1}, respectively. MIP (AAm) of CYZ had its maximum adsorption efficiency in 6 ppm CYZ solution at pH 7, 0.1 g of polymer and 240 mins of contact time. MIP (MAA) of AME had its highest adsorption efficiency in 7 ppm AME solution at pH 7, 0.1 g of polymer and 210 mins of contact time. MIP (2VP) of ATZ exhibited its maximum adsorption efficiency in 8 ppm of ATZ solution at pH 7, 0.3 g of polymer and 15 mins of contact time. The thermogravimetric analysis (TGA) of MIPs of triazine herbicides depicted that the decomposition of polymers was between ~320 °C to ~500 °C. MIP (AAm) of CYZ, MIP (MAA) of AME and MIP (2VP) of ATZ were more selective towards their target compounds with relative selectivity coefficients of 2.36, 2.66 and 2.77, respectively. The synthesized MIP (AAm) of CYZ, MIP (MAA) of AME and MIP (2VP) of ATZ were successfully applied

to remove CYZ, AME and ATZ from different water samples (distilled water, tap water and river water) with removal efficiencies between ~84% to ~95%.

Keywords: Cyanazine, Ametryn, Atrazine, precipitation polymerization, molecularly imprinted polymers

Sintesis dan Pencirian Molekul Polimer Tercetak untuk Penyingkiran Herbisida Triazin daripada Sampel Air

ABSTRAK

Sianazin (CYZ), Ametrin (AME), dan Atrazin (ATZ) adalah herbisida triazin yang banyak digunakan untuk mengawal pertumbuhan rumput dan rumpai daun lebar. Namun, penggunaannya yang berleluasa memberikan kesan buruk kepada alam sekitar, organisma bukan sasaran, dan kesihatan manusia. Oleh itu, molekul polimer tercetak (MIPs) digunakan untuk menyingkirkan herbisida triazin daripada alam sekitar. Dalam kajian ini, MIPs herbisida triazin disintesis menggunakan pempolimeran pemendakan dengan menggunakan molekul templat (CYZ, AME dan ATZ), monomer berfungsi (metakrilik,, akrilamida, 2-vinilpiridin dan 4-vinilpiridin), penggabung silang (etilena glikol dimetakrilat), bahan pemula (azo-bis-isobutironitril) serta pelarut (toluen dan asetonitril). Sebagai perbandingan, molekul polimer tidak tercetak (NIPs) disintesis tanpa penambahan molekul templat. Analisa Spektrum Inframerah Transformasi Fourier (FTIR) menunjukkan bahawa kewujudan CYZ, AME dan ATZ dapat dikenalpasti di ~756 cm^{-1}, ~1450 cm^{-1}, dan ~1389 cm^{-1}. Kadar optimum penjerapan maksimum bagi MIP (AAm) CYZ diperolehi dalam larutan CYZ 6 ppm pada pH 7, 0.1 g polimer dengan jangka waktu penjerapan selama 240 mins. MIP (MAA) AME mempunyai kadar penjerapan tertinggi dicapai dalam larutan AME 7 ppm pada pH 7, 0.1 g polimer dengan jangka waktu penjerapan selama 210 mins. MIP (2VP) ATZ mencapai kadar penjerapan maksimum dalam larutan ATZ 8 ppm pada pH 7, 0.3 g polimer dengan jangka waktu penjerapan selama 15 mins. Analisa termogravimetrik (TGA) bagi MIP herbisida triazin menunjukkan penguraian polimer antara ~320 °C to ~500 °C. MIP (AAm) CYZ, MIP (MAA) AME, dan MIP (2VP) ATZ lebih selektif terhadap molekul sasaran dengan koefisien relatif selektif iaitu 2.36, 2.66, dan 2.77, masing-masingnya. MIP

(AAm) CYZ, MIP (MAA) AME dan MIP (2VP) ATZ telah berjaya menyingkirkan CYZ, AME dan ATZ dalam pelbagai sampel air (air suling, air paip dan air sungai) dengan kadar penyingkiran antara ~84% to ~95%.

Kata kunci: *Cyanazin, ametrin, atrazin, pempolimeran mendakan, molekul polimer tercetak*

TABLE OF CONTENTS

		Page
DECLARATION		i
ACKNOWLEDGEMENT		ii
ABSTRACT		iii
ABSTRAK		v
TABLE OF CONTENTS		vii
LIST OF TABLES		xiv
LIST OF FIGURES		xvi
LIST OF ABBREVIATIONS		xix
CHAPTER 1	**INTRODUCTION**	1
1.1	Research Background	1
1.2	Problem Statement	4
1.3	Objectives	6
1.4	Scope of Study	7
1.5	Chapter Summary	8
CHAPTER 2	**LITERATURE REVIEW**	10
2.1	Triazine Herbicides	10
2.1.1	Cyanazine	11
2.1.2	Ametryn	12

2.1.3 Atrazine 13

2.2 Molecular Imprinting Technology 15

2.3 Molecular Imprinting Pre-Polymerization Mixture 18

2.3.1 Template Molecule 18

2.3.2 Functional Monomer 21

2.3.3 Cross-Linker 25

2.3.4 Initiator 27

2.3.5 Solvent 30

2.4 Molecular Imprinting Process 31

2.5 Molecular Imprinting Approaches 34

2.5.1 Covalent Imprinting 35

2.5.2 Non-Covalent Imprinting 37

2.5.3 Semi Covalent Imprinting 38

2.6 Molecular Imprinting Techniques 39

2.7 Characterizations of Molecularly Imprinted Polymers 42

2.7.1 Physical Characterizations of Molecularly Imprinted Polymers 43

2.7.2 Chemical Characterizations of Molecularly Imprinted Polymers 45

2.8 Thermal Study of Molecularly Imprinted Polymers 47

2.9 Parameters Affecting Binding Efficiency of Molecularly Imprinted Polymers 49

2.9.1 Effect of Contact Time 50

2.9.2 Effect of Initial Concentration 51

2.9.3 Effect of pH 51

2.9.4 Effect of Polymer Dosage 52

2.10 Selectivity Test of Molecularly Imprinted Polymers 52

2.11 Applications of Molecularly Imprinted Polymers 53

2.11.1 MIP Application in Separation Techniques 54

2.11.2 MIP Application in Sensors 57

2.11.3 MIP Application in Drug Delivery 59

2.11.4 MIP Application in Catalysis 59

2.12 Molecularly Imprinted Polymers of Triazine Herbicides 60

2.12.1 Molecularly Imprinted Polymers of Cyanazine Herbicides 60

2.12.2 Molecularly Imprinted Polymers of Ametryn Herbicides 61

2.12.3 Molecularly Imprinted Polymers of Atrazine Herbicides 63

2.13 Other Methods Applied for the Removal Triazine Herbicides 64

CHAPTER 3 MATERIALS AND METHODS 65

3.1 Materials 65

3.2 Summary of Methods Involved in the Research 66

3.3 Synthesis of MIPs of Triazine Herbicides 67

3.4 Template Removal of Triazine Herbicides from MIPs 70

3.5 Fourier Transform Infra-Red (FTIR) Spectroscopy 71

3.6 Field Emission Electron Microscopy (FESEM) 71

3.7 Batch Binding Studies on MIPs of Triazine Herbicides 72

3.8 Kinetic Isotherm Study on of MIPs of Triazine Herbicides 73

3.9 Brunauer-Emmett-Teller (BET) Analysis 74

3.10 Energy Dispersive X-Ray (EDX) 74

3.11 Thermal Study of MIPs of Triazine Herbicides 75

3.12 Adsorption Studies of MIPs of Triazine Herbicides 75

3.12.1 Effect of Initial Concentration on Adsorption Efficiency 76

3.12.2 Effect of pH on Adsorption Efficiency 77

3.12.3 Effect of Polymer Dosage on Adsorption Efficiency 79

3.13 Adsorption Isotherm Study on MIPs of Triazine Herbicides 80

3.14 Selectivity Test of MIPs of Triazine Herbicides 81

3.15 Application of MIPs for Triazine Herbicides Removal 84

CHAPTER 4 RESULTS AND DISCUSSION 87

4.1 Synthesis of MIPs of Triazine Herbicides 87

4.2 FTIR Analysis 90

4.2.1 FTIR Analysis of MIPs of CYZ 90

4.2.2 FTIR Analysis of MIPs of AME 94

4.2.3 FTIR Analysis of MIPs of ATZ 100

4.3 FESEM Analysis 108

4.3.1 FESEM Analysis of MIPs of CYZ 109

4.3.2 FESEM Analysis of MIPs of AME 110

4.3.3 FESEM Analysis of MIPs of ATZ 112

4.4 Batch Binding Analysis 114

4.4.1 Batch Binding Analysis of MIPs of CYZ 114

4.4.2 Batch Binding Analysis of MIPs of AME 116

4.4.3 Batch Binding Analysis of MIPs of ATZ 120

4.5 Kinetic Study 125

4.5.1 Kinetic Study of MIP (AAm) of CYZ 125

4.5.2 Kinetic Study of MIP (MAA) of AME 127

4.5.3 Kinetic Study of MIP (2VP) of ATZ 129

4.6 BET Analysis 131

4.6.1 BET Analysis of MIP (AAm) of CYZ 131

4.6.2 BET Analysis of MIP (MAA) of AME 132

4.6.3 BET Analysis of MIP (2VP) of ATZ 133

4.7 EDX Analysis 135

4.7.1 EDX Analysis of MIP (AAm) of CYZ 135

4.7.2 EDX Analysis of MIP (MAA) of AME 136

4.7.3 EDX Analysis of MIP (2VP) of ATZ 137

4.8 Thermal Analysis 139

4.8.1 TGA of MIP (AAm) of CYZ 139

4.8.2 TGA of MIP (MAA) of AME 141

4.8.3 TGA of MIP (2VP) of ATZ 143

4.9 Effect of Initial Concentration 145

4.9.1 Effect of Initial Concentration on MIP (AAm) of CYZ 145

4.9.2 Effect of Initial Concentration on MIP (MAA) of AME 146

4.9.3 Effect of Initial Concentration on MIP (2VP) of ATZ 149

4.10 Effect of pH 151

4.10.1 Effect of pH on MIP (AAm) of CYZ 151

4.10.2 Effect of pH on MIP (MAA) of AME 152

4.10.3 Effect of pH on MIP (2VP) of ATZ 154

4.11 Effect of Polymer Dosage 156

4.11.1 Effect of Polymer Dosage of MIP (AAm) of CYZ 157

4.11.2 Effect of Polymer Dosage of MIP (MAA) of AME 158

4.11.3 Effect of Polymer Dosage of MIP (2VP) of ATZ 160

4.12 Adsorption Isotherm Study 162

4.12.1 Adsorption Isotherm Study of MIP of CYZ 162

4.12.2 Adsorption Isotherm Study of MIP (MAA) of AME 164

4.12.3 Adsorption Isotherm Study of MIP (2VP) of ATZ 166

4.13 Selectivity Test 168

4.13.1 Selectivity Test of MIP (AAm) of CYZ 168

4.13.2 Selectivity Test of MIP (MAA) of AME 170

4.13.3 Selectivity Test of MIP (2VP) of ATZ 171

4.14 MIP Applications in Water Samples 172

4.14.1 Application of MIP (AAm) for CYZ Removal 172

4.14.2 Application of MIP (MAA) for AME Removal 174

4.14.3 Application of MIP (2VP) for ATZ Removal 174

CHAPTER 5 CONCLUSION AND RECOMMENDATIONS 176

5.1 Conclusion 176

5.2 Recommendations 178

REFERENCES 179

APPENDICES 218

LIST OF TABLES

		Page
Table 2.1:	Comparison between CYZ, AME and ATZ	10
Table 2.2:	Common Examples of Acidic, Neutral, and Basic Functional Monomers	22
Table 2.3:	Classification and Examples of Cross-Linker (Nishchaya et al., 2023)	26
Table 2.4:	Classification of Molecular Imprinting Approaches	35
Table 2.5:	Methods for the Removal of Triazine Herbicides	64
Table 3.1:	Ratio of Chemicals for the Synthesis of MIPs and NIP of CYZ	69
Table 3.2:	Ratio of Chemicals for the Synthesis of MIPs and NIP of AME	69
Table 3.3:	Ratio of Chemicals for the Synthesis of MIPs and NIPs of ATZ	70
Table 3.4:	Summary of Overall Adsorption Studies of MIPs of Triazine Herbicides	75
Table 3.5:	Parameters Involved in Adsorption Study of Initial Concentration	77
Table 3.6:	Parameters Involved in Adsorption Study of pH	78
Table 3.7:	Parameters Involved in Adsorption Study of Polymer Dosage	79
Table 3.8:	Important Compounds and Parameters Used in Selectivity Test	82
Table 3.9:	Parameters for MIP Application in Water Samples	85
Table 4.1:	Kinetic Models Examined on MIP (AAm) of CYZ	127
Table 4.2:	Kinetic Models Examined on MIP (MAA) of AME	129
Table 4.3:	Kinetic Models Examined on MIP (2VP) of ATZ	131
Table 4.4:	BET Analysis of MIP (AAm) and NIP (AAm) of CYZ	132
Table 4.5:	BET Analysis of MIP (MAA) and NIP (MAA) of AME	133
Table 4.6:	BET Analysis of MIP (2VP) and NIP (2VP) of ATZ	134
Table 4.7:	Adsorption Isotherm Models of MIP (AAm) of CYZ	164
Table 4.8:	Adsorption Isotherm Models of MIP (MAA) of AME	166
Table 4.9:	Adsorption Isotherm Models of MIP (2VP) of ATZ	168

Table 4.10: Selectivity Test of MIP (AAm) and NIP (AAm) of CYZ 169

Table 4.11: Selectivity Test of MIP (MAA) and NIP (MAA) of AME 170

Table 4.12: Selectivity Test of MIP (2VP) and NIP (2VP) of ATZ 171

Table 4.13: Removal of CYZ Using MIP (AAm) and NIP (AAm) 173

Table 4.14: Removal of AME Using MIP (MAA) and NIP (MAA) 174

Table 4.15: Removal of ATZ Using MIP (2VP) and NIP (2VP) 175

LIST OF FIGURES

Page

Figure 2.1: Chemical Structure of Cyanazine 11

Figure 2.2: Chemical Structure of Ametryn 13

Figure 2.3: Chemical Structure of Atrazine 14

Figure 2.4: Development of MIPs from 1800s until 2023 17

Figure 2.5: Five Important Chemicals for Pre-Polymerization Mixture 18

Figure 2.6: Classifications and Examples of Commonly Used Template Molecule 20

Figure 2.7: List of Common Initiators for MIP Synthesis 28

Figure 2.8: General Steps in the Molecular Imprinting Process 32

Figure 2.9: Different Types of MIP Preparation Techniques 40

Figure 2.10: Analyses of Physical and Chemical Characterizations of MIPs 43

Figure 2.11: Parameters Affecting MIP Performance 49

Figure 2.12: Important MIP Applications and Examples 54

Figure 3.1: Locality Map of Sampling Point at Kota Samarahan (Google Maps, n.d.) 65

Figure 3.2: Experimental Design Involved Throughout the Research 67

Figure 4.1: Proposed Mechanism for the MIP Preparation 89

Figure 4.2: FTIR Spectra of MIP (MAA), MIP (AAm) and MIP (4VP) of CYZ 91

Figure 4.3: FTIR Spectra of MIP (AAm) and NIP (AAm) of CYZ 93

Figure 4.4: FTIR Spectra of MIP (MAA), MIP (AAm) and MIP (2VP) of AME 95

Figure 4.5: FTIR Spectra of MIP (MAA) and NIP (MAA) of AME 98

Figure 4.6: FTIR Spectra of MIP (MAA), MIP (AAm) and MIP (2VP) of ATZ 101

Figure 4.7: FTIR Spectra of MIP (2VP) and NIP (2VP) of ATZ 106

Figure 4.8: FESEM Micrographs of MIPs and NIP of CYZ 109

Figure 4.9: FESEM Micrographs of MIPs and NIP of AME 111

Figure 4.10: FESEM Micrographs of MIPs and NIP of ATZ 113
Figure 4.11: Batch Binding of MIPs of CYZ 115
Figure 4.12: Batch Binding of MIP (AAm) and NIP (AAm) of CYZ 116
Figure 4.13: Batch Binding of MIPs of AME 117
Figure 4.14: Batch Binding of MIP (MAA) and NIP (MAA) of AME 119
Figure 4.15: Batch Binding of MIPs of ATZ 121
Figure 4.16: Batch Binding of MIP (2VP) and NIP (2VP) of ATZ 124
Figure 4.17: Pseudo-First-Order Kinetic Model of MIP (AAm) of CYZ 125
Figure 4.18: Pseudo-Second-Order Kinetic Model of MIP (AAm) of CYZ 126
Figure 4.19: Pseudo-First-Order Kinetic Model of MIP (MAA) of AME 128
Figure 4.20: Pseudo-Second-Order Kinetic Model of MIP (MAA) of AME 128
Figure 4.21: Pseudo-First-Order Kinetic Model of MIP (2VP) of ATZ 129
Figure 4.22: Pseudo-Second-Order Kinetic Model of MIP (2VP) of ATZ 130
Figure 4.23: EDX Analysis of MIP (AAm) of CYZ 136
Figure 4.24: EDX Analysis of MIP (MAA) of AME 137
Figure 4.25: EDX Analysis of MIP (2VP) of ATZ 138
Figure 4.26: TGA Analysis of MIP (AAm) of CYZ 140
Figure 4.27: TGA Analysis of MIP (MAA) of AME 142
Figure 4.28: TGA Analysis of MIP (2VP) of ATZ 144
Figure 4.29: Effect of Initial Concentration on MIP (AAm) and NIP (AAm) of CYZ 146
Figure 4.30: Effect of Initial Concentration on MIP (MAA) and NIP (MAA) of AME 147
Figure 4.31: Effect of Initial Concentration on MIP (2VP) and NIP (2VP) of ATZ 150
Figure 4.32: Effect of pH on MIP (AAm) and NIP (AAm) of CYZ 152
Figure 4.33: Effect of pH on MIP (MAA) and NIP (MAA) of AME 153
Figure 4.34: Effect of pH on MIP (2VP) and NIP (2VP) of ATZ 155
Figure 4.35: Effect of Polymer Dosage on MIP (AAm) and NIP (AAm) of CYZ 157

Figure 4.36: Effect of Polymer Dosage on MIP (MAA) and NIP (MAA) of AME 159

Figure 4.37: Effect of Polymer Dosage on MIP (2VP) and NIP (2VP) of ATZ 161

Figure 4.38: Langmuir Isotherm Model of MIP (AAm) of CYZ 163

Figure 4.39: Freundlich Isotherm Model of MIP (AAm) of CYZ 163

Figure 4.40: Langmuir Isotherm Model of MIP (MAA) of AME 164

Figure 4.41: Freundlich Isotherm Model of MIP (MAA) of AME 165

Figure 4.42: Langmuir Isotherm Model of MIP (2VP) of ATZ 167

Figure 4.43: Freundlich Isotherm Model of MIP (2VP) of ATZ 167

LIST OF ABBREVIATIONS

%	Percentage
°C	Degree Celsius
µg/mL	Microgram Per Millilitre
2VP	2-Vinylpyridine
4VP	4-Vinylpyridine
AA	Acrylic Acid
AAm	Acrylamide
ABDV	Azobisdimethylvaleronitrile
Ace	Acetone
ACN	Acetonitrile
AcOH	Acetic Acid
AIBN	Azobisisobutyronitrile
AME	Ametryn
BET	Brunauer-Emmett-Teller
BIPB	Bis-(1-Tert-Butylperoxy)-1-Methylethyl)-Benzene
BPO	Bensoylperoxide
C	Another Kinetic Constant
C_e	Analyte Concentration at Equilibrium
CEC	Capillary Electro Chromatography
C_f	Final Concentration in the Solution After Binding
C_i	Initial Concentration in the Solution Before Binding
cm	Centimetre
cm^{-1}	Per Centimetre

CYZ	Cyanazine
DAD	Diode Array Detection
DCP	Dicumyl peroxide
DEA	Dielectric Thermal Analysis
DIPB	1,3-Diisopropenylbenzene
DIW	Distilled Water
DMA	Dynamic Mechanical Analysis
DSC	Differential Scanning Calorimetry
DSPE	Dispersive Solid-Phase Extraction
DTA	Differential Thermal Analysis
DVB	Divinylbenzene
EDCs	Endocrine Disrupting Chemicals
EDX	Energy Dispersive X-Ray
EGDMA	Ethylene Glycol Dimethacrylate
EPA	Environmental Protection Agency
EtOH	Ethanol
FESEM	Field Emission Scanning Electron Microscopy
FRP	Free Radical Polymerization
FTIR	Fourier Transform Infra-Red
g	Gram
GC	Gas Chromatography
GC-MS	Gas Chromatograph-Mass Spectrometer
GPC	Gel Permeation Chromatography
h	Hour
HEMA	2-Hydroethylmethacrylate

HPLC-UV	High Performance Liquid Chromatography-UltraViolet
IR	Infra-Red
ISEC	Inverse Size Exclusion Chromatography
K	Kelvin
k’	Relative Selectivity Coefficient
K_1	Pseudo-First-Order
K_2	Pseudo-Second-Order
K_D	Distribution Ratio
K_{diff}	Pseudo-First-Order Equilibrium Rate Constant
K_F	Maximum Adsorption Capacity of MIP
K_L	Langmuir Constant
KPS	Potassium Persulfate
K_{sel}	Selectivity Coefficient
m	Mass
MAA	Methacrylic Acid
MBAm	N, N-Methylenebisacrylamide
MeOH	Methanol
mg	Milligram
min	Minute
MIP	Molecularly Imprinted Polymer
MISPE	Molecular Imprinted Solid Phase Extraction
MIT	Molecular Imprinting Technology
mL	Millilitre
mmol	Millimoles
mol	Moles

MSPE	Magnetic Solid-Phase Extraction
n	Constant for the Intensity of Adsorption
NIP	Non-Imprinted Polymer
nm	Nanometre
NMR	Nuclear Magnetic Resonance
O/W	Oil-in-Water
PDMS	Diphenyldiethoxysilane
PhTMS	Phenyltrimethoxysilane
ppm	Parts Per Million
q_e	Amount of Analyte Adsorbed at Equilibrium Time
q_{max}	Maximum Adsorption Capacity of MIP
q_t	Amount of Analyte Adsorbed at Any Given Time
R_L	Parameter of Equilibrium
RP-HPLC	Reversed Phase-High Performance Liquid Chromatography
rpm	Round Per Minute
SBSE	Stir Bar Sorptive Extraction
SEM	Scanning Electron Microscopy
SERS	Surface-Enhanced Raman Scattering
SPE	Solid Phase Extraction
SPME	Solid-Phase Microextraction
t	Time
TAIC	Triallyl Isocyanurate
TEM	Transmission Electron Microscopy
TEOS	Tetrathoxysilane
TGA	Thermogravimetric Analysis

TMA	Tetramethylene Dimethacrylate
TMS	Tetramethoxysilan
Tol	Toluene
TRIM	Trimethylolproapne Trimethacrylate
USEPA	United States Environmental Protection Agency
UV	UltraViolet
UV-Vis	UltraViolet-Visible
V	Volume
v/v	Volume Per Volume
W/O	Water-in-Oil
wt.	Weight
XRD	X-Ray Diffraction

CHAPTER 1

INTRODUCTION

1.1 Research Background

Herbicides are chemical substances that are essential for agriculture and landscaping to kill unwanted plants, commonly known as weeds and broadleaf grasses as they are designed to selectively target and eliminate weeds and broadleaf grasses while minimizing the damage to the desirable plants or crops. Generally, herbicides are applied during pre-emergence or post-emergence of crop planting so that the growth of weeds and broadleaf grasses will not compete with desired plants or crops for nutrients, sunlight, and water. The utilization of herbicides is not only cost-effective and involves simple preparation, but they are also effective and efficient in managing weed and broadleaf grass infestation in plants or crops. Besides that, it also helps to improve and increase crop quality and productivity in the agriculture sector, as well as maintain the desired appearance of various areas for landscaping. For example, the usage of herbicides as weedkillers to eliminate unwanted vegetation in corn crops increased the corn yield by 6% (Ackerman, 2007). For these reasons, herbicides are progressively utilized in agriculture and applied by other fields such as railway companies, landscapers, greenkeepers, sports field managers, municipalities, and private gardeners (Mesnage et al., 2021).

Among the classes of herbicides mentioned by Rao (2000), only triazine herbicides including Cyanazine (CYZ), Ametryn (AME) and Atrazine (ATZ) were discussed in this research. The class of these herbicides is the first group chemical herbicides that classified according to chemical composition. These herbicides are specifically known as 1,3,5-triazine herbicides which can be further classified into chloro-1,3,5-triazine herbicides (CYZ and

ATZ) and methylthio-1,3,5-triazine herbicides (AME). These 1,3,5-triazine herbicides have pros and cons as weed and broadleaf grasses control, and hence, they have become a compound of interest in much research to study their reaction mechanism, toxicity on the ecosystem and living things, detection, and removal from the environment. The extensive usage of CYZ, AME and ATZ in agriculture can especially contribute to environmental pollution and their toxicity has adverse effects on living organisms including amphibians, aquatic life, and human health. This is due to herbicides being more persistent in the environment due to their bioaccumulation, lipophilicity, long half-life, and numerous modes of transport for these chemicals (Bhaskar et al., 2022). Therefore, an appropriate approach is necessary to cope with this problem for the sustainability of a safe environment and healthy living organisms with longevity.

In this regard, a selective and effective approach for the removal of contaminants such as CYZ, AME and ATZ in the environment is essential and this can be performed by molecular imprinting technology (MIT). Generally, MIT is an assuring method that can produce molecularly imprinted polymers (MIPs), which are extensively cross-linked polymers with highly specific binding sites and highly selective towards their target compound also known as template compound. The production of MIPs involves three main steps including the preparation of a pre-polymerization mixture (template or target molecule, functional monomer, cross-linker, initiator, and solvent), the polymerization reaction takes place at a designated time and temperature, and lastly the removal of template or target molecule from the MIP matrix. Schirhagl (2013) further explained that the molecular imprinting process begins with the organization of the functional monomer and the template molecule, then functional monomer-template complexes co-polymerize in the presence of excess cross-linker and initiator in a suitable solvent, and finally, the removal of the template

from the polymer cavity. Hence, MIPs are generated whereby the functional groups' shape, size, position, and polymer cavities are complementary to the template or target molecule.

There are various types of molecular imprinting methods to synthesize MIPs such as bulk polymerization (Jin et al., 2013), in situ polymerization (Ye, 2016), suspension polymerization (Nabavi et al., 2017), emulsion polymerization (Sun et al., 2018;; Bhawani et al., 2022), grafting polymerization (Yu, et al., 2018), seed polymerization (Tian et al., 2018) and precipitation polymerization (Lim et al., 2018; Bhawani et al., 2019;; Bhawani et al., 2020a; Bhawani et al., 2020b; Bhawani et al., 2020c). Different types of polymerization methods may generate various forms of MIPs such as hydrogels (Bergmann and Peppas, 2008), inorganic or organic composites (Oxelbark et al., 2007), nanoparticles or nanogels (Guan et al., 2008), nanofibres or nanofilaments (Linares et al., 2009), or thin films (Weetall and Rogers, 2004). Yusof et al. (2010) stated that bulk polymerization generates bulk monolith polymers which need to be crushed and sieved to get uniform particle size. Other than that, precipitation and microemulsion polymerizations can produce microsphere polymers (Bhawani et al., 2018) and nanosphere polymers (Bhawani et al., 2022), respectively.

Khajeh, Heidari and Sanchooli (2011) highlighted one of the advantages of MIP preparation as a straightforward and economical method to generate specific and selective polymers with high storage stability, mechanical strength, and durability in extreme chemical conditions. Haupt and Mosbach (2000) also explained that the highly cross-linked nature of MIPs had contributed to their remarkable stability, strength, and resilience to both heat and pressure. Additionally, Mahony et al. (2004) emphasized that MIPs exhibited excellent storage stability, allowing them to be stored for extended periods without losing

their affinity for rebinding with the template or target molecule. Therefore, MIPs have been widely used in various applications including separation materials (Balamurugan et al., 2011) sensors (Reimhult et al., 2008) drug delivery (Zaidi, 2016) and catalysis (Strikovsky et al., 2003). For example, MIPs have been a versatile material for the effective removal of numerous contaminants such as melamine (Anirudhan et al., 2017), organochlorine fungicides (Xu and Liang, 2019), 2–phenylphenol (Bakhtiar et al., 2019), 2,4,6-trichlorophenol (Bhawani et al., 2019), as well as dyes including Congo red (Shafqat et al., 2020) and Sudan III (Bhawani et al., 2022).

1.2 Problem Statement

CYZ is one of the herbicides that had been found in increasing amounts in both surface water and groundwater (Blahová et al., 2013). Karimi-Maleh et al. (2022) stated that CYZ has been reported by the Environmental Protection Agency (EPA) as a hazardous substance and dangerous compound applied in the agriculture method. For example, CYZ can cause contamination in the soil where it is applied, and rainwater may transport CYZ to other areas or waterways such as nearby rivers. Besides that, Gao et al. (2019) mentioned that CYZ has poor solubility in water and hence it is commonly dissolved in an organic solvent when used, which later causes water pollution. Moreover, CYZ might travel into the groundwater supply and contaminate the water sources. Much research has been more focused on the determination of CYZ in the environment (Lerch et al., 2015; Dong et al., 2016) and its toxicity towards mankind and the ecosystem (Abass et al., 2021; Chidya et al., 2021).

Another 1,3,5-triazine herbicide discussed in this study is AME which the U.S. Environmental Protection Agency (EPA) had classified as a Class III herbicide (Grillo et al.,

2011), indicating that it is slightly toxic due to its high solubility in water, weak adsorption behaviour, high environmental persistency (in soil and water), and very mobile in the environment (Britto et al., 2012). For these reasons, AME is called an environmental contaminant as it can be detected in surface water (Kunene and Mahlambi, 2019; Wang et al., 2019), groundwater (Scheel and Tarley, 2017) and soil (Cavalcante et al., 2021).

The widespread application of ATZ for agricultural use has led to drinking water and soil contaminations, posing risks to living organisms even at ATZ minimal concentrations (Kaur et al., 2007). For this reason, the usage of ATZ has been banned in October 2003 by various European countries, however, this herbicide is still illegally used in agriculture which contributed to persistent ATZ contamination in surface water and groundwater (Jablonowski et al., 2011). The prolonged persistence of ATZ in soil which is attributed to its low biodegradability property (Zajíček et al., 2015), and hence ATZ was transported into groundwater sources through rainwaters (Yilmaz et al., 2017). Besides that, ATZ has been detected in drinking water sources, surpassing regulatory limits, and raising concerns for vulnerable populations. The United States, the European Union, Japan, and the United States Environmental Protection Agency (USEPA) had set that 3 ppb of ATZ is the maximum contaminant level that can be found in drinking water (Zadaka et al., 2009). The toxic nature and persistent presence of ATZ in the aquatic environment had led many research studies to continually concentrate on eliminating this herbicide from water sources (Konstantinou et al., 2006). However, Malaysia has shown limited awareness regarding the occurrence of herbicides in drinking water sources and their potential implications for human health (Ahmad et al., 2015).

1.3 Objectives

The main objectives for this research are;

i) To synthesize MIPs of CYZ, AME and ATZ via precipitation polymerization method using different functional monomers including methacrylic acid, acrylamide, 2-vinylpyridine and 4-vinylpyridine.

ii) To characterize the physical, chemical, and thermal properties of MIPs of CYZ, AME and ATZ by using Fourier Transform Infrared Red (FTIR) spectroscopy, Field Emission scanning Electron Microscopy (FESEM), Energy Dispersive X-Ray (EDX), Brunauer-Emmett-Teller (BET) analyser, and Thermogravimetric analyser (TGA).

iii) To identify the binding efficiencies and adsorption parameters (contact time, adsorbent dosages, initial concentrations, and pH) of MIPs of Cyanazine, Ametryn, and Atrazine by using UltraViolet-Visible spectrophotometer (UV-Vis).

iv) To determine the selectivity efficiencies of synthesized MIPs towards CYZ, AME and ATZ by using Reversed-Phase High Performance Liquid Chromatography (RP-HPLC).

v) To demonstrate the removal efficiency of CYZ, AME and ATZ in distilled water, tap water and river water by using MIPs of CYZ, AME and ATZ, respectively.

1.4 Scope of Study

MIPs of CYZ, AME and ATZ were synthesized by precipitation polymerization with a non-covalent imprinting approach which indicated the non-covalent bond interactions between the template molecule (CYZ, AME and ATZ) and the functional monomer (MAA, AAm, 2VP and 4VP) used. Different functional monomers were used to produce MIPs of CYZ, AME and ATZ in order to obtain the best combination of template molecule and functional monomer with highest binding efficiency. The non-imprinted polymers (NIPs) that aced as the control were also synthesized as the MIPs but without addition of CYZ, AME and ATZ.

The FTIR analysis and EDX analysis were conducted to chemically characterized the synthesized MIPs of CYZ, AME and ATZ. Besides that, the FESEM analysis and BET analysis were performed to study the physical characterization of the synthesized MIPs of CYZ, AME and ATZ in terms of size, shape, pore volume, pore radius, and surface area. The thermal study was carried out via TGA to determine the thermal stability of the synthesized MIPs of CYZ, AME and ATZ.

The adsorption efficiencies of MIPs of CYZ, AME and ATZ were evaluated based on the four parameters including contact time, initial concentration, pH, and polymer dosage to determine the optimum parameters for each MIP. Kinetic study and adsorption isotherm study were also important to understand the sorption mechanism involved within the MIP cavity. Moreover, selectivity test also crucial to determine the capability of the synthesized MIPs to selectively remove their respective target compound (CYZ, AME and ATZ). The successful removal efficiencies of CYZ, AME and ATZ in several water samples (DIW, tap water and river water) by using MIPs of CYZ, AME and ATZ were determined.

1.5 Chapter Summary

This thesis comprises five main chapters namely, Introduction, Literature Review, Material and Methods, Results and Discussion, as well as Conclusion which will be further discussed below.

In Chapter 1 (Introduction), the background of this study was introduced to provide a better understanding of this research especially on topics of triazine herbicides (CYZ, AME and ATZ) and MIT. Then, the significance of the research was highlighted, along with the gaps in the existing literature that motivated this research. There were five main objectives of this research were outlined. This chapter concluded by presenting the structure of the thesis and how each subsequent chapter contributes to addressing the research objectives.

For Chapter 2 (Literature Review), extensive literature reviews on the 1,3,5-triazine herbicides (CYZ, AME and ATZ) and MIPs were performed to investigate the existing body of knowledge correlated to this research. The contents of this chapter embodied the concepts, theories, and experimental studies pertinent to this research to have profound knowledge of molecular imprinting technology.

The Chapter 3 (Materials and Methods) thoroughly indicated the experimental methodologies applied in this research which include the synthesis of MIPs and NIPs of the 1,3,5-triazine herbicides (CYZ, AME and ATZ), template removal, chemical and physical characterizations, thermal study, batch binding study, adsorption studies (initial concentration, pH, and polymer dosage), selectivity test and applications in the spiked environmental samples (distilled water, tap water and river water).

In Chapter 4 (Results and Discussion), the findings of the empirical data of this research were presented, interpreted, and discussed. The data were analysed by using Microsoft Excel and Origin software. A clear presentation of the experimental results, supported by relevant figures and tables with the interpretation of the research findings was included. A comprehensive discussion on the comparison of this research finding with previous studies as well as the theories was also provided.

The final chapter which is Chapter 5 (Conclusion) of this thesis is comprised of the conclusion and future recommendations on this research. The main research objectives mentioned in Chapter 1 (Introduction) were answered and discussed how they were achieved throughout the study. The key findings were highlighted and integrated research findings were provided. The conclusion also discussed the practical implications of the research and suggested recommendations for practitioners. Finally, the limitations of this research were reflected and suggested potential directions for future research.

CHAPTER 2

LITERATURE REVIEW

2.1 Triazine Herbicides

In this research, the 1,3,5-triazine herbicides namely CYZ, AME and ATZ are further discussed in this section. CYZ, AME and ATZ are pre-emergent and post-emergent herbicides that bear a 1,3,5-triazine group in their chemical structure and serve a similar purpose as weed and broadleaf control to eliminate unwanted vegetation. The comparison of chemical properties among CYZ, AME and ATZ were displayed in Table 2.1. Ackerman (2007) stated that the utilization of herbicides can maximize the production and quality of harvests. Moreover, Masnage et al. (2021) mentioned that herbicides are often used in public or private gardens, railways, sports fields, and golf courses to preserve the desired appearance of various landscaped areas.

Table 2.1: Comparison between CYZ, AME and ATZ

Template molecule	**CYZ**	**AME**	**ATZ**
Chemical formula	$C_9H_{13}ClN_6$	$C_9H_{17}N_5S$	$C_8H_{14}ClN_5$
Herbicide group	Chloro-1,3,5-triazine herbicide	Methylthio-1,3,5-triazine herbicide	Chloro-1,3,5-triazine herbicide
Derivative(s)	–	Prometryn	Terbuthylazine Simazine
Solubility	Poor	High	High
Environmental Persistency	Moderate	High	High

2.1.1 Cyanazine

Based on Figure 2.1, CYZ is a chloro-1,3,5-triazine herbicide, which is relatively persistent in the environment, so the exploitation of CYZ in agriculture can be detrimental to mankind and the ecosystem, causing water pollution. CYZ has been reported by the Environmental Protection Agency (EPA) as a hazardous substance and dangerous compound applied in the agriculture method (Karimi-Maleh et al., 2022). For example, CYZ can cause soil contamination, and rainwater may transport CYZ to other areas or waterways such as nearby rivers eventually killing the aquatic life. Besides that, Gao et al. (2019) mentioned that CYZ has a chemical property of poor solubility in water and hence it is commonly dissolved in an organic solvent when used, which later causes environmental pollution. Moreover, CYZ might travel into the groundwater supply and contaminate the water sources. Studies conducted by Jin et al. (2010) and Blahová et al. (2013) exposed that CYZ is one of the herbicides that had been found in increasing amounts in both surface water and groundwater.

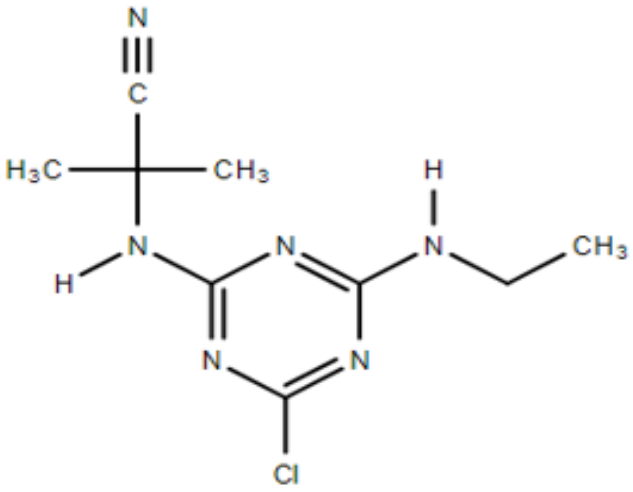


Figure 2.1: Chemical Structure of Cyanazine

Furthermore, Saka et al. (2018) indicated that CYZ is among seven 1,3,5-triazine herbicides that cause growth inhibition, development retardation, thyroid gland histology and axial malformation in amphibian tadpoles. Several adverse effects of CYZ towards human health such as diabetes, chronic bronchitis and danger of birth defects have been reported by Montgomery et al. (2003), Valcin et al. (2007) and Weselak et al. (2008), respectively. Until recently, the detection of CYZ in the environment (Lerch et al., 2015; Dong et al., 2016) and its toxicity towards mankind and the ecosystem (Abass et al., 2021; Chidya et al., 2021) are the main concern worldwide while the studies on CYZ removal in the environment is not broadly explored.

2.1.2 Ametryn

Grillo et al. (2011) testified that AME (Figure 2.2), a methylthio-1,3,5-triazine herbicide which the U.S. Environmental Protection Agency (EPA) had classified as a Class III herbicide. Britto et al. (2012) also highlighted several properties of AME as slightly toxic due to its high solubility in water, weak adsorption behaviour, high environmental persistency (in soil and water), and very mobile in the environment. For these reasons, AME is called an environmental contaminant as it can be detected in surface water (Kunene and Mahlambi, 2019; Wang et al., 2019), groundwater (Scheel and Tarley, 2017) and soil (Cavalcante et al., 2021).

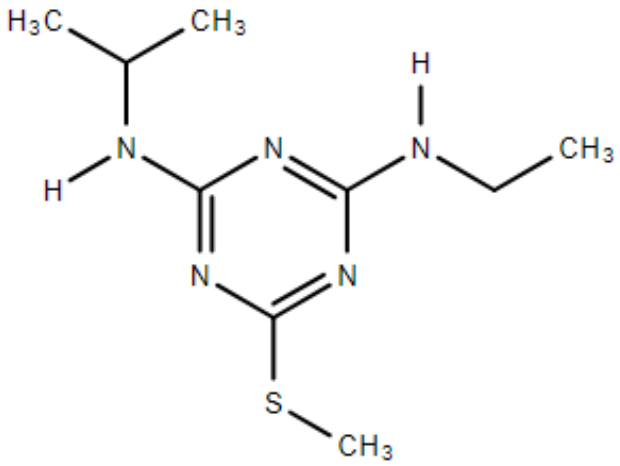


Figure 2.2: Chemical Structure of Ametryn

Moreover, AME contamination in water compartments will be very challenging to be treated and eventually harmful to human health and the ecosystem such as animals, aquatic life, as well as water sources. Studies conducted by Ali et al. (2016) and Mahesh and Manu (2019) proved that AME poisoning in humans can cause nausea, diarrhoea, salivation, muscle weakness, dermatitis, eye irritation and respiratory tract irritation. According to Ali et al (2016), prolonged exposure to AME can cause serious effects such as cancer due to its functionality as an endocrine-disrupting compound. In addition, Koutnik et al. (2015) exposed that the presence of AME in aquatic environments possesses high to moderate toxicity to fish, high toxicity to crustaceans and moderate to high toxicity to molluscs. Sanchez-Domene et al. (2022) also observed that a lower abundance of various tadpole species was noticeably associated with the presence of AME in those agricultural areas.

2.1.3 Atrazine

Kaur et al. (2007) reported that the widespread application of ATZ, a chloro-1,3,5-triazine herbicide (Figure 2.3) for agricultural use has led to drinking water and soil contaminations, posing risks to living organisms even at ATZ minimal concentrations.

Jablonowski et al. (2011) also mentioned that the usage of ATZ was banned in October 2003 by various European countries, however, this herbicide is still illegally used in agriculture which contributed to persistent ATZ contamination in surface water and groundwater. This is due to the prolonged persistence of ATZ in soil which is attributed to its low biodegradability property (Zajíček et al., 2015), and hence ATZ was transported into groundwater sources through rainwaters (Yilmaz et al., 2017). Besides that, ATZ has been detected in drinking water sources, surpassing regulatory limits, and raising concerns for vulnerable populations. It was set by the United States, the European Union and Japan, as well as the United States Environmental Protection Agency (USEPA) that 3 ppb of ATZ is the maximum contaminant level that can be found in drinking water (Zadaka et al., 2009).

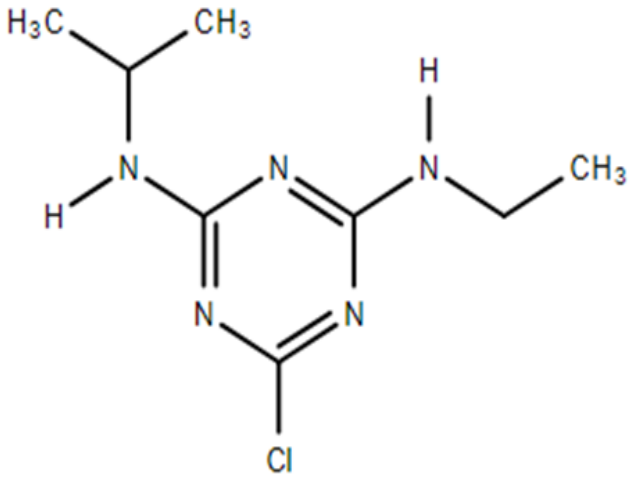


Figure 2.3: Chemical Structure of Atrazine

In aquatic ecosystems, ATZ inhibits algae growth, reducing oxygen levels and disrupting the food chain. Vryzas et al. (2009) confirmed that phytoplankton and zooplankton are examples of aquatic plants containing ATZ toxicity levels of 3100 and 5 µg/L, respectively. Moreover, freshwater vertebrates such as fish and amphibians (Rohr and McCoy, 2010) are exposed to ATZ contamination in ponds, lakes, and rivers. Additionally,

Hayes et al. (2010) revealed that amphibians are particularly sensitive to ATZ exposure, experiencing developmental abnormalities and reproductive impairments. Non-target plants, including important wildflowers and crops, can also be affected by the uncontrolled usage of ATZ, leading to reduced biodiversity and agricultural yield losses. Concerns regarding human health including the disruption of the human endocrine system (Beaulieu et al., 2020) and increased risks of mutagenesis (Cooper, 2000), carcinogenesis (Kucka et al., 2012) and teratogenesis (Stayner et al., 2017, Almberg et al., 2018) which are due to the ATZ-contaminated water that enters the human body through the food chain (Gao et al., 2017). The persistence of ATZ in the environment, its ecological disruptions, and potential health risks highlight the need to develop sustainable alternatives to cope with the issues of ATZ contamination. Konstantinou et al. (2006) indicated that more research nowadays is focusing on the removal of ATZ in water sources due to the toxic nature and persistency of ATZ in the aquatic environment.

2.2 Molecular Imprinting Technology

Molecular Imprinting Technology (MIT) is a significant approach for designing molecular recognition materials known as molecularly imprinted polymers (MIPs), capable of emulating natural recognition entities like antibodies and biological receptors (Vasapollo et al., 2011). The knowledge of polymer chemistry provides insight into the discovery of molecular imprinting as well as the development of conventional to contemporary MIT, with applications studied and implemented for various purposes in recent times as shown in Figure 2.4.

Spivak and Shea (2001) stated that the concept of MIPs traces back to the late 1800s when Fischer proposed the analogy between enzyme-substrate interactions and the lock and

key mechanism. Then, in the year 1930, Breinl and Haurowitz proposed the antibodies–antigens interaction concept in the study of immunology which later led to the adaptation of the template molecule-functional monomer interaction for the MIP concept (Ghasemzadeh, 2010). Then, Harun (2010) stated that Polyakov had interpreted the antibodies-antigen mechanism from immunology into chemistry by producing imprinted silica gel back in 1931. Xu et al. (2013) also mentioned that Polyakov was the first person who described the selective effects as a template effect, albeit additives were included after polymerization.

Nevertheless, the original idea of MIPs was inspired by Pauling's theory on antibodies' ability to produce specific three-dimensional corresponding recognition sites back in the 1940s. Subsequently, Dickey and co-workers synthesized MIPs of silica gel in the 1950s, generating affinity sites for organic dyes as mentioned by Raof (2014). Wulff and Sarhan (1972) amplified the interest in imprinting materials, meanwhile Vlatakis et al. (1993) reported the successful preparation of molecular imprinting polymers (MIPs) in the early 1980s, employing non-covalent MIT techniques. Therefore, covalent, non-covalent, and semi-covalent imprinting are the three types of molecular imprinting protocols that were established from the 1970s to the 1990s, interpreting the binding interactions of template molecule-functional monomer and polymers-analyte which provide deeper understanding regarding the MIT nowadays. Until recent years, MIP has been applied for various applications including separation techniques, catalysis, drug delivery and sensors.

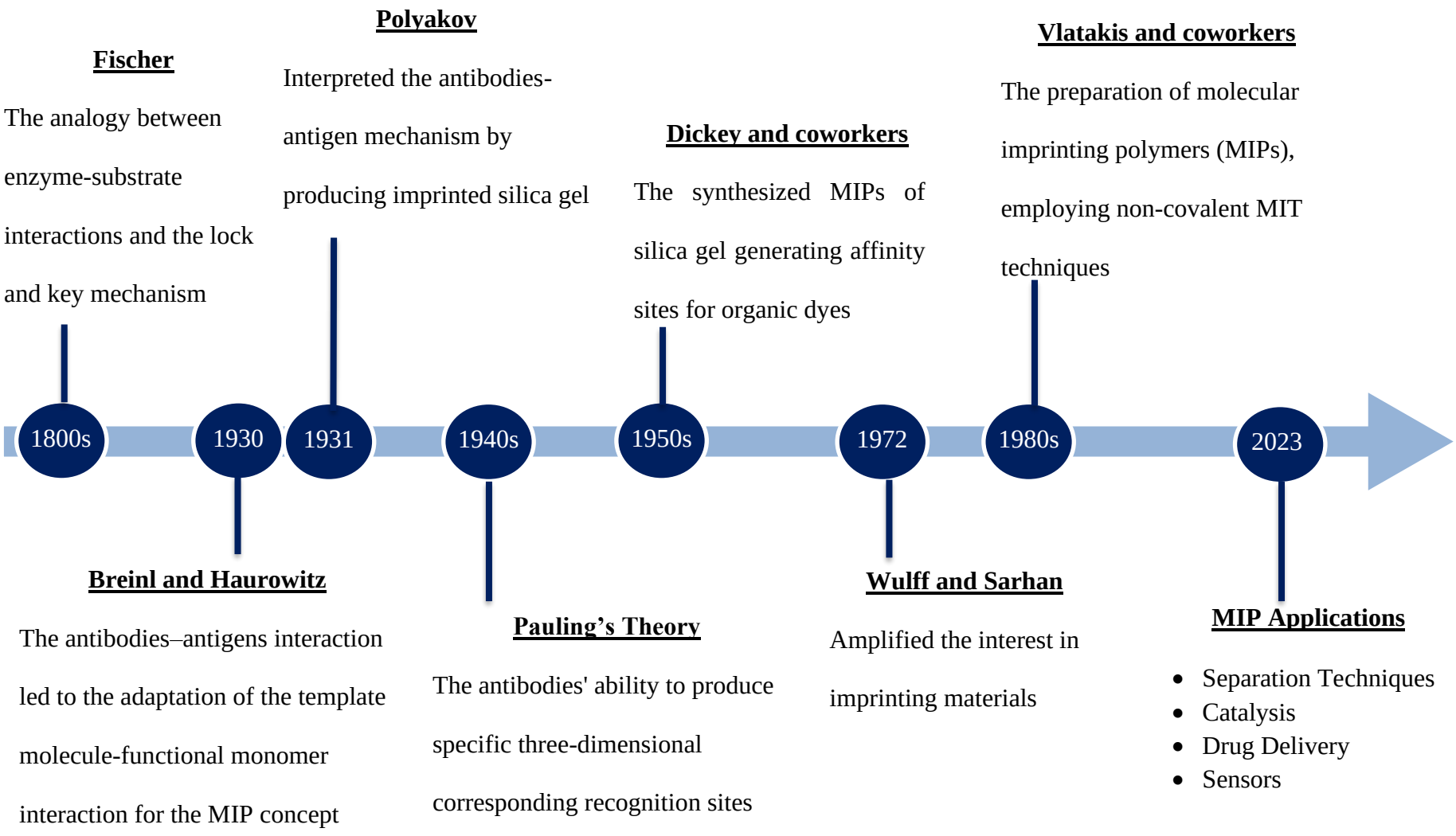


Figure 2.4: Development of MIPs from 1800s until 2023

2.3 Molecular Imprinting Pre-Polymerization Mixture

The fabrication of MIPs involved five essential chemical constituents including template molecule, functional monomer, cross-linker, initiator, and solvent are compulsory in the MIP synthesis (Liu et al., 2021) as depicted in Figure 2.5.

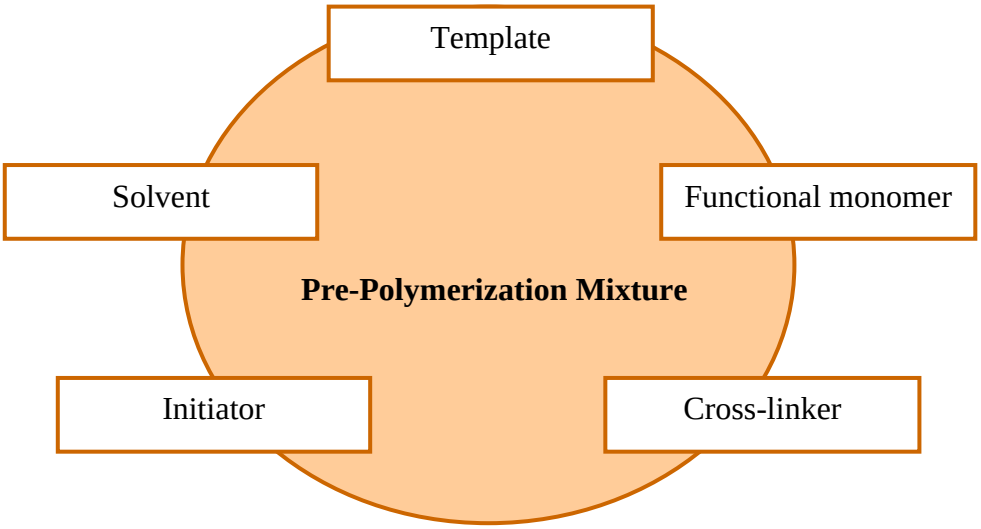


Figure 2.5: Five Important Chemicals for Pre-Polymerization Mixture

This mixture is also known pre-polymerization mixture and each of the chemicals plays an important role in successfully generating MIPs with high specificity and affinity towards the template molecule or target compound. Hence, it is crucial to properly select the right combination of the pre-polymerization mixture as their choice can significantly impact the binding performance of the produced MIPs.

2.3.1 Template Molecule

In molecular imprinting, a template molecule which is also known as a target compound plays a significant role in fabricating MIPs with specific recognition sites in its polymer cavity. This is because the template molecule serves as a blueprint that guides its interaction with the functional groups that are attached to the functional monomer during the

pre-polymerization reaction (Sajini and Mathew, 2021). Hence, the presence of a template molecule in the molecular imprinting reaction is essential to produce MIPs which consist of specific binding sites. Meanwhile, the absence of a template molecule in the polymer synthesis leads to the production of non-imprinted polymers (NIPs) which lack specific binding sites.

The selection of a template molecule for MIP synthesis depends on several factors such as the nature, availability, accessibility, and cost of the compound of interest (template molecule) are important aspects to consider in choosing a template or target molecule which later can affect the performance of MIPs. For example, the selected template molecule should be readily available in great amounts and inexpensive (Zare et al., 2022). Chen et al. (2016) stated there are three necessary criteria any analyte should meet to be an ideal template molecule for MIP synthesis including; it should have functional groups that do not impede the MIP polymerization reaction, display exceptional chemical stability during the MIP synthesis process, and possess functional groups that can interact effectively with the functional monomers by forming template-functional monomer complexes before the polymerization reaction.

The production of MIPs involved the selection of a template or target molecule is subjected to the specific application and the desired target molecule to be recognized by the MIP. Haupt (2001) emphasized that small organic molecules (amino acids, peptides, nucleotide bases, steroids, and sugars) are typically more favourable to be chosen as template molecules in MIP synthesis because of their greater structural rigidity as compared to larger template molecules. Yan and Row (2006) also stated that smaller template molecules have a higher tendency to promote the formation of well-defined binding cavities throughout the

polymerization reaction. Wloch and Datta (2019) stated that commonly used template molecules for molecular imprinting can be classified into four categories; ions, organic molecules, biomacromolecules, and cells and viruses as displayed in Figure 2.6.

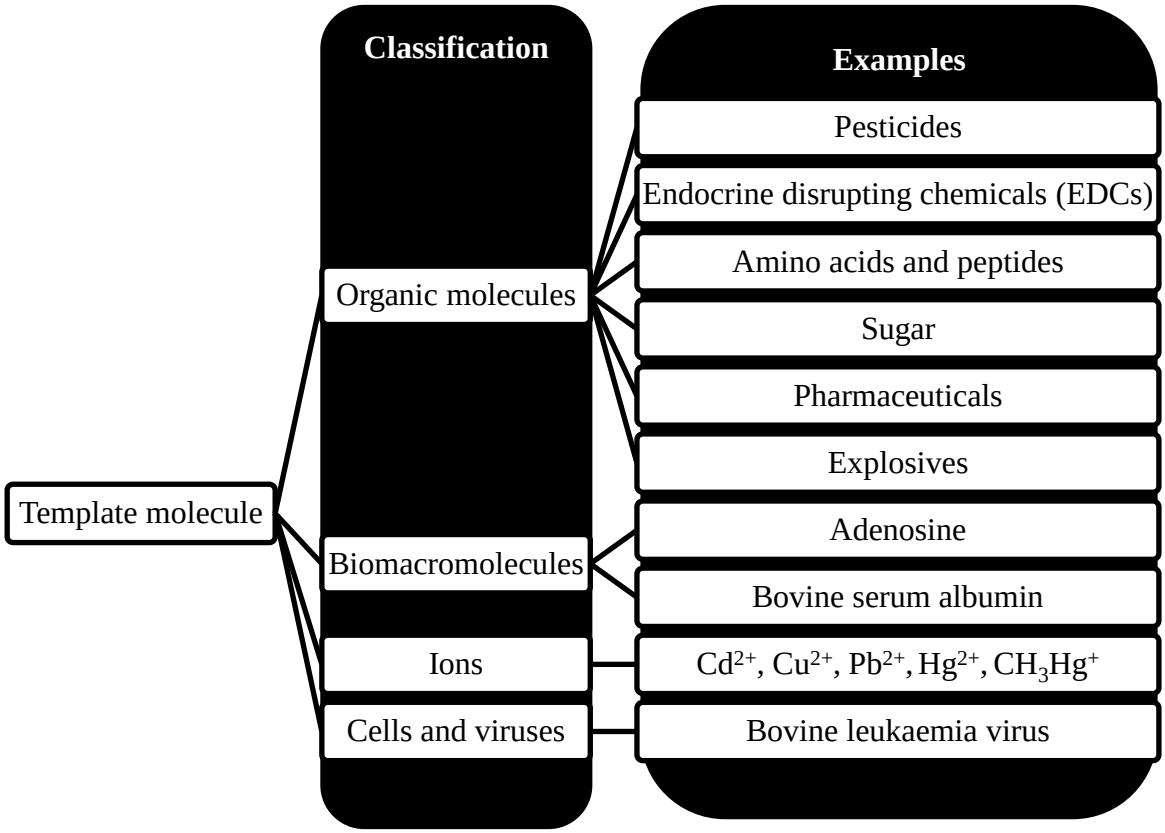


Figure 2.6: Classifications and Examples of Commonly Used Template Molecule

Sajini and Mathew (2021) emphasized that the nature of the template molecule specifically its properties and functionalities can contribute to the successful fabrication of MIPs. Besides that, Herrera-Chaćon et al. (2021) stated the choice of template molecule for MIP synthesis should consist of at least a single functional group such as alcohol, amine, amide, aromatic rings, carboxylic acid, and nitrile groups. This is because a template molecule consisting of numerous functional groups could be a factor that influences the capability of a strong template molecule-functional monomer interaction. Since a template

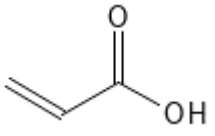
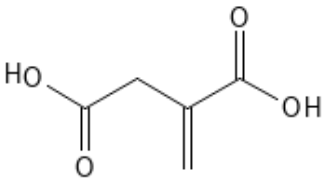
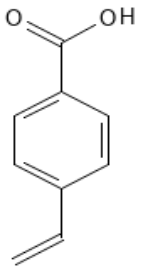
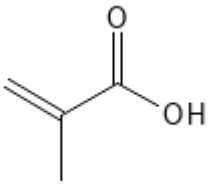
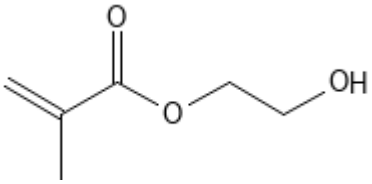
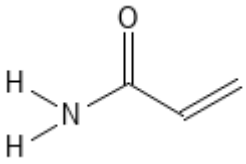
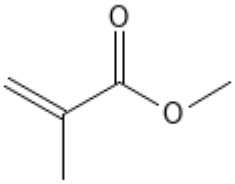
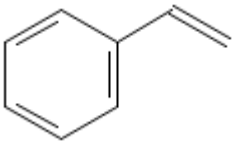
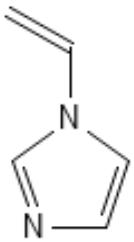
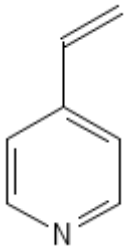
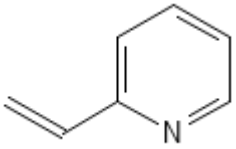
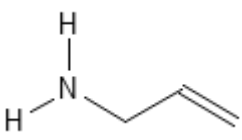
or target molecule contains multiple functional groups, it has multiple sites that promote greater binding interaction with the functional monomer thus fabricating MIPs with greater affinity and selectivity towards their template or target molecule (Samarth et al., 2015).

2.3.2 Functional Monomer

A functional monomer is functioned to interact directly with the template molecule to form complexes between the template molecule and the functional monomer. The formation of stable template molecule-functional monomer complexes contributes to the successful establishment of molecular recognition of MIPs (Pratiwi et al., 2018). Sajini and Mathew (2021) stated that a functional monomer has two components, namely recognition and polymerization. Chen et al. (2022) further explained that the recognition component of the functional monomer gives access to its functional groups to interact and bind with the target molecule, meanwhile, the polymerization component of the functional monomer with the assistance of cross-linker comprehends the fabrication of polymeric cavity.

Table 2.2 indicates the commonly used acidic, neutral, and basic functional monomers for the MIPs preparation. Nishchaya et al. (2023) stated that the most employed functional monomers for MIP synthesis of covalent and non-covalent imprinting approaches are methacrylic acid (MAA) and acrylic acid (AA). MAA is well-known as a universal functional monomer due to its capability as an H-bond acceptor and donor (Chen et al., 2016), as well as its ability to boost the imprinting effect due to the dimerization of MAA (Zhang et al., 2010).

Table 2.2: Common Examples of Acidic, Neutral, and Basic Functional Monomers

Functional monomer	Example(s)	
Acidic	 Acrylic acid (AA)	 Itaconic acid
	 p-vinyl benzoic acid	 Methacrylic acid (MAA)
Neutral	 2-hydroethylmethacrylate (HEMA)	 Acrylamide (AAm)
	 Methyl methacrylate	 Styrene
Basic	 1-vinylimidazole	 2-vinylpyridine
	 4-vinylpyridine	 Allylamine

In general, the choice of a functional monomer for MIP synthesis is based on the chemical properties of the template molecule. Sajini and Mathew (2021) stated that the functionality of both the template molecule and the functional monomer should be complementary to each other to maximise the creation of the pre-polymerization complex, in which an H-bond donor of the template molecule is suitably paired with an H-bond acceptor of the functional monomer, reciprocally.

A template molecule composed of basic functional groups is compatible with an acidic functional monomer to promote hydrogen bonding or ionic interactions, whereas a template molecule containing acidic functional groups is suitable with weak bases (Urriza-Arsuaga et al., 2023). This is because the ideal matching between a template molecule and a functional monomer with better stability and suitability of its functional groups affects the affinity and selectivity of produced MIPs (Chen et al., 2022).

Moreover, the selection of a functional monomer for the MIP preparation is also depending on the selected solvent in which the functional monomer must have high stability and solubility in the solvent (Lafarge et al., 2020). Murdaya et al. (2022) also added that the use of a suitable functional monomer in a designated solvent would probably display strong interactions, resulting in binding cavities with greater capacity and homogeneity. The chosen functional monomer for MIP synthesis must have high resistance to extreme temperatures, harsh chemical media, and other environmental factors (Lim et al., 2020; Ozcelikay et al., 2022). When the selected functional monomer for molecular imprinting has met all requirements mentioned above, the subsequent MIPs would have greater imprinting effects that are capable of selectively binding with the template molecule even after the template removal.

The simplest and easiest way to select a suitable functional monomer is by conducting trial-and-error experiments. However, there are diverse reliable and convenient strategies for the determination of effective functional monomers for molecular imprinting such as Fourier Transform Infrared Spectroscopy (FTIR) (Lv et al., 2007), morphological characteristics, Nuclear Magnetic Resonance (NMR) (Ansell and Wang, 2009), UV spectroscopic titrations (Luo et al., 2008), isothermal titration calorimetry (Su et al., 2009), computer simulation (Cowen et al., 2016), and combinational screening.

Additionally, it is crucial to determine a proper ratio of functional monomer to template molecule because it affects the number of generated binding sites and thus influences the MIP performance. To allow the creation of template molecule-functional monomer complexes, the functional monomer is used in excess to which the typical ideal molar ratio of a functional monomer to template molecule is 4:1 (Wloch and Datta, 2019). For example, the use of a high molar ratio of MAA generated MIPs with large pore sizes and promoted higher MIP binding capacity (Golker et al., 2013).

However, an excessively high molar ratio of functional monomer could lead to an abundance of non-specific recognition sites and weaken the specific recognition of template molecule whereas the insufficient molar ratio of functional monomer results in limited specific recognition sites in the polymer cavity or even hinders the polymerization reaction (Chen et al., 2022). Other than that, the ratio of functional monomer to cross-linker is also vital to retain the efficiency, selectivity, and rigidity of the synthesized MIPs. Azizi and Bottaro (2020) reported that the standard ratio of functional monomer to cross-linker is 1:2.

2.3.3 Cross-Linker

Cross-linker is also an essential chemical constituent in molecular imprinting because it assists the functional monomers in gathering around the template molecule rigidly and generates a highly cross-linked polymer network.

Sajini and Mathew (2021) exposed that cross-linker has three main roles in the molecular imprinting process which is responsible for the polymer morphology, stability of the imprinted recognition sites, and mechanical strength of the polymer cavity.

Various cross-linkers used in the molecular imprinting process can be classified into a few categories including covalent, non-covalent and semi-covalent as listed in Table 2.3. The most common cross-linkers used in MIP synthesis are ethylene glycol dimethacrylate (EGDMA), divinylbenzene (DVB) and trimethylolpropane trimethacrylate (TRIM).

A comparison study on TRIM and EGDMA as cross-linkers was conducted by Esfandyari-Manesh et al. (2013) and Pengkamta et al. (2020) proved that TRIM had established better performance in producing MIPs of a higher number of binding sites and greater binding efficiency than that EGDMA. Another study also demonstrated that the usage of TRIM as the cross-linker yielded more MIPs as compared to the DVB cross-linker (Nishchaya et al., 2023).

The amount of cross-linker utilized in the molecular imprinting process is one of the profound features of generating MIPs with excellent binding efficiency and selectivity towards its template or target molecule (Wloch and Datta, 2019). This is because an inadequate amount of cross-linker leads to a low crosslinking degree thus producing MIP with unstable mechanical strength while an excessively high amount of cross-linker causes

a lower number of active binding sites produced per unit mass of MIPs. Therefore, a sufficiently high amount of cross-linker is necessary to generate permanently porous MIPs, ensuring that the functional groups are evenly distributed and spatially configured for improved rebinding efficiency with the template or target molecule (Ma et al., 2019).

Table 2.3: Classification and Examples of Cross-Linker (Nishchaya et al., 2023)

Classification	Examples
Covalent cross-linker	▪ Bis-(1-tert-butylperoxy)-1-methylethyl)-benzene (BIPB) ▪ Dicumyl peroxide (DCP) ▪ Triallyl isocyanurate (TAIC)
Non-covalent cross-linker	▪ 1,3-diisopropenylbenzene (DIPB) ▪ 1,4-diacryloyl piperazine ▪ Divinylbenzene (DVB) ▪ Ethylene glycol dimethacrylate (EGDMA) ▪ N, N-1,4-phenylenediacrylamine ▪ N, N-methylenebisacrylamide (MBAm) ▪ N, O-bisacryloyl-phenylalaninol ▪ N, O-bismethacryloyl ethanolamine ▪ Tetramethylene dimethacrylate (TMA) ▪ Trimethylolpropane trimethacrylate (TRIM)
Semi-covalent cross-linker	▪ Diphenyldiethoxysilane (PDMS) ▪ Phenyltrimethoxysilane (PhTMS) ▪ Tetramethoxysilan (TMS) ▪ Tetrathoxysilane (TEOS)

Another important aspect of molecular imprinting is to choose a suitable type of cross-linker because it can affect the characteristics of the subsequent polymers. The selection of cross-linker further depends on the functional monomer used in the synthesis,

the type of bond present due to the template molecule-functional monomer interactions, the type of polymerization reaction involved, as well as the type of solvent applied in the MIP synthesis (Chen et al., 2016; Sooraj et al., 2020). Sooraj et al. (2020) mentioned that both types of cross-linkers and functional monomers should have similar reactivity to promote an even distribution of functional groups of the functional monomers upon random copolymerization. Besides that, Chen et al. (2016) stated that the type of bond interaction between the template molecule and the functional monomer must be identified so that the chosen cross-linker will not disrupt the bond interaction.

The type of polymerization which involved the presence or absence of free radicals has influenced the generated MIPs (Sooraj et al., 2020). This is because the free radical polymerizations for non-covalent bonds are utilizing EGDMA, DVB and TRIM, while the free radical polymerizations for covalent bonds use triallyl isocyanurate (TAIC), dicumyl peroxide (DCP), and bis-(1-tert-butylperoxy)-1-methylethyl)-benzene (BIPB) (Wypych, 2019; Sooraj et al., 2020).

Lastly, the selection of a cross-linker also depends on the type of solvent as it must be insoluble in that solvent. Often, N, N-methylenebisacrylamide cross-linker is employed in inorganic solvents meanwhile EGDMA and DVB cross-linkers are applied in organic solvents (Sooraj et al., 2020).

2.3.4 Initiator

An initiator in the pre-polymerization mixture functions to start or trigger the polymerization reaction (Kryscio and Peppas, 2012). Free radical polymerization (FRP), photopolymerization and electropolymerization are the three common types of polymerization reactions applied for MIP formation (Sajini and Mathew, 2021). Among

them, FRP is the most employed polymerization reaction to produce MIPs because it can be initiated by heat or photochemical for a vast variety of functional monomers and template molecules (Chen et al., 2016).

Generally, FRP's polymerisation mechanism involves three stages: initiation, propagation, and termination. Murdaya et al. (2022) further explained that the initiation phase takes place when the initiator undergoes decomposition into stable fragments known as free radicals which possess free electrons that form bonds with the carbon double bonds present in the functional monomer, initiating the polymerization reaction. For this reason, an initiator used in molecular imprinting can be an indicator to evaluate the success of the polymerization reaction.

Since Murdaya et al. (2022) exposed that an effective initiator for MIP synthesis should be a compound that readily undergoes decomposition, a careful choice of initiator that is suitable for the type of polymerization applied in the molecular imprinting process is an important aspect to consider. Figure 2.7 shows the list of common initiators used for the molecular imprinting process (Wloch and Datta, 2019).

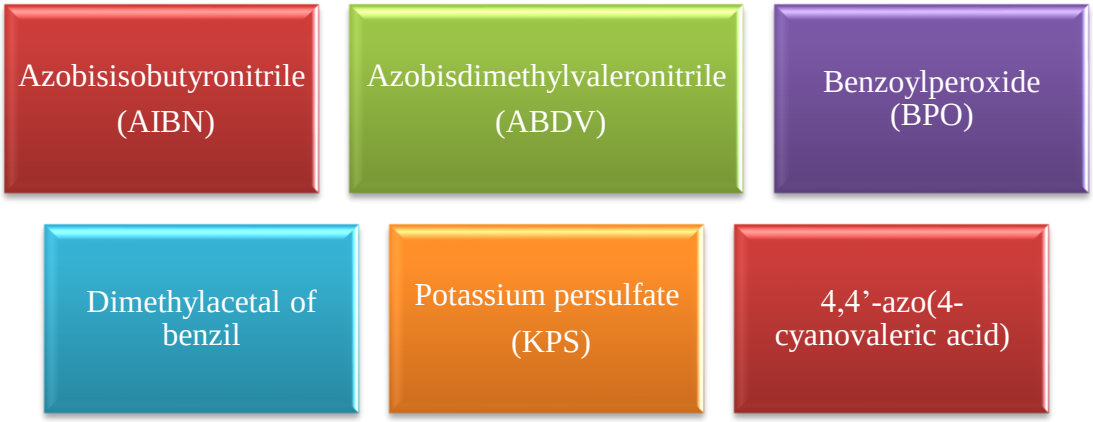


Figure 2.7: List of Common Initiators for MIP Synthesis

For MIP synthesis by FRP, azo compounds and peroxy compounds are the frequently applied initiators. Nishchaya et al. (2023) stated that azo compounds are preferable initiators because they consist of tertiary carbon on both ends that carry the alkyl group along with the ester or nitrile group, which serves as the essential atom for FRP. For instance, azobisisobutyronitrile (AIBN), an azo compound is the most common initiator used for MIP synthesis because it can be decomposed by photolysis and thermolysis at a temperature ranging between 50 °C to 70 °C (Haupt et al., 2012) to generate stabilized carbon-centred radicals that effectively initiate the various vinyl monomers (Sajini and Mathew, 2021). Yoew et al. (2018) also added that it is essential to remove oxygen in the pre-polymerization mixture by purging with inert gas to minimize the oxidation and following deactivation of polymerization.

Other than that, the selection of an initiator is also based on the nature of the template molecule used in the molecular imprinting process. Turkewitsch et al. (2005) clarified that a thermally unstable template or target molecule is ideal for photochemical initiation, which occurs at low temperatures as well as its favourability for the non-covalent molecular imprinting that exhibits stronger interactions at lower temperatures. On the contrary, a template molecule with characteristics of low solubility and sensitivity to light is suitable for thermal initiation.

In addition, the amount of initiator added to the pre-polymerization mixture is also important to allow a successful molecular imprinting process. A previous study conducted by Haupt and Mosbach (1998) stated that the rate of the radical polymerization process is influenced by the amount of initiator applied in the MIP synthesis. A study conducted by Mohebali et al. (2018) indicated that the usage of a high amount of initiator causes an

increased number of generated free radicals, resulting in MIP formation of very small pores which later influence the MIP performance. Both Wackerlig and Schirhagl (2016) proved that only a low amount of initiator is required where the polymerization condition needs to be adjusted (longer duration and lower temperature of polymerization reaction) to produce MIPs consisting of good recognition sites with average pore size. Lusina and Ceglowski (2022) also revealed that the MIP synthesis only requires a low amount of initiator, about 1 wt. % or 1 mol % relative to the total amount of moles of polymerizable double bonds.

2.3.5 Solvent

The use of solvent in the molecular imprinting process is crucial to serve as dispersion media and agents for pore formation. Li and Row (2017) revealed that a solvent is responsible as a reaction media for dissolving the template molecule, functional monomer, cross-linker, and initiator into a homogeneous solution known as a pre-polymerization mixture. Besides that, the solvent is in control for the formation of macroporous polymers with their pores (Murdaya et al., 2022). Sajini and Mathew (2021) also emphasized that the solvent selected for MIP synthesis must comply with these three conditions including the solubility of the template molecule, functional monomer, cross-linker, and initiator in the solvent, the ability to generate large pores, as well as low polarity to minimize interferences during pre-polymerized complex production. Due to these reasons, the solvent used in MIP synthesis is often referred to as the porogen or porogenic solvent.

To choose a suitable porogenic solvent for the MIP synthesis, the nature in terms of polarity and solubility, as well as the volume of the porogenic solvent applied are very crucial because they can influence the morphology, the template molecule-functional monomer, as well as the adsorption efficiency of the fabricated MIPs. Lusina and Ceglowski (2022) stated

that the polarity of a solvent affects the template molecule-functional monomer interactions. Therefore, non-polar or less polar solvents with low dielectric constants are commonly employed for the non-covalent imprinting method to promote the formation of complexes that involve non-covalent interactions, such as hydrogen bonding (Murdaya et al., 2022). Such porogenic solvents are toluene, acetonitrile, and chloroform. In contrast, when a more polar solvent such as water is used as the porogenic solvent, it will disrupt the interactions in the generated complexes (Vasapollo et al., 2011).

Moreover, Chen et al. (2022) stated that the porogenic solvents with characteristics of low polarity and high solubility phase are likely to separate later, generating small pores and large surface areas that give MIPs adequate adsorption and rebinding sites. A study conducted by Chen et al. (2016) mentioned that type of solvent also affects the morphology whereby a variety of porogenic solvents produced MIPs of several sizes (eg. micro-sized or nano-sized) and shapes (eg. irregular or spherical).

The volume of porogenic solvent used in the MIP synthesis is also important to maximize the imprinting effects of MIP because a higher volume of solvent will increase its pore size. Wolch and Datta (2019) revealed that an increasing volume of solvent leads to an increase in pore size, and therefore, the usage of an appropriate volume of porogenic solvent for MIP synthesis is essential to improve the production of specific binding sites in the polymer cavity that complementary to the template molecule.

2.4 Molecular Imprinting Process

The knowledge of the molecular imprinting process provides a better understanding of the important role of each chemical constituent (template molecule, functional monomer, cross-linker, initiator and porogenic solvent) in generating MIPs of highly specific and

selective towards its target compound. This is because the physical and chemical characterizations as well as the binding performance of resultant MIPs are influenced by the choice of template molecule, functional monomer, cross-linker, initiator and porogenic solvent. Briefly, MIP preparation comprises three essential stages namely the organization between the functional monomer and the target molecule; followed by the co-polymerization of the complexes facilitated by an excess of cross-linker; and thirdly, the elimination of the template molecule from the polymer cavity (Schirhagl, 2013) as displayed in Figure 2.8.

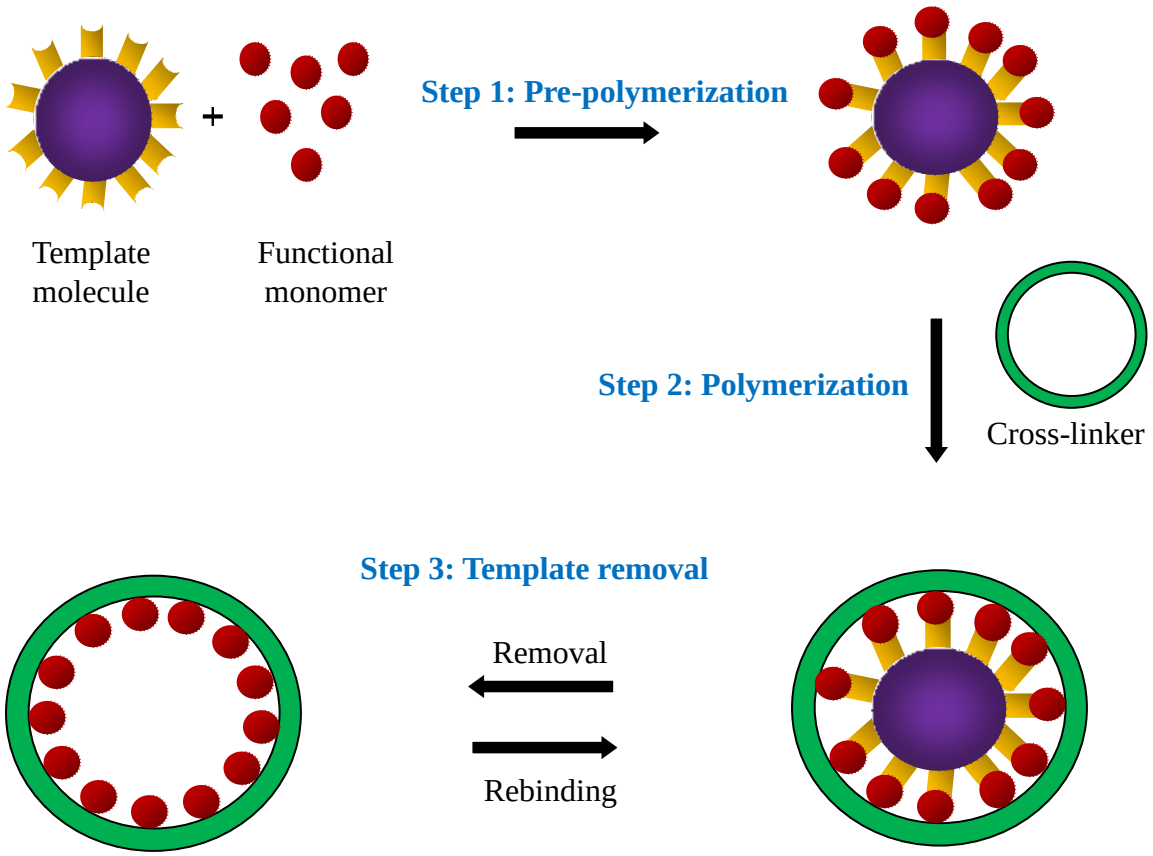


Figure 2.8: General Steps in the Molecular Imprinting Process

In the first step of the molecular imprinting process, the pre-polymerization mixture is prepared by dissolving the template molecule, functional monomer, cross-linker, and initiator in a porogenic solvent. At this stage, the template or target molecule takes control

of the molecular imprinting process by organizing the functional monomer around it during the pre-polymerization reaction to form template molecule-functional monomer complexes (Mafu et al., 2013) and thus creating specific binding sites and selectivity of the subsequent MIPs. The binding interaction that may occur due to the arrangement of the functional monomer around the template molecule is either a covalent bond, non-covalent bond or semi-covalent bond which will be further described in the next section. These template molecule-functional monomer complexes are also known as pre-polymerization complexes because the polymer structure had been formed but without rigidity (Haupt et al., 2012).

During the second stage of the molecular imprinting process, a significant excess of cross-linker in the pre-polymerization mixture would favour the polymerization reaction to occur. This stage showed the incorporation of cross-linkers in the pre-polymerization complexes to provide them with a stable and rigid polymer structure (Yan and Row, 2006). This is because the copolymerization of the cross-linker helps fix the functional monomer's position around the template molecule. The initiator in the pre-polymerization mixture plays its role as an activator to start the polymerization reaction either through thermal or photo initiation (Fitzhenry, 2011). The reaction is carried out at a specific temperature and duration to ensure complete polymerization of all complexes, resulting in the formation of stable and rigid three-dimensional polymer networks.

The final stage of the molecular imprinting process involves the removal of the template molecule from the generated polymer matrix, and this can be performed by continuous solvent extraction. Suitable solvents are required to remove the template molecule and other impurities without disrupting the non-covalent interactions that occurred between the template molecule and synthesized MIPs (Zare et al., 2022). Such solvent

extraction mixture that can be used for MIP washing is a solvent mixture of methanol and acetic acid at a designated ratio. Subsequently, the template molecule is removed from the polymer cavity leaving the MIPs consisting of highly specific and selective recognition sites (Iskierko et al., 2016). This explained that the imprinted recognition sites in the MIP cavity retained the original template's shape, size, and chemical functionality which possess a high affinity for the target molecule, allowing for selective binding and recognition even after the template removal.

2.5 Molecular Imprinting Approaches

Molecular imprinting approaches are used to describe the binding interactions that happened throughout the polymerization reaction and such approaches are covalent imprinting, non-covalent imprinting, and semi-covalent imprinting (Yemis et al., 2013). Typically, the selection of an appropriate molecular imprinting approach depends on the suitable reaction mechanism, desired properties, and intended purposes of the subsequent MIPs (Chen et al., 2022).

Each molecular imprinting approach has its advantages and limitations, and understanding these factors can lead to the development of highly efficient and selective MIPs for various analytical, sensing, and separation applications. Table 2.4 shows the classification of molecular imprinting approaches based on the template molecule-functional monomer interactions during the polymerization reaction and the synthesized polymers-analyte interactions during the rebinding process in which the template molecule (analyte) is restored.

Table 2.4: Classification of Molecular Imprinting Approaches

Molecular imprinting approach	Bond interactions between chemical components	
	Template & functional monomer	Polymers & analytes
Covalent imprinting	Covalent bond	Covalent bond
Non-covalent imprinting	Non-covalent bond	Non-covalent bond
Semi-covalent imprinting	Covalent bond	Non-covalent bond

2.5.1 Covalent Imprinting

The covalent imprinting approach, also called the pre-organized approach was pioneered by Wulff and co-workers, indicating the creation of reversible covalent bonds within the complex of template molecule and functional monomer in the solution before the polymerization reaction takes place, leading to molecular recognition through the formation and breakage of the covalent bonds (Wulff et al., 1977). Acetal bonds, boronic ester bonds (Sallacan et al., 2002), ketals (Shea and Sasaki, 1991), and shift base bonds (Wulff and Vietmeier, 1989) are the examples of the establishment of covalent bond interactions in molecular imprinting.

Typically, in the covalent imprinting approach, the template molecule and functional monomer are connected by the reversible covalent bonds before the polymerization reaction. For this approach, the choice of template molecule must possess at least one functional group that can undergo derivatization including aldehyde, amines, ketones, carboxylic acids, or alcohol group (Herrera-Chacón et al., 2021). Then, the MIP polymerization process occurred in the presence of a cross-linker to form rigid polymers. This approach requires a substantial amount of cross-linker for the polymerization to occur and generate an insoluble rigid polymer network (Sajini and Mathew, 2021). After that, the template removal step whereby

the covalent bonds in the generated polymer structure are cleaved and the template molecule is released from the synthesized MIPs. Sajini and Mathew (2021) also stated that template removal is conducted by chemical interaction whereby the covalent bonds are cleaved, resulting in the MIP formation of distinct binding cavities that specifically correspond to the template molecule in terms of steric and functional topography. These covalent bonds can be re-established during the rebinding process of the MIPs with the previously removed template molecule (Lusina and Ceglowski, 2022) because the same covalent bond can be regenerated to bind with its template molecule specifically and selectively.

The covalent imprinting approach has several advantages including producing precise recognition sites in the polymer cavity, high stability and minimized non-specific recognition sites in the MIP matrix. The stoichiometric complexes of template molecule-functional monomer led to the production of MIPs containing recognition sites that are precisely situated in the imprinted cavities (Amorim et al., 2022)., thereby minimizing the occurrence of non-specific interactions (Parisi et al., 2022). The high stability of the template molecule-functional monomer complexes during polymerization contributed to the formation of the MIP network with homogenous recognition site distribution and excellent specificity in comparison with the MIP based on the non-covalent imprinting approach (Sajini and Mathew, 2021).

Despite that, this covalent imprinting approach has numerous disadvantages that make it an unfavourable approach for MIP synthesis. Firstly, the options for template molecules and functional monomers are limited because these chemical components should have functional groups of alcohols, amines, aldehydes, ketones, or carboxylic acids (Sajini and Mathew, 2021). Secondly, Chen et al. (2022) also revealed that strong covalent bond

interactions lead to slow binding and dissociation, hence it is intractable to reach thermodynamic equilibrium. Thus, the rebinding process would take longer time and the template removal would be difficult to extract out of the polymer cavity.

2.5.2 Non-Covalent Imprinting

The non-covalent imprinting approach also known as the self-assembly approach was first revealed by the Mosbach group which describes the non-covalent bond interactions between the template molecule and functional monomer (Arshady and Mosbach, 1981). Such non-covalent bonds are van der Waals forces, hydrogen bonding, π-π interactions, dipole-dipole interaction, and ion-dipole interactions that have weak interactions between the template molecule and functional monomer and thus only require minimal synthetic effort for the binding and template removal process. Shah et al. (2012) reported that the most employed non-covalent imprinting approach involved the utilization of MAA (functional monomer) and EGDMA (cross-linker) because MAA exhibits the capability to form hydrogen bonds with a wide range of template molecules in this approach.

Generally, the template molecule interacts with the functional monomer via the non-covalent bond to form the pre-polymerization complexes before the polymerization reaction. This non-covalent imprinting approach requires the usage of an excess amount of functional monomer to favour the complete binding interaction with the template molecule (Sajini and Mathew, 2021). Then, these pre-polymerization complexes will undergo a polymerization process with the aid of a cross-linker to generate a rigid highly cross-linked polymer structure. Finally, the template removal from the MIP cavity can be conducted using solvent extraction that will provide MIP with highly specific and selective recognition sites towards its template compound. Tóth (2010) explained that template removal can be performed under

mild conditions and the rebinding process of MIP with the template molecule is a rapid method.

Among the types of molecular imprinting approaches, the non-covalent molecular imprinting approach is the most employed approach to produce polymers because it has a wide variety of choices for functional monomers and template molecules that can establish the non-covalent bond interactions (Haupt et al., 2012). It is also the most preferred approach due to its numerous advantages including; (i) a simple procedure for the formation of template molecule-functional monomer complexes, (ii) the binding interactions are flexible, quick, and simple, (iii) the template molecule can be easily removed from the polymer cavity, and (iv) produce MIPs with high affinity and selectivity towards its target compound or template molecule (BelBruno, 2019).

Nevertheless, this non-covalent imprinting approach has few drawbacks as this approach requires massive usage of functional monomers and the non-covalent bonds are weak interactions. In the non-covalent imprinting approach, the usage of an excess amount of functional monomer is necessary, however, this can contribute to the formation of non-specific binding sites which can affect the performance of resulting MIPs (Zare et al., 2022). Chen et al. (2022) also emphasized that since the non-covalent bonds are weak interactions and therefore, they can be readily interrupted by the presence of water in the reaction solvent system.

2.5.3 Semi Covalent Imprinting

Semi-covalent molecular imprinting approach as the name described is the combination of covalent and non-covalent imprinting approaches that use the advantages of both approaches to generate MIPs with excellent characteristics in terms of stability,

strength, and fast binding interactions. This approach is pioneered by Whitcombe and co-workers (Whitcombe et al., 1995), where the covalent imprinting approach is implemented in the interactions between the template molecule and functional monomer during the polymerization reaction, meanwhile, the non-covalent imprinting approach is executed in the rebinding interactions between the generated polymers and the template molecule (Azizi and Bottaro, 2020; Parisi et al., 2022) as shown in Table 2.3.

In this approach, the preparation of complexes between the template molecule and functional monomer during the polymerization is conducted by covalent bonds can reduce the formation of non-specific recognition sites in comparison with the non-covalent imprinting approach (Chen et al., 2022). This semi-covalent imprinting approach also involved the non-covalent bonds in the rebinding interaction between the polymers and template molecule, resulting in a tremendous enhancement in the rebinding sensitivity and efficiency (Qi et al., 2010). In contrast with the single molecular imprinting approach, this approach can generate MIPs with much greater specificity and sensitivity towards its target compound (Chen et al., 2022).

2.6 Molecular Imprinting Techniques

There are a variety of techniques that can be applied to fabricate MIPs as shown in Figure 2.9. The choice of MIP synthesis technique depends on the required properties of the polymers in terms of the particle sizes. In this section, only four types of commonly used polymerization techniques including bulk polymerization, precipitation polymerization, emulsion polymerization and suspension polymerization are further discussed. These polymerization techniques are utilizing a free-radical polymerization mechanism.

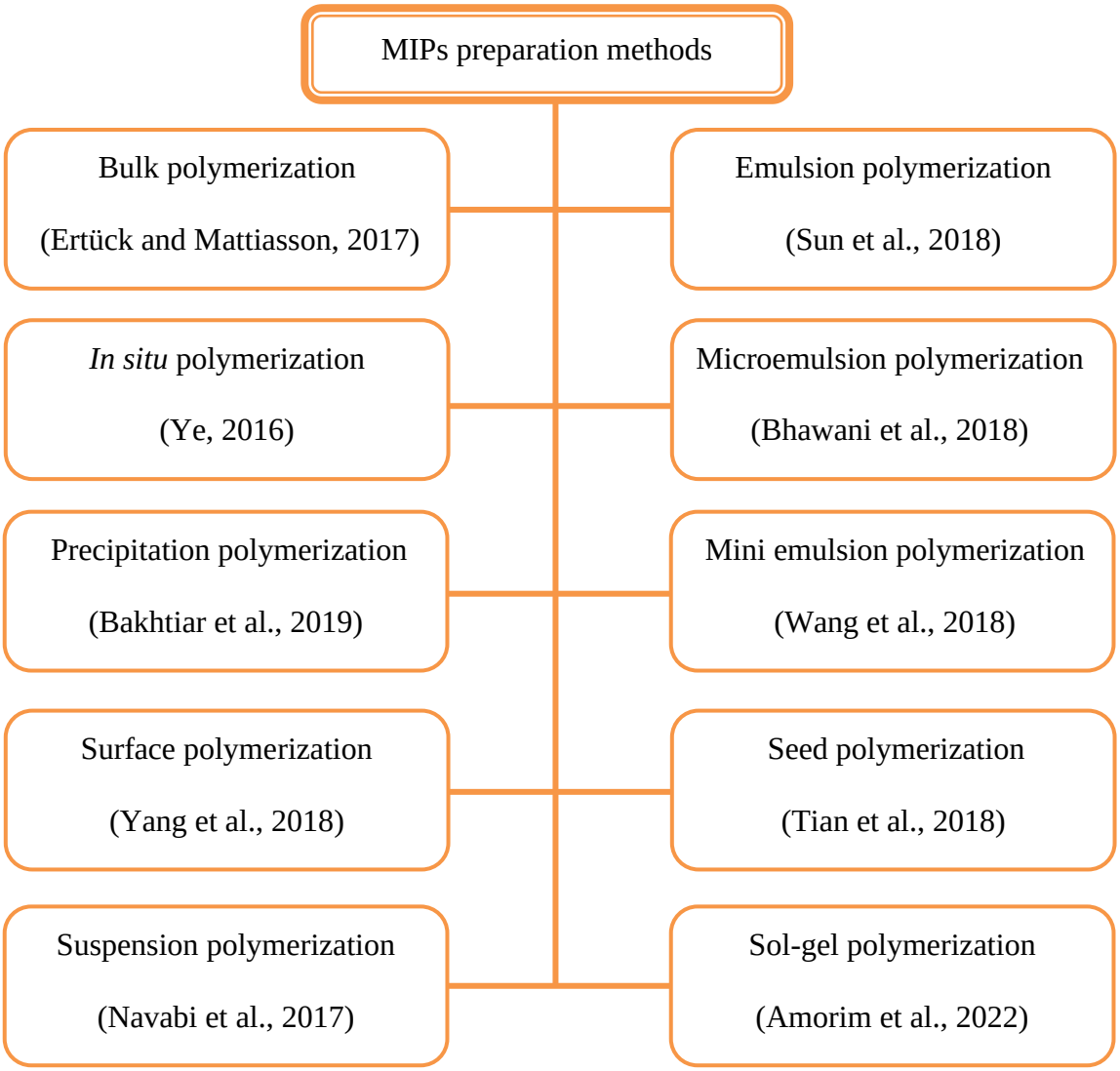


Figure 2.9: Different Types of MIP Preparation Techniques

Bulk polymerization is the most conventional type of polymerization method for MIP preparation which was first introduced by Mosbach and Ramström (1996). This technique involves rapid and easy preparation, simple apparatus setup and produces MIPs with high purity (Sajini and Mathew, 2021). Also, bulk polymerization could produce polymers on a large scale (He et al., 2021; Lin et al., 2021). However, Sajini and Mathew (2021) also highlighted the drawbacks of bulk polymerization which are time-consuming due to MIPs

requiring to be ground and sieved, contributing to low-affinity sites, and irregular polymer particles in terms of size and shape.

Suspension polymerization has been chosen as an alternative to bulk polymerization because it offers the benefits of consistent results, high yields, monodispersity, and regular microspheres (Liang et al., 2017; Prasad and Pathak, 2017; Wang et al., 2018). In suspension polymerization, the droplets of pre-polymerization mixes are suspended in a liquid continuous phase, either oil in water (O/W) or water in oil (W/O) droplets and to lower surface tension at the liquid contact, stabilisers or surfactants are applied (Chen et al., 2022). Correspondingly, the droplet sizes can vary depending on the reaction conditions. Hence, suspension polymerization has been applied in diverse applications, including the production of MIPs, microrattles, nanospheres, and microspheres. However, the disadvantages of this polymerization method include the production of big polymer particle-size with poor recognition (Sajini and Mathew, 2021).

Besides that, precipitation polymerization is another commonly employed type of MIP polymerization approach which was invented by Ye and Mosbach (2001). Typically, during the precipitation polymerization, the polymer chains develop until they are large enough to be insoluble in the liquid phase, at which point the polymers precipitate and thus the polymers can be recovered by washing and centrifugation steps (Chen et al., 2022). This type of polymerization is considered a versatile MIP technique due to its ability to generate spherical shapes and uniform sizes of polymer particles (Fauziah et al., 2021; Masumoto et al., 2021; Nguyen et al., 2021). Another advantage of precipitation polymerization is it can produce a high yield of water-soluble polymers which does not require any sieving or grinding steps (Sajini and Mathew, 2021). For these reasons, MIP produced by precipitation

polymerization has been tremendously applied in solid phase extraction (SPE) applications (Chen et al., 2022). Nevertheless, precipitation polymerization has a few limitations because it requires a high dilution factor and a large amount of template molecules during MIP synthesis (Saji and Mathew, 2021).

Lastly, emulsion polymerization is an example of a polymerization method that can generate monodispersed MIP nanoparticles (Haupt et al., 2020) consisting of surface-exposed recognition sites (Vaihinger et al., 2002). This polymerization method can be further derived into two types of emulsion polymerization techniques namely oil-in-water (O/W) emulsion and water-in-oil (W/O) emulsion which both require the presence of a surfactant (Zhao et al., 2020). Moreover, emulsion polymerization can be conducted in the form of mini-emulsion and micro-emulsion polymerization, producing nanoparticle polymers with diameters of 30-500 nm and 5-50 nm, respectively (Refaat et al., 2019). In this type of polymerization, the monomers are stabilized by a co-surfactant, and subsequently, homogenization is accomplished using sonication or stirring (Marchyk et al., 2014). The advantages of emulsion polymerization are the high yield of polymer particles and the propriety for protein imprinting (Haupt et al., 2020). Nonetheless, the restrictions of this polymerization technique are the low imprinting capacity and the presence of remnants of surfactant used in the emulsion polymerization method (Sajini and Mathew, 2021).

2.7 Characterizations of Molecularly Imprinted Polymers

In molecular imprinting, MIP characterizations are one of the important studies conducted to assess the properties of the synthesized polymers that subsequently influence the analytical performance and applications of the MIPs. Hence, the characterizations of MIPs can be categorized into two groups namely physical and chemical characterizations as

shown in Figure 2.10, which are further discussed below. Farooq et al. (2022) stated that the evaluations of the chemical and physical properties of synthesized MIPs were performed to confirm the successful formation and efficiency of MIPs.

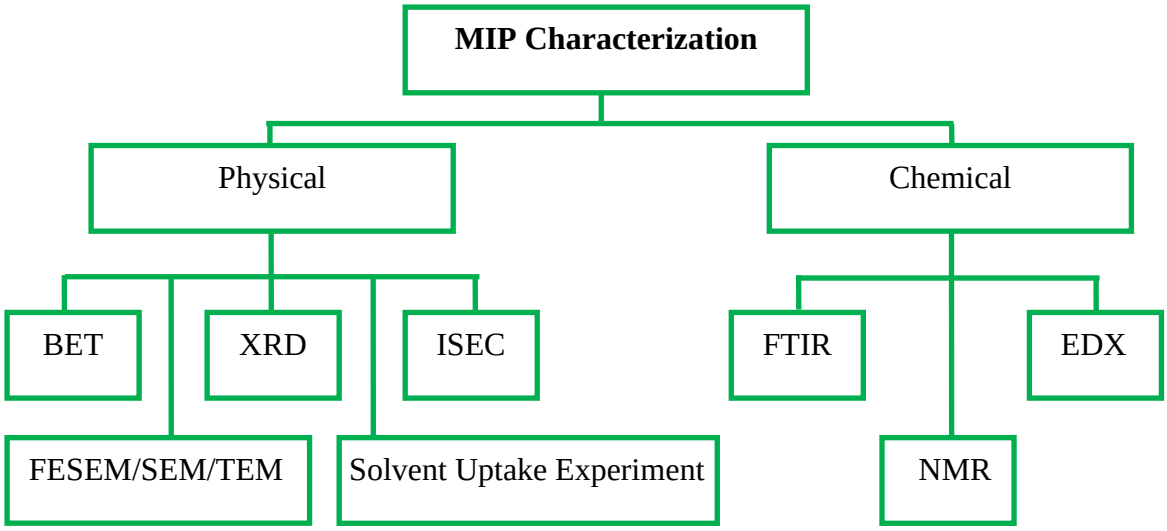


Figure 2.10: Analyses of Physical and Chemical Characterizations of MIPs

2.7.1 Physical Characterizations of Molecularly Imprinted Polymers

The physical characterizations of MIPs involve the evaluation of their physical properties in terms of morphological characteristics (size and shape), surface area, pore volume and porosity of the polymer particles.

For morphological analysis of MIPs, several types of electron microscopy such as Scanning Electron Microscopy (SEM), Field Emission Scanning Electron Microscopy (FESEM) and Transmission Electron Microscopy (TEM) can be employed to determine the surface morphology and size of the synthesized polymer particles as shown in Figure 2.9. Feng et al. (2016) mentioned that SEM can be conducted to observe the morphology specifically the uniform size and shape of the polymers which is the essential physical characterization in MIP preparation. For example, the SEM analysis showed that the

synthesized MIP of 2-phenylphenol were globular in shape with a diameter of 1.22 µm (Bakhtiar et al., 2019). Besides that, Han et al. (2017) stated that TEM micrographs showed the fractions and imprinted layers because the high resolution of TEM displayed electron diffraction from a single nanoparticle, whereas the low resolution of TEM micrographs exposed the particle core size and monodispersity. For example, the TEM analysis of MIP nanoparticles of Sudan III was sphered-shape with a diameter of 82 nm (Bhawani et al., 2022).

Other physical characterization that can be performed on MIPs is via the Brunauer Emmett Teller (BET) analysis using nitrogen adsorption experiments. This instrumental analysis gives information on the specific surface areas, specific pore volume, pore sizes and pore size distributions of the synthesized polymers. Kumar and Agrawal (2014) reported that the BET analyzer is the best instrumentation option for detailed analysis of medium-sized (meso-) and small (micro-) pores. Bhawani et al. (2019) stated that the MIP of 2,4,6-trichlorophenol had surface area, average pore radius and total pore volume of 19.931 m^2/g, 3.9679 Å and 3.954 cc/g, respectively. Meanwhile, its NIP had much smaller surface area, average pore radius and total pore volume of 7.961 m^2/g, 1.2453 Å and 2.653 cc/g, respectively.

Moreover, the Inverse Size Exclusion Chromatography (ISEC) technique is another physical characterization that can be conducted on MIP to examine the porosity structure of the synthesized polymers in the swollen state (Landry, 2005). ISEC is utilized to physically characterise MIP by employing a porous material as the stationary phase and determining the time it takes for a set of linear soluble polymer standards of known molar mass to pass down the column at a constant flow rate (Kumar and Agrawal, 2014).

The usage of the X-Ray Diffraction (XRD) method is a rapid analytical approach in MIP characterizations for the determination of polymer morphology specifically the crystal composition, ideal configuration, grain size, and the identification of several phases present in the microcrystalline mixtures (Yanti et al., 2016). Su et al. (2009) revealed that the recognition of the amorphous materials in the partially crystalline mixtures can be conducted by XRD. Zhan et al. (2011) also stated that XRD can be used to distinguish the changes in the magnetic structure of the imprinted and non-imprinted polymer particles.

Another type of analytical method for the physical characterization of polymers is the solvent uptake experiment technique whereby a solvent is required to enter the pore network of the permanently macroporous polymers. Kumar and Agrawal (2014) emphasized that the volume of solvent taken up by the polymers can be used to estimate its specific pore volume.

2.7.2 Chemical Characterizations of Molecularly Imprinted Polymers

The importance of chemical characterizations of MIPs is to identify the chemical interactions that occur between the chemical constituents throughout the polymerization reaction. Such common examples of chemical characterizations in molecular imprinting are Fourier Transform Infra-Red (FTIR) spectroscopy and Nuclear Magnetic Resonance (NMR) spectroscopy as indicated in Figure 2.9. Chen et al. (2016) explained that FTIR and NMR can be employed for the chemical characterization of MIPs because these spectroscopic methods can determine the template molecule-functional monomer interactions that happened during MIP synthesis by screening of functional monomer due to its interaction with template molecule or the validation of computational design data.

Generally, FTIR spectroscopy can be utilized for analysing a variety type of samples such as liquids, solutions, gases, powders, and pastes (Fan et al., 2012). Prati et al. (2010) stated that FTIR spectroscopy is a crucial instrumental approach for the identification of the presence of any functional group in unknown samples. This is because it generates the FTIR spectra, indicating the type of bonds and bond vibration of the functional groups present in the analysed samples. For instance, FTIR has been widely employed to detect chemical bond formation specifically hydrogen bonds between template molecules and functional monomers as they can be observed based on the adsorption of the IR spectrum and peak shifting (Munajad et al., 2018; Xie et al., 2019). In molecular imprinting, FTIR spectroscopy is employed for the chemical characterization of MIPs to determine the template molecule-functional monomer interactions that happened during MIP synthesis (Chen et al., 2016). Atlabachew et al. (2015) also described that FTIR analysis could show identical characteristics peaks, indicating the resemblances in the backbone structures of the non–leached MIP, leached MIP, and NIP of the target compound. A study conducted by Yanti et al. (2016) mentioned that FTIR analysis of MIP samples was observed from the range of 500 cm^{-1} to 4000 cm^{-1} with 24 scans. Another study also emphasized that FTIR analysis can check the purity and presence of organic and/or other compounds in the synthesized nanoparticles which were recorded within the range of 500 cm^{-1} to 3800 cm^{-1} (Asfaram et al., 2017).

NMR is another commonly employed chemical characterization for MIPs due to its function to assess the interaction strength of each chemical component involved in the pre-polymerization mixture for MIP preparation. Kumar and Agrawal (2014) clarify that the proton NMR or 1 H NMR is not only used to examine the formation of complexes in the pre-polymerization mixture but also to distinguish the specific sites in the polymer structure

that are involved during the complexation reaction. Additionally, the NMR spectra also provide information on the chemical shift changes, resulting from the interactions that happened in the pre-polymerization mixture that were also probably used to show the dissociation constants of the generated complexes (Li and Row, 2017). For instance, Shen and Ren (2014) reported that numerous NMR characterization studies were performed on vast types of functional monomers and template molecules to investigate their interactions.

Besides FTIR and NMR analyses, the Energy Dispersive X-ray (EDX) technique as listed in Figure 2.9 is also a useful analysis for the chemical characterizations of polymers because it can be used to investigate the elemental compositions in synthesized polymers. Jalilian et al. (2021) stated that EDX analysis could determine the elemental content in the prepared MIP sorbents. For example, Ali et al. (2023) conducted EDX analyses to verify the element loading on the prepared nanoparticles, silica core-shell, and MIPs for the target drug delivery application. Previous studies performed by Khalifa et al. (2020) and Shadabfar et al. (2020) also applied EDX analysis for the chemical characterizations of their synthesized MIPs.

2.8 Thermal Study of Molecularly Imprinted Polymers

Peñalver et al. (2020) stated that thermal methods are frequently employed for the characterization of polymers. It is one of the important techniques that study the response of polymers to changes in temperature that eventually give insights into the thermal stability and properties of synthesized MIPs. Such examples of thermal analyses are Dielectric Thermal Analysis (DEA), Differential Scanning Calorimetry (DSC), Differential Thermal Analysis (DTA), Dynamic Mechanical Analysis (DMA) and Thermogravimetric Analysis (TGA). Schindler et al. (2017) highlighted that both DSC and TGA were the most employed

conventional thermal techniques to examine a thorough characterization of polymer samples as DSC demonstrated the glass transition, crystallization and melting points of polymer while TGA studied the pyrolytic decomposition and combustion of polymers.

The DSC analysis quantifies the heat exchange of a sample as the temperature changes this technique provides insights into phase transitions, glass transition temperatures, melting points, and thermal stability of MIPs. Hence, the occurrence of template desorption, polymer degradation, or structural changes may be due to the changes in heat flow. Previous studies explained that DSC facilitates the identification of melting, crystallization, and transition temperatures, along with associated enthalpy and entropy changes that display variations in either heat capacity or latent heat, indicating that it is a reliable analytical tool for the physical characterization of polymers (Baltes et al., 2019). The thermal study of MIPs has been performed by using DSC in numerous research (Ceglowski et al., 2020; Jian et al., 2020; Quinto et al., 2020; Wadie et al., 2022; Shah et al., 2023).

Commonly, TGA is applied to MIPs to measure the change in their weight corresponding to temperature variations and thus, give insights into the thermal stability (Sajini and Mathew, 2021) and decomposition behaviour of MIPs. Moreover, TGA is used to identify the temperature initiating the MIPs degradation and assess the degree of decomposition of MIPs. Shabaka et al. (2020) further explained that TGA reports the reduction in sample mass as temperature increases steadily while the combustion reaction quantifies weight loss by subjecting the sample to a consistent temperature for a specified duration to ensure complete thermal degradation of materials. In molecular imprinting, various research had performed TGA that successfully investigated the thermal stability of the synthesized polymers (Ceglowski et al., 2020; Jian et al., 2020; Liu et al., 2020; Quinto

et al., 2020; Zhang et al., 2020; Karrat et al., 2022; Li et al., 2022; López et al., 2023; Shafqat et al., 2023; Shah et al., 2023).

2.9 Parameters Affecting Binding Efficiency of Molecularly Imprinted Polymers

Several parameters can influence the binding efficiency of the MIPs including contact time, initial concentrations, pH, and polymer dosages as shown in Figure 2.11. These studies are the most crucial part of molecular imprinting because they provide knowledge and a better understanding of the factors affecting the binding efficiency of fabricated MIPs, indicating them as effective adsorbents for the removal of target analytes or environmental contaminants such as triazine herbicides from environmental samples.

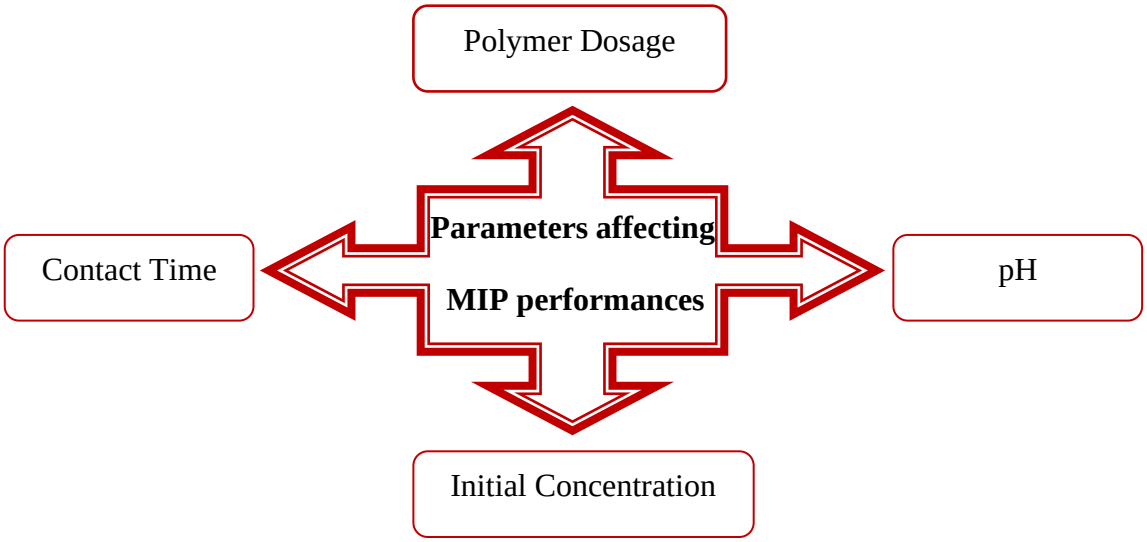


Figure 2.11: Parameters Affecting MIP Performance

Previous studies indicated that the adsorption studies of MIPs were performed using the batch binding experiment and accompanied by suitable instrumental analysis under various conditions of different initial concentrations of the solvent, types of the eluent, volume of the solution, pH solution, polymer dosages, contact time and temperature of the adsorption reaction (Madikizela et al., 2018; Mehamod et al., 2018; Saavedra et al., 2018).

Therefore, the effects of contact time, initial concentrations, pH, and polymer dosage are further discussed in this topic.

Multiple options of instrumental analyses such as Ultraviolet-Visible (UV-Vis) spectrophotometry, High Performance Liquid Chromatography (HPLC) and Reversed-Phase Liquid Chromatography (RP-HPLC) can be performed to determine the binding efficiency of MIPs. This is because the selection of instrumental analysis depends on the target analyte and its wavelength of detection. For instance, the binding efficiencies of MIPs of Gallic Acid (Bhawani et al., 2018), 2,4,6-tricholorophenol (Bhawani et al., 2019), 2-phenylphenol (Bakhtiar et al., 2019), Vanillic Acid (Bhawani et al., 2020a) and p-Coumaric (Bhawani et al., 2020b) were conducted using RP-HPLC, meanwhile, the binding efficiency of dyes such as Xylenol Orange (Bhawani et al., 2020c), Sudan III (Bhawani et al., 2022) and methyl red (Shafqat et al., 2023) were conducted via UV-Vis spectrophotometer.

2.9.1 Effect of Contact Time

Contact time is one of the parameters that affect the binding efficiency of MIPs, and this study can be carried out by batch binding experiments. A previous study conducted by Gajovic-Eichelmann et al. (2012) showed that batch binding experiments were essential to explain the equilibrium binding isotherms of synthesized MIPs and NIPs. In batch binding experiments, the binding efficiencies of fabricated polymers at different contact times were observed as different contact times result in diverse percentages of binding efficiency of polymers. This is due to many empty binding sites and less steric hindrance in synthesized polymers, allowing the binding of the target analyte to the MIPs' binding sites (Jusoh et al., 2022). Eventually, the optimum contact time for the binding between MIPs and target analyte can be distinguished based on their highest binding efficiency. This indicated that

the MIP had reached its saturation point as the MIP binding sites had completely bound with the target analyte (Yusof et al., 2017)

2.9.2 Effect of Initial Concentration

In adsorption studies, the influence of initial concentrations of the target analyte towards the adsorption efficiency of polymers can be tested by using various ranges of initial concentrations while other parameters (contact time, pH, and polymer dosage) remain unchanged. A graph of the adsorption efficiency of polymers versus different initial concentrations of target analyte can be tabulated to provide a better understanding of their relationship. Typically, higher initial concentrations of a target analyte have a higher number of binding sites for MIP and thus lead to higher adsorption efficiency of MIPs (Abraham and Mathew, 2014). This study also helps to determine the ideal initial concentration of the target analyte whereby the MIPs are attaining their highest adsorption efficiency. A too-low or too-high initial concentrations of the target analyte may negatively affect the MIP adsorption efficiency (Wang et al., 2016).

2.9.3 Effect of pH

The pH condition also plays a crucial role in ensuring excellent adsorption efficiency of the target analyte by the fabricated MIPs because a suitable pH condition allows the MIPs to effectively extract the target analyte from the aqueous medium. Certain pH conditions can disturb the original functionality of the target analyte and the target analyte becomes less matched with the MIP binding sites, contributing to poor MIP adsorption efficiency (Yusof et al., 2013). Besides that, different pH conditions may influence intermolecular interactions such as electrostatic and hydrogen bonding interactions among the MIPs and target analyte (Anirudhan et al., 2017) which later the bond interactions that occurred will affect the MIP

adsorption efficiency. Kumar et al. (2018) stated that low pH conditions can cause the protonation of certain functional groups in the target analyte thus disturbing its interactions with the MIP binding. Hence, an optimum pH condition is necessary to allow MIP adsorption for the target analyte with its highest efficiency.

2.9.4 Effect of Polymer Dosage

Another parameter that has an impact on the MIP adsorption efficiency is polymer dosage because different amounts of polymer can either increase or decrease its adsorption efficiency, depending on its optimum condition to attain the highest adsorption efficiency. Generally, a higher amount of polymer leads to higher adsorption efficiency due to a higher number of binding sites and surface area of polymers for binding interaction with the target analyte (Gomes et al., 2017). Then, at an ideal polymer dosage, MIP attained its highest adsorption efficiency as all the binding sites had fully bound to the target analyte. However, excess polymer dosage can cause aggregation and thus negatively affect the MIP adsorption efficiency (Mor et al., 2016).

2.10 Selectivity Test of Molecularly Imprinted Polymers

In molecular imprinting, a selectivity study is an essential test that can distinguish the success of MIPs as effective and selective adsorbent materials towards their target compounds of interest. The Scatchard analysis (Garcia-Mayor et al., 2017) and the rebinding analysis (Bhawani et al., 2022; Shafqat et al., 2023) are the two methods used to determine the selectivity of MIPs. Li and Row (2017) explained that Scatchard analysis was used to evaluate the binding capabilities of the synthesized polymers, while the rebinding experiment was used to assess the selectivity of the generated polymers towards both the

template molecule and the competitive compound, which shares structural similarities with the template molecule.

The rebinding experiment, employed as a selectivity test, stands as a prominent method to evaluate the effectiveness of the polymer's attributes as a reliable adsorbent material. The outcomes of the selectivity assessment can be analyzed using instrumental techniques such as HPLC or UV spectrophotometry. For example, the selectivity of MIPs using dyes as the template molecules can be determined by using a UV-Vis spectrophotometer (Bhawani et al., 2022; Shafqat et al., 2023). Besides that, an HPLC system can be conducted to evaluate the selectivity of MIPs that used environmental contaminants such as 2-phenylphenol (Bakhtiar et al., 2019), and 2,4,6-trichlorophenol (Bhawani et al., 2019) as the template molecules, in which the MIPs were more selective towards their template molecules than the competitive compounds.

2.11 Applications of Molecularly Imprinted Polymers

To date, the applications of MIPs have been extensively explored due to their versatility and promising techniques, offering the potential for numerous practical applications in diverse fields of science and technology, as depicted in Figure 2.12. Kudupoje (2017) declared that the advantages of MIP techniques that have led to significant advancements in their applications within the field of polymer chemistry include the simplicity of MIP preparation procedures, the capacity of MIPs to emulate the binding selectivity and sensitivity of biological receptors, and their ability to uphold stability even under harsh conditions encompassing temperature, pressure, and pH variations.

For instance, the MIP application has shown great potential in detecting and extracting contaminants such as heavy metals, pesticides, and endocrine disruptors from

water and soil samples. Numerous studies have highlighted the ability of MIPs to selectively extract and quantify a wide range of target compounds, even at trace levels that ultimately help society by protecting human health and preserving ecosystems. The applications of MIPs for separation techniques, sensors, catalysis, and drug delivery are further discussed below.

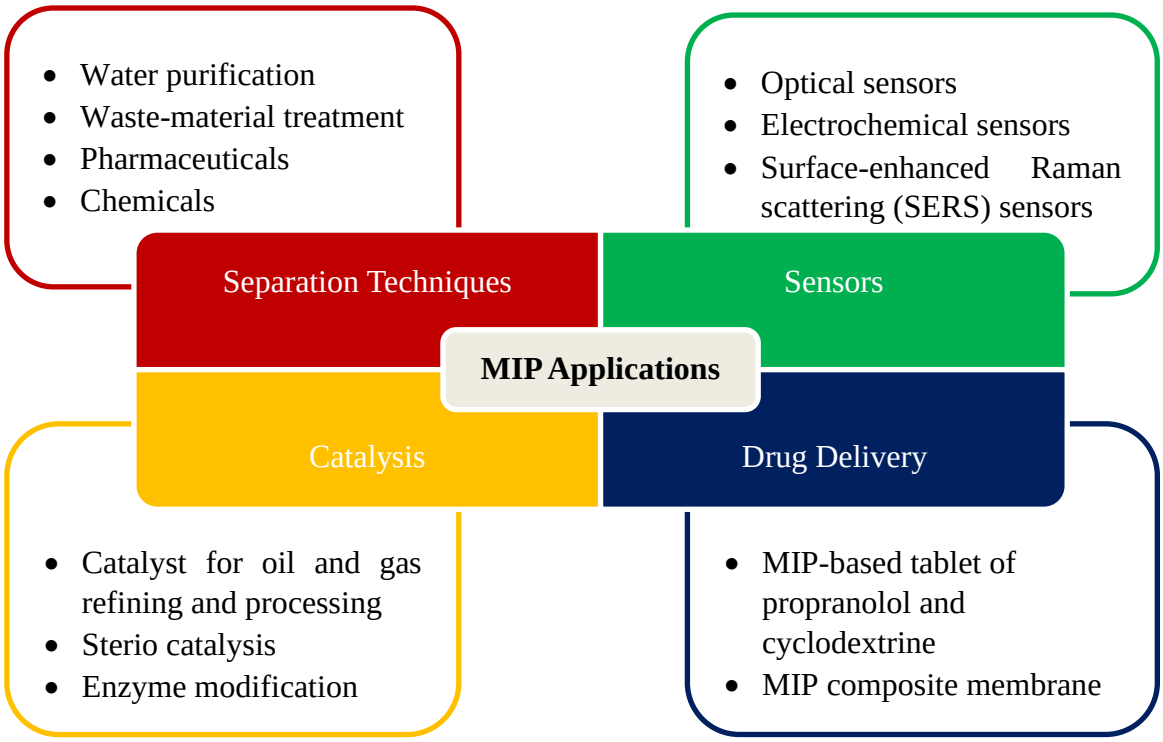


Figure 2.12: Important MIP Applications and Examples

2.11.1 MIP Application in Separation Techniques

Diverse industries including pharmaceutical, chemical, waste-material treatment and water purification have contributed to the rapidly expanding and rising field of separation science (Ansell, 2005). This is because proper separation techniques play a crucial role in sample pre-treatment for trace or ultra-trace level analysis, enhancing treatment efficiency and sample quality as Chen et al. (2022) emphasised. Hence, various techniques like

chromatographic separation, solid-phase extraction (SPE), and solid-phase microextraction (SPME) have been developed for sample pre-treatment and separation. Each of these techniques has its limitations and advantages.

Nevertheless, the challenges of separation techniques are the utilization of a large amount of organic solvent and the cross-pollution of sorbents that led to limitations in enhancement efficiency and purity (Chen et al., 2022). For this reason, integrating the separation techniques and MIPs, resulting in alternative sorbent materials with high selectivity, affinity, and low risk of cross-pollution can enhance extraction efficiency for target molecules. Sajini and Mathew (2021) also revealed that MIPs have shown potential in various separation applications including SPE, dispersive SPE, SPME, magnetic SPE, and HPLC stationary phase. This is because they can be used as sorbents for removing environmental pollutants, drugs, DNA and RNA, peptides, amino acids (Gao et al., 2011), carbohydrates, hormones, and flavoured compounds. MIPs also play a crucial role in enantiomeric separation of drug design (Ansell, 2005), optics and polymer chemistry (Ansell, 2005), as well as the removal of heavy metals and rare metals (Aravind and Mathew, 2018) with high selectivity.

Chromatographic separation is one of the examples of separation techniques that are coupled with MIPs. Examples of chromatographic separation techniques are capillary electrochromatography (CEC), gel permeation chromatography (GPC), gas chromatography (GC), and high-performance liquid chromatography (HPLC) (Hashemi-Moghaddam et al., 2017; Luo et al., 2017). Incorporating chromatographic separation with MIPs allows for efficient separation because MIPs are designed to have excellent selectivity, high affinity towards specific target analytes, and a low risk of cross-pollution. Besides that, MIPs serve

as stationary phases in both packed columns and monolithic columns, simplifying the conventional steps, and accelerating the analysis (Yang et al., 2018). MIP-based chromatographic separation also can be applied in various applications such as environmental monitoring, food safety, biomedical analysis, and drug extraction (Chen et al., 2022). For instance, Xue et al. (2013) successfully extracted shikimic acid from Chinese star anise by using flash column chromatography, equipped with preloaded MIPs. This showed that the MIPs-packed chromatography column is a reliable technique due to its rapid process, efficiency, and cost-effectiveness (Chen et al., 2022) which can be carried out for large-scale extraction of active compounds from plants. However, MIP for chromatographic separation may have limitations in synthesizing MIPs with desired properties for specific applications, requiring careful optimization of polymerization conditions.

Another example of MIP application in separation techniques is SPE, a sample preparation method conducted for the preconcentration and purification of target compounds before analysis. In the context of MIPs, this technique is known as MIP for SPE or MISPE, in which SPE refers to the utilization of MIPs as sorbent materials in the extraction process. The synthesis of appropriate MIP sorbents, packaging of SPE columns, uploading of samples, washing out of interferents, and elution of target components are the typical steps in the creation of MISPE (Chen et al., 2022). MISPE offers several advantages as it has high selectivity, high affinity, and low cross-pollution risk, making it favourable for the removal of target compounds in a variety of applications including chem-biological samples, environmental contaminants, drug screening, and food safety inspection (Maranata et al., 2021; Farooq et al., 2022; Madikizela et al., 2022). On the contrary, MIP for SPE also has limitations. MIP-based SPE needs manual loading of reagents such as samples, sorbents,

solvents, and additives, which can be time-consuming and require skilled operators (Guo et al., 2017).

Generally, SPME is the advancement of conventional SPE, pursues miniaturization and high quantity in which it has effectively reduced separation times and solvent usage while increasing the efficacy of the final extraction. MIP in SPME is also known as MISPME whereby using MIP with tailored functions provides a wide range of raw materials options and fulfils complex demands for various applications (Chen et al., 2022). MIPs can be easily coated on SPME fibers, enabling sensitive capture of targets and simple dissociation for purification and collection (Wang et al., 2019). Nonetheless, one of the limitations of MISPME is the challenge of coating MIPs onto SPME fibers, requiring in situ polymerization methods that can be technically challenging (Chen et al., 2022). Additionally, the extraction efficiency of MISPME may vary depending on the specific coating method used and the compatibility between the target analyte and the MIP coating.

2.11.2 MIP Application in Sensors

MIPs also have been used in various sensor applications as they can be employed as specific and sensitive recognition elements in different types of sensors, including optical sensors, electrochemical sensors, and surface-enhanced Raman scattering (SERS) sensors. The incorporation of MIPs in sensor applications enhances selectivity improves sensitivity, higher stability, and reusability, more versatility and customizability, as well as cost-effectiveness, making them valuable tools for various sensing technologies (Gui et al., 2018).

In optical sensors, MIPs can be used to transfer changes in optical properties into electronic signals and thus types of MIP-based optical sensors can be further categorized into two groups namely MIP-affinity optical sensors and MIP-optoelectronic sensors. For

MIP-affinity optical sensors, it is targeting the analytes with inherent optical properties (refractive index, fluorescence intensity, and absorbance), meanwhile, MIP-optoelectronic sensors integrate MIPs with functional reagents that have optical reporting capabilities, allowing them to respond sensitively to changes in the surrounding environment (Chen et al., 2022)

Moreover, MIPs can be incorporated into electrochemical sensors by modifying the surface of electrodes with electroactive MIP nanoparticles or films. This allows for the selective detection of target analytes through the electro-polymerization of conductive polymer monomers. The applications of MIP-based electrochemical sensors for on-line monitoring target analytes have benefitted various fields including drug delivery, pharmaceutical screening, environmental contaminants, and food chemistry (Wang and Kan, 2020). The advancements in MIP-based electrochemical sensors are also due to the numerous applications of carbon nanotubes or NCTs (Akhoundian et al., 2018; Zhang et al., 2018). Due to the progression of varied electrodes, MIP-based electrochemical sensors offer advantages such as miniaturization, automation, and lower production costs (Chen et al., 2022). On the other hand, the drawbacks of MIP-based electrochemical sensors including shielding interference signals, production of thinner MIP membranes and closer packing have constrained their further progression (Chen et al., 2022).

In addition, MIP can be combined with Surface-Enhanced Raman Scattering (SERS) substrates to create MIP-SERS sensors. These sensors utilize the strong affinity of MIPs to target analytes, generating SERS signals when the analytes enter the imprinted cavities upon activation by incident light (Chen et al., 2022). Hence, MIP-SERS sensors are particularly useful for the ultra-sensitive detection of analytes in biological samples.

2.11.3 MIP Application in Drug Delivery

The applications of MIPs also have been extensively explored as drug delivery systems, offering controlled release of therapeutics in a targeted manner. This is because MIP has properties of good selectivity, memory and rebinding ability that are useful for applications in drug release (Sellergren and Allender, 2005). By imprinting the polymer with the desired drug molecule, MIPs can entrap and release the drug in response to specific stimuli, such as changes in pH or temperature.

Norell et al. (1998) emphasized that MIP-based theophylline beads were successfully employed for continuous drug release. The MIP-based tablets consisting of propranolol (Suedee et al., 2002) and cylclodextrine (Alvarez-Lorenzo and Concheiro, 2004) also demonstrated selective drug release. In addition, the MIP composite membrane was created to selectively rebind uric acid (Cristallini et al., 2004) and propranolol (Suedee et al., 2002). These showed that MIP for drug delivery has immersed applications in the pharmaceutical field that enhance drug efficacy, reduce side effects, and improve patient compliance. Hence, MIP-based drug delivery systems have highlighted its potential to revolutionize the treatment of various diseases, thereby improving healthcare outcomes and enhancing the quality of life for patients.

2.11.4 MIP Application in Catalysis

Enzymes have specific interactions in the active site between key amino acid residues and substrates, making them naturally and proficiently catalyse a diversity of chemical reactions, however, enzymes have some restrictions to their extensive applications due to their poor stability in organic solvents, as well as in extreme temperatures and pH (Amorim et al., 2022). For these reasons, MIPs have significant implications in catalysis applications

because they can be designed to mimic the catalytic activity of enzymes, allowing for the development of enzyme-like catalysts with improved stability and reusability (Wulff, 2002) and tailored to have high selectivity towards specific substrates, enabling selective catalytic reactions for various applications.

MIPs are commonly applied as catalysts in the preparation of zeolites for oil and gas refining and processing (Tang et al., 2010), stereo catalysis, and enzyme modification (Wulff, 2002). Besides that, MIP can aid as synthetic enzymatic resources through imprinting acid-base catalysts, reaction intermediates, or metal complexes (Kuhn et al., 1992). Nonetheless, MIP-based catalytic reactions may have some drawbacks including closely packed substrate binding and the rigidity of the recognition sites resulting in low reactivity and product inhibition (Mirata and Remini, 2015). Besides that, MIP application in catalysis may have limited catalytic activity compared to natural enzymes or other conventional catalysts (Wulff, 2002).

2.12 Molecularly Imprinted Polymers of Triazine Herbicides

MIPs of Triazine herbicides namely CYZ, AME and ATZ are synthetic polymers that are designed to selectively recognize and bind to their target compounds, known as the template molecule for detection or extraction of CYZ, AME and ATZ, respectively. There were studies conducted on MIPs of CYZ, AME and ATZ for their extractions in various samples but many studies were performed for their detections and thus, the MIPs of CYZ, AME and ATZ are further discussed in this section.

2.12.1 Molecularly Imprinted Polymers of Cyanazine Herbicides

The presence of CYZ herbicide as one of the environmental contaminants in the environment has gained interest in the detection of CYZ in the environment due to its toxicity

effects. For instance, Breton et al. (2006) fabricated MIPs of CYZ that combined the photosynthetic-based biosensor and a preconcentration step to detect the photosynthesis-inhibiting herbicides in water at the level demanded by the European community. Another study conducted by Gholivand et al. (2012) successfully synthesized computationally designed MIPs for the application of electrochemical sensors to detect CYZ in food samples such as tomatoes, onions, lettuces, and rice. Gholivand et al. (2012) also performed other studies on a chemometrics technique based on a carbon paste electron modified by MIPs for the simultaneous detection of CYZ in foodstuffs and river water samples with good and satisfactory detection results.

Besides that, the extraction of CYZ herbicide by using MIPs is another crucial research for environmental sustainability. For instance, Guzzela et al. (2007) prepared the MIP of CYZ by using the bulk polymerization technique which later the elimination of herbicides from water samples was analysed using HPLC-UV. The MIP synthesis of CYZ by suspension polymerization was utilized for the efficient removal of CYZ from environmental water (Qiao et al., 2014).

2.12.2 Molecularly Imprinted Polymers of Ametryn Herbicides

Like CYZ, AME is another example of a Triazine herbicide that is commonly used in the agriculture field due to its effectiveness in inhibiting the growth of broadleaf grasses and weeds. The extensive usage of AME for various purposes such as agriculture and landscaping has contributed to environmental pollution thus negatively affecting not only the environment but also living organisms. Therefore, research on MIPs of AME has been employed for both detection and extraction of CYZ in various samples.

Koohpaei et al. (2008) reported that the MIP-based SPE approach was fabricated by bulk polymerization and its applications showed that the synthesized MIP was capable of detecting AME. Another study carried out by Koohpaei et al. (2009) indicated successful trace determination of AME in environmental matrices by employing an optimized MISPE as a modern sorbent. A magnetic superhydrophilic MIP composite resin based on multi-walled carbon nanotubes was designed by Zhou et al. (2018) for the detection of triazine herbicides including AME in environmental water, resulting in good linearity, lower limit of detection and excellent precision. Moreover, Yu et al. (2021) established a modified QuEChERs technique based on the MIPs coupled with gas chromatography-mass spectrometry/mass spectrometry (GC-MS/MS) analysis to detect the presence of fourteen Triazine herbicides including AME in shellfish samples like mussels, scallops, and cockles.

Other than that, MIPs of AME are also utilized for the extraction of AME in a variety of samples including foods, beverages, soil, and especially river water. For instance, the application of MIP-based SPE efficiently extracted the AME analyte from grape juice and soil extracts (Chapuis et al., 2004). In other studies, MIP-based SPME fiber of AME was successfully prepared by Djozan et al. (2009) to analyse and selectively remove Triazine herbicides in tap water, rice, maize, and onion. Djozan et al. (2010) also designed a new approach employing MIPs of AME coated with anodized-silylated aluminum wire coupled with SPME fiber for the withdrawal of AME and other Triazine herbicides. Research conducted by Khan et al. (2018) proved that magnetic MIPs as a feasible tool for the elimination of AME in fruit and vegetable extracts specifically capsicum, strawberry, and tomato.

2.12.3 Molecularly Imprinted Polymers of Atrazine Herbicides

The utilization of ATZ has both pros and cons for mankind and the environment because ATZ helps to control the growth of weeds and broadleaves grass, however, the extensive usage of ATZ can be detrimental to human health and cause environmental pollution, causing some European countries to prohibit the usage of ATZ. The toxicity of ATZ has developed research interest in its detection in various samples by a variety of adsorbents, especially MIP, a versatile sorbent material with high affinity and selectivity towards its target analyte.

Ahmad et al. (2018) synthesized MIPs of ATZ by bulk polymerization for electrochemical ATZ detection in water solution. Another study on the rapid detection of ATZ in apple juice by employing MIPs coupled with gold nanoparticles-colorimetric/SERS dual sensor proved that this method is highly feasible for rapid analysis of ATZ in food samples (Zhao et al., 2019). Nsibande and Forbes (2019) also successfully designed a quantum dot (QD) MIP sensor for fluorescence screening of ATZ in real water samples that showed satisfactory recoveries, indicating a promising technique for monitoring water quality. Moreover, Lah et al. (2019) studied the influence of porogen towards the synthesized MIP of ATZ as an electrochemical sensor in water. Research conducted by Salahshoor et al. (2022) demonstrated the ability of photonic MIPs to selectively detect and monitor ATZ and two of its water-soluble metabolites in aqueous solutions.

In addition, the research on the extraction of ATZ in any samples by using MIPs is also equally important to sustain a healthy ecosystem. For example, Chen et al. (2019) successfully prepared MIP-based SPE, also known as MISPE as the sorbent accompanied by HPLC analysis to detect and separate ATZ from seawater. Another application of MIP as

an effective adsorbent material was coupled with the accelerated solvent extraction and pipette tip solid-phase extraction followed by UPLC-DAD analysis for the elimination of ATZ in Chinese Yam was demonstrated by Wu et al. (2021). Yin et al. (2022) performed a study for the fabrication of porous carbon-based MIPs to extract Triazine herbicides including ATZ in various corn samples.

2.13 Other Methods Applied for the Removal Triazine Herbicides

Table 2.5 showed a variety of methods were applied for the removal of triazine herbicides specifically CYZ, AME and ATZ which these removal methods of Triazine herbicides had good removal efficiencies, however they are time-consuming, expensive, complicated, and less environmentally friendly.

Table 2.5: Methods for the Removal of Triazine Herbicides

Triazine Herbicide	Removal Method	Analytical Instrument	Sample(s)	Reference
CYZ AME ATZ	Dispersive Solid-Phase Extraction (DSPE) using graphene	Gas Chromatograph-Mass Spectrometer (GC-MS)	Tap water River water	Wu et al., 2015
CYZ	Magnetic Solid-Phase Extraction (MSPE)	HPLC-Diode Array Detection (DAD)	Environmental water	Liu et al., 2023
AME ATZ	Stir Bar Sorptive Extraction (SBSE)	High Performance Liquid Chromatography-UltraViolet detector (HPLC-UV)	Lake water Pond water	Lei et al., 2017
ATZ	Granular activated carbon	High Performance Liquid Chromatography-UltraViolet detector (HPLC-UV)	Drinking water	Ilavaský et al., 2020

CHAPTER 3

MATERIALS AND METHODS

3.1 Materials

Cyanazine (CYZ), ametryn (AME), atrazine (ATZ), methacrylic acid (MAA), ethylene glycol dimethacrylate (EGDMA), 2-vinylpyridine (2VP) and 4-vinylpyridine (4VP) were purchased from Sigma-Aldrich. Acrylamide (AAm), azo-bis-isobutyronitrile (AIBN), methanol (MeOH) and ethanol absolute (EtOH abs) were obtained from R & M Chemicals. Toluene (Tol) and acetonitrile (ACN) were supplied by HmbG Chemicals and Fisher Scientific, respectively. Acetic acid (AcOH) and acetone (Ace) are purchased from Bendosen Laboratory Chemical. Distilled water (DIW) was also used in the research. The river water was collected from Sabang River, Kota Samarahan (Figure 3.1).

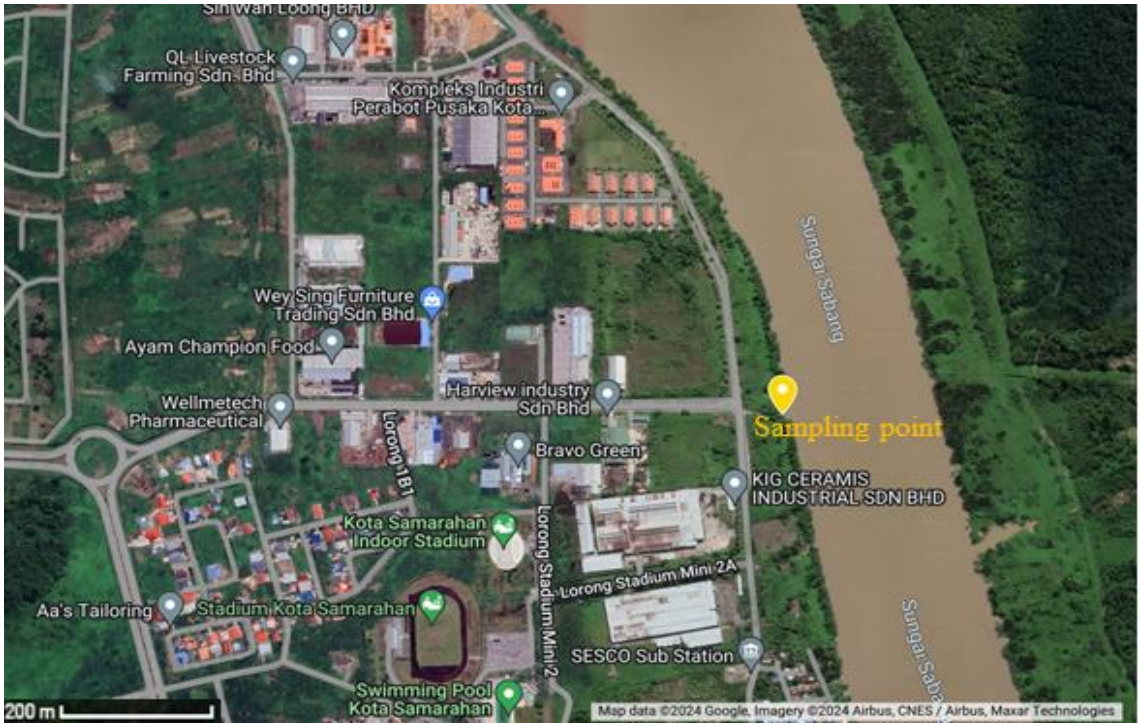


Figure 3.1: Locality Map of Sampling Point at Kota Samarahan (Google Maps, n.d.)

3.2 Summary of Methods Involved in the Research

In this study, three compounds of interest namely CYZ, AME and ATZ were used to generate MIPs. About eight main procedures were employed in this study as summarized in Figure 3.1. Firstly, the syntheses of MIPs and NIPs of Triazine herbicides were conducted via the precipitation polymerization. Then, the synthesized MIPs underwent template removal by washing process using a mixture of methanol and acetic acid.

Thirdly, the characterizations by FTIR and FESEM were performed on all polymers. After that, the batch binding experiments were carried out on all polymers. Only the MIP of each triazine herbicide with the highest rebinding efficiency was selected for further studies such as characterization by BET and EDX, adsorption studies, selectivity tests and applications in environmental samples. For comparison purposes, NIP was also evaluated to distinguish the molecular recognition of the selected MIP.

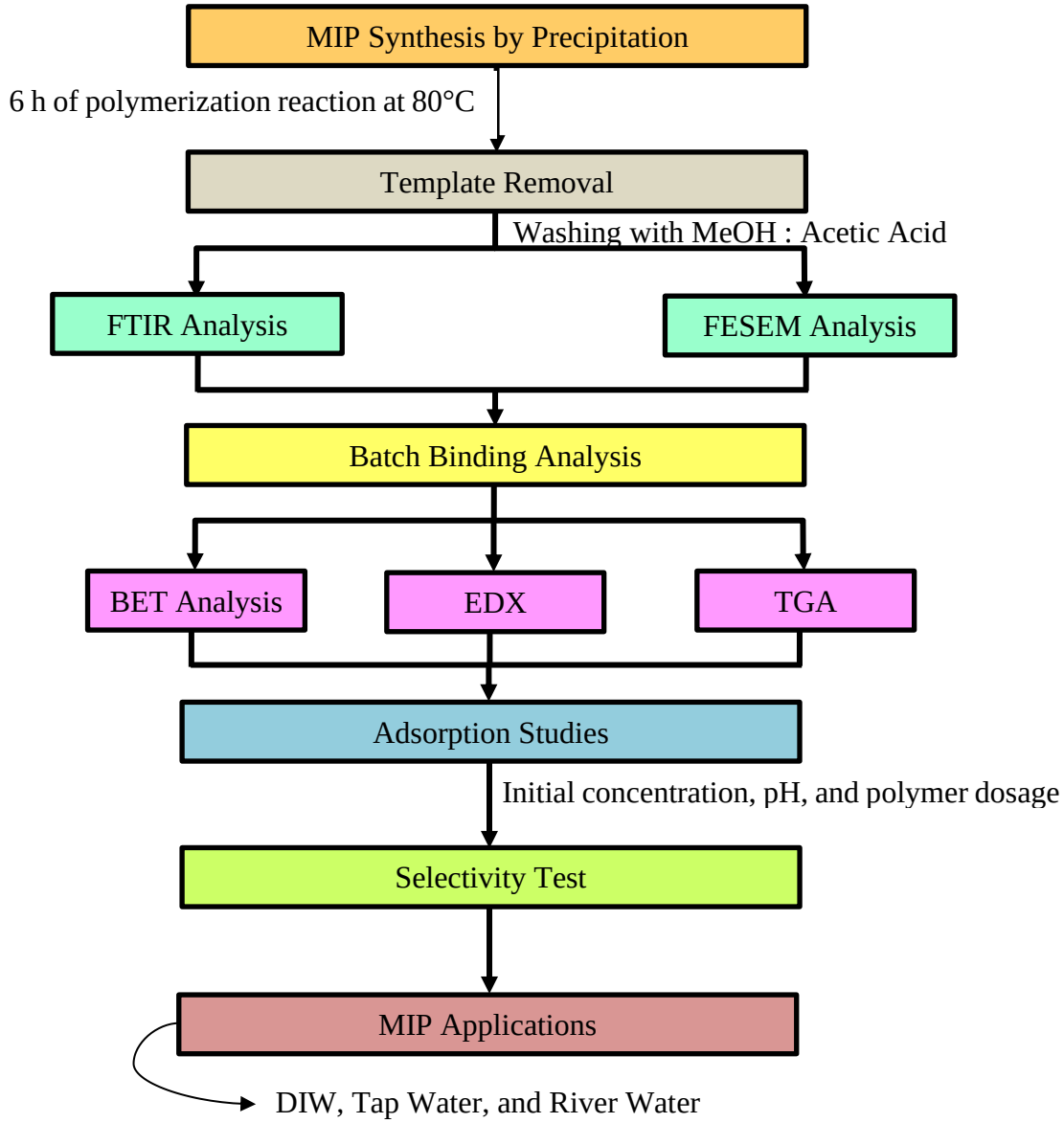


Figure 3.2: Experimental Design Involved Throughout the Research

3.3 Synthesis of MIPs of Triazine Herbicides

The MIPs and NIPs of CYZ, AME and ATZ were synthesized via the precipitation polymerization method. Three different types of functional monomers were applied in this study such as acidic (MAA), neutral (AAm), and basic (2VP or 4VP) with molar ratio employed as given in Table 3.1, Table 3.2, and Table 3.3, respectively.

For the preparation of MIP (MAA) of CYZ, about 100 mL of 1.0 mmol template solution (CYZ as template molecule and Tol as solvent), 6.0 mmol of functional monomer (MAA), 12.0 mmol cross-linker (EGDMA) and 30 mg of initiator (AIBN) were poured into 250 mL conical flask. The pre-polymerization mixture was sonicated (Brandson 2510 ultrasonic cleaner, USA) for 10 mins and then degassed with nitrogen in an ice water bath for 15 mins. Then, the conical flask containing the mixture was sealed tightly and immersed in a water bath (Biobase XMTD-204 NUOHAI, China) at 80 °C for 6 h to complete the polymerization reaction.

The synthesized polymer particles were collected by centrifugation (Gyrozen-406 Low-Speed Centrifuge, South Korea) at 4000 rpm for 15 mins and dried overnight at room temperature, 25 °C.

After that, the MIP (AAm) and MIP (2VP) of CYZ were prepared using similar methods as mentioned above, using other functional monomers such as AAm and 2VP as shown in Table 3.1. The non-imprinted polymer (NIP) was synthesized similarly but without the addition of the template molecule.

A similar experimental procedure of MIPs and NIP of CYZ was followed for the preparation of MIPs and NIP of AME, as well as, MIPs and NIP of ATZ using different types and ratios of functional monomers, as well as, types of solvent as depicted in Table 3.2 and Table 3.3, respectively.

Table 3.1: Ratio of Chemicals for the Synthesis of MIPs and NIP of CYZ

Code		MIP (MAA)	MIP (AAm)	NIP (AAm)	MIP (2VP)
CYZ (mmol)		1.0	1.0	–	1.0
Functional monomer (mmol)	MAA	6.0	–	–	–
	AAm	–	6.0	6.0	–
	4VP	–	–	–	6.0
EGDMA cross-linker (mmol)		12.0	12.0	12.0	12.0
AIBN initiator (mg)		30	30	30	30
Tol solvent (mL)		100	100	100	100

Table 3.2: Ratio of Chemicals for the Synthesis of MIPs and NIP of AME

Code		MIP (MAA)	NIP (MAA)	MIP (AAm)	MIP (2VP)
AME (mmol)		1.0	–	1.0	1.0
Functional monomer(mmol)	MAA	5.0	5.0	–	–
	AAm	–	–	5.0	–
	2VP	–	–	–	5.0
EGDMA cross-linker (mmol)		20.0	20.0	20.0	20.0
AIBN initiator (mg)		30	30	30	30
ACN solvent (mL)		100	100	100	100

Table 3.3: Ratio of Chemicals for the Synthesis of MIPs and NIPs of ATZ

Code		MIP (MAA)	MIP (AAm)	MIP (2VP)	NIP (2VP)
ATZ (mmol)		1.0	1.0	1.0	–
Functional monomer (mmol)	MAA	5.0	–	–	–
	AAm	–	5.0	–	–
	2VP	–	–	5.0	5.0
EGDMA cross-linker (mmol)		12.0	12.0	12.0	12.0
AIBN initiator (mg)		30	30	30	30
ACN solvent (mL)		100	100	100	100

3.4 Template Removal of Triazine Herbicides from MIPs

Each of the triazine herbicides (CYZ, AME and ATZ) was removed from their synthesized MIPs by the washing process. Firstly, the MIPs of triazine herbicides were added to their respective conical flasks. Secondly, the MIPs were soaked in a mixture of MeOH and AcOH (7:3, v/v). Thirdly, the conical flasks containing the mixture were sonicated for about 30 mins. Then, the mixtures were centrifuged for about 15 mins at the speed of 4000 rpm. The supernatant was collected and analyzed using the UV-Visible spectrophotometer (Agilent Cary 60) at 220 nm.

The synthesized MIPs were continuously washed until the Triazine herbicides (template molecule) were not detected by UV analysis. After that, the MIPs were rinsed with MeOH to remove the AcOH from the polymer matrix. Finally, the synthesized MIPs were

collected by centrifugation for 15 mins at 4000 rpm. After that, the attained MIPs were dried overnight at room temperature, 25 ℃ for further studies.

3.5 Fourier Transform Infra-Red (FTIR) Spectroscopy

In this study, the FTIR analyses of the MIPs and NIPs of triazine herbicides were performed using the Fourier Transform Infra-Red spectrometer (Thermo Scientific Nicolet iS10 FTIR with Diamond ATR). Before conducting this analysis, the synthesized MIPs and NIPs underwent a drying process at 100 ºC for 6 h.

Initially, the pressure applicator's tip of FTIR-ATR was ensured at its maximum distance above the crystal. The tip, crystal surface and nearby area were cleaned with EtOH absolute to avoid any contamination in the analysis. Then, approximately 0.01 g of polymer was placed on the crystal surface of the FTIR-ATR. The FTIR spectra were recorded within the range of 4000-500 cm^{-1}. The NIPs of triazine herbicides were also performed following the same procedure as the MIPs. Later the FTIR spectra of MIPs and NIPs of CYZ, AME and ATZ were compared accordingly.

3.6 Field Emission Electron Microscopy (FESEM)

The FESEM analysis of MIPs and NIPs of triazine herbicides was employed using the Field Emission Electron Microscope (JOEL JSM-IT500HR). Before this analysis, all polymers were dried at 100 ºC for 6 h.

Small sizes of carbon tapes were cut and pasted on bigger flat aluminium plates, onto which the MIPs and NIPs were affixed. Subsequently, a layer of gold was applied to coat the polymer samples. The MIPs and NIP of triazine herbicides were then subjected to

FESEM analysis, and the morphology of both MIPs and NIPs of triazine herbicides was determined based on the scanning electron micrographs.

3.7 Batch Binding Studies on MIPs of Triazine Herbicides

Initially, 50 ppm of CYZ stock solution in a mixture of MeOH and DIW (1:9, v/v) was prepared and diluted to 5 ppm of CYZ solution. Besides that, the MIPs and NIPs were dried in an oven at 100 ºC for 6 h.

A series of 100 mL conical flasks containing 0.1 g of MIPs and NIPs of CYZ were added with 10 mL of 5 ppm CYZ solution, respectively. The conical flasks containing the mixture were agitated on an orbital shaker (Heathrow Scientific) at the speed of 150 rpm and the samples were collected at different time intervals (0, 5, 10, 15, 20, 25, 20, 60, 90, 120, 150, 180, 210, 240, 270 and 300 mins).

After agitation, the conical flasks containing samples were placed on a table to facilitate the settling of polymer particles at the bottom of the conical flasks. Subsequently, the supernatants were obtained and filtered using a syringe filter for UV analysis.

The concentrations of CYZ after the rebinding were observed by using a UV-Visible spectrophotometer (Agilent Cary 60) at 220 nm. The rebinding efficiencies of MIPs and NIPs of CYZ were evaluated by using the following Equation 3.1 (Yusof et al., 2010):

$$\text{Binding efficiency} = \frac{C_i - C_f}{C_i} \times 100\ \% \qquad \text{Equation 3.1}$$

Where, C_i: The initial CYZ concentration in the solution before binding

C_f: The final CYZ concentration in the solution after binding

For the batch binding analysis of MIPs and NIP of both AME and ATZ, a similar experimental procedure was followed. Three sets of MIPs were generated with each CYZ, AME and ATZ, however, only one set of each MIP of CYZ, AME and ATZ were selected for further studies due to its highest rebinding efficiency.

3.8 Kinetic Isotherm Study on of MIPs of Triazine Herbicides

Three different kinetic models such as the pseudo-first-order model and pseudo-second-order model were applied in this study to investigate the rate and kinetic mechanism of MIP (AAm) of CYZ, MIP (MAA) of AME and MIP (2VP) of ATZ adsorptions.

The experimental data of the batch binding study of MIP (AAm) of CYZ, MIP (MAA) of AME and MIP (2VP) of ATZ were examined using these kinetic models. Equation 3.2 and Equation 3.3 represented the linear equations of pseudo-first-order and pseudo-second-order, respectively (Alamrani and AL-Aoh, 2021).

Among these kinetic models, only one kinetic model with a higher correlation coefficient (R^2) was selected as the best-fitted kinetic model which describes the adsorption of MIP (AAm) of CYZ, MIP (MAA) of AME and MIP (2VP) of ATZ.

$$\text{Pseudo-first-order: } \log (q_e - q_t) = \log (q_e) - K_1 \frac{t}{2.303} \qquad \text{Equation 3.2}$$

Where, q_e: The amount of CYZ/AME/ATZ adsorbed at equilibrium time

q_t: The amount of CYZ/AME/ATZ adsorbed at any given time

K_1: The pseudo-first-order equilibrium rate constant

t: The time interval of CYZ/AME/ATZ adsorption

$$\text{Pseudo-second-order: } \frac{t}{q_t} = \frac{1}{K_2 (q_e)^2} + \frac{t}{q_e} \qquad \text{Equation 3.3}$$

Where, q_e: The amount of CYZ/AME/ATZ adsorbed at equilibrium time

q_t: The amount of CYZ/AME/ATZ adsorbed at any given time

K_2: The pseudo-second-order equilibrium rate constant

t: The time interval of CYZ/AME/ATZ adsorption

3.9 Brunauer-Emmett-Teller (BET) Analysis

Firstly, about 0.5 g of each selected MIPs and their NIPs of Triazine herbicides were degassed at 393 K for 6 h. Then, the nitrogen adsorption measurement of selected MIPs and NIPs of Triazine herbicides were carried out at 77 K using the Brunauer-Emmett-Teller analyzer (Brunauer-Emmett-Teller Quantachrome Autosorb). Based on the BET results, the surface area, total pore volume and pore radius of the selected MIPs and their NIPs of triazine herbicides were evaluated.

3.10 Energy Dispersive X-Ray (EDX)

The EDX analysis of MIPs and NIPs of triazine herbicides were employed using the Energy Dispersive X-Ray spectroscopy (JOEL JSM-IT500HR). Prior this analysis, MIP (AAm) of CYZ, MIP (MAA) of AME and MIP (2VP) of ATZ were dried at 100 ºC for 6 h.

Small sizes of carbon tapes were cut and pasted on bigger flat aluminium plates, onto which the MIPs were affixed. Subsequently, a layer of gold was applied to coat the polymer samples. The MIPs of triazine herbicides were then subjected to EDX analysis, and their elemental compositions were observed based on the EDX spectra.

3.11 Thermal Study of MIPs of Triazine Herbicides

For this study, the rate of decomposition of the selected MIPs of Triazine herbicides were monitored by using Thermogravimetric Analyzer, TGA (Universal Analyzer 2000 with Universal V4.7A software).

About 0.5 g of selected MIPs of Triazine herbicides were analysed by the TGA instrument at a temperature range between 30 to 900 °C with a heating rate of 10 °C/min under nitrogen flow. The stability and rate of decomposition of the selected MIPs of Triazine herbicides were determined based on the generated thermogram.

3.12 Adsorption Studies of MIPs of Triazine Herbicides

The selected MIP (AAm) and NIP (AAm) of CYZ, MIP (MAA) and NIP (MAA) of AME, as well as MIP (2VP) and NIP (2VP) of ATZ were utilized in the adsorption studies of different parameters such as initial concentration, pH, and polymer dosage (Table 3.4). Before the adsorption studies, the selected MIPs and NIPs of Triazine herbicides were dried in an oven for 6 h at 100 ºC.

Table 3.4: Summary of Overall Adsorption Studies of MIPs of Triazine Herbicides

Parameter	Variation in Parameters	Constant parameters
Initial concentration	1 ppm, 2 ppm, 3 ppm, 4 ppm, 5 ppm, 6 ppm, 7 ppm, 8 ppm, 9 ppm, and 10 ppm	Polymer dosage, pH condition, agitation period, agitation speed, and temperature
pH	pH 3, pH 5, pH 7, pH 9 and pH 11	Initial concentration, polymer dosage, agitation period, agitation speed, and temperature

Table 3.4 continued

Polymer dosage	0.1 g, 0.2 g, 0.3 g, 0.4 g, 0.5 g, 0.6 g, and 0.7 g	Initial concentration, pH condition, agitation period, agitation speed, and temperature

3.12.1 Effect of Initial Concentration on Adsorption Efficiency

0.1 g of the selected MIP (AAm) and NIP (AAm) of CYZ were added into a series of 100 mL conical flasks containing 10 mL of different CYZ concentrations (1, 2, 3, 4, 5, 6, 7, 8, 9 and 10 ppm). The conical flasks containing the mixture were agitated on an orbital shaker at 240 mins with the speed of 150 rpm as shown in Table 3.4.

After agitation, the conical flasks containing samples were placed on a table to facilitate the settling of polymer particles at the bottom of the conical flasks. Subsequently, the supernatants were obtained and filtered using a syringe filter for UV analysis.

The concentrations of CYZ after the rebinding were observed by using UV-Visible spectrophotometer. The rebinding efficiencies of MIP and NIP of CYZ were evaluated by using the following Equation 3.1.

The above methods were also employed on the MIP (MAA) and NIP (MAA) of AME, as well as MIP (2VP) and NIP (2VP) of ATZ with different contact time as displayed in Table 3.5

.

Table 3.5: Parameters Involved in Adsorption Study of Initial Concentration

Selected Polymers	Variation in parameter	Constant Parameter(s)
MIP (AAm) of CYZ NIP (AAm) of CYZ	CYZ Initial concentrations: 1 ppm, 2 ppm, 3 ppm, 4 ppm, 5 ppm, 6 ppm, 7 ppm, 8 ppm, 9 ppm and 10 ppm	(i) Polymer dosage: 0.1 g (ii) pH condition: pH 7 (iii) Agitation period: 240 mins (iv) Agitation speed: 150 rpm (v) Temperature: 25 °C
MIP (MAA) of AME NIP (MAA) of AME	AME Initial concentrations: 1 ppm, 2 ppm, 3 ppm, 4 ppm, 5 ppm, 6 ppm, 7 ppm, 8 ppm, 9 ppm and 10 ppm	(i) Polymer dosage: 0.1 g (ii) pH condition: pH 7 (iii) Agitation period: 210 mins (iv) Agitation speed: 150 rpm (v) Temperature: 25 °C
MIP (2VP) of ATZ NIP (2VP) of ATZ	ATZ Initial concentrations: 1 ppm, 2 ppm, 3 ppm, 4 ppm, 5 ppm, 6 ppm, 7 ppm, 8 ppm, 9 ppm and 10 ppm	(i) Polymer dosage: 0.1 g (ii) pH condition: pH 7 (iii) Agitation period: 15 mins (iv) Agitation speed: 150 rpm (v) Temperature: 25 °C

3.12.2 Effect of pH on Adsorption Efficiency

0.1 g of MIP (AAm) and NIP (AAm) of CYZ were added into a series of 100 mL conical flasks containing 10 mL of 6 ppm CYZ solution at different pH conditions (pH 3, pH 5, pH 7, pH 9 and pH 11). The conical flasks containing the mixture were agitated on an orbital shaker at the speed of 150 rpm for 240 mins.

After agitation, the conical flasks containing samples were placed on a table to facilitate the settling of polymer particles at the bottom of the conical flasks. Subsequently, the supernatants were obtained and filtered using a syringe filter for UV analysis.

The concentrations of CYZ after the rebinding were observed by using UV-Visible spectrophotometer. The rebinding efficiencies of MIP and NIP of CYZ were evaluated by using the following Equation 3.1.

Similar procedures were employed on the MIP (MAA) and NIP (MAA) of AME, as well as MIP (2VP) and NIP (2VP) of ATZ based on the parameters indicated in Table 3.6.

Table 3.6: Parameters Involved in Adsorption Study of pH

Selected Polymers	**Variation in parameter**	**Constant Parameter(s)**
MIP (AAm) of CYZ NIP (AAm) of CYZ	pH of CYZ solution: pH 3, pH 5, pH 7, pH 9 and pH 11	(i) Initial concentration: 6 ppm (ii) Polymer dosage: 0.1 g (iii) Agitation period: 240 mins (iv) Agitation speed: 150 rpm (v) Temperature: 25 °C
MIP (MAA) of AME NIP (MAA) of AME	pH of AME solution: pH 3, pH 5, pH 7, pH 9 and pH 11	(i) Initial concentration: 7 ppm (ii) Polymer dosage: 0.1 g (iii) Agitation period: 210 mins (iv) Agitation speed: 150 rpm (v) Temperature: 25 °C
MIP (2VP) of ATZ NIP (2VP) of ATZ	pH of ATZ solution: pH 3, pH 5, pH 7, pH 9 and pH 11	(i) Initial concentration: 8 ppm (ii) Polymer dosage: 0.1 g (iii) Agitation period: 15 mins (iv) Agitation speed: 150 rpm (v) Temperature: 25 °C

3.12.3 Effect of Polymer Dosage on Adsorption Efficiency

Different amounts of MIP (AAm) and NIP (AAm) of CYZ (0.1 g, 0.2 g, 0.3 g, 0.4 g, 0.5 g, 0.6 g and 0.7 g) were added into a series of 100 mL conical flasks containing 10 mL of 6 ppm of CYZ solution at pH 7. The conical flasks containing the mixture were agitated on an orbital shaker at the speed of 150 rpm for 240 mins.

After agitation, the conical flasks containing samples were placed on a table to facilitate the settling of polymer particles at the bottom of the conical flasks. Subsequently, the supernatants were obtained and filtered using a syringe filter for UV analysis.

The concentrations of CYZ after the rebinding were observed by using UV-Visible spectrophotometer. The rebinding efficiencies of MIPs and NIPs of CYZ were evaluated by using the following Equation 3.1.

Based on the parameters specified in Table 3.7, the MIP (MAA) and NIP (MAA) of AME, along with the MIP (2VP) and NIP (2VP) of ATZ, were subjected to similar procedures as mentioned above.

Table 3.7: Parameters Involved in Adsorption Study of Polymer Dosage

Selected Polymers	Variation in parameter	Constant Parameter(s)
MIP (AAm) of CYZ NIP (AAm) of CYZ	Polymer dosage: 0.1 g, 0.2 g, 0.3 g, 0.4 g, 0.5 g, 0.6 g, and 0.7 g	(i) Initial concentration: 6 ppm (ii) pH condition: pH 7 (iii) Agitation period: 240 mins (iv) Agitation speed: 150 rpm (v) Temperature: 25 °C
MIP (MAA) of AME NIP (MAA) of AME	Polymer dosage: 0.1 g, 0.2 g, 0.3 g, 0.4 g,	(i) Initial concentration: 7 ppm (ii) pH condition: pH 7 (iii) Agitation period: 210 mins

Table 3.7 continued

	0.5 g, 0.6 g, and 0.7 g	(iv) Agitation speed: 150 rpm (v) Temperature: 25 °C
MIP (2VP) of ATZ NIP (2VP) of ATZ	Polymer dosage: 0.1 g, 0.2 g, 0.3 g, 0.4 g, 0.5 g, 0.6 g, and 0.7 g	(i) Initial concentration: 8 ppm (ii) pH condition: pH 7 (iii) Agitation period: 15 mins (iv) Agitation speed: 150 rpm (v) Temperature: 25 °C

3.13 Adsorption Isotherm Study on MIPs of Triazine Herbicides

The Langmuir and Freundlich isotherm models were employed in this study that described the adsorption capability and surface of the MIP (AAm) of CYZ, MIP (MAA) of AME and MIP (2VP) of ATZ. The experimental data of the adsorption study (initial concentration) of MIP (AAm) of CYZ, MIP (MAA) of AME and MIP (2VP) of ATZ were examined using both isotherm models. Equations 3.4 and 3.6 represented the linear equations of Langmuir and Freundlich isotherm models, respectively (Alamrani and AL-Aoh, 2021). Between these two isotherm models, only one model with higher correlation coefficient (R_2) was selected as the best–fitted isotherm model.

Langmuir Isotherm: $$\frac{C_e}{q_e} = \frac{1}{q_{max}\, K_L} + \frac{C_e}{q_{max}}$$ Equation 3.4

Where, C_e: The CYZ/AME/ATZ concentration at equilibrium

q_e: The amount of CYZ/AME/ATZ adsorbed at equilibrium time

q_{max}: The maximum adsorption capacity of MIP of CYZ/AME/ATZ

K_L: The Langmuir constant

Moreover, the R_L value (parameter of equilibrium) related to the fundamental characteristics of the Langmuir isotherm model was calculated by using Equation 3.6 (Alamrani and AL-Aoh, 2021).

$$R_L = \frac{1}{1 + K_L C_e} \quad \text{Equation 3.5}$$

Where, K_L: The Langmuir constant

C_e: The CYZ/AME/ATZ concentration at equilibrium

$$\text{Freundlich isotherm: } \ln(q_e) = \ln(K_F) + \frac{1}{n} \ln(C_e) \quad \text{Equation 3.6}$$

Where, C_e : The CYZ/AME/ATZ concentration at equilibrium

q_e : The amount of CYZ/AME/ATZ adsorbed at equilibrium time

K_F : The maximum adsorption capacity of MIP of CYZ/AME/ATZ

n : Constants associated with intensity of adsorption

3.14 Selectivity Test of MIPs of Triazine Herbicides

Prior to the selectivity test, MIP (AAm) and NIP (AAm) of CYZ, MIP (MAA) and NIP (MAA) of AME, along with MIP (2VP) and NIP (2VP) of ATZ were dried in an oven at 100 ºC for 6 hr. The template molecules with their analogous competitive compounds and several parameters involved in this study were summarized in Table 3.8.

Table 3.8: Important Compounds and Parameters Used in Selectivity Test

Selected Polymers	Template molecule	Competitive compound	Parameters
MIP (AAm) of CYZ NIP (AAm) of CYZ	6 ppm of CYZ solution	6 ppm of AME solution	(i) Polymer dosage: 0.1 g (ii) pH condition: pH 7 (iii) Agitation period: 240 mins (iv) Agitation speed: 150 rpm (v) Temperature: 25 °C
MIP (MAA) of AME NIP (MAA) of AME	7 ppm of AME solution	7 ppm of CYZ solution	(i) Polymer dosage: 0.1 g (ii) pH condition: pH 7 (iii) Agitation period: 210 mins (iv) Agitation speed: 150 rpm (v) Temperature: 25 °C
MIP (2VP) of ATZ NIP (2VP) of ATZ	8 ppm of ATZ solution	8 ppm of AME solution	(i) Polymer dosage: 0.3 g (ii) pH condition: pH 7 (iii) Agitation period: 15 mins (iv) Agitation speed: 150 rpm (v) Temperature: 25 °C

Initially, the conical flask containing a 10 mL mixture of 6 ppm CYZ solution (template molecule) and 6 ppm AME solution (competitive compound) was added with 0.1 g of MIP (AAm) and NIP (AAm) of CYZ, respectively. Then, the conical flasks were agitated on an orbital shaker at 150 rpm for 240 mins.

After agitation, the conical flasks containing samples were placed on a table to facilitate the settling of polymer particles at the bottom of the conical flasks. Afterward, the

supernatants were obtained and filtered using a syringe filter for Reversed Phase-High Performance Liquid Chromatography analysis (Shimadzu LC-20A, Japan).

The RP-HPLC was conducted by using C_{18} column (250 X 4 mm, 5µm) with the mobile phase consisting of MeOH, ACN and ultra-pure water in the ratio of 70:20:10, v/v/v, respectively. The flow rate was set at 0.5 mL/min with the UV detection at 220 nm and the injection volume was set at 20 µL.

The concentrations of CYZ after the rebinding were observed by using RP-HPLC. The selectivity of MIP (AAm) and NIP (AAm) towards CYZ were expressed in terms of the distribution ratio (K_D), using the following Equation 3.7 (Arabzadeh and Abdouss, 2010).

$$K_D = \frac{C_i - C_f}{C_i} \times \frac{V}{m} \qquad \text{Equation 3.7}$$

Where, C_i: The initial CYZ concentration in the solution before adsorption

C_f: The final CYZ concentration in the solution after adsorption

V: The volume of solvent used

m: The mass of MIP/NIP used

The selectivity coefficients for CYZ (template molecule) relative to AME (binding competitor) for MIP (AAm) and NIP (AAm) were determined according to Equation 3.8 (Arabzadeh and Abdouss, 2010).

$$\text{Selectivity coefficient, } K_{sel} = \frac{K_D^{CYZ}}{K_D^{AME}} \qquad \text{Equation 3.8}$$

Where, K_D^{CYZ}: The batch binding assay of MIP or NIP for CYZ

K_D^{AME}: The batch binding assay of MIP or NIP for AME

Hence, the relative selectivity coefficient (k') defined by Equation 3.9 (Arabzadeh and Abdouss, 2010), as below.

$$k' = \frac{K_{MIP}}{K_{NIP}} \qquad \text{Equation 3.9}$$

Moreover, the MIP (MAA) and NIP (MAA) of AME, along with the MIP (2VP) and NIP (2VP) of ATZ, were also underwent similar procedure of selectivity test with different competitive compounds and parameters applied as shown in Table 3.8.

3.15 Application of MIPs for Triazine Herbicides Removal

Initially, the selected MIPs and NIPs of CYZ, AME and ATZ were dried in an oven at 100 °C for 6 h. Among the water samples, DIW was the control sample for the removal of CYZ, AME and ATZ by using synthesized MIPs. The Sabang River water was murky brown with muddy odour and containing floating debris of tree branches. The locality map of the sampling point at Sabang River was shown in Figure 3.1. The collected tap water (Environmental Lab 1, FRST) and river water (Sabang River, Kota Samarahan) were filtered by using vacuum filtration to eliminate any suspended particles. The presence of AME in the collected tap water and river water were monitored using UV-Visible spectrophotometer.

Firstly, the filtered river water, tap water and DIW were spiked with 25 µg/mL of CYZ, respectively. Secondly, 0.1 g of MIP (AAm) and NIP (AAm) of CYZ were added to

respective conical flasks containing 10 mL of spiked CYZ solution. The conical flasks containing mixture were agitated on a shaker at 150 rpm for 240 mins.

After agitation, the conical flasks containing samples were placed on a table to facilitate the settling of polymer particles at the bottom of the conical flasks. Later, the supernatants were obtained and filtered using a syringe filter for UV analysis.

Finally, the CYZ concentrations after adsorption were observed via UV-Visible spectrophotometer. The CYZ removal efficiency in river water, tap water and DIW by using MIP (AAm) and NIP (AAm) were calculated using Equation 3.1.

Similarly, the selected MIP (MAA) and NIP (MAA) of AME, together with MIP (2VP) and NIP (2VP) of ATZ were underwent the application methods above. Table 3.9 summarized the substantial parameters involved in application study.

Table 3.9: Parameters for MIP Application in Water Samples

Selected polymers	**Environmental samples**			**Parameters**
	DIW	**Tap water**	**River Water**	
MIP (AAm) of CYZ NIP (AAm) of CYZ	25 µg/mL of spiked CYZ	25 µg/mL of spiked CYZ	25 µg/mL of spiked CYZ	(i) Polymer dosage: 0.1 g (ii) pH condition: pH 7 (iii) Agitation period: 240 mins (iv) Agitation speed: 150 rpm (v) Temperature: 25 °C
MIP (MAA) of AME NIP (MAA) of AME	25 µg/mL of	25 µg/mL of	25 µg/mL of	(i) Polymer dosage: 0.1 g (ii) pH condition: pH 7 (iii) Agitation period: 210 mins (iv) Agitation speed: 150 rpm

Table 3.9 continued

	spiked AME	spiked AME	spiked AME	(v) Temperature: 25 °C
MIP (2VP) of ATZ NIP (2VP) of ATZ	25 µg/mL of spiked ATZ	25 µg/mL of spiked ATZ	25 µg/mL of spiked ATZ	(i) Polymer dosage: 0.3 g (ii) pH condition: pH 7 (iii) Agitation period: 15 mins (iv) Agitation speed: 150 rpm (v) Temperature: 25 °C

CHAPTER 4

RESULTS AND DISCUSSION

4.1 Synthesis of MIPs of Triazine Herbicides

The precipitation polymerization was chosen to synthesize MIPs of CYZ, AME and ATZ for the removal of CYZ, AME and ATZ as the contaminants in water samples such as polluted tap water and river water. This is because it is an effective technique for producing numerous types of uniform polymer particles which has remarkable benefits of ease of operation and the absence of any surfactant (Zhang et al., 2022).

Non-covalent imprinting approach was implemented in the synthesis of MIPs of CYZ, AME and ATZ that explained the non-covalent interactions between the template molecules of triazine herbicides and different functional monomers such as MAA, AAm and 2VP or 4VP. Non-covalent imprinting approach is more favourable because it has more flexibility for the types of template molecule-functional monomer interactions, involves easy and rapid binding and removal of template molecules from the polymer matrix (Wloch and Datta, 2019).

In this research, precipitation polymerization was successfully synthesizing MIPs and NIPs of CYZ, AME and ATZ because polymers are produced at the prescribed duration of 6 h and temperature of 80 °C for the complete polymerization reaction. During the synthesis of MIPs and NIPs of CYZ, AME and ATZ, the colourless solution began to change colour to cloudy solution after 2 h and then the white polymer precipitates were observed on the bottom of the conical flask after completing 6 h of polymerization reaction.

Turiel and Esteban (2019) thoroughly explained that the preparation of MIPs involved several crucial phases: firstly, dissolving template molecule, functional monomer, cross-linker, and initiator in the solvent; secondly, the formation of stable template molecule-functional monomer complex due to the interactions between the template molecule and functional monomer; thirdly, the functional monomer is arranged around the template molecule due to the copolymerization with cross-linker; fourthly, the template molecule removal from the polymer cavity; and thus leaving the polymer cavity with recognition sites corresponding to the target analyte based on the functionalities, size, and shape. Figure 4.1 described an example of proposed mechanisms for the formation of MIP of Triazine herbicides specifically CYZ.

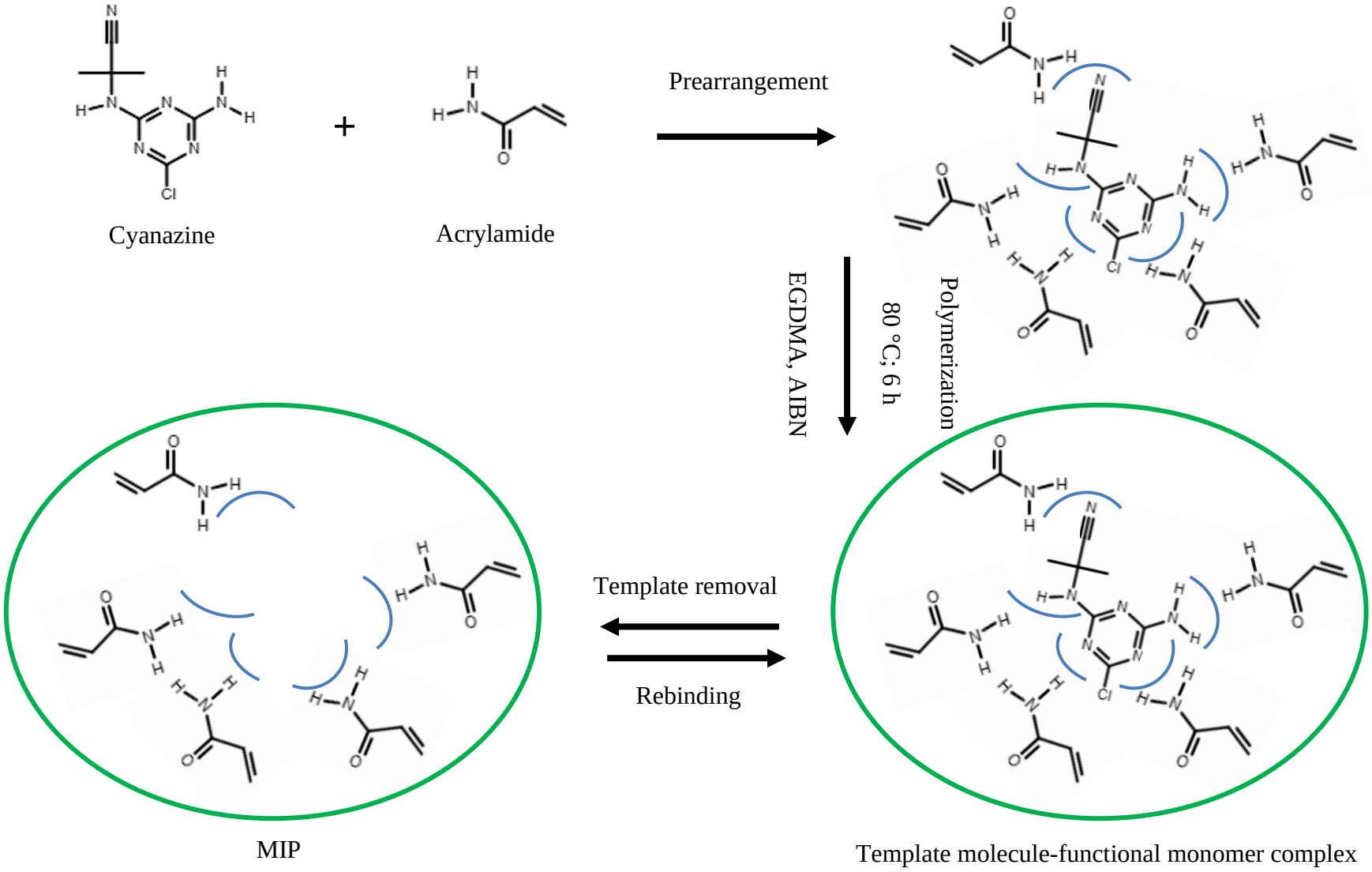


Figure 4.1: Proposed Mechanism for the MIP Preparation

4.2 FTIR Analysis

FTIR analysis was employed to distinguish the chemical bonds formed particularly Hydrogen bonding that occurred among the template molecule and functional monomer based on the FTIR spectra of the polymer sample and peak shifting (Munajad et al., 2018; Xie et al., 2019).

4.2.1 FTIR Analysis of MIPs of CYZ

Figure 4.2 showed the FTIR analysis of MIPs and NIP of CYZ, associated with the interaction among the CYZ as the template molecule, while MAA, AAm and 4VP as functional monomers, as well as EGDMA as the cross-linker. Only MIP (AAm) of CYZ showed a weak and broad peak at 3355.60 cm^{-1}, demonstrating the N-H stretching of the amide group from AAm (functional monomer). All FTIR spectra of MIP (MAA), MIP (AAm) and MIP (4VP) of CYZ showed peaks at the band of 2884.42 cm^{-1} to 2985.68 cm^{-1}, indicating the C-H stretching of an alkyl group from CYZ (template molecule) and EGDMA (cross-linker). These peaks may also indicate the C-H stretching of the alkyl group from MAA as shown in the FTIR spectrum of MIP (MAA) of CYZ.

Besides that, a strong peak in FTIR spectra of MIP (MAA), MIP (AAm) and MIP (4VP) of CYZ (Figure 4.2) can be detected from the range of 1721.38 cm^{-1} to1723.01 cm^{-1}, which corresponded to the C=O stretching of ester group from EGDMA (cross-linker). The peak at 1721.38 cm^{-1} of MIP (MAA) of CYZ may also correspond to the C=O stretching of the carboxylic acid group from MAA (functional monomer). The peaks of MIP (AAm) of CYZ at 1671.56 cm^{-1} and 1614.52 cm^{-1} attributed to the C=O stretching of the amide group from AAm (functional monomer). A medium peak of MIP (MAA) of CYZ at 1636.72 cm^{-1} showing the C=C stretching of the alkenyl group from MAA (functional monomer).

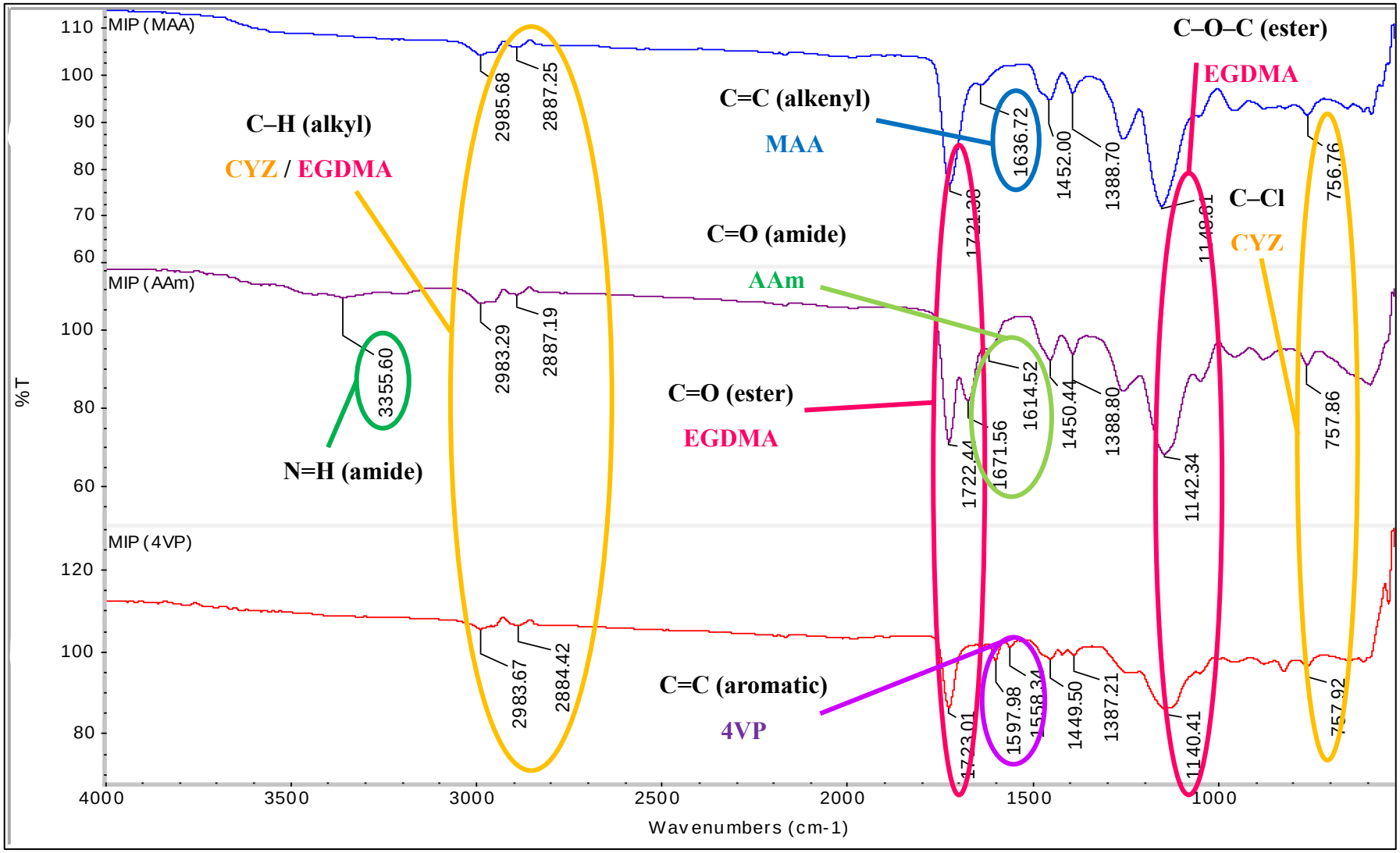


Figure 4.2: FTIR Spectra of MIP (MAA), MIP (AAm) and MIP (4VP) of CYZ

Based on Figure 4.2, medium peaks present in the FTIR spectrum of MIP (4VP) of CYZ at 1558.34 cm^{-1} and 1597.98 cm^{-1} was displaying the C=C bending of an aromatic group from 4VP. Moreover, MIP (MAA), MIP (AAm) and MIP (4VP) of CYZ had medium peaks at 1452.00 cm^{-1}, 1450.44 cm^{-1} and 1449.50 cm^{-1}, respectively. These peaks were attributed to CH_2 bond bending and CH_3 bending of CYZ (template), EGDMA (cross-linker) and either MAA or AAm or 4VP (functional monomers). The peaks present between 1140.41 cm^{-1} to 1388.80 cm^{-1} in FTIR spectra of MIP (MAA), MIP (AAm) and MIP (4VP) of CYZ were showing a strong peak of C-O-C stretching and medium peak of CH_3 bending of EGDMA (cross-linker). In addition, the peaks present in FTIR spectra of MIP (MAA), MIP (AAm) and MIP (4VP) of CYZ from the range of 756.76 cm^{-1} to 757.92 cm^{-1} showing the C-Cl stretching of CYZ (template). These peaks may also represent the C-H bending of the alkene group in EGDMA (cross-linker).

For comparison, the FTIR spectra of MIP (AAm) and NIP (AAm) of CYZ were shown in Figure 4.3. The FTIR spectra showed that the peaks of MIP (AAm) of CYZ were similar but slightly shifted as compared to NIP (AAm). This is due to the interaction between AAm (functional monomer) with CYZ, the template molecule during the synthesis of MIP (AAm) of CYZ. The presence of N–H stretching of the amide group from AAm (functional monomer) was detected in the FTIR spectrum of NIP (AAm) with a slight band shifting at 3361.96 cm^{-1} as compared to MIP (AAm) of CYZ (3350.60 cm^{-1}). The peaks of NIP (AAm) were at 2888.06 cm^{-1} and 2984.03 cm^{-1}, meanwhile, the peaks of MIP (AAm) of CYZ were slightly shifted at 2887.19 cm^{-1} and 2983.29 cm^{-1}. These peaks were corresponding to the C-H stretching of EGDMA (cross-linker). For MIP (AAm) of CYZ, these peaks may also have been associated with the C-H stretching of CYZ (template), due to the addition of CYZ during the synthesis of imprinted polymer.

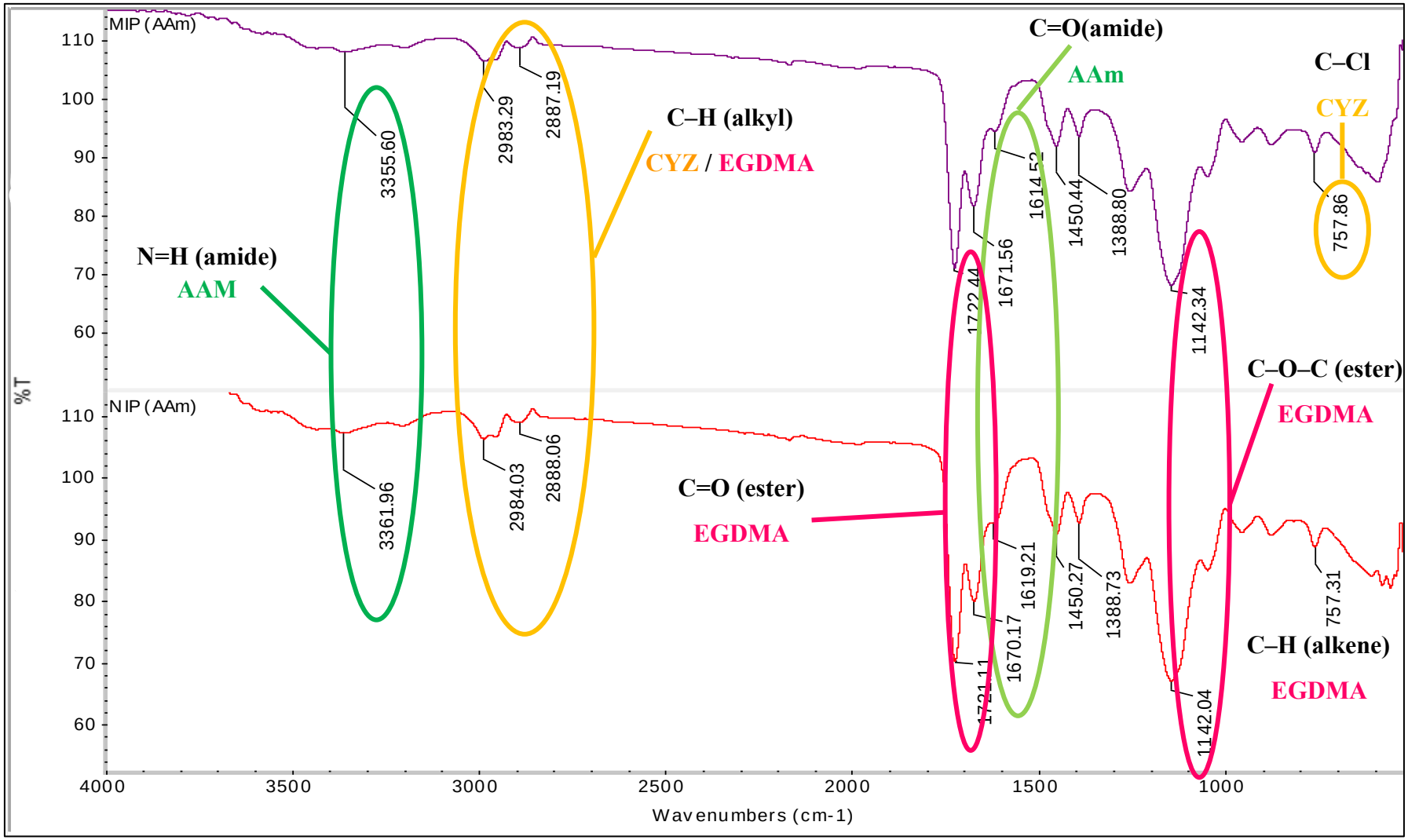


Figure 4.3: FTIR Spectra of MIP (AAm) and NIP (AAm) of CYZ

The presence of C=O stretching of the amide group from AAm (functional monomer) can be observed from the peaks of NIP (AAm) at 1670.17 cm^{-1} and 1619.21 cm^{-1} (Figure 4.3). Similarly, MIP (AAm) of CYZ had slight band shifting at 1614.52 cm^{-1} and 1671.56 cm^{-1}, showing the C=O stretching of the amide group from AAm (functional monomer). Both of NIP (AAm) and MIP (AAm) of CYZ had a medium peak at 1450.27 cm^{-1} and 1450.44 cm^{-1}, respectively. This showed the CH_2 bending and CH_3 bending of EGDMA (cross-linker) in both NIP (AAm) and MIP (AAm) of CYZ. This peak may also indicate the CH_3 bending of CYZ (template) in the MIP (AAm) of CYZ that causes a slight band shifting than that of NIP (AAm). Another CH_3 bending from EGDMA (cross-linker) was detected in MIP (AAm) and NIP (AAm) of CYZ at 1450.44 cm^{-1} and 1388.73 cm^{-1}, respectively.

A strong peak at 1142.04 cm^{-1} of NIP (AAm) was associated with the C-O-C stretching of the ester group from EGDMA (cross-linker). Similarly, a strong and slightly shifted peak at 1142.34 cm^{-1} of MIP (AAm) of CYZ was related to the C-O-C stretching of the ester group from EGDMA (cross-linker). Another medium peak was detected at 757.86 cm^{-1} and 757.31 cm^{-1} for MIP (AAm) and NIP (AAm) of CYZ, respectively. These peaks were associated with the C-H bending of the alkene group in EGDMA (cross-linker) and AAm (functional monomer). Slight band shifting at the peak of MIP (AAm) of CYZ (757.86 cm^{-1}) may also be due to the presence of the C-Cl stretching of CYZ (template).

4.2.2 FTIR Analysis of MIPs of AME

The FTIR analysis on MIPs and NIP of AME attributed to the functional groups present in the synthesized polymers due to the interaction among template molecule (AME), functional monomer (MAA/AAm/2VP) and cross-linker (EGDMA) were shown in Figure 4.4 and Figure 4.5.

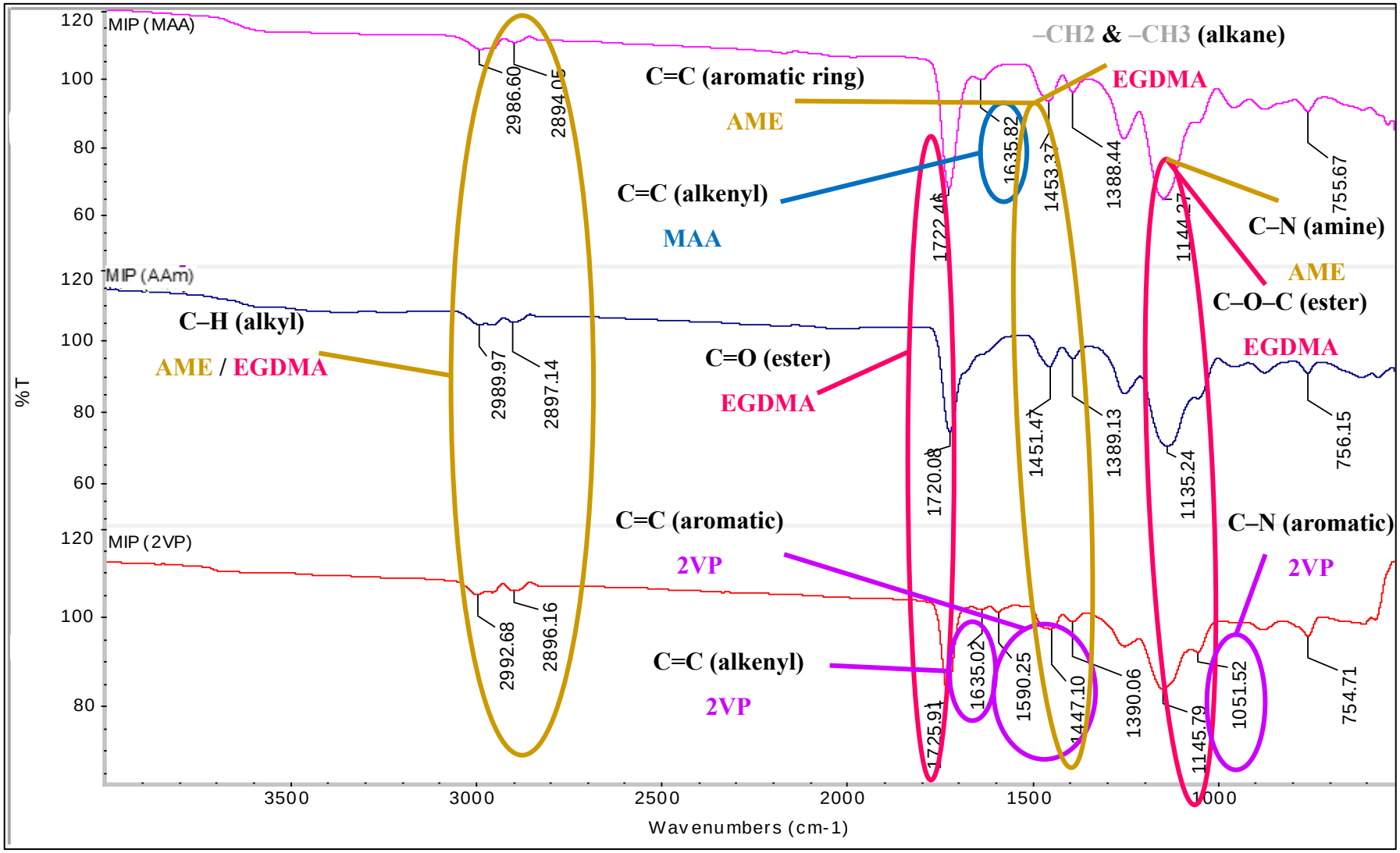


Figure 4.4: FTIR Spectra of MIP (MAA), MIP (AAm) and MIP (2VP) of AME

The medium peak at 2986.60 cm^{-1}, 2994.09 cm^{-1} and 2992.68 cm^{-1} may indicate the C–H stretching of alkane group of AME (template molecule) and EGDMA (cross-linker) in FTIR spectra of MIP (MAA), MIP (AAm) and MIP (2VP) of AME, respectively (Figure 4.4). The peak at 2986.60 cm^{-1} of MIP (MAA) of AME might also imply the O-H stretching of carboxylic acid group in methacrylic acid (MAA), functional monomer. Similarly, the small peaks at 2894.05 cm^{-1}, 2897.14 cm^{-1} and 2896.16 cm^{-1} may refer to the C-H stretching of alkane group of AME and EGDMA in MIP (MAA), MIP (AAm) and MIP (2VP) of AME, respectively. The peak of MIP (MAA) of AME at 2897.14 cm^{-1} might also denote the O-H stretching of carboxylic acid group in MAA.

Based on Figure 4.4, a strong peak appeared in FTIR spectra of MIP (MAA), MIP (AAm) and MIP (2VP) of AME at 1722.48 cm^{-1}, 1720.08 cm^{-1} and 1725.91 cm^{-1}, respectively, and these peaks may represent the C=O stretching of ester group in EGDMA, cross-linker. Besides that, the peak of MIP (MAA) of AME at 1722.48 cm^{-1} may show the presence of C=O stretching of carboxylic acid group in MAA. The weak peak of MIP (MAA) of AME at 1635.82 cm^{-1} and MIP (2VP) of AME at 1635.02 cm^{-1} may display the presence of C=C stretching of alkenyl group in MAA and 2VP, respectively and no peak of MIP (AAm) of AME was detected at this adsorption band. Only MIP (2VP) of AME had a weak peak at 1590.25 cm^{-1} and this assigned to C=C stretching of aromatic ring in 2VP.

A medium peak in FTIR spectra of MIP (MAA), MIP (AAm) and MIP (2VP) of AME at 1453.37 cm^{-1}, 1451.47 cm^{-1} and 1447.10 cm^{-1}, respectively, may prove the C=C stretching of aromatic ring in AME template. These peaks might also attribute to the $-CH_2$ bending and the $-CH_3$ bending of MAA, AAm and 2VP in MIP (MAA), MIP (AAm) and NIP (AAm) of AME, respectively as well as the EGDMA. The identical peak at 1447.10

cm^{-1} of MIP (2VP) of AME might also indicate the presence of C=C stretching of aromatic ring in 2VP. Another medium peak at 1388.44 cm^{-1}, 1389.13 cm^{-1} and 1390.66 cm^{-1} may indicate the $–CH_3$ bending of alkane group in AME template and EDGMA cross-linker as shown in FTIR spectra of MIP (MAA), MIP (AAm) and MIP (2VP) of AME. The peak of MIP (MAA) of AME at 1388.44 cm^{-1} may also show the CH_3 bending of alkane group in MAA, functional monomer. Moreover, this peak at 1388.44 cm^{-1} might imply the presence of $-CH_3$ bending of alkane group in MAA, functional monomer of MIP (MAA) of AME.

A strong peak at 1144.27 cm^{-1}, 1135.24 cm^{-1} and 1447.10 cm^{-1} of MIP (MAA), MIP (AAm) and MIP (2VP) of AME, respectively, may represent the C-O-C stretching of ester in EGDMA and the C-N stretching of amine group in AME template. Only FTIR spectra of MIP (2VP) of AME had peak at 1051.52 cm^{-1}, showing the presence of C-N stretching of amine group in 2VP, functional monomer. The peaks of MIP (MAA), MIP (AAm) and MIP (2VP) of AME at 755.67 cm^{-1}, 756.15 cm^{-1} and 754.71 cm^{-1} may show the C-H bending of alkene group in EGDMA.

Figure 4.5 showed the comparison between the FTIR spectra of MIP (MAA) and NIP (MAA) of AME. Since MIP (MAA) of AME was synthesized in the presence of AME template molecule a slight absorption band shifting might occurred in comparison to NIP (MAA) that was synthesized without presence of AME template molecule. In FTIR spectra of MIP (MAA) of AME, a medium peak at 2894.05 cm^{-1} and 2986.60 cm^{-1} may assign to the C-H stretching of alkane group of AME (template molecule) and EGDMA (cross-linker) as well as the O-H stretching of carboxylic acid group in MAA (functional monomer).

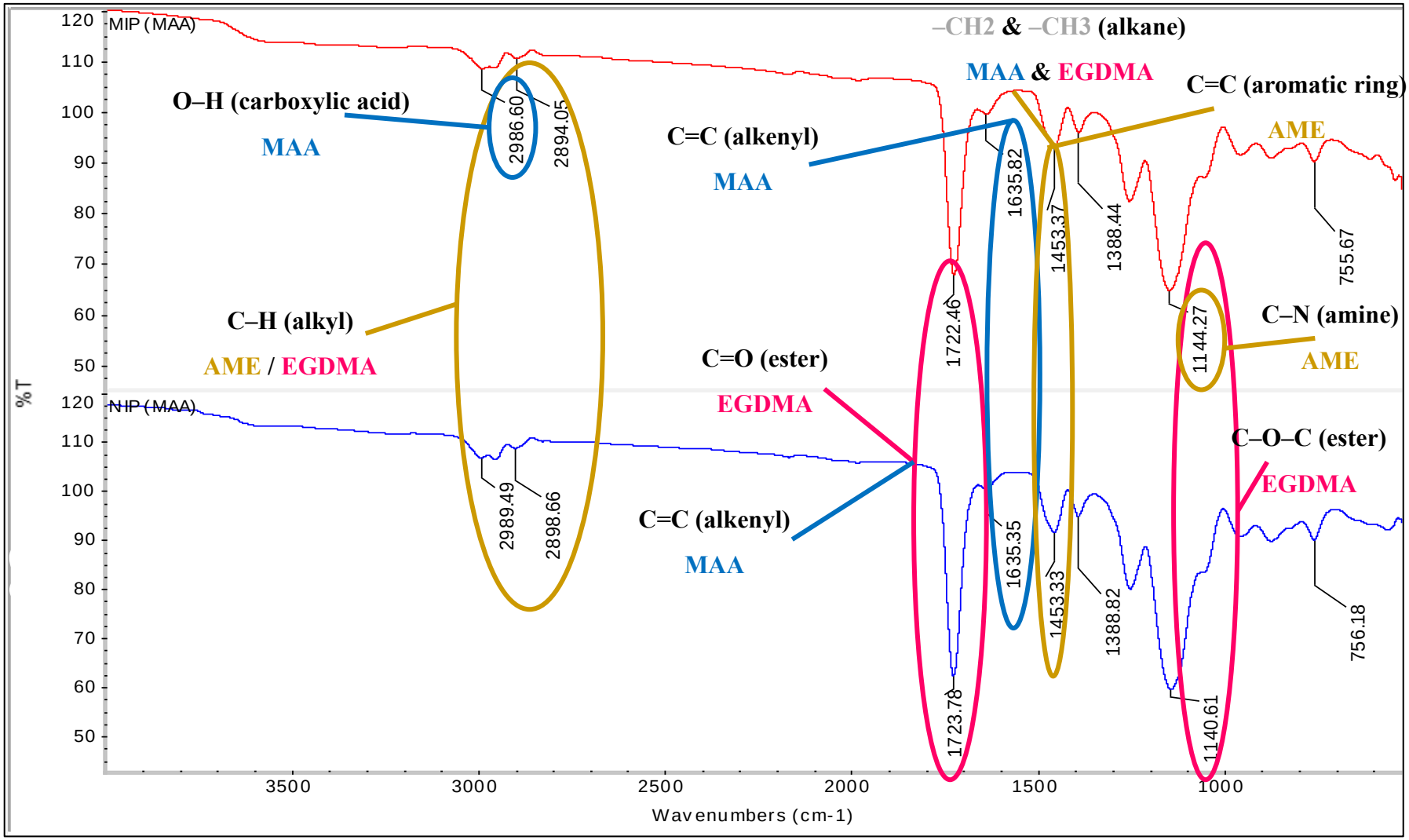


Figure 4.5: FTIR Spectra of MIP (MAA) and NIP (MAA) of AME

While in FTIR spectra of NIP (MAA), a slight shifting of the peak at 2898.66 cm^{-1} and 2989.49 cm^{-1} that indicate the -CH stretching of alkane group of EGDMA and the O-H stretching of carboxylic acid group in MAA. A strong peak at 1722.46 cm^{-1} in MIP (MAA) of AME (Figure 4.5) showed the C=O stretching of ester group and carboxylic acid group in EGDMA and MAA, respectively. A small peak shifting at 1723.78 cm^{-1} in NIP (MAA) display the presence of C=O stretching of ester group and C=C stretching of alkenyl group in EGDMA and MAA, respectively. The peaks present from 1700 cm^{-1} to 1750 cm^{-1} showed the C=O stretching of the crosslinking polymerization between EGDMA crosslinker and MAA monomer (Sanagi et al., 2013).

A weak peak of MIP (MAA) of AME at 1635.82 cm^{-1} imply the presence of the C=C stretching of alkenyl group in MAA. A minor peak shifting at 1635.82 cm^{-1} of NIP (MAA) was observed indicating the C=C stretching of alkenyl group in MAA. The peak of MIP (MAA) of AME at 1453.37 cm^{-1} represent the C=C stretching of aromatic ring in AME template as well as the $-CH_2$ bending and $-CH_3$ bending of MAA and EGDMA (Figure 4.5). Due the absence of AME template in the NIP (MAA), a very small shifting of the peak at 1453.33 cm^{-1}, indicating the $-CH_2$ bending and $-CH_3$ bending of MAA and EGDMA.

In addition, the MIP (MAA) of AME peak at 1388.44 cm^{-1} may display the $-CH_3$ bending of alkane group in AME template, MAA and EDGMA. While a small shift in NIP (MAA) at 1388.82 cm^{-1}, might show the $-CH_3$ bending of alkane group in MAA and EDGMA only. The FTIR spectra of MIP (MAA) of AME has a strong peak at 1144.27 cm^{-1} that assign to the C-O-C stretching of ester and C-N stretching of amine group in EGDMA and AME template, respectively. However, a strong peak of NIP (MAA) was shifted at 1140.61 cm^{-1} due to the C-O-C stretching of ester in EGDMA and no presence of AME

template. The small peaks of MIP (MAA) and NIP (MAA) of AME at 755.67 cm^{-1} and 756.18 cm^{-1}, respectively, may imply the C-H bending of alkene group in EGDMA.

4.2.3 FTIR Analysis of MIPs of ATZ

The FTIR spectra of MIPs of ATZ would exhibit peaks corresponding to ATZ template molecule, functional monomer (MAA, AAm and 2VP) and EGDMA cross-linker (Figure 4.6). Both MIP (AAm) and MIP (2VP) of ATZ revealed characteristic absorption band at 3669.55 cm^{-1} and 3666.50 cm^{-1}, respectively. This confirmed the presence of N-H stretching vibration (Jawaid et al., 2013), characteristic of an amide group and an amine group in MIP (AAm) and MIP (2VP) of ATZ, respectively.

Besides that, a medium peak was observed around 2982.47 cm^{-1}, 2978.45 cm^{-1} and 2978.74 cm^{-1} of MIP (MAA), MIP (AAm) and MIP (2VP) of ATZ, respectively, indicating the C-H stretching and CH_2 stretching (asymmetric and symmetric) vibrations due to the presence of alkyl groups. This was consistent with the inclusion of the ATZ template molecule and EGDMA cross-linker, as intended in the MIP synthesis. However, a slight band shifting in the FTIR spectrum of MIP (MAA) of ATZ in comparison with MIP (AAm) and MIP (2VP) of ATZ was suggesting to the presence of the O-H stretching vibration in the carboxylic acid group from MAA functional monomer.

Similarly, the peaks of MIP (MAA), MIP (AAm) and MIP (2VP) of ATZ at 2899.57 cm^{-1}, 2903.40 cm^{-1} and 2902.23 cm^{-1}, respectively. These peaks were corresponding to the C-H stretching vibrations of alkyl groups from ATZ template molecule and EGDMA cross-linker. Nevertheless, the peak of MIP (MAA) of ATZ had slightly shifted than other MIPs because of the O-H stretching vibration of the carboxylic acid group from MAA functional monomer.

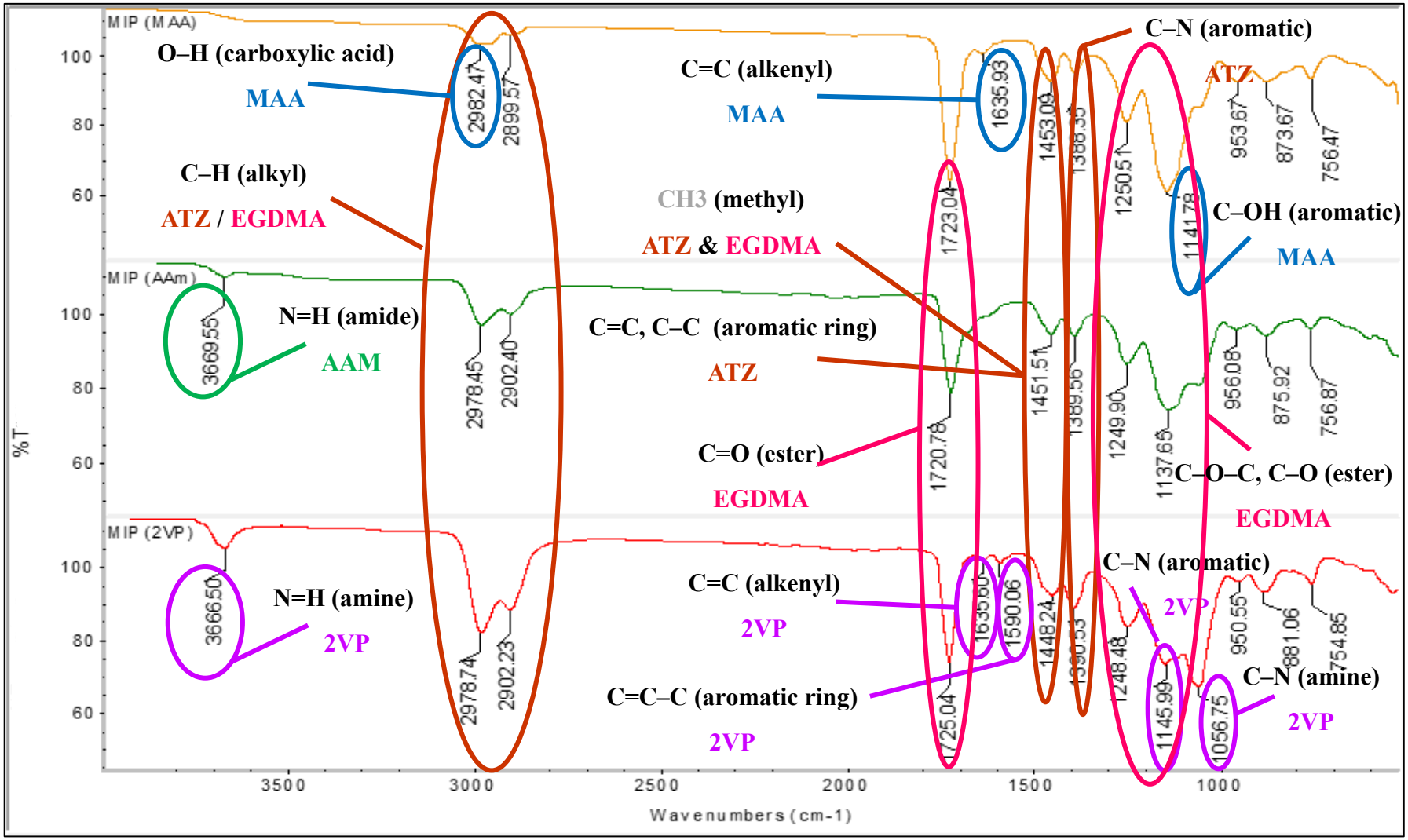


Figure 4.6: FTIR Spectra of MIP (MAA), MIP (AAm) and MIP (2VP) of ATZ

Moreover, strong absorption band at 1723.04 cm^{-1}, 1720.78 cm^{-1} and 1725.04 cm^{-1} of MIP (MAA), MIP (AAm) and MIP (2VP) of ATZ interpreted the presence of C=O stretching vibrations (Royani et al., 2014), which confirmed the successful incorporation of the carbonyl group from EGDMA cross-linker in the MIPs structure. This peak intensity varied among different MIPs, suggesting the usage of different functional monomers such as MAA, AAm and 2VP.

The peak of MIP (MAA) of ATZ at 1723.04 cm^{-1} and MIP (AAm) of ATZ at 1720.78 cm^{-1} may also indicate the presence of a carbonyl group in the carboxylic acid group from MAA functional monomer and an amide group of AAm functional monomer, respectively. Moreover, both MIP (MAA) and MIP (2VP) of ATZ exhibited a weak absorption band at 1635.93 cm^{-1} and 1635.60 cm^{-1}, respectively. These peaks may demonstrate the presence of C=C stretching vibration of alkenyl groups (Nandiyanto et al., 2019) from MAA and 2VP functional monomers, respectively.

In contrast, only MIP (2VP) of ATZ had a weak absorption band at 1590.06 cm^{-1} (Figure 4.6), which shows the presence of C=C-C stretching vibrations associated with an aromatic ring group (Nandiyanto et al., 2019) in 2VP functional monomer. MIP (MAA), MIP (AAm) and MIP (2VP) of ATZ have medium absorption bands at 1453.09 cm^{-1}, 1451.51 cm^{-1} and 1448.24 cm^{-1}, respectively. These peaks may represent the asymmetric or symmetric C-H bending vibration of the methyl group (Nandiyanto et al., 2019) from ATZ template molecule and EGDMA cross-linker. Comparably, the peak of MIP (2VP) of ATZ was slightly shifted, also implying the presence of C=C stretching and C-C vibrations corresponding to aromatic groups of the 2VP functional monomer.

Small peaks have appeared at 1388.35 cm^{-1}, 1389.56 cm^{-1} and 1390.53 cm^{-1} of MIP (MAA), MIP (AAm) and MIP (2VP) of ATZ (Figure 4.6) indicating the presence of C-N stretching from an aromatic group in ATZ template molecule. Similar peaks might show the presence of C-H bending vibration from the methyl group the in ATZ template molecule and EGDMA cross-linker. These peaks also display the incorporation of MAA and 2VP as functional monomers in their respective MIPs. The peak at 1388.35 cm^{-1} may also show the O-H bending vibration in carboxylic acid group (Royani et al., 2014) of MAA while peak at 1390.53 cm^{-1} may signify the C-N stretching in the aromatic ring of 2VP.

Additionally, the successful interaction of EGDMA as the cross-linker in the synthesis of MIP (MAA), MIP (AAm) and MIP (2VP) of ATZ can be further confirmed with the strong peaks at 1250.51 cm^{-1}, 1249.90 cm^{-1} and 1248.48 cm^{-1}, suggesting the C-O stretching vibration of ester group in EGDMA. These peaks may also display the presence C-N stretching aromatic amine group of ATZ template molecule in MIP (MAA), MIP (AAm) and MIP (2VP) of ATZ. The peak of MIP (MAA) of ATZ at 1250.51 cm^{-1} was slightly shifted to the left than the other MIPs may be due to the presence of C-O stretching vibration of the carboxylic acid group in MAA. Meanwhile, the peak of MIP (2VP) of ATZ at 1248.48 cm^{-1} was partially shifted to the right than the other MIPs due to the presence of C-N stretching vibration in the aromatic ring group of 2VP.

Figure 4.6 also showed other prominent peaks at 1141.78 cm^{-1}, 1137.65 cm^{-1} and 1145.99 cm^{-1} were observed from the FTIR spectra of MIP (MAA), MIP (AAm) and MIP (2VP) of ATZ, respectively. These peaks revealed the C-O-C stretching and C-O stretching vibrations, characteristics of the ester group in EGDMA as a cross-linker in the polymer network. These peaks might also indicate the presence of C-N stretching vibration of the

triazine ring group (Pareek et al., 2015) in the ATZ template molecule in all MIPs. The peak band shifting of MIP (MAA) and MIP (2VP) of ATZ were due to the presence of the C-OH stretching vibration in MAA functional monomer and the C-N stretching vibration in 2VP functional monomer, respectively. Only MIP (2VP) of ATZ had a medium peak at 1056.75 cm^{-1}, implying the presence of C-N stretching vibration of an amine group in 2VP functional monomer.

In addition, the synthesized MIP (MAA), MIP (AAm) and MIP (2VP) of ATZ had weak peaks at 953.67 cm^{-1}, 956.08 cm^{-1} and 950.55 cm^{-1}, respectively (Figure 4.6). These peaks indicated the presence of =C-H bending vibration of vinyl groups in EGDMA cross-linker as well as in different functional monomers such as MAA, AAm and 2VP. MIP (MAA), MIP (AAm) and MIP (2VP) of ATZ had medium peaks at 873.67 cm^{-1}, 875.92 cm^{-1} and 881.06 cm^{-1}, respectively. These peaks might indicate the C=C bending vibration of an alkene group in EGDMA cross-linker and functional monomers including MAA, AAm and 2VP.

Lastly, the presence of C-Cl stretching (Nandiyanto et al., 2019) and C-H bending vibrations resulting from the addition of ATZ template molecule for MIP synthesis can be denoted by peaks observed in FTIR spectra of MIP (MAA), MIP (AAm) and MIP (2VP) of ATZ at 756.47 cm^{-1}, 756.87 cm^{-1} and 754.85 cm^{-1}, respectively (Figure 4.6). These peaks may also indicate the ortho or 1,2-disubstituted C-H bending vibration of an aromatic ring group (Nandiyanto et al., 2019) in 2VP of MIP (2VP) of ATZ.

Figure 4.7 showed the comparison of the FTIR spectra of MIP (2VP) and NIP (2VP) of ATZ which provide insights into the polymer imprinting process, confirm the presence of specific binding sites and differentiate between the imprinted and non-imprinted polymers

on their spectral features. The peaks at 3666.50 cm^{-1} and 3665.38 cm^{-1} imply the presence of N-H stretching (Jawaid et al., 2013) of an amine group in the 2VP functional monomer of MIP (2VP) and NIP (2VP) of ATZ. This provides strong evidence for the presence of 2VP in the samples analysed. MIP (2VP) and NIP (2VP) of ATZ had two peaks that appeared in the range of ~ 2978 cm^{-1} to ~ 2902 cm^{-1}, revealing the presence of the C-H stretching and CH_2 stretching (asymmetric and symmetric) vibrations, an alkyl group in the EGDMA cross-linker as shown in Figure 4.7. It is observed that the peaks of MIP (2VP) of ATZ at 2978.74 cm^{-1} and 2902.23 cm^{-1} were shifted as compared to the peak of NIP (2VP) at 2978.66 cm^{-1} and 2903.45 cm^{-1} due to the presence of ATZ template molecule in MIP (2VP) of ATZ, resulting in an abundance of specific binding sites and template-monomer interactions.

Strong peaks at 1725.04 cm^{-1} and 1723.75 cm^{-1} of MIP (2VP) and NIP (2VP) of ATZ, respectively, indicate the C=O stretching vibration (Nandiyanto et al., 2019) of the ester group in EGDMA cross-linker. Besides that, these band absorptions may also show the presence of C-H bending vibration of an aromatic group the in 2VP functional monomer. The MIP (2VP) of ATZ was slightly shifted as compared to NIP (2VP) due to the presence of ATZ template molecule that had a bond characteristic of C-H bending vibration in the aromatic ring group. Based on Figure 4.7, both MIP (2VP) and NIP (2VP) of ATZ had small peaks at 1635.60 cm^{-1} and 1635.82 cm^{-1}, respectively, which reveal the presence of C=C stretching vibrations (Nandiyanto et al., 2019), associated with the alkenyl group in EGDMA cross-linker and aromatic rings in 2VP functional monomer. The presence of 2VP functional monomer in the polymer structure of MIP (2VP) and NIP (2VP) of ATZ can be observed at 1590.06 cm^{-1} and 1589.93 cm^{-1}, respectively. These peaks implied the C=C-C stretching vibrations of the aromatic rings group (Nandiyanto et al., 2019).

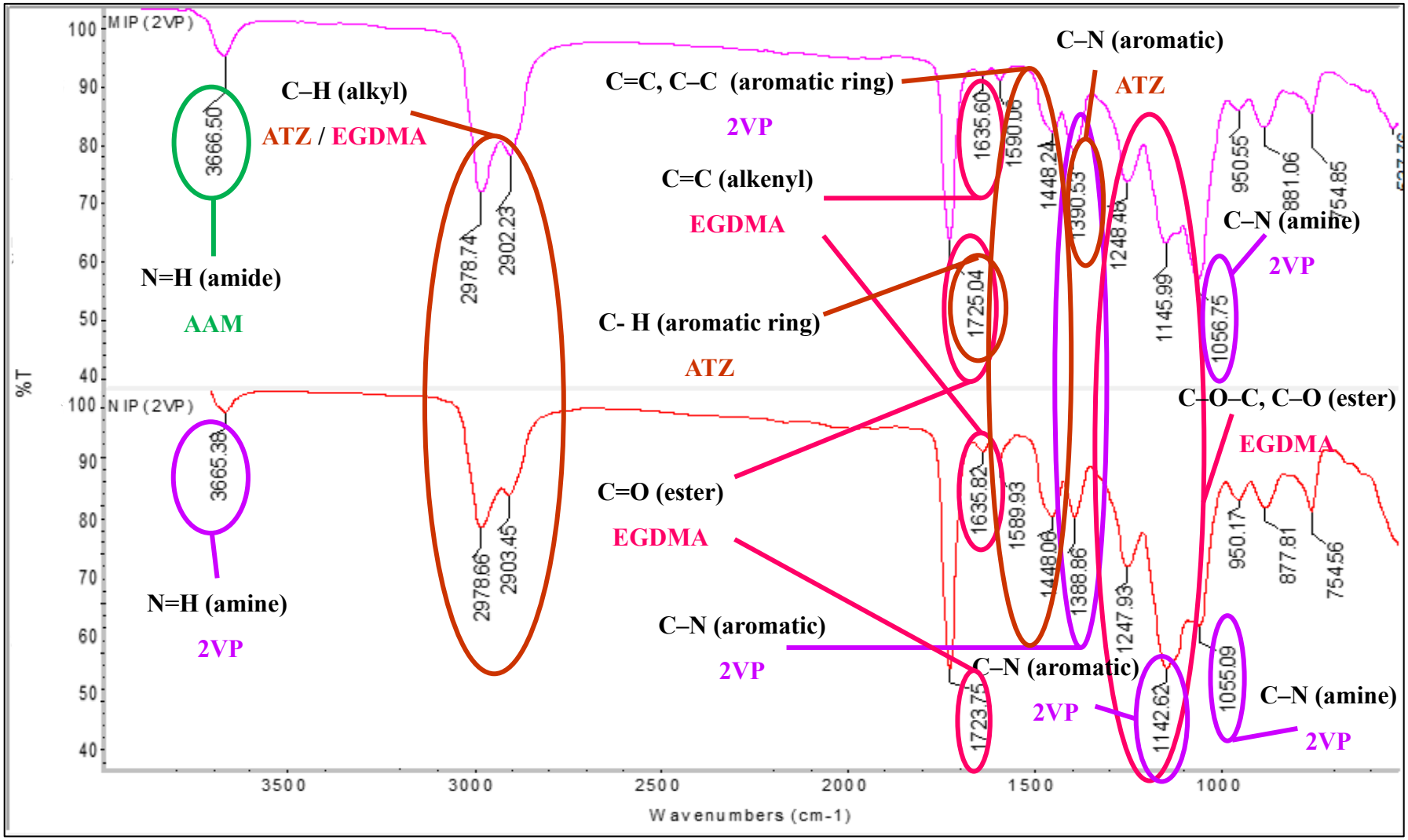


Figure 4.7: FTIR Spectra of MIP (2VP) and NIP (2VP) of ATZ

Moreover, medium peaks of MIP (2VP) and NIP (2VP) of ATZ at 1448.24 cm^{-1} and 1448.06 cm^{-1} also indicated the C=C stretching and C-C stretching vibrations of the aromatic rings group in the 2VP functional monomer. Similar peaks also showed the C-H bending vibration (Nandiyanto et al., 2019) of the EGDMA as the cross-linker in the synthesized polymers. The peak of MIP (2VP) of ATZ was slightly shifted from that NIP (2VP) due to the presence of C-H bending vibration of the alkyl group in the ATZ template molecule.

Figure 4.7 also showed medium absorption bands at 1390.53 cm^{-1} and 1388.86 cm^{-1} of MIP (2VP) and NIP (2VP) of ATZ, respectively, suggested the presence of C-H bending vibration of the methyl group in EGDMA cross-linker and C-N stretching vibration of aromatic amines group in 2VP functional monomer. It was clear that the band shifting in MIP (2VP) of ATZ due to the C-H bending and C-N stretching vibrations in the ATZ template molecule.

Furthermore, MIP (2VP) and NIP (2VP) of ATZ had medium peaks at 1248.48 cm^{-1} and 1247.93 cm^{-1}, respectively. These absorption bands distinguish the presence of C-O stretching and C-N stretching vibrations of the ester group in the EGDMA cross-linker and the aromatic ring group in the 2VP functional monomer, respectively. However, the peak of MIP (2VP) of ATZ had shifted because of the C-N stretching vibration of the aromatic ring group in the ATZ template molecule.

The FTIR spectra of MIP (2VP) and NIP (2VP) of ATZ (Figure 4.7) displayed a strong peak at 1145.99 cm^{-1} and 1142.62 cm^{-1}, respectively. These peaks imply the C-O-C stretching and C-O stretching vibrations, representing the ester group in the EGDMA cross-linker. These absorption bands were also associated with the C-N stretching vibration that proved the identification of 2VP functional monomer in both polymers. The observed shift

in the IR spectrum of MIP (2VP) of ATZ indicated the successful imprinting and specific interactions between the ATZ template molecule and the 2VP functional monomer in the imprinted polymer, resulting in excellent molecular recognition capabilities.

The peaks at 1056.75 cm^{-1} and 1055.09 cm^{-1} were corresponding to the C-N stretching vibration of 2VP functional monomer in both MIP (2VP) and NIP (2VP) of ATZ, respectively. MIP (2VP) and NIP (2VP) of ATZ had weak peaks at 950.55 cm^{-1} and 950.17 cm^{-1}, respectively, indicating the presence of =C-H bending vibration of vinyl group in 2VP functional monomer and EGDMA cross-linker. Additionally, MIP (2VP) of ATZ had a medium peak at 881.06 cm^{-1} while NIP (2VP) had peak at 877.81 cm^{-1} which revealed the C=C bending vibrations of alkene group in 2VP functional monomer and EGDMA cross-linker. MIP (2VP) of ATZ was shifted due to the N-H wagging vibration of the secondary amine group in the ATZ template molecule.

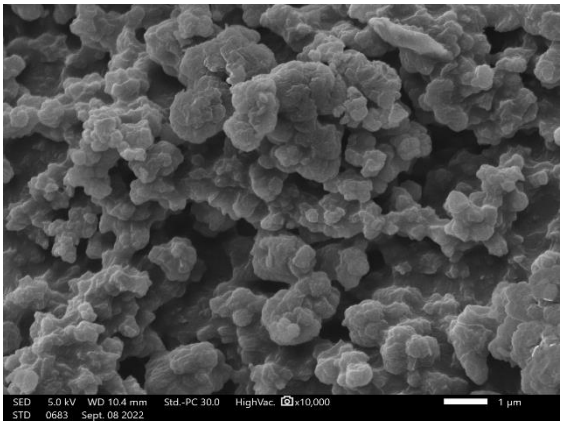
Both MIP (2VP) and NIP (2VP) of ATZ had medium peaks at 754.85 cm^{-1} and 754.56 cm^{-1}, respectively which represent the C-H bending vibration of an aromatic group in the 2VP functional monomer. The presence of ATZ template molecule in MIP (2VP) of ATZ can be further confirmed with the appearance of a similar peak due to the C-Cl stretching (Nandiyanto et al., 2019) and C-H bending vibrations of ATZ template molecule which the absorption band of MIP (2VP) of ATZ was slightly shifted than that NIP (2VP).

4.3 FESEM Analysis

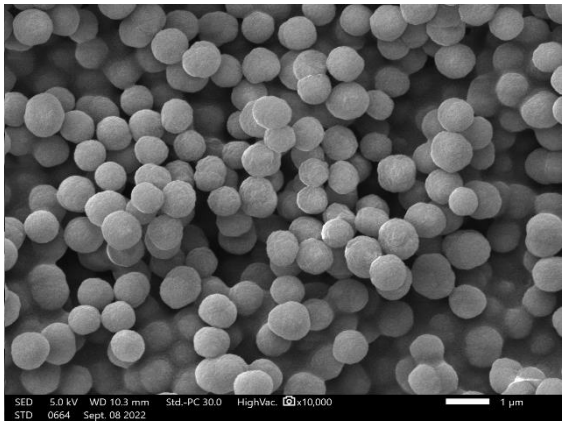
In this study, the morphologies of MIPs and NIPs of Triazine herbicides were analysed using FESEM to provide crucial insights into the polymer surface morphology and structural characteristics at a high resolution of 10k magnification as portrayed in Figure 4.8, Figure 4.9, and Figure 4.10.

4.3.1 FESEM Analysis of MIPs of CYZ

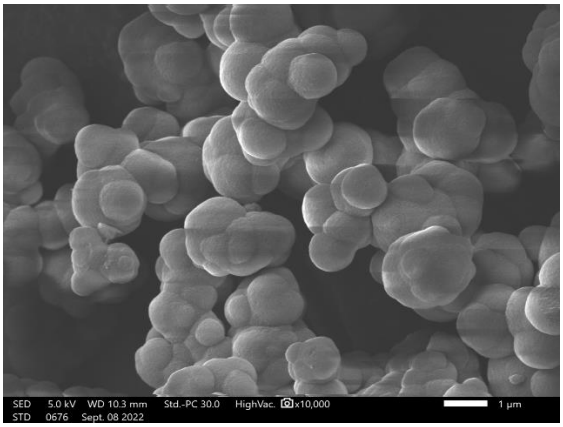
Based on Figure 4.8, it was observed that MIP (MAA) and MIP (4VP) of CYZ were agglomerated and in irregular shape, meanwhile, MIP (AAm) and NIP (AAm) of CYZ were spherical and nearly regular in shape. Arabzadeh and Abdouss (2010) emphasized that the template-monomer interaction affects the polymer production of regular-size distribution with a dispersed polymer surface.



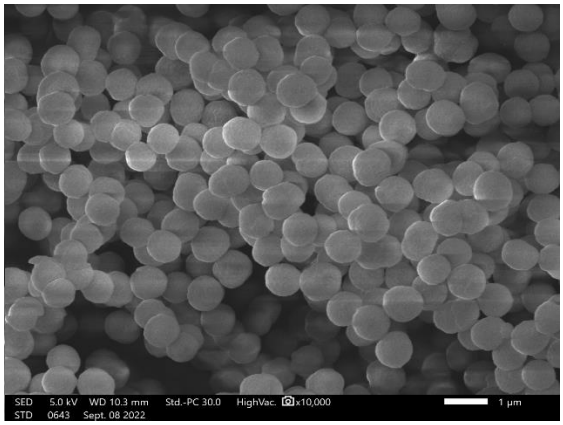
MIP (MAA) of CYZ



MIP (AAm) of CYZ



MIP (4VP) of CYZ



NIP (AAm) of CYZ

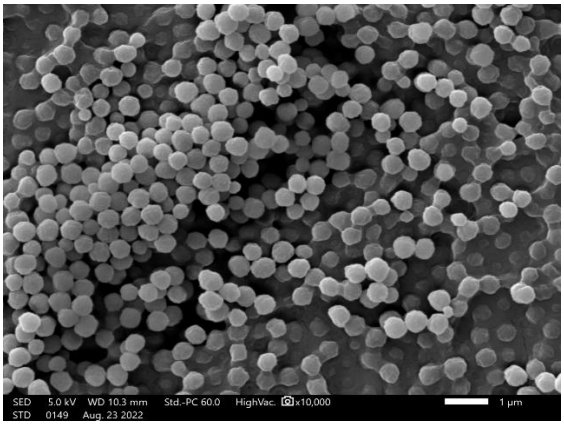
Figure 4.8: FESEM Micrographs of MIPs and NIP of CYZ

It was calculated that the average diameter size of MIP (MAA), MIP (AAm) and MIP (4VP) of CYZ were 0.64 µm, 0.86 µm and 0.98 µm, respectively (Appendix 1). This may be due to the usage of different functional monomers such as MAA, AAm and 4VP for the fabrication of the MIPs of CYZ.

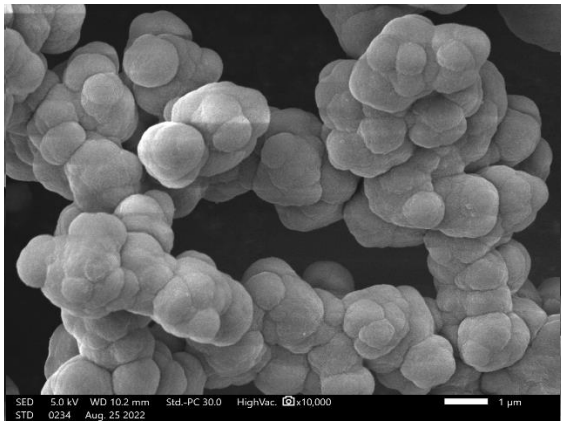
Since MIP (AAm) of CYZ was selected for further studies, its NIP (AAm) was also prepared in similar way without addition of CYZ for comparison purpose. In comparison to MIP (AAm) of CYZ, the average diameter of NIP (AAm) was 0.98 µm. The polymer particles of NIP (AAm) were slightly bigger than MIP (AAm) of CYZ due to the absence of the CYZ template added for the synthesis of the NIPs.

4.3.2 FESEM Analysis of MIPs of AME

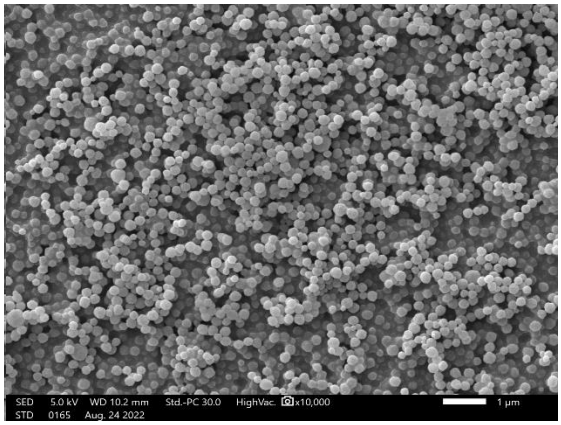
Figure 4.9 indicated the synthesized MIP (MAA), MIP (2VP) and NIP (MAA) of AME were regular in size and spherical in shape. This is due to precipitation polymerization method which synthesize polymers in circular shape and its particles size within a particular range (Xiao et al., 2018). However, the synthesized MIP (AAm) was not only irregular in shape and size, but also the polymer particles were agglomerated even though the precipitation polymerization method was used. This may be due to high concentration of co-monomers (the total concentration of functional monomer and the cross-linker) that constrain the particle growth (Xia et al., 2017). This indicated that the usage of 5 mmol of AAm functional monomer and 20 mmol of EGDMA cross-linker was improper concentration of co-monomers for the preparation of MIP (AAm) of AME.



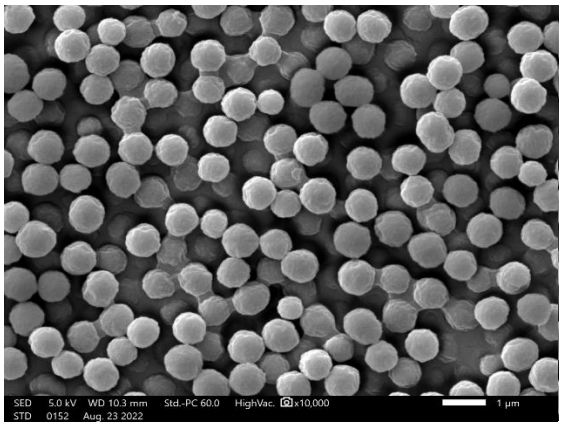
MIP (MAA) of AME



MIP (AAm) of AME



MIP (2VP) of AME



NIP (MAA) of AME

Figure 4.9: FESEM Micrographs of MIPs and NIP of AME

It was calculated that the mean diameter sizes of MIP (MAA), MIP (AAm) and MIP (2VP) of AME were 0.52 µm, 1.23 µm and 0.36 µm, respectively (Appendix 2). The mean diameter sizes of the synthesized MIPs of AME were arranged in ascending order: MIP (2VP) < MIP (MAA) < MIP (AAm). This showed that MIP (2VP) had the smallest polymer particles size, followed by the MIP (MAA), and MIP (AAm) had the largest polymer particle size among the imprinted polymers.

Among those MIPs, MIP (MAA) of AME was selected for further studies and therefore its NIP (MAA) of AME was synthesized for comparison purpose. In contrast, the

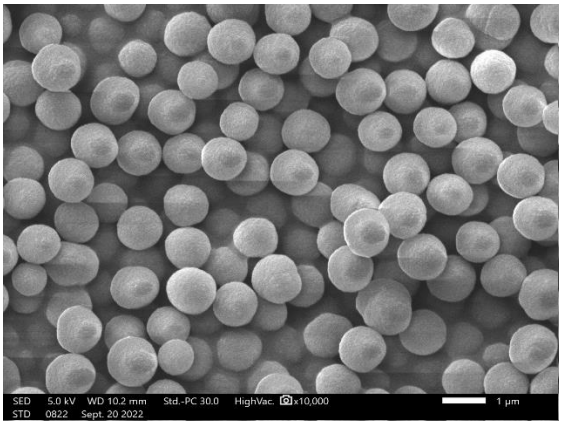
mean diameter size of MIP (MAA) of AME was 0.52 µm, which was smaller than that NIP (MAA) of 0.80 µm. The presence of template molecule in the MIP polymerization reaction had influence on the particle size of the synthesized MIP (Lu et al., 2020). In addition, smaller particles size of polymers had larger surface area-to volume ratio and therefore it had better binding capability with more substance on its surface (Nabavi et al., 2017).

4.3.3 FESEM Analysis of MIPs of ATZ

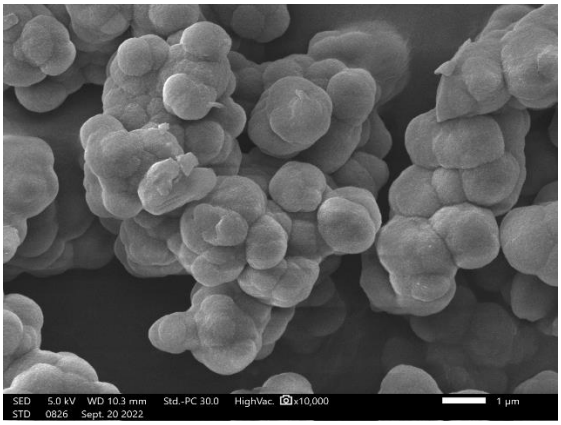
Both MIP (MAA) and MIP (2VP) of ATZ were nearly uniform in size and spherical in shape while MIP (AAm) of ATZ was not uniform in size and irregular in shape as shown in Figure 4.10. However, precipitation polymerization is anticipated to produce microspherical polymer particles with regular size and shape (Xiao et al., 2018). These are due to the polymer chains continuing to grow individually without overlapping or merging during precipitation polymerization, capturing newly formed oligomers and monomers in a diluted reaction system, forming microspheres upon separation from the solution, meanwhile, the presence of irreversible chain transfer reactions causes aggregation of small globular particles into larger irregular particles (Xu et al., 2011).

The FESEM analysis of MIP (MAA) and MIP (2VP) of ATZ as shown in Figure 4.10 exhibited relatively uniform sizes which is crucial for consistent performance and reproducibility. The uniform particle size distribution ensures that the synthesized polymers can be densely packed, optimizing their adsorption capacity and promoting efficient ATZ removal. Moreover, the surface of the synthesized MIP (MAA), MIP (AAm) and MIP (2VP) of ATZ appeared rough and uneven, indicating the presence of numerous pores and cavities throughout the material. These porous structures are important for the effective adsorption and recognition of ATZ, the target molecule. The presence of these pores also suggests that

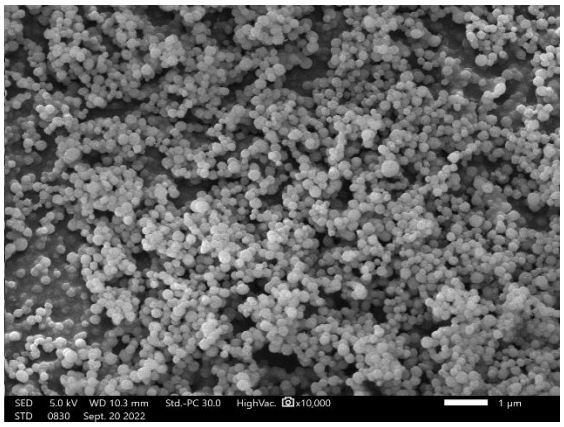
the MIPs can provide a large surface area for molecular interactions, enhancing their binding capacity and selectivity (Chen et al., 2019).



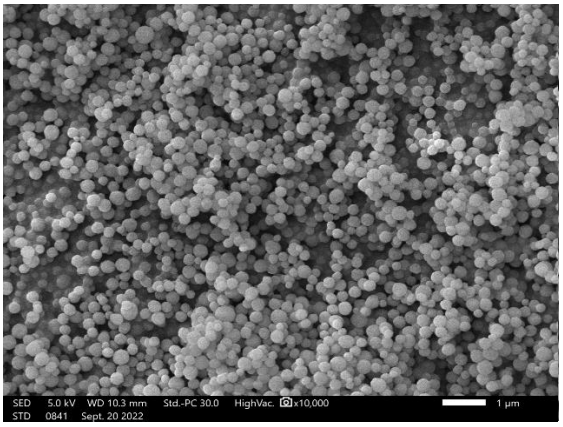
MIP (MAA) of ATZ



MIP (AAm) of ATZ



MIP (2VP) of ATZ



NIP (2VP) of ATZ

Figure 4.10: FESEM Micrographs of MIPs and NIP of ATZ

The calculated mean diameter of MIP (MAA), MIP (AAm) and MIP (2VP) of ATZ were 1.04 µm, 1.20 µm and 0.30 µm, respectively (Appendix 3). Among the three MIPs of ATZ, MIP (2VP) had the smallest mean diameter of polymer particles. This may be due to the choice of functional monomer for the MIP synthesis, as well as the polymerization conditions such as duration (6 h) and temperature of synthesis. These factors can affect the polymer particles of the synthesized polymers.

In comparison, NIP (2VP) was uniform and spherical in shape but had a slightly larger diameter of 0.40 µm than that of MIP (2VP) of ATZ. This explains that smaller particle size results in a larger surface area-to-volume ratio, allowing MIP to effectively adsorbed a greater amount of template or target molecule on its surface and thus enhance its binding capacity (Nabavi et al., 2017).

4.4 Batch Binding Analysis

The studies on batch binding were conducted to evaluate the rebinding efficiencies of the fabricated MIPs and NIPs of Triazine herbicides at various contact times.

4.4.1 Batch Binding Analysis of MIPs of CYZ

Figure 4.11 presented the rebinding efficiency of the synthesized MIP (MAA), MIP (AAm) and MIP (4VP) of CYZ as calculated in Appendix 4, Appendix 5, and Appendix 6, respectively. These MIPs of CYZ showed a similar trend as the rebinding efficiencies of MIP (MAA), MIP (AAm) and MIP (4VP) of CYZ were increasing with the increasing contact time until 240 min, and then the rebinding efficiencies were decreasing gradually until 300 min. This indicated that at a contact time of 240 min, the rebinding of MIPs with the CYZ template had been achieved and the adsorption phase had reached its equilibrium.

At 240 min, MIP (MAA), MIP (AAm) and MIP (4VP) of CYZ attained their highest rebinding efficiencies of 53.87%, 83.30% and 60.14%, respectively. MIP (AAm) of CYZ had the highest rebinding efficiency than that MIP (MAA) and MIP (4VP) of CYZ, indicating that the mixture of CYZ (template), AAm (neutral functional monomer), EGDMA (cross-linker), AIBN (initiator) and toluene (porogen) are the best combination of a pre-polymerization mixture to produce imprinted polymers with higher binding efficiency. This is because a suitable choice of functional monomer in MIP synthesis provides stronger

interactions with the template molecule to generate more stable template-monomer complexes, resulting MIPs with greater imprinting effect (Zhong et al., 2018; Sánchez-González et al., 2019; Wu et al., 2019). It was clear that MIP (AAm) of CYZ had the highest rebinding efficiency with CYZ and therefore, the batch binding study on the NIP (AAm) was also conducted for comparison purposes.

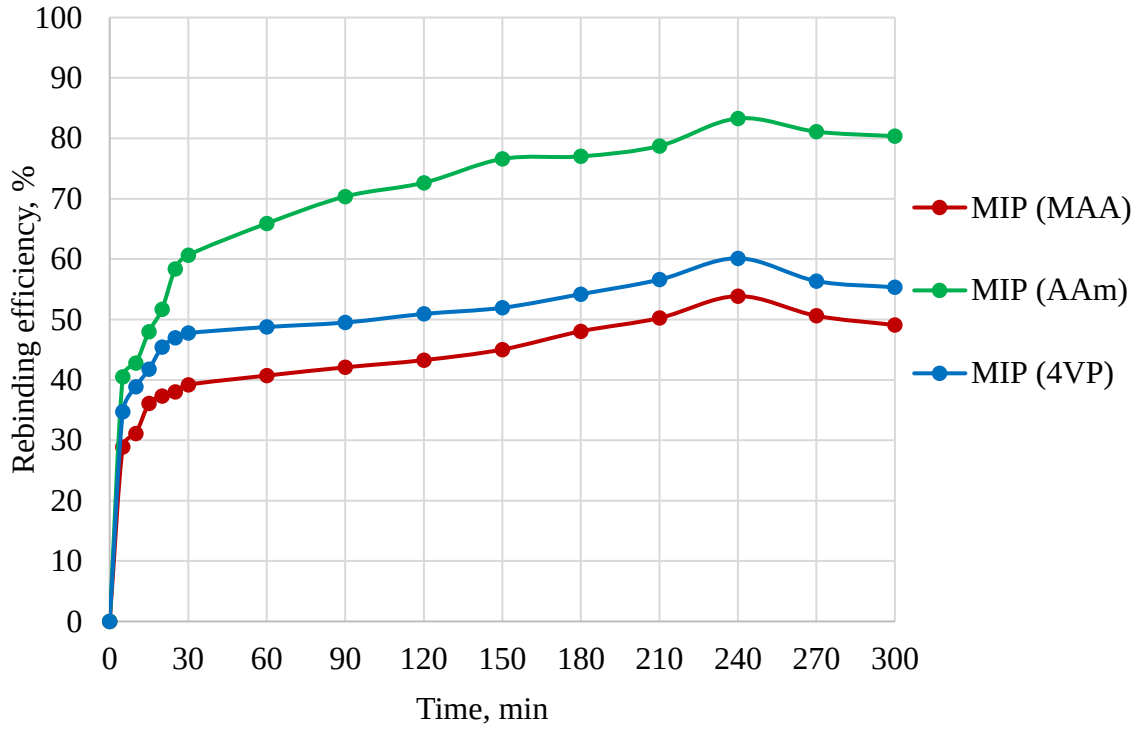


Figure 4.11: Batch Binding of MIPs of CYZ

Figure 4.12 indicated that the rebinding efficiency of NIP (AAm) also had a similar trend but is much lower than that of MIP (AAm) of CYZ. The highest rebinding efficiency of NIP (AAm) was recorded at 240 min, which was only 56.17% (Appendix 7), much lower than the rebinding efficiency of MIP (AAm) of CYZ. This is because NIP (AAm) was synthesized without the presence of a CYZ template and therefore having non-specific binding sites. NIP had lower binding efficiency because it lacked specific recognition sites complementary to the template molecule (Arabzadeh and Abdouss, 2010). Therefore, MIP

(AAm) and NIP (AAm) of CYZ were selected for further studies such as adsorption studies, selectivity tests and the application of polymers in environmental samples.

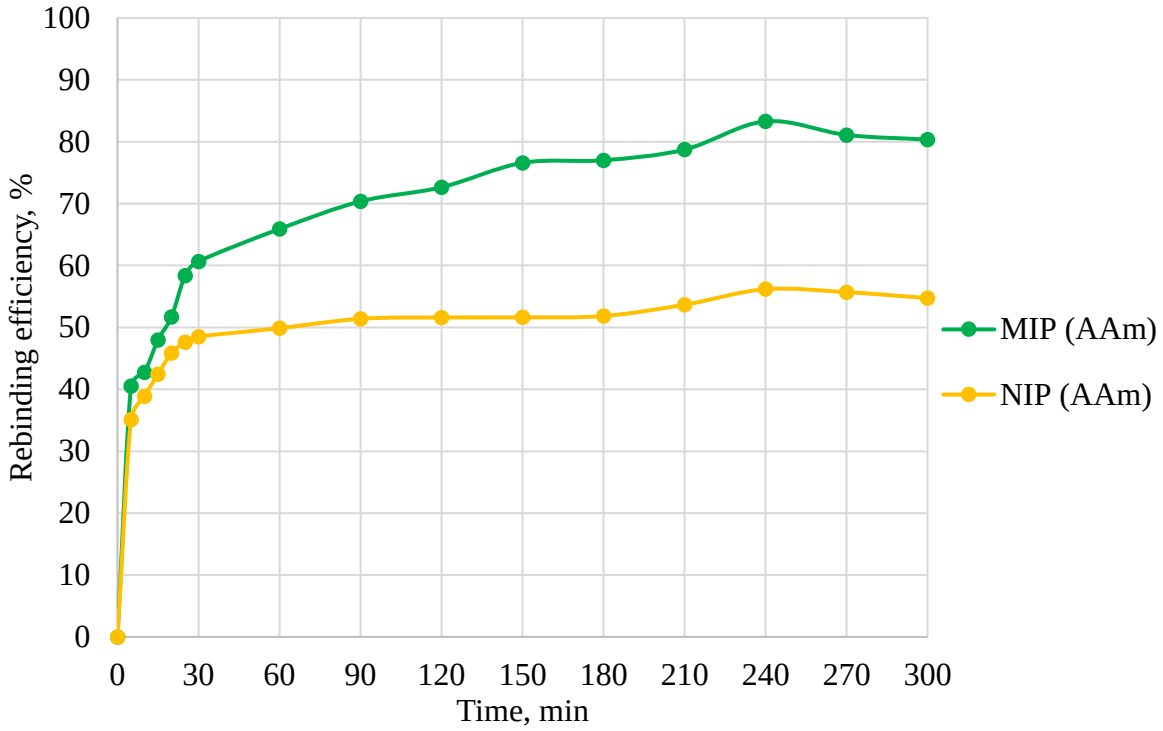


Figure 4.12: Batch Binding of MIP (AAm) and NIP (AAm) of CYZ

4.4.2 Batch Binding Analysis of MIPs of AME

Based on Figure 4.13, the amount of AME adsorbed by the three MIPs increased with the rebinding time, up to a maximum at 210 mins and after that, the adsorption of AME steadily decreased until 300 mins. Numerous vacant binding sites and less mass transfer resistance in the polymer cavity permit the active sites to capture the target analyte (template molecule), resulting the increase in rate of adsorption of the analyte on the surface of synthesized polymers, and hence increased the binding efficiency (Jusoh et al., 2022). Nevertheless, the quantity of active sites in the polymer cavity reduced with the increase of contact time as the binding sites are progressively attached with the analyte (template

molecule) and the mass transfer resistance of analyte to the binding sites also increased, causing the decrease in rate of adsorption, and thus slow decrease in binding efficiency (Abouzarzadeh et al., 2012).

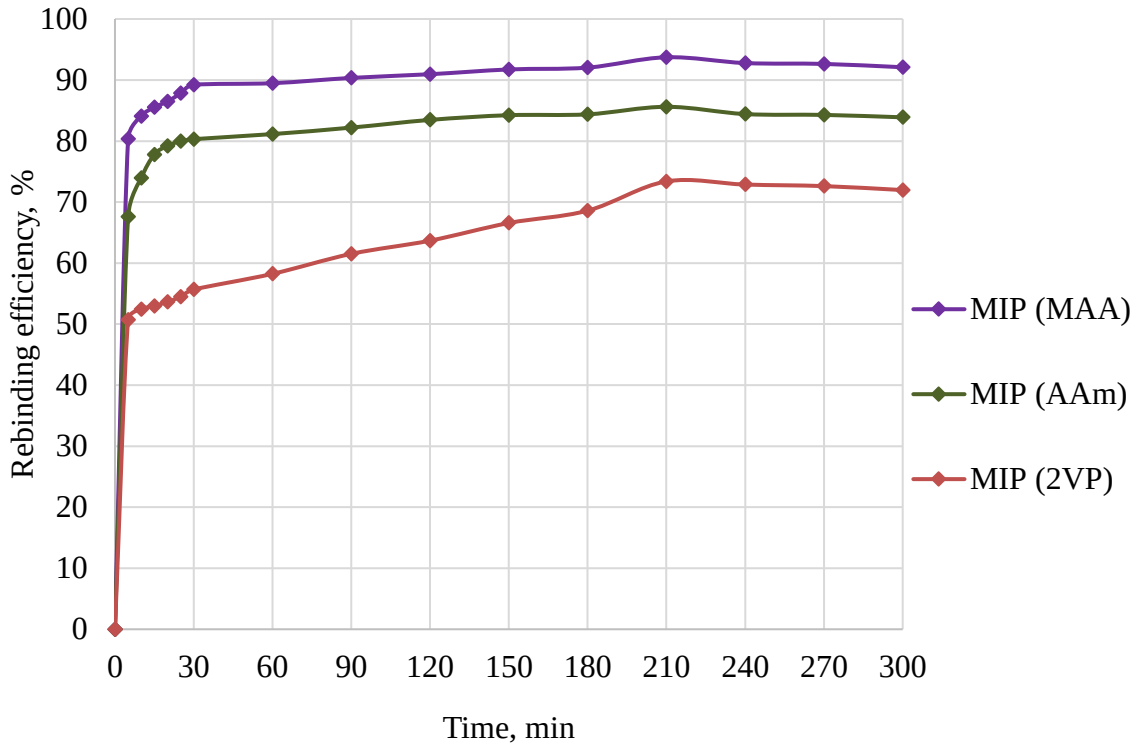


Figure 4.13: Batch Binding of MIPs of AME

As the contact time increased, more specific binding sites in the MIPs matrix can be occupied by AME template molecule until it reached its saturation, resulting the highest rebinding efficiencies at 210 mins. The increase in contact time of binding process leads to the increased in the adsorption of target analyte onto the synthesized polymeric surface until the equilibrium is attained (Yusof et al., 2017).

But after this point of saturation (210 mins), further increase in contact time leading to no rebinding of template after that or slight decrease in the polymers rebinding efficiencies because the available binding sites in the polymer matrix had been completely occupied with

AME. Since the binding sites in the polymeric surface have been adequately occupied with the target analyte, the extended contact time for the binding process did not affecting its percentage efficiency (Jusoh et al., 2022).

At 210 mins, MIP (MAA), MIP (AAm) and MIP (2VP) of AME attained their highest rebinding efficiencies with AME which were 93.73 %, 85.61 % and 73.87 %, respectively as shown in Figure 4.13 (Appendices 8-10). This indicated that the best contact time for the rebinding of MIPs with AME template was at 210 mins. When the adsorption phase of an analyte (template molecule) by the imprinted polymers had achieved its equilibrium, no obvious changes were observed in equilibrium concentration with additional rise in contact time.

Among these three MIPs of AME, MIP (MAA) had the highest rebinding efficiency with AME while MIP (2VP) had the lowest rebinding efficiency with AME. A suitable choice of functional monomer used in MIP synthesis allows stronger interactions between the template molecule and functional monomer which could generate more stable template-monomer complex before the polymerization takes place, and hence, resulting in production of MIPs with greater imprinting efficiency (Zhong et al., 2018; Sánchez-González et al., 2019; Wu et al., 2019). So, this showed that MIP made up of AME (template molecule) with MAA (acidic functional monomer) was the best combination of template-monomer to obtain the highest rebinding efficiency.

Figure 4.14 displayed the comparison on the rebinding efficiencies between MIP (MAA) and NIP (MAA) of AME. Both MIP (MAA) and NIP (MAA) of AME depicted similar trend as the rebinding efficiencies of imprinted and non-imprinted polymers were increased from 0 min to 210 mins and then further decreased until 300 mins.

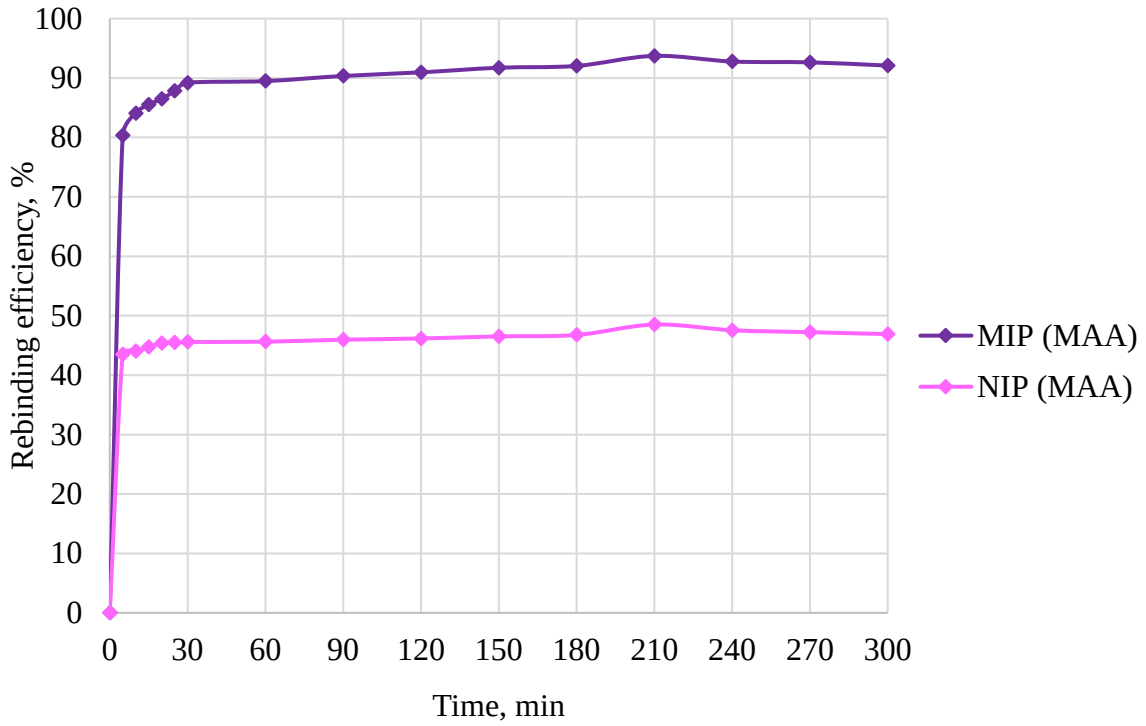


Figure 4.14: Batch Binding of MIP (MAA) and NIP (MAA) of AME

The highest rebinding efficiencies of both MIP (MAA) and NIP (MAA) of AME were 93.73 % and 48.52 %, respectively (Appendix 8 and Appendix 11). MIP (MAA) of AME had much higher rebinding efficiency than that NIP (MAA) due to the imprinting effect of AME in the MIP (MAA) cavity. The MIP particles with a larger surface area and total pore volume were displaying good imprinting effect (Hasanah et al., 2021). The imprinting effect is due to the addition of template molecule during MIP synthesis which produces more specific binding sites complementary with the template molecule. Viveiros et al. (2023) revealed that the presence of template molecule during the polymerization process of the MIP had generated several specific interactions that corresponds to the template molecule.

As expected, NIP (MAA) had much lower rebinding efficiency than that MIP (MAA) of AME due to no imprinting effect as AME was absent during NIP synthesis, hence lack of specific binding sites in the NIP cavity for the rebinding with AME.

4.4.3 Batch Binding Analysis of MIPs of ATZ

Figure 4.15 showed that the rebinding efficiencies of MIP (MAA), MIP (AAm) and MIP (2VP) towards the ATZ template molecule were increased as the contact time increased from 0 min to 15 mins and then gradually decrease from 20 mins to 300 mins.

The highest rebinding efficiencies of MIP (MAA), MIP (AAm) and MIP (2VP) towards the ATZ template molecule were attained at a contact time of 15 mins with rebinding efficiencies of 80.63 %, 74.71 % and 88.44 %, respectively (Appendices 12-14). This explained that 15 mins was the ideal contact time for complete binding between the vacant recognition sites in the MIPs with the ATZ template molecule, where the MIPs had reached their saturation point. This also demonstrated rapid binding property of the MIPs serves as a crucial validation of their successful synthesis and affirms their efficacy for facilitating time-efficient extraction of target or template molecule (Zhao et al., 2019).

Any further increase in contact time may lead to slightly lower rebinding efficiencies between MIPs and ATZ template molecules due to the lack of empty recognition sites and increased mass transfer in the MIPs matrixes.

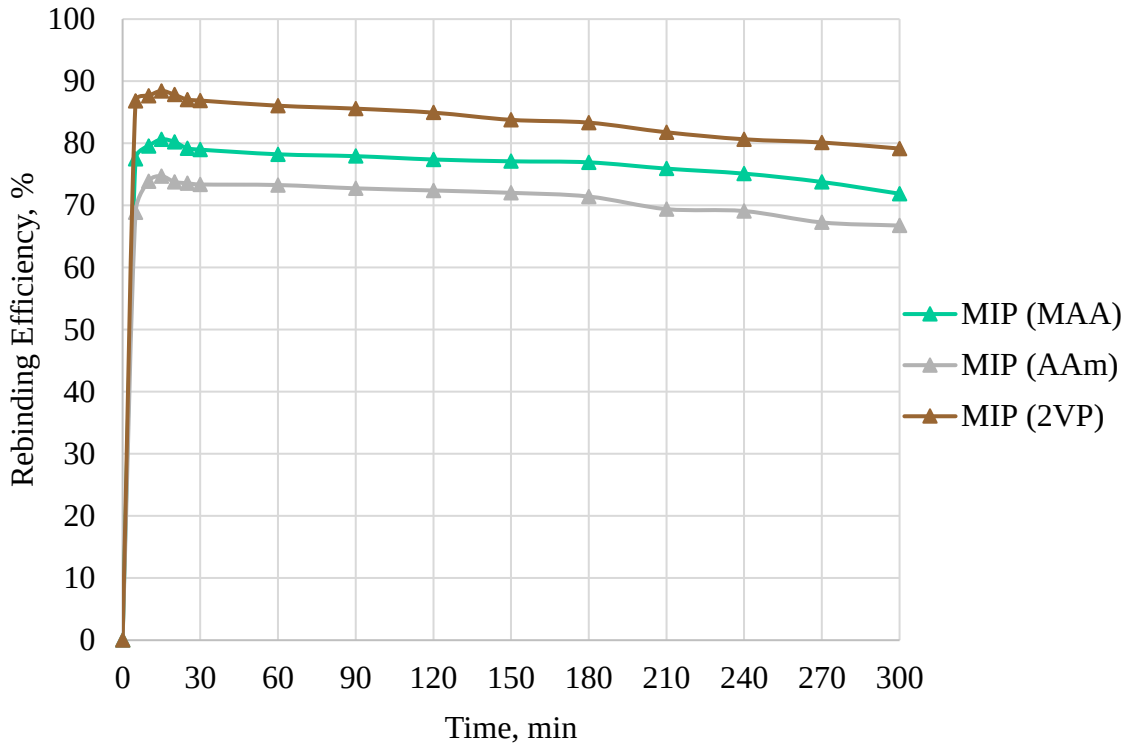


Figure 4.15: Batch Binding of MIPs of ATZ

Generally, the MIP (MAA), MIP (AAm) and NIP (AAm) of ATZ had exceptional batch binding efficiencies due to factors such as the washing and drying methods of MIPs. Optimizing the washing method is crucial for removing non-selective sites and irregularly shaped cavities with weaker molecule adsorption, enabling the interaction of target molecules with specific cavities, and eliminating co-extracted non-target substances, hence increasing the binding efficiency (Chapuis et al., 2003). The binding efficiency of MIPs is also influenced by the drying process, as incomplete drying leading to residual water after sample application can alter the binding affinity between MIPs and ATZ (Pap et al., 2002).

The synthesized MIPs of ATZ were arranged in ascending order based on their percentage rebinding efficiencies as followed: MIP (AAm) > MIP (MAA) > MIP (2VP). Among these three synthesized MIPs, MIP (2VP) of ATZ had the highest rebinding towards

the ATZ template molecule while MIP (AAm) of ATZ had the lowest rebinding efficiency towards the ATZ template molecule. The uniform size and spherical shape of the synthesized polymer particles are factors affecting the highest rebinding efficiency of MIP (2VP) towards the ATZ template molecule. Besides that, MIP (2VP) of ATZ had the smallest mean pore diameter (0.30 µm) than that MIP (MAA) of ATZ (1.04 µm) and MIP (AAm) of ATZ (1.20 µm) which provides a larger surface area for the binding affinity of MIP (2VP) with the ATZ template molecule. In contrast, MIP (MAA) particles had regular size and spherical shape but larger mean pore diameter while MIP (AAm) particles had irregular size and shape as well as the largest mean pore diameter.

Several other factors influence the highest rebinding efficiency of MIP (2VP) of ATZ towards the ATZ template molecule as compared with the other two MIPs of ATZ such as its ionic interactions (Vasapollo et al., 2011), hydrophobicity (Cui et al., 2020), template-functional monomer compatibility (Ibarra et al., 2020), complementary binding sites (Nikoleli et al., 2018) and polymer network structure (Cui et al., 2020).

The 2VP is the best functional monomer for the MIP synthesis of ATZ because of its ability to form strong interactions with the ATZ template molecule. The presence of the basic pyridine ring in 2VP allows for specific interactions with the ATZ template molecule, leading to a more stable and high binding affinity between MIP (2VP) and ATZ template molecule. Other than that, the hydrophobic interactions between 2VP and the ATZ's hydrophobic regions further contribute to higher binding efficiency in MIP (2VP). AAm, being a neutral functional monomer, can also exhibit some hydrophobic interactions, but it may not be as strong or specific as those formed by 2VP. The polymeric structure of MIP (2VP) of ATZ may provide more complementary binding sites for the ATZ template

molecule binding because MIP (2VP) of ATZ can accommodate the shape and size of the ATZ template molecule more effectively than MIP (MAA) of ATZ and MIP (AAm) of ATZ due to the presence of the pyridine ring and its associated aromatic interactions. This complementary binding site enhances the rebinding efficiency of MIP (2VP) of ATZ by facilitating the formation of stronger interactions and promoting better spatial fit.

Moreover, the compatibility between the ATZ template molecule and 2VP functional monomer is another important factor influencing rebinding efficiency. 2VP exhibits a higher degree of chemical compatibility with the ATZ template molecule compared to MAA and AAm because the specific chemical groups present in the 2VP functional monomer enable a more favourable interaction with ATZ, resulting in improved binding efficiency. The specific combination of 2VP with the EGDMA cross-linker may lead to a more porous and accessible structure, allowing for efficient binding and rebinding of the ATZ template molecule. The network structure of the MIP (MAA) of ATZ and MIP (AAm) of ATZ may differ slightly, affecting their overall binding efficiencies.

Figure 4.16 depicted the comparison of the rebinding efficiency between the MIP (2VP) and NIP (2VP) of ATZ at different contact times. The rebinding efficiencies of MIP (2VP) and NIP (2VP) of ATZ increased from 0 min to 15 mins and then decreased from 20 mins to 300 mins. Both MIP (2VP) and NIP (2VP) of ATZ attained their highest rebinding efficiencies at a contact time of 15 mins with 88.44 % (Appendix 14) and 51.04 % (Appendix 15), respectively.

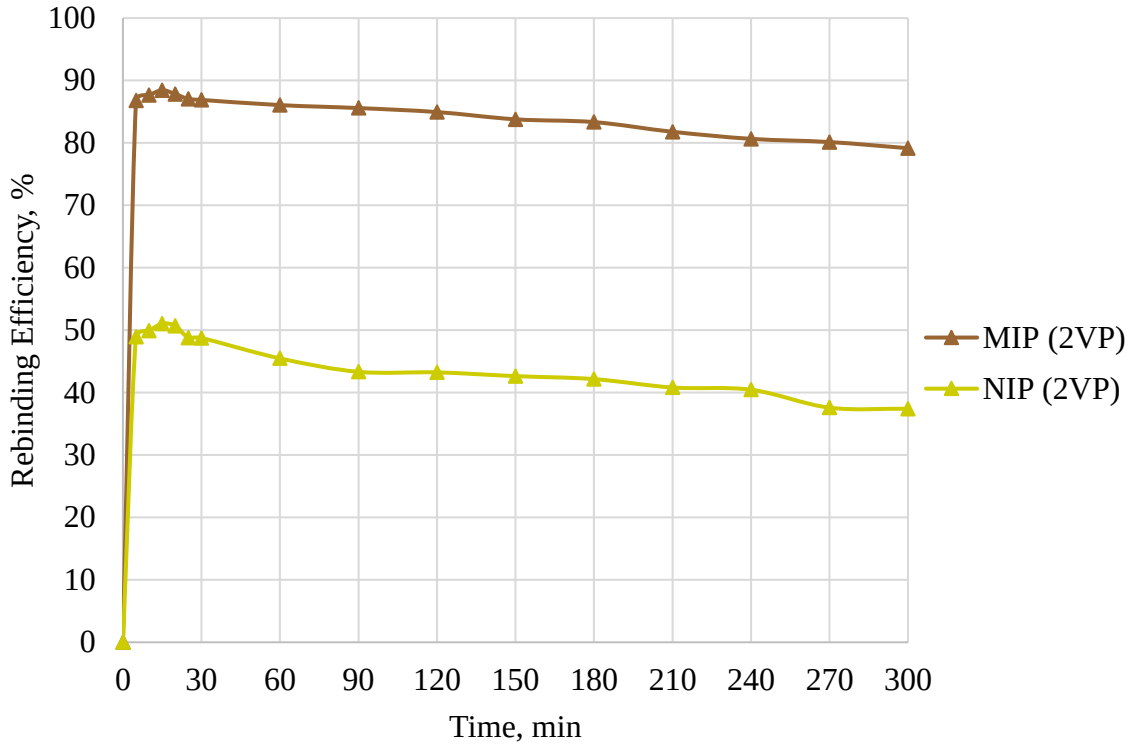


Figure 4.16: Batch Binding of MIP (2VP) and NIP (2VP) of ATZ

At various contact times, MIP (2VP) of ATZ exhibited much higher rebinding efficiencies as compared to NIP (2VP). The presence of the ATZ template molecule during MIP (2VP) of ATZ synthesis leads to the formation of complementary recognition sites, enabling specific interaction with the ATZ template molecule. As a result, MIP (2VP) of ATZ can bind to the ATZ template molecule more effectively, leading to enhanced binding affinity. In contrast, NIP (2VP) lacks these specific recognition sites, resulting in non-selective interactions with the ATZ template molecule. Lack of the imprinting effect may lead to lower binding affinities (Arabzadeh and Abdouss, 2010). Hence, the difference in rebinding efficiency between MIP and NIP has proven the success of the MIP imprinting process which bears physical and chemical characteristics of ATZ within the MIP matrix (Zhao et al., 2019).

4.5 Kinetic Study

Three different kinetic models such as pseudo-first-order and pseudo-second-order were applied in kinetic studies to distinguish the adsorption process of Triazine herbicides on the surface of the MIPs of Triazine herbicides.

4.5.1 Kinetic Study of MIP (AAm) of CYZ

Only MIP (AAm) of CYZ was selected for kinetic study to find the most suitable kinetic model that describe the adsorption process of CYZ on the surface of MIP (AAm) of CYZ. Figure 4.17 and Figure 4.18 indicated the adsorption process of CYZ on the surface of the MIP (AAm) based on the two different kinetic models known as pseudo-first-order and pseudo-second-order, respectively.

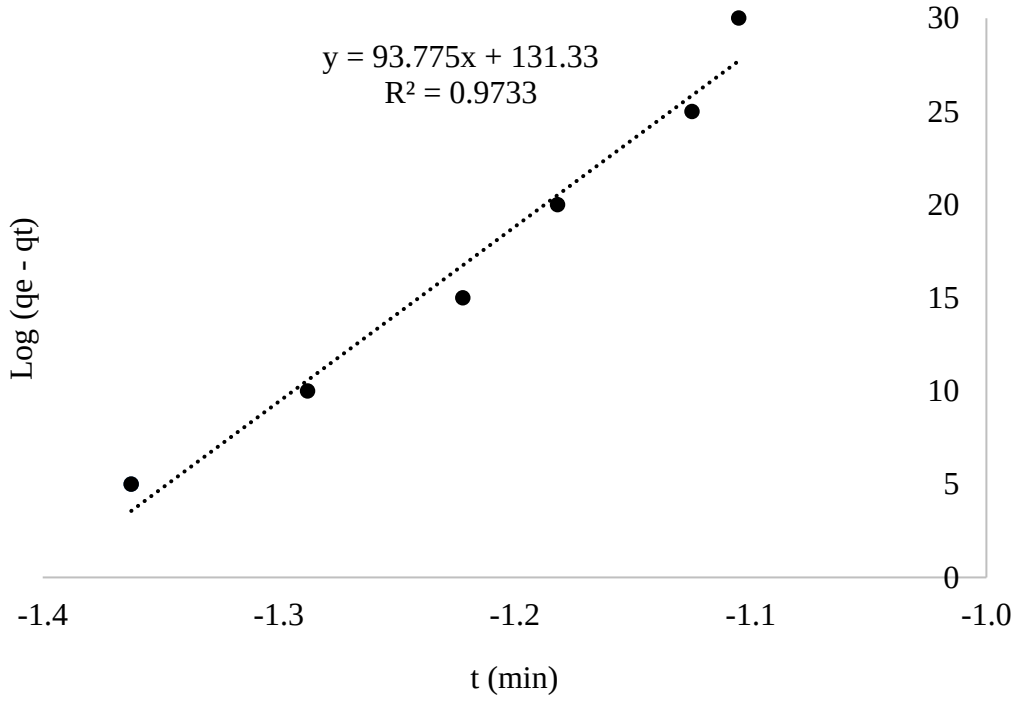


Figure 4.17: Pseudo-First-Order Kinetic Model of MIP (AAm) of CYZ

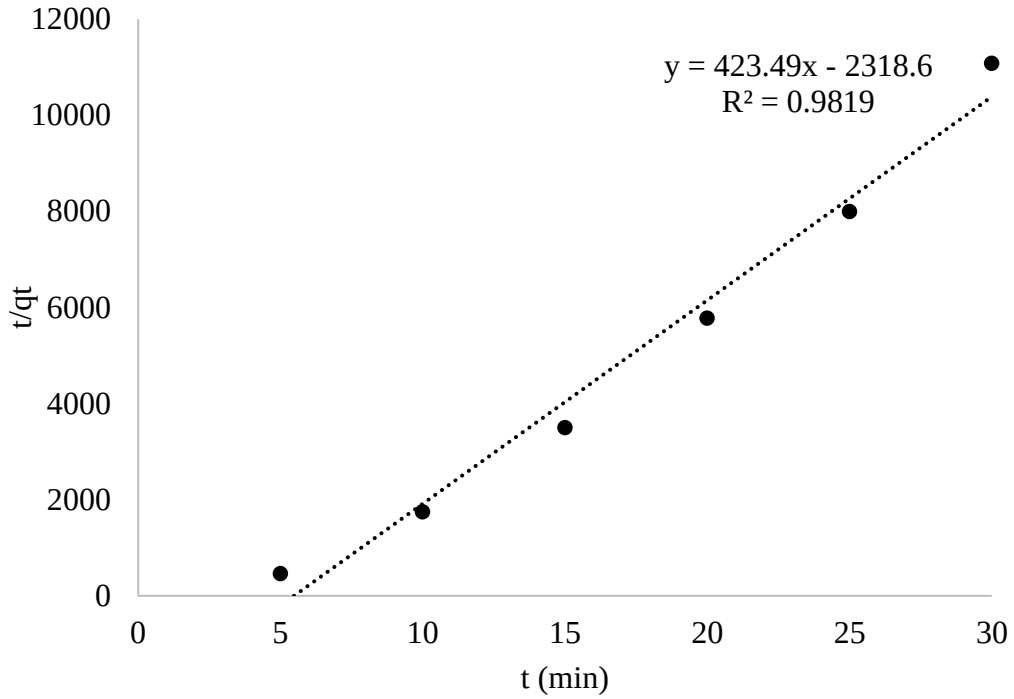


Figure 4.18: Pseudo-Second-Order Kinetic Model of MIP (AAm) of CYZ

In comparison with the two kinetic models (Table 4.2), the pseudo-second-order kinetic model had the greatest correlation coefficient value that was closest to 1 ($R^2 = 0.9819$) as compared to the pseudo-first-order kinetic model ($R^2 = 0.9733$) As a result, the pseudo-second-order kinetic model was the best-fitted kinetic model for MIP (AAm) of CYZ, showing that the CYZ molecule and the MIP (AAm) were involved in the rate-determining stage of the adsorption process. The chemisorption process also entailed the creation of a strong chemical bond interactions between CYZ as the solute and MIP as the adsorbent material. Furthermore, the adsorption rate of CYZ as the solute is proportional to the accessible binding sites on the MIP (AAm) of CYZ as the adsorbent material, according to this pseudo-second-order kinetic model.

Table 4.1: Kinetic Models Examined on MIP (AAm) of CYZ

Kinetic models of MIP (AAm) of CYZ					
Pseudo-1st-order			**Pseudo-2nd-order**		
q_{e1} (mg/g)	**K_1 (1/h)**	**R^2**	**q_{e2} (mg/g)**	**K_2 (g/mgh)**	**R^2**
1.08616E+57	-93.775	0.9733	0.0024	77.350	0.9819

4.5.2 Kinetic Study of MIP (MAA) of AME

The kinetic results of AME adsorption onto the selected MIP of AME which was MIP (MAA) were evaluated by using different kinetic models including pseudo-first-order and pseudo-second-order as depicted in Figure 4.19 and Figure 4.20, respectively. The calculated values of the amount of AME (absorbate) adsorbed at equilibrium time (qe), rate constants (k) and correlation coefficients (R^2) were given in Table 4.3.

Between the two kinetic models, the pseudo-second-order kinetic model had the highest correlation coefficient (R^2) value of 0.9633 and therefore it was selected as the best fitted kinetic model for describing the AME (absorbate) uptake by the MIP (MAA) during the adsorption process. This explained that the chemical adsorption was primarily affecting the adsorption rates of absorbate (Bedin et al., 2016).

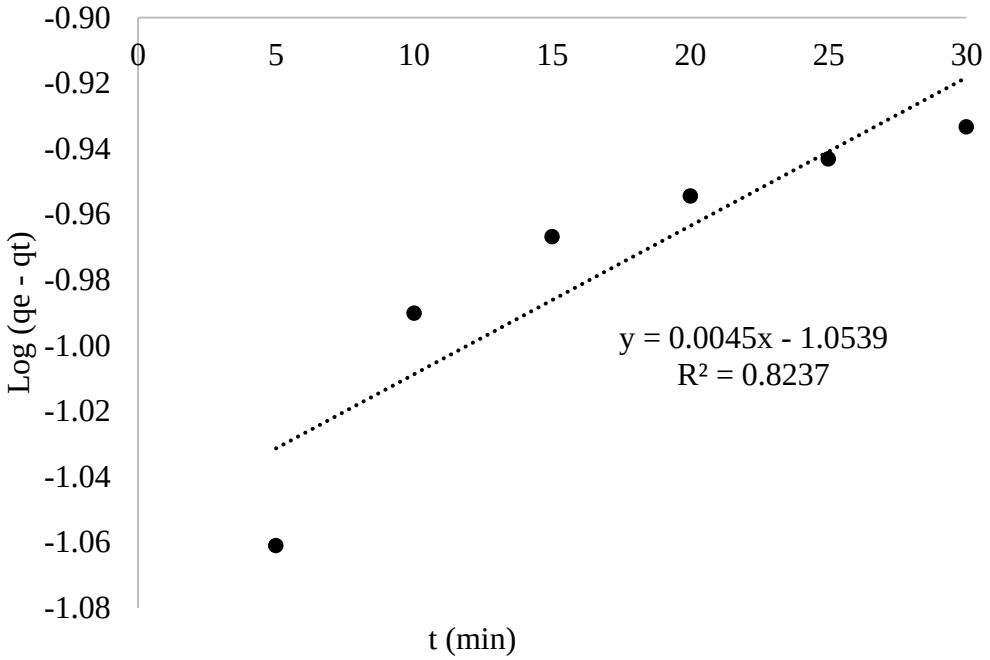


Figure 4.19: Pseudo-First-Order Kinetic Model of MIP (MAA) of AME

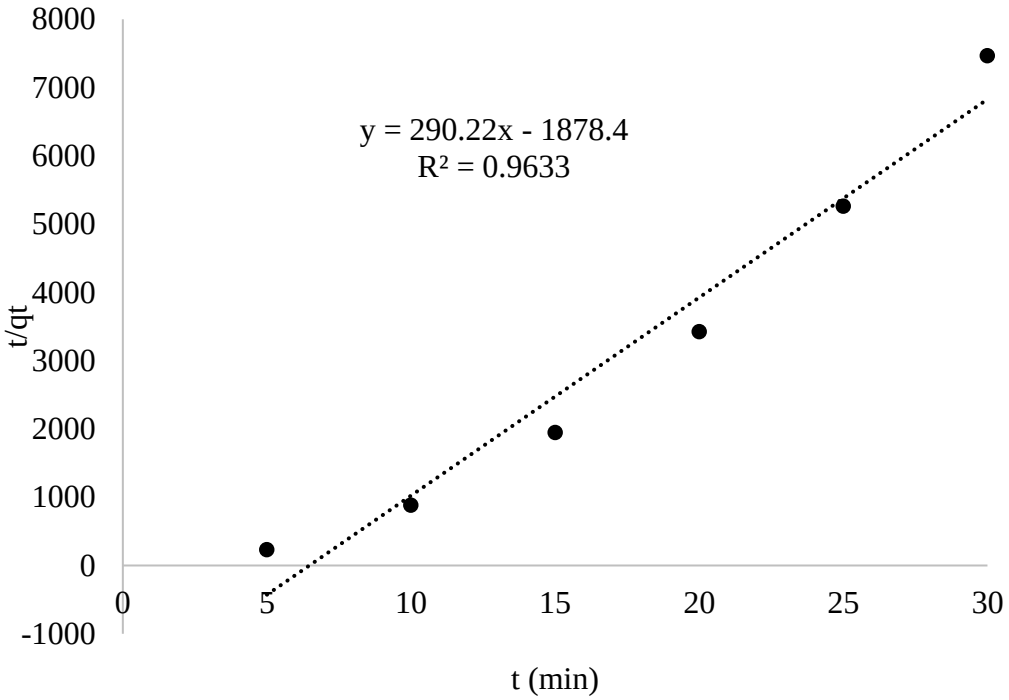


Figure 4.20: Pseudo-Second-Order Kinetic Model of MIP (MAA) of AME

Table 4.2: Kinetic Models Examined on MIP (MAA) of AME

Kinetic models of MIP (AAm) of CYZ					
Pseudo-1st-order			**Pseudo-2nd-order**		
q_{e1} (mg/g)	**K_1 (1/h)**	**R^2**	**q_{e2} (mg/g)**	**K_2 (g/mgh)**	**R^2**
0.3486	-0.0045	0.8237	0.0034	44.840	0.9633

4.5.3 Kinetic Study of MIP (2VP) of ATZ

Two kinetic isotherm models including the pseudo-first-order model and pseudo-second-order model were applied to experimental data of MIP (2VP) as shown in Figure 4.21 and Figure 4.22, respectively.

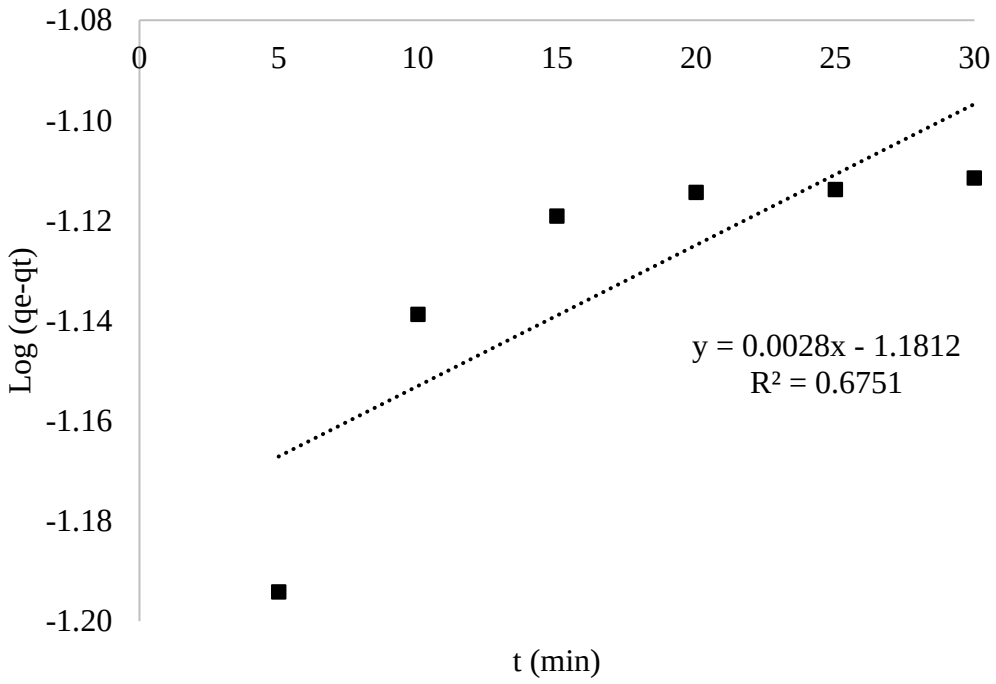


Figure 4.21: Pseudo-First-Order Kinetic Model of MIP (2VP) of ATZ

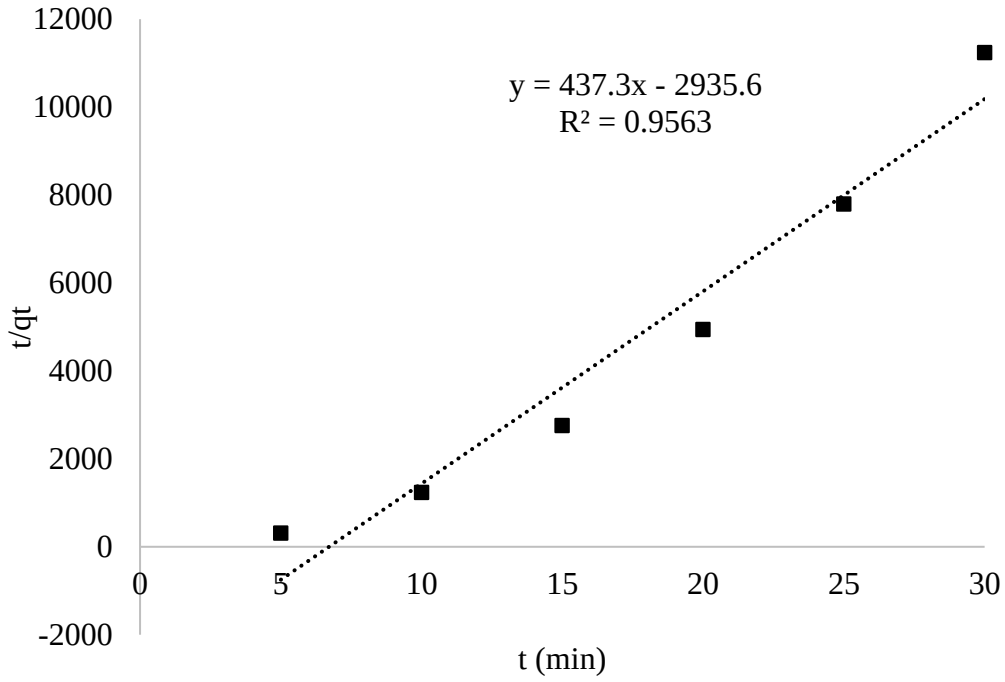


Figure 4.22: Pseudo-Second-Order Kinetic Model of MIP (2VP) of ATZ

Based on Figure 4.21 and Figure 4.24, the amount of ATZ adsorbed at equilibrium time (qe), rate constants (k) and correlation coefficients (R^2) were calculated and tabulated as shown in Table 4.4. The correlation coefficient value is important to distinguish the adsorption process of the MIP. Based on these results, the correlation coefficients or R^2 values of the pseudo-first-order model and pseudo-second-order model were 0.6751 and 0.9563, respectively. This indicated that the pseudo-second-order is the best kinetic model to describe the kinetic isotherm of MIP (2VP) of ATZ with the highest value of correlation coefficients than the other two kinetic models.

This also assumes that the rate-limiting step in the adsorption process (Men et al., 2012) is the chemisorption between the ATZ molecules and the binding sites of the MIP (2VP) surface. The rate of adsorption is proportional to the product of the remaining

concentration of ATZ and the number of available binding sites in the MIP (2VP) of ATZ. Moreover, the chemisorption behaviour of the adsorbent as indicated by the pseudo-second-order model highlights the essential factors in the ATZ removal process such as the significant influence of electron transfer, surface complexation and supplementary interactions species shared between the adsorbent and ATZ (Magesh et al., 2022).

Table 4.3: Kinetic Models Examined on MIP (2VP) of ATZ

Pseudo-1st-order			**Pseudo-2nd-order**			**Intra-particle diffusion**			
q_{e1} (mg/g)	**K_1 (1/h)**	**R^2**	**qe2 (mg/g)**	**K_2 (1/h)**	**R^2**	**Co (mg/L)**	**Kdiff (mg/h $^{1/2}$g)**	**C**	**R^2**
0.3069	-0.0028	0.6751	0.0023	65.1421	0.9563	0.9210	-0.0039	0.0222	0.8696

4.6 BET Analysis

The Brunauer-Emmett-Teller (BET) analysis was performed to distinguish the surface area, average pore radius and total pore volume of selected MIPs and NIPs of Triazine herbicides.

4.6.1 BET Analysis of MIP (AAm) of CYZ

The surface area (21.019 m^2/g), average pore radius (104.900 Å) and total pore volume (1.868 cm^3/g) of MIP (AAm) of CYZ were greater than that of NIP (AAm), as displayed in Table 4.5. This is because the addition of the CYZ template molecule in the MIP preparation generated specific binding sites that influenced the particle growth. The surface area of polymer particle is also influenced by its particle size. In previous section, the FESEM results revealed that MIP (AAm) had smaller particle size than the NIP (AAm)

of 0.86 µm and 0.98 µm, respectively, and therefore MIP (AAm) of CYZ (21.019 m^2/g) had larger surface area than the NIP (AAm) of CYZ (10.870 m^2/g). Nabavi et al. (2017) explained that polymers with smaller particle size had larger surface area-to volume ratio which later contributing to improved binding efficiency with the target compound.

Table 4.4: BET Analysis of MIP (AAm) and NIP (AAm) of CYZ

Properties	**MIP (AAm)**	**NIP (AAm)**
Surface area (m^2/g)	21.019	10.870
Average pore radius (Å)	104.900	91.824
Total pore volume (cm^3/g)	1.868	0.025

Table 4.5 also depicted the average pore radius of MIP (AAm) of CYZ was 104.900 Å, indicating a porous polymer. In this research, toluene was selected as the porogen for the MIP synthesis which also contributed to the morphological characteristics of the resulting polymers. It has been reported that the concentration, volume, and structure of the porogen can affect the morphology, pore volume and surface area of the synthesized MIP and NIP (Reimhult et al., 2008).

4.6.2 BET Analysis of MIP (MAA) of AME

The surface area (13.6801 m^2/g), average pore radius (103.1369 Å) and total pore volume (0.03178 cm^3/g) of MIP (MAA) of AME were larger than the surface area (11.593 m^2/g), average pore radius (92.9228 Å) and total pore volume (0.029892 cm^3/g) of NIP (MAA) as shown in Table 4.6. A larger surface area of MIP (MAA) of AME as compared

to the NIP (MAA) of AME was due to the smaller particle size of MIP (MAA) of AME (0.52 µm) than that NIP (MAA) of AME (0.80 µm). It was reported that the smaller the particle size of polymers, the larger its surface areas (Nabavi et al., 2017). A larger surface area of MIP than that NIP showed that the specific binding sites were generated in the MIP cavities for the recognition of the template compound, resulting in greater MIP adsorption capacity (Sadia et al., 2022).

Table 4.5: BET Analysis of MIP (MAA) and NIP (MAA) of AME

Properties	**MIP (MAA)**	**NIP (MAA)**
Surface area (m^2/g)	13.6801	11.593
Average pore radius (Å)	103.1369	92.9228
Total pore volume (cm^3/g)	0.03178	0.029892

4.6.3 BET Analysis of MIP (2VP) of ATZ

Based on Table 4.7, the surface area of the MIP (2VP) was reported as 41.5923 m^2/g, while the NIP (2VP) had a surface area of 28.6062 m^2/g. The higher surface area of the MIP (2VP) suggested that it had a greater accessible area for molecular recognition and binding of the ATZ template molecule. This is desirable as it provides more binding sites for ATZ template molecules and increases the selectivity of the MIP (2VP) than that of the NIP (2VP).

The average pore radius of the MIP (2VP) of ATZ was stated as 170.5645 Å, whereas the NIP (2VP) had an average pore radius of 151.8012 Å. The larger average pore radius in the MIP (2VP) of ATZ indicates the presence of relatively larger pores within the polymer

matrix. These pores contribute to better accessibility of the ATZ template molecule to the binding sites within the MIP (2VP), facilitating efficient binding and recognition of the ATZ template molecule. The larger average pore radius is advantageous as it allows the template molecules to diffuse more freely within the polymer and enhances the rebinding efficiency.

Table 4.6: BET Analysis of MIP (2VP) and NIP (2VP) of ATZ

Properties	**MIP (2VP)**	**NIP (2VP)**
Surface area (m^2/g)	41.5923	28.6062
Average pore radius (Å)	170.5645	151.8012
Total pore volume (cm^3/g)	0.1774	0.1086

The total pore volume of the MIP (2VP) of ATZ was calculated as 0.1774 cm^3/g, while the NIP (2VP) had a total pore volume of 0.1086 cm^3/g (Table 4.7). The higher total pore volume in the MIP (2VP) of ATZ implied a greater volume available for the ATZ template molecule to interact and bind within the polymer matrix. The increased pore volume provides more space for the template molecules to reside, promoting the higher binding capacity and potentially enhancing the selectivity of the MIP.

The presence of template molecule in the MIP synthesis allows the production of MIP with larger surface area, average pore radius and total pore volume as compared to the NIP, thus leading to improved recognition performance for the template molecule (Chen et al., 2014). Hence, the higher surface area, average pore radius and total pore volume of the MIP (2VP) of ATZ than that of NIP (2VP) in Table 4.7 had shown that MIP (2VP) of ATZ

had a more favourable structure for ATZ recognition and binding. These properties are essential for achieving high specificity and affinity of MIP (2VP) towards ATZ template molecule, making the MIP (2VP) an efficient and selective material for ATZ detection and removal applications.

4.7 EDX Analysis

EDX analysis is a commonly used technique to determine the elemental composition in material science and polymer research, including the analysis of molecularly imprinted polymers (MIPs).

4.7.1 EDX Analysis of MIP (AAm) of CYZ

The amount of main chemical elements in the synthesized MIP (AAm) of CYZ such as carbon (C) and oxygen (O) were determined by using EDX analysis. Figure 4.23 showed a significant amount of carbon (82.88 %) and oxygen (17.12%) that were present in the MIP (AAm). This explained that carbon was the main element present in the polymer backbone of MIP (AAm) of CYZ due to the presence of AAm functional monomer and EGDMA cross-linker during MIP synthesis.

The high carbon-rich content (Figure 4.23) in the synthesized MIP (AAm) of CYZ also implied that this polymer is rigid and capable to withstand extreme conditions. The oxygen content of 17.12% was detected in MIP (AAm) of CYZ (Figure 4.23) due to the presence of oxygen atom in AAm (functional monomer), EGDMA (cross-linker) and AIBN (initiator). Moreover, MIP (AAm) of CYZ may have the functional groups containing oxygen due to the polymerization reaction or to improve particular interactions with the CYZ template molecule.

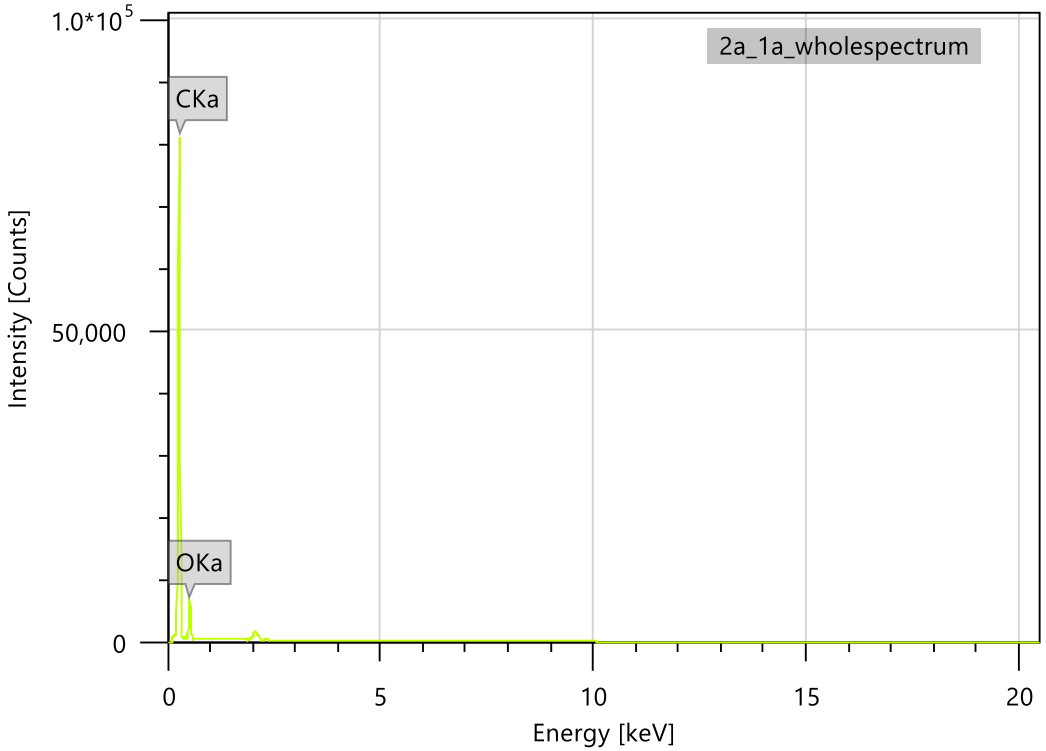


Figure 4.23: EDX Analysis of MIP (AAm) of CYZ

4.7.2 EDX Analysis of MIP (MAA) of AME

The EDX analysis in Figure 4.24 of MIP (MAA) of AME demonstrated the mass percentage of carbon (C) element in MIP (MAA) was 88.52 %, much higher than that oxygen (O) element which was only 11.48 %, indicated that the C was the main element in the backbone of MIP (MAA) of AME. This is because MIP (MAA) was made up of carbon-based compounds which MAA as the functional monomer, EGDMA as the cross-linker and AIBN as initiator. Due to its carbon-rich content, the synthesized MIP (MAA) of AME had high stability, mechanical strength, and resistance to extreme conditions. MIP (MAA) of AME also consisted of 11.48 % oxygen content as a result of polymerization process or to increase specific interactions with the AME (template molecule).

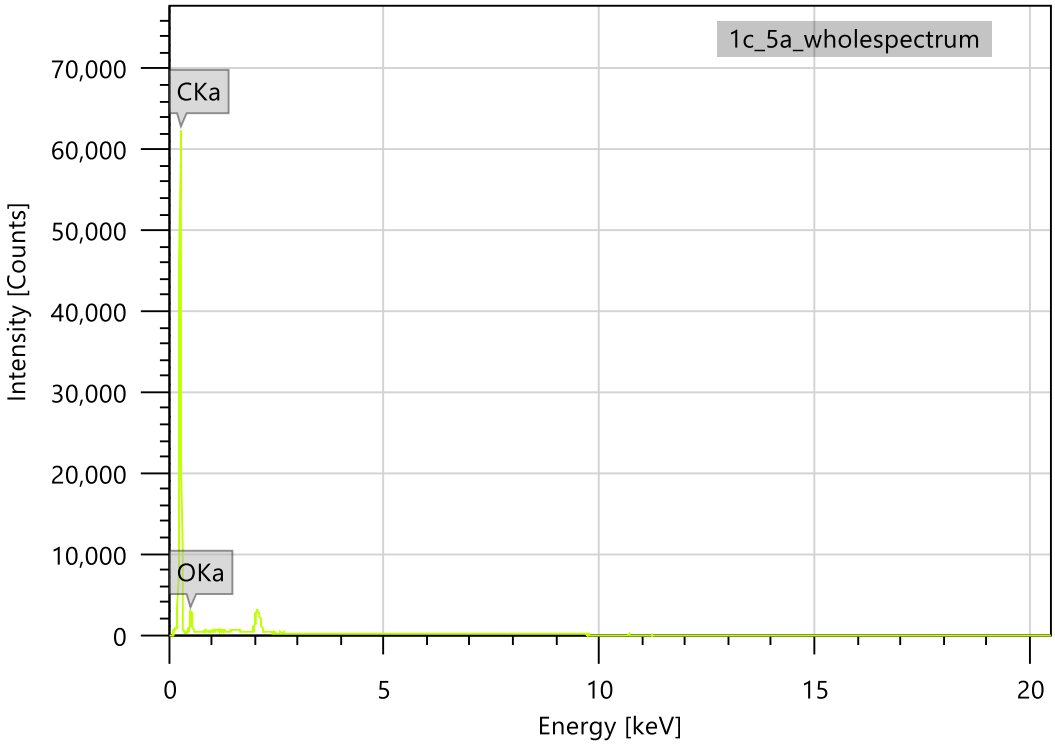


Figure 4.24: EDX Analysis of MIP (MAA) of AME

4.7.3 EDX Analysis of MIP (2VP) of ATZ

Figure 4.28 showed the qualitative and quantitative analysis of the elements present in the MIP (2VP) of ATZ. In this case, the EDX analysis of MIP (2VP) of ATZ confirmed the presence of carbon (C) and oxygen (O) at 87.87% and 12.13%, respectively. The high carbon content (87.87%) suggests that the MIP (2VP) of ATZ was primarily composed of carbon-based compounds since the MIP (2VP) of ATZ was synthesized using a combination of 2VP as the functional monomer and EGDMA as the cross-linker. Both chemical components are carbon-based compounds, contributing significantly to the carbon content in the MIP (2VP) of ATZ. MIP (2VP) of ATZ possesses a significant carbon-rich polymer matrix which is favourable for applications where high stability, mechanical strength, and resistance to environmental factors are desired. Hence, MIP (2VP) of ATZ can potentially withstand hard conditions and maintain its structural rigidity during application.

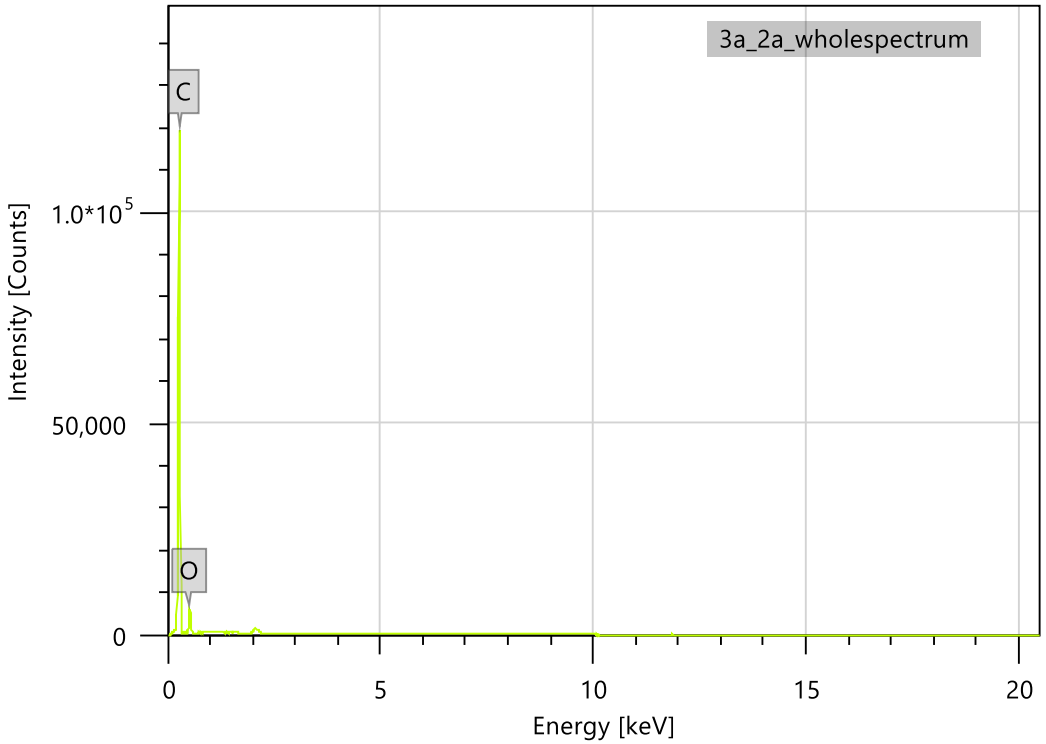


Figure 4.25: EDX Analysis of MIP (2VP) of ATZ

The oxygen content of 12.13% suggested the presence of oxygen-containing functional groups or residue oxygen in the MIP (2VP) of ATZ. Oxygen is commonly found in polymer systems due to the presence of oxygen atoms in the functional monomer, cross-linker and initiator used during the polymerization process. Besides that, oxygen-containing functional groups such as carbonyl groups (-C=O) or hydroxyl groups (-OH) may be present in the imprinted polymers, either because of the polymerization process or to enhance specific interactions with the template molecule. In this case, the EGDMA cross-linker contributed to the presence of oxygen content in the MIP (2VP) of ATZ due to the presence of oxygen-containing functional groups such as carbonyl groups (C=O and C-O-C). Oxygen-containing functional groups can contribute to specific interactions such as hydrogen bonding or polar interactions, which can enhance the selectivity and affinity of the MIP

(2VP) for ATZ template molecule or similar molecules. The presence of oxygen can also impact the overall hydrophilicity of the synthesized MIP, potentially influencing its performance in aqueous samples.

4.8 Thermal Analysis

The thermogravimetric analysis (TGA) provides the study on the decomposition characteristics of the synthesized polymers (Burkanudeen et al., 2022) of the synthesized MIPs of CYZ, AME and ATZ.

4.8.1 TGA of MIP (AAm) of CYZ

The TGA curve of the synthesized MIP (AAm) of CYZ was shown in Figure 4.26, showing its weight percentage at a temperature of 31.76 °C was 99.56 %. The initial stage of MIP (AAm) of CYZ weight loss was started from ~31 °C to ~48 °C, with a weight loss of about 4.45 %. No significant weight loss can be found from ~ 48 °C to ~ 254 °C. This weight loss was attributed to the moisture content in the MIP (AAm) of CYZ. Then, a drastic weight loss can be observed starting from ~334 °C to ~420 °C with a weight loss of 81.36 %, due to the decomposition of functional group such as CO, OH and NH_2 of MIP (AAm) of CYZ backbone. The final weight loss was continued until ~900 °C in which the remaining MIP (AAm) of CYZ was less than 20 %, indicating its thermal resistance.

Different endothermic curves were observed through the DTA curve (Figure 4.26). The first endothermic curve showed the removal of moisture in the MIP (AAm) of CYZ. The second endothermic curve was observed in the range of >334 °C, indicating the breakage of crosslinking and thermal degradation of the synthesized MIP (AAm) of CYZ. This indicated the good thermal stability of the synthesized polymer due to the usage of EGDMA cross-linker which provide stability and rigidity to the MIP (AAm) of CYZ structure.

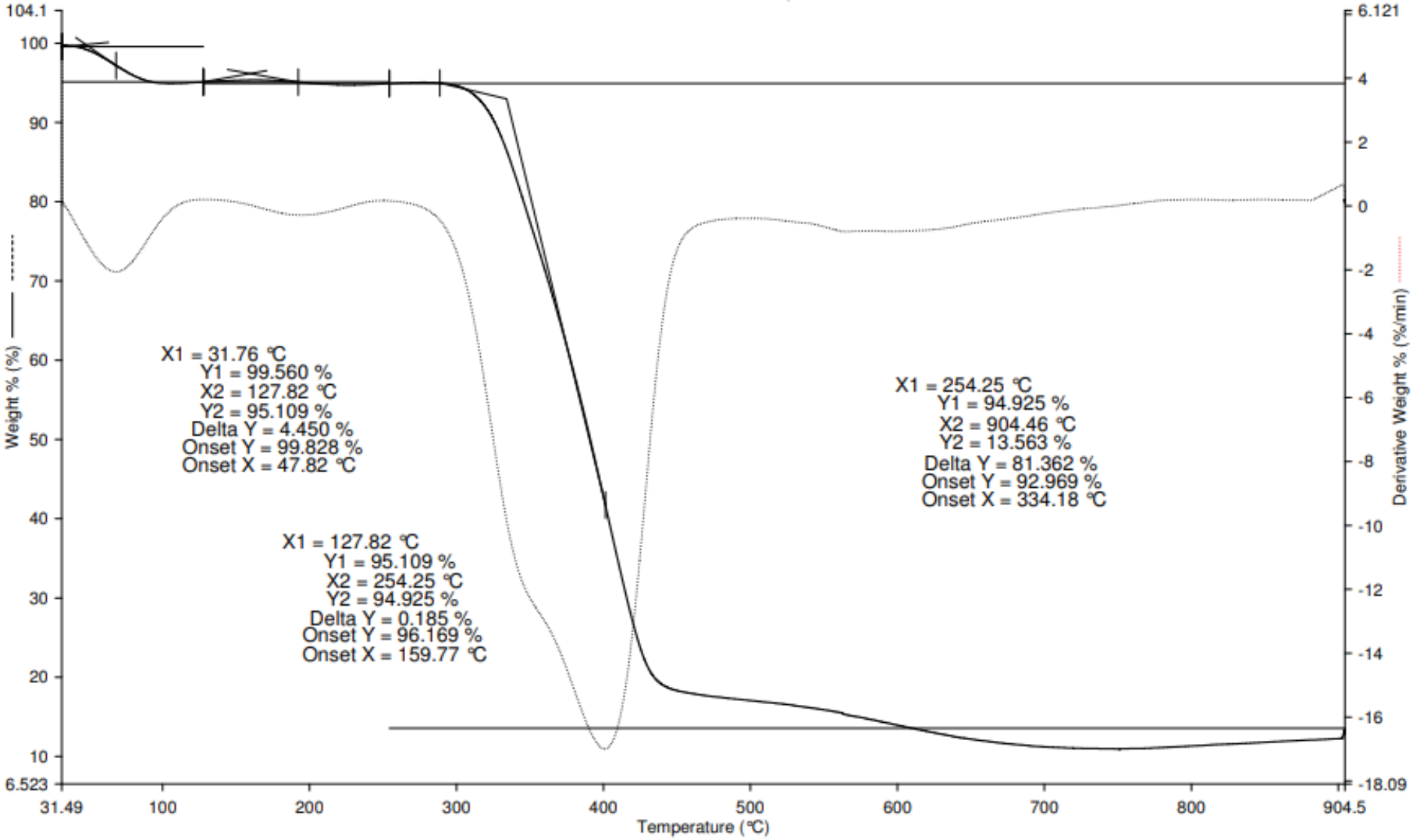


Figure 4.26: TGA Analysis of MIP (AAm) of CYZ

4.8.2 TGA of MIP (MAA) of AME

The thermal degradation activity MIP (MAA) of AME was performed from ~30 °C to ~900 °C, in an atmosphere of nitrogen as shown in Figure 4.27. Based on Figure 4.27, the MIP (MAA) of AME had a slight weight loss of about 4 % within the range of 30.57 °C to 109.73 °C. The weight loss may be due to the loss of moisture content in the polymer matrix of MIP (MAA) of AME.

Then, the TGA thermogram of MIP (MAA) of AME remained constant from 109.73 °C until 320.51 °C whereby no weight loss was observed. This exposed that MIP (MAA) of AME had excellent thermal stability until the temperature of 320.51 °C. The presence of EGDMA (cross-linker) had greatly influenced the thermal stability and structure rigidity of MIP (MAA) of AME.

However, Figure 4.27 also showed a drastic weight loss of ~92 % at the temperature of 320.51 °C to ~480 °C which was due to the degradation of functional groups including CO, OH and NH of the main MIP (MAA) of AME framework. After that, the curve remained consistent until ~900 °C, showing that no further degradation reaction took place.

Thus, the generated MIP (MAA) of AME had no significant weight loss until a temperature of 320.51 °C while dramatic weight loss was detected at the temperature between 320.51 °C to ~480 °C. The remaining mass of MIP (MAA) of AME was due to its thermal resistance and the amount of MIP (MAA) of AME particles left after the decomposition process was less than 10 %.

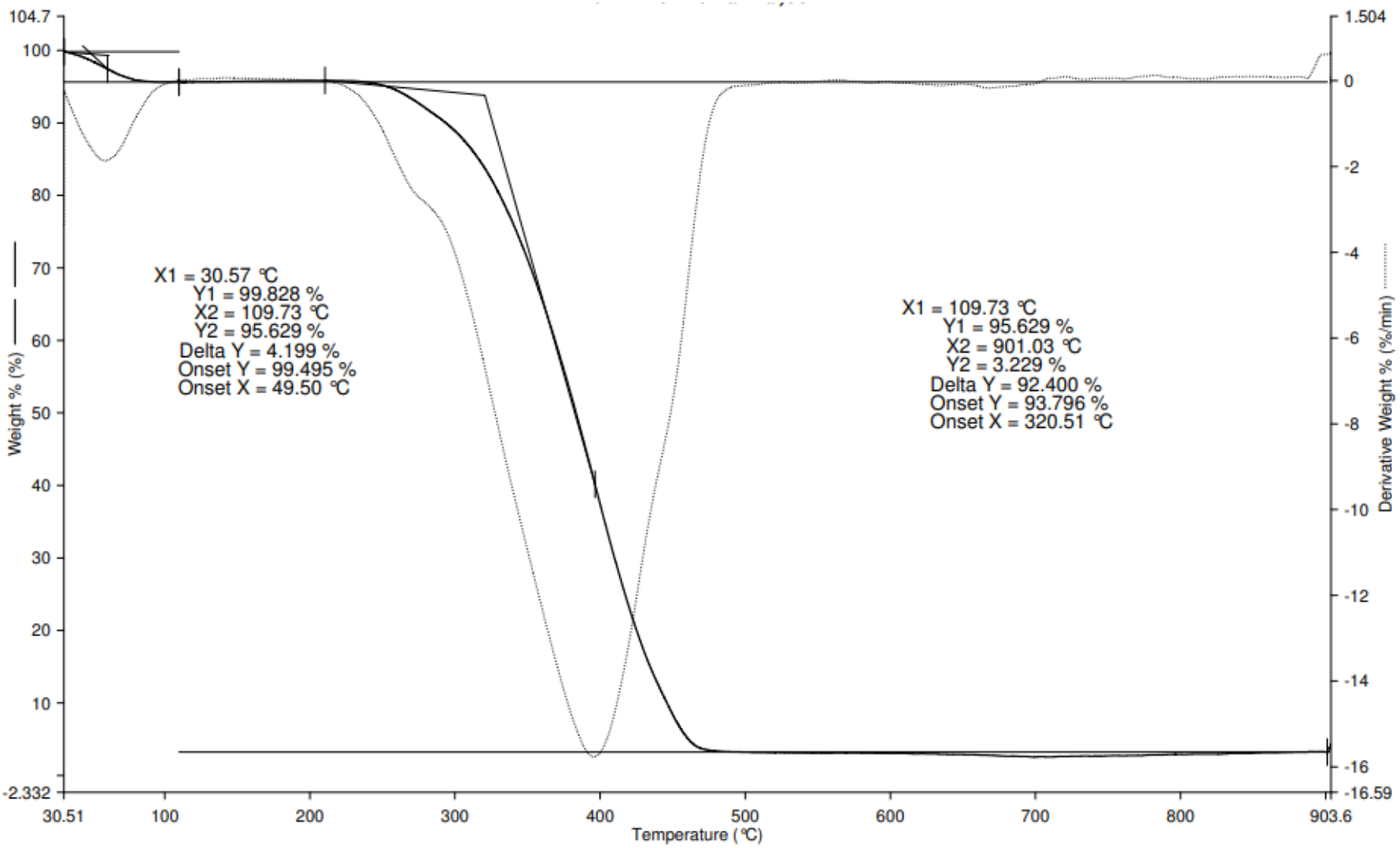


Figure 4.27: TGA Analysis of MIP (MAA) of AME

4.8.3 TGA of MIP (2VP) of ATZ

Figure 4.28 displayed the TGA curve of the MIP (2VP) which indicates the stability of the polymer at different temperatures. It was observed that the weight percentage of MIP (2VP) was 99.806 % at the temperature of 30.07°C. The weight percentage of MIP (2VP) of ATZ began to reduce at the temperature of 39.65°C to 108.64°C with a slow weight loss of 1.729 %. Then, another weight loss of about 4.521% was detected at the temperature of 195.81°C to 268.40°C. These two stages of weight loss indicated the removal of moisture or water content in the MIP (2VP) of ATZ.

Besides that, this TGA analysis also revealed that the MIP (2VP) of ATZ exhibited minimal weight loss up to a certain temperature (268.40°C), indicating excellent thermal stability. The usage of EGDMA cross-linker provides stability and rigidity to the MIP (2VP) of ATZ structure as the tightly cross-linked polymer network requires more energy to degrade.

After that, the TGA curve of MIP (2VP) of ATZ showed a steep slope at the temperature of 335.84°C to ~ 450°C with a rapid weight loss of 89.814 % which implied the degradation of the MIP (2VP) of ATZ backbone as presented in Figure 4.31. The decrease in weight percentage is attributed to the decomposition of MIP (Men et al., 2012).

Finally, the TGA curve was at a plateau at about 450°C to 896.3°C, proving that there was no further decomposition process. Hence, the synthesized MIP (2VP) of ATZ has no dramatic weight loss until a temperature of 268.40°C while significant mass loss was between 335.84°C to ~450°C. The remaining mass of MIP (2VP) of ATZ was attributed to its thermal resistance and the amount of MIP (2VP) of ATZ beads was about 5 %.

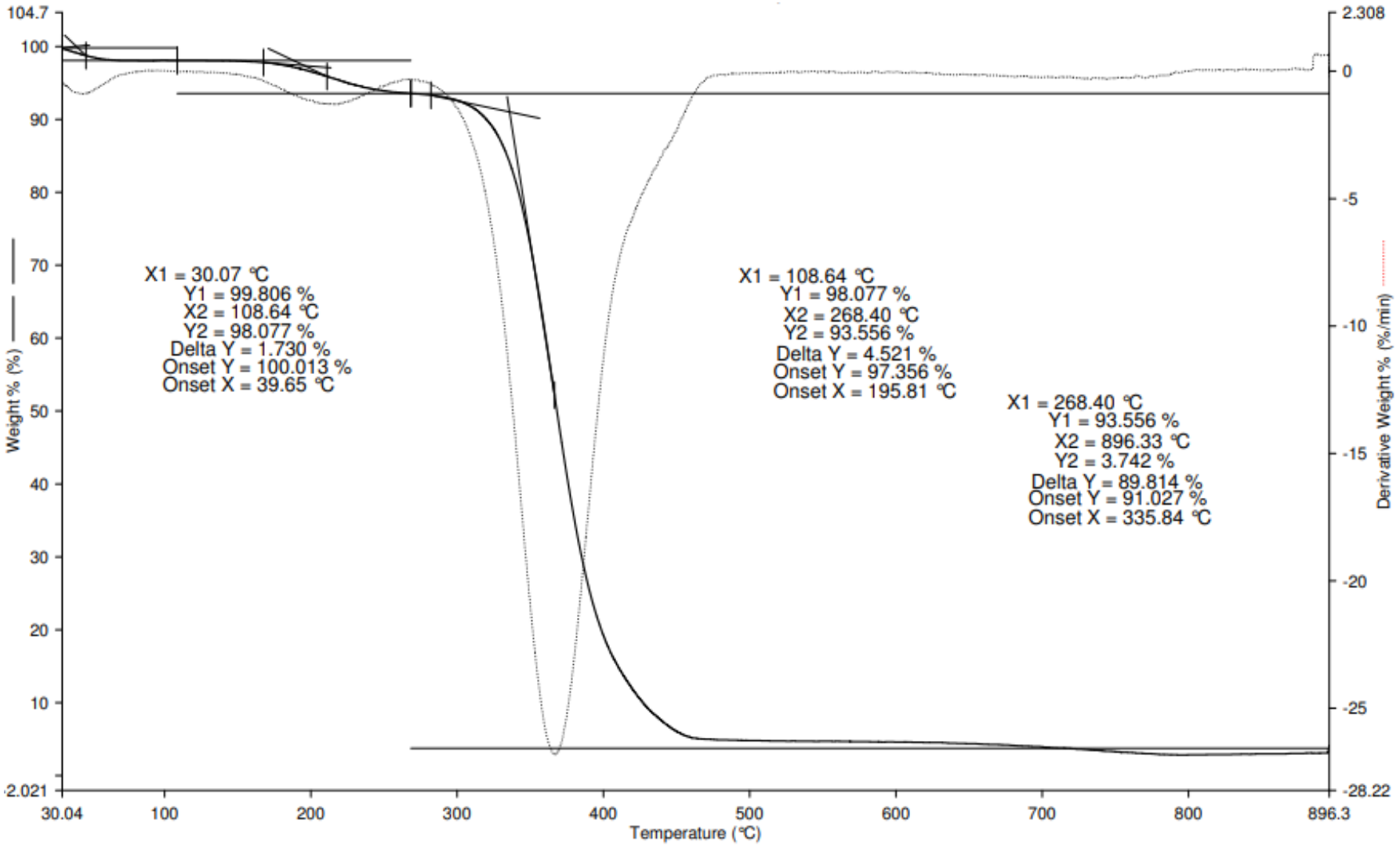


Figure 4.28: TGA Analysis of MIP (2VP) of ATZ

4.9 Effect of Initial Concentration

In this adsorption study, different initial concentrations (1, 2, 3, 4, 5, 6, 7, 8, 9 and 10 ppm) of Triazine herbicides (CYZ, AME and ATZ) solution were applied to study its effect towards the adsorption efficiency of the synthesized polymers and determine the optimum initial concentration of Triazine herbicides with the highest adsorption efficiency. Meanwhile, other parameters such as the polymer dosage, pH of the solution and the contact time were kept unchanged.

4.9.1 Effect of Initial Concentration on MIP (AAm) of CYZ

As the initial concentration of CYZ solution was increased (1 to 6 ppm), the adsorption efficiencies of MIP (AAm) of CYZ also increased, and then a further increase in initial concentrations of CYZ solution (7 to 10 ppm) lead to decrease in the adsorption efficiency of MIP (AAm) of CYZ as shown in Figure 4.29. A similar trend was detected in NIP (AAm) but with much lower adsorption efficiency.

Figure 4.29 indicated that the highest adsorption efficiency of MIP (AAm) of CYZ (Appendix 16) was obtained at an initial concentration of 6 ppm CYZ solution (86.26%), meanwhile, the lowest adsorption efficiency of MIP (AAm) of CYZ was observed at an initial concentration of 1 ppm CYZ solution (25.51%). This showed that different initial concentrations of CYZ influenced the adsorption efficiency of MIP (AAm) because an adequate number of CYZ complementary binding sites were required to sufficiently bind with the available recognition sites in the MIP (AAm).

As expected, the highest adsorption efficiency of NIP (AAm) (53.54%) at 6 ppm CYZ solution was much lower than that of MIP (AAm) of CYZ (Appendix 17). This revealed the successful incorporation of CYZ as a template molecule in MIP synthesis that

produces specific binding that had high affinity and selectivity towards its target molecule. Thus, the optimum initial concentration for the highest adsorption efficiency of MIP (AAm) of CYZ and NIP (AAm) was at 6 ppm of CYZ solution, because at this stage all the sites on the polymers have been occupied by the template molecule and had attained a saturation (Madikizela et al., 2018).

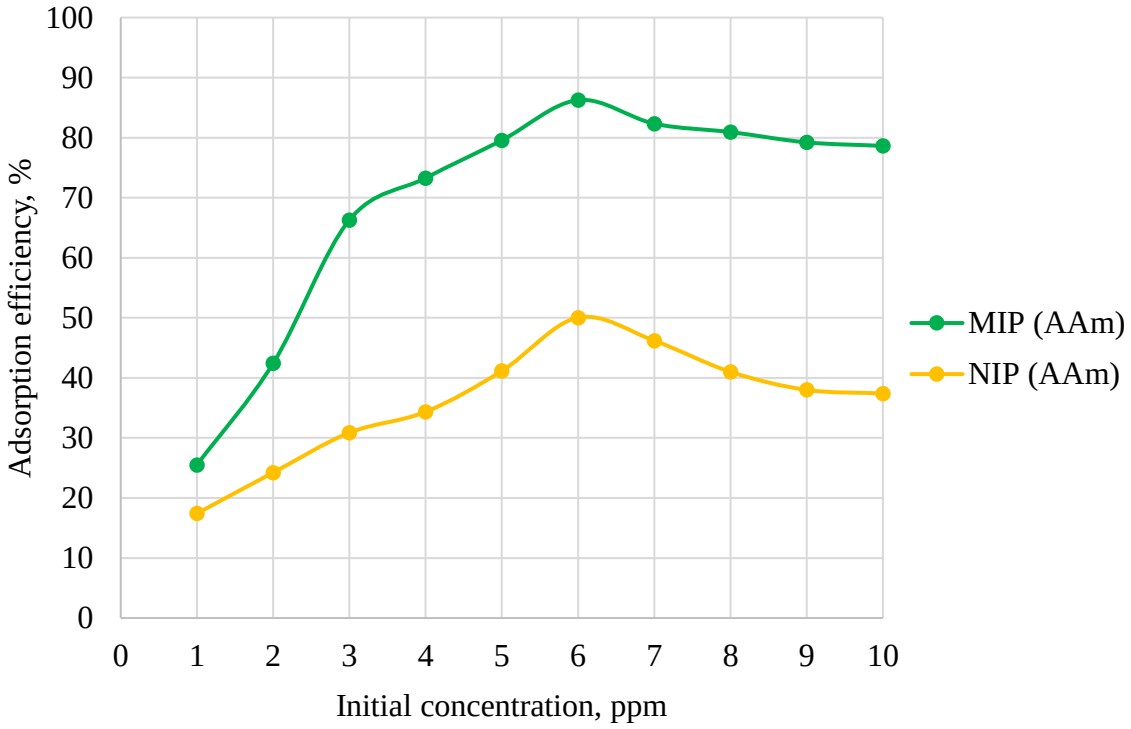


Figure 4.29: Effect of Initial Concentration on MIP (AAm) and NIP (AAm) of CYZ

4.9.2 Effect of Initial Concentration on MIP (MAA) of AME

Figure 4.30 described the adsorption efficiency of MIP (MAA) and NIP (MAA) of AME at different AME initial concentrations (1 ppm to 10 ppm). It revealed that as the AME initial concentration increased, the adsorption efficiencies also increased, however, the adsorption efficiency had slightly decreased at much higher AME initial concentration.

The adsorption efficiencies of MIP (MAA) towards AME were increased regularly from 1 ppm to 7 ppm, then decreased gradually until 10 ppm (Figure 4.30). As the initial concentration of AME increased, the possibility for greater adsorption by MIP (MAA) of AME also increased until it reached its saturation (at 7 ppm). The increment of AME adsorption efficiency by MIP (MAA) of AME starting from 1 ppm until 7 ppm indicated that there were plenty of binding sites present in the MIP (MAA) of AME cavity that can bind with AME template molecule. Abraham and Mathew (2014) also mentioned that the MIP binding sites can be easily attached with the template molecule in increasing analyte (template molecule) concentration, and hence, promote better adsorption of template molecule by the synthesized MIP.

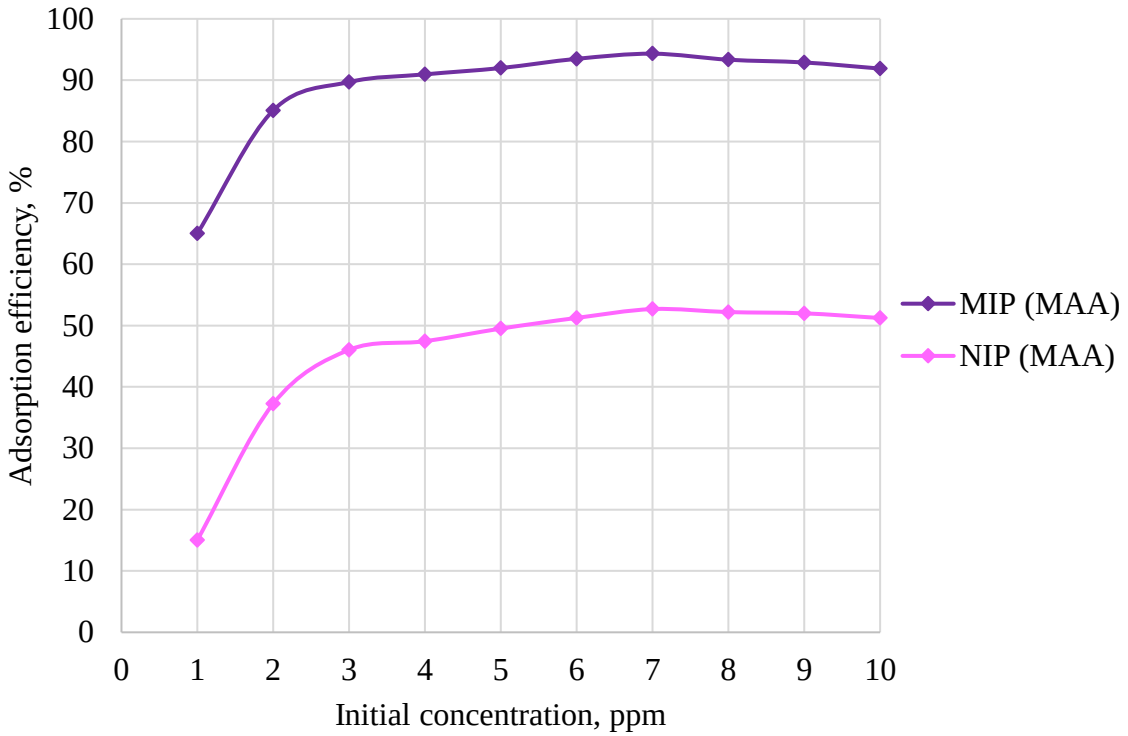


Figure 4.30: Effect of Initial Concentration on MIP (MAA) and NIP (MAA) of AME

Figure 4.30 also showed the highest adsorption efficiencies of MIP (MAA) and NIP (MAA) of AME were observed at 7 ppm of AME which were 94.32 % and 52.69 %,

respectively (Appendix 18 and Appendix 19). This indicated that 7 ppm of AME was the optimum concentration to obtain the highest adsorption efficiency of the synthesized MIP (MAA) of AME. The MIP (MAA) of AME had much higher adsorption efficiency due to the availability of specific binding sites in its polymer matrix that are complementary to the template molecule (AME) in terms of size and shape. At 7 ppm, the AME adsorption by the MIP (MAA) of AME reached its saturation or in other words, equilibrium has been achieved. At this point, the vacant binding sites in the MIP (MAA) cavity were sufficiently filled up by the AME template molecule. Sadia et al. (2022) indicated that the adsorption process has reached its plateau and no more binding sites can be accessed by template molecule for further adsorption at much higher concentration.

However, the adsorption efficiencies of both MIP (MAA) and NIP (MAA) of AME were decreased gradually at 8 ppm to 10 ppm because the synthesized polymers had reached its adsorption equilibrium at 7 ppm (Figure 4.30). After the adsorption equilibrium point, further increase in AME initial concentrations will cause the accumulation of AME template molecule to gather around the MIP (MAA) of AME binding sites which could hinder efficient adsorption of AME in the binding sites of MIP (MAA) of AME cavity, hence decreases the adsorption efficiency. It can be further explained that abundance of AME template molecule surrounds the MIP (MAA) of AME will limit the binding ability between the AME template molecule and MIP (MAA) binding sites because each MIP (MAA) binding site can only attach with single AME template molecule to increase the adsorption efficiency. Since the polymer dosages used were constant in all concentrations so the number of available binding sites were also constant, however, the concentration of analyte was increased, explaining the increase in the number of moles of analyte in the solution which contributed to the decrease in MIP adsorption efficiencies (Wang et al., 2016).

In contrast, similar trend was detected on the adsorption efficiencies of NIP (MAA) towards AME but in much lower efficiencies (Figure 4.30). This is because NIP (MAA) does not have specific binding sites in its cavity that can promote efficient adsorption with AME template molecule since the non-specific binding sites were not corresponding to the AME template molecule (Jusoh et al., 2022).

4.9.3 Effect of Initial Concentration on MIP (2VP) of ATZ

Figure 4.31 displayed the comparison of adsorption efficiencies between MIP (2VP) and NIP (2VP) of ATZ at several initial concentrations of ATZ solution as the target molecule (Appendix 20 and Appendix 21). Based on Figure 4.31, increasing the initial concentration of ATZ solution from 1 ppm to 8 ppm tends to enhance the adsorption efficiency of the MIP (2VP) of ATZ. A higher initial concentration means a larger number of ATZ molecules are present in the MIP matrix, increasing the chances of successful binding interactions with the MIP (2VP) of ATZ binding sites. Consequently, a higher initial concentration provides a greater opportunity for molecular recognition and stronger binding between ATZ and the MIP (2VP) of ATZ, resulting in higher adsorption efficiency.

At the initial concentration of 8 ppm ATZ solution, MIP (2VP) of ATZ achieved its highest adsorption efficiency of 91.43% (Figure 4.31). This indicated that 8 ppm of ATZ solution was the optimal initial concentration for obtaining the highest adsorption efficiency of MIP (2VP) of ATZ. At this point, the saturation capacity of the polymer had been reached, meaning that all available binding sites are already occupied (Madikizela et al., 2018). However, any further increase in the initial concentration of 9 ppm and 10 ppm ATZ solution did not enhance the adsorption efficiency, as the MIP (2VP) of ATZ had reached its maximum adsorption capacity at 8 ppm of ATZ solution as shown in Figure 4.31.

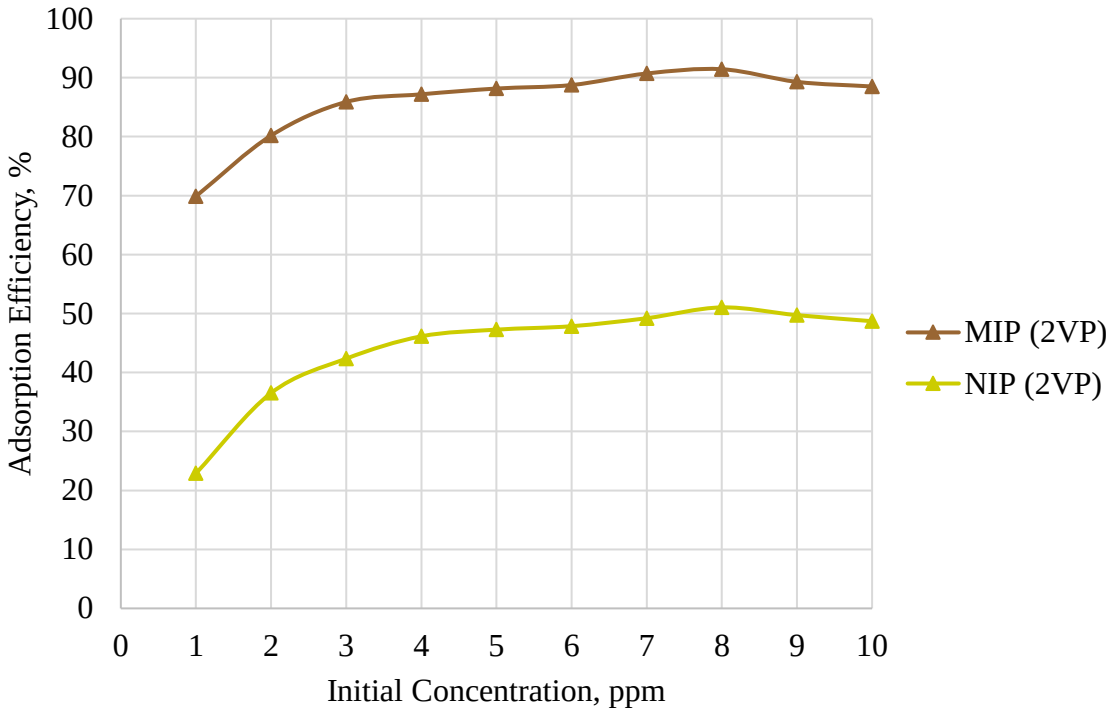


Figure 4.31: Effect of Initial Concentration on MIP (2VP) and NIP (2VP) of ATZ

At 9 ppm and 10 ppm of ATZ solution, MIP (2VP) of ATZ had lower adsorption efficiencies because excessively high initial concentrations may lead to increased non-specific interactions between the imprinted polymer and other components present in the polymer matrix. The non-specific adsorption can reduce the binding affinity and selectivity of MIP (2VP) towards the ATZ target compound, resulting in the binding of non-target compounds. Hence, this can lower the adsorption efficiency and affect the specificity of ATZ removal by the MIP (2VP) of ATZ.

Similarly, the NIP (2VP) had an identical trend as MIP (2VP) which its adsorption efficiency increased with increasing initial concentration from 1 ppm to 8 ppm of ATZ solution and then further increase in initial concentration from 9 ppm to 10 ppm of ATZ solution leads to decrease in adsorption efficiencies of NIP (2VP) (Figure 4.31). NIP (2VP) also exhibited its highest adsorption efficiency of 51.04% at an initial concentration of 8

ppm of ATZ solution. As expected, NIP (2VP) had a much lower efficiency than the MIP (2VP) of ATZ due to the lack of specific binding sites in the NIP cavity. Due to the presence of specific and non-specific binding sites, MIP exhibits greater adsorption capacity than NIP, especially at high atrazine concentrations where specific recognition binding sites are activated (Liu et al., 2015).

4.10 Effect of pH

For this study, the pH of CYZ solutions was adjusted to acidic, neutral, and basic such as pH 3 and pH 5, pH 7, pH 9 and pH 11, respectively. Meanwhile, other parameters such as the Triazine herbicides (CYZ, AME and ATZ) concentration, polymer dosage and contact time remained unchanged.

4.10.1 Effect of pH on MIP (AAm) of CYZ

Based on Figure 4.32, the adsorption efficiency of MIP (AAm) towards CYZ was increased from an acidic condition (pH 3 and pH 5) to a neutral condition (pH 7), and then, decreased at the basic condition (pH 9 and pH 11). The highest adsorption efficiency of MIP (AAm) of CYZ was attained at pH 7, neutral condition (86.39 %) while the lowest adsorption efficiency of MIP (AAm) was obtained at pH 11, strong basic condition (14.41 %) (Appendix 22 and Appendix 23).

This revealed that pH condition had an influence on the MIP adsorption efficiency as too low or too high pH condition may disrupt the characteristics of the CYZ template molecule. Yusof et al. (2013) emphasized that certain pH conditions that may alter the functionality of the template molecule, hence not fitting suitably with the binding sites of the synthesized MIP. Therefore, the rebinding of the synthesized MIP (AAm) of CYZ is pH dependent.

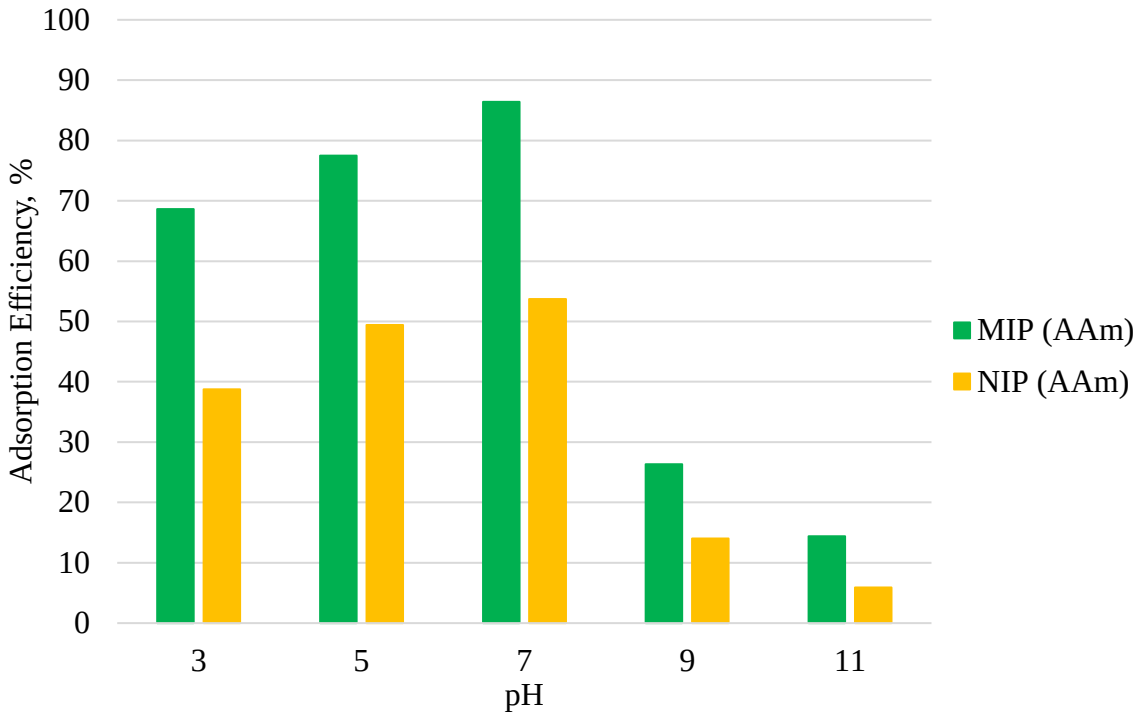


Figure 4.32: Effect of pH on MIP (AAm) and NIP (AAm) of CYZ

As expected, the adsorption efficiencies of NIP (AAm) were much lower than the adsorption efficiencies of MIP (AAm) of CYZ (Figure 4.32). This is because NIP does not have an imprinting effect in its polymer matrix, resulting in the formation of non-specific binding sites (Zhang et al., 2016). Since NIP (AAm) did not have specific binding sites, the binding affinity and specificity between the NIP (AAm) and CYZ was weak, thus resulting in lower adsorption efficiency. NIP (AAm) also showed a similar trend as the MIP (AAm) of CYZ, whereby its adsorption efficiency towards CYZ was increased from acidic condition (pH 3 and pH 5) to neutral condition (pH 7), and then, decreased in basic conditions (pH 9 and pH 11).

4.10.2 Effect of pH on MIP (MAA) of AME

Figure 4.33 represented the adsorption efficiencies of MIP (MAA) of AME and NIP (MAA) of AME at several pH (pH 3, pH 5, pH 7, pH 9 and pH 11) conditions (Appendix 24

and Appendix 25). At pH 3 (strong acidic condition), the adsorption efficiencies of MIP (MAA) of AME and NIP (MAA) of AME were 80.56 % and 42.06 %, respectively. At pH 5 (weaker acidic condition), the adsorption efficiencies of MIP (MAA) of AME and NIP (MAA) of AME were 86.44 % and 49.83 %, respectively. Lower pH value of analyte solution than the MIP will allows the MIP to be protonated and become positively charged, so it can simply adsorb the negatively charged analyte (Li et al., 2013), resulting an increase in the adsorption efficiency.

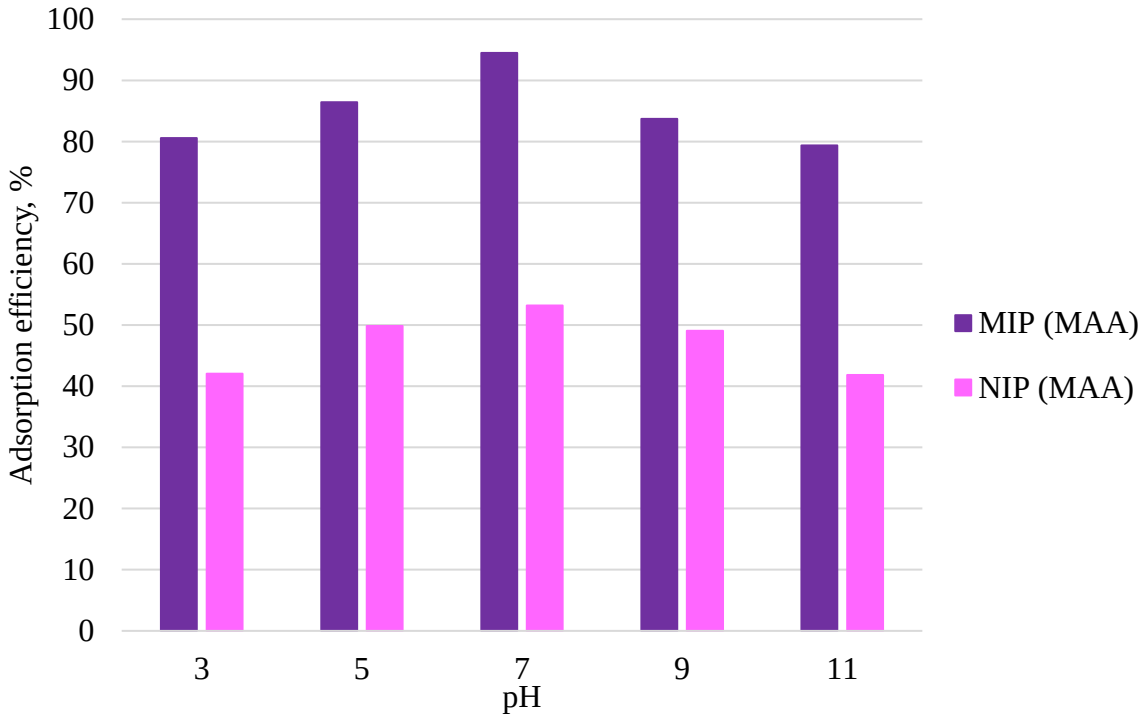


Figure 4.33: Effect of pH on MIP (MAA) and NIP (MAA) of AME

It was calculated that the highest adsorption efficiency of MIP (MAA) of AME and NIP (MAA) of AME were 94.51 % and 53.21 %, respectively at pH 7 (neutral condition) as shown in Figure 4.33. Güzel and Sayğili (2016) explained that greater adsorption performance between the analyte and MIP can be achieved in the range of pH 5 to pH 7 because the analyte has practically no charge and the non-electrostatic interactions, for

example hydrogen bonding and π-π accumulation were involved in the adsorption process. The highest adsorption of MIP at certain pH value is governed by the neutral condition of the analytes and hydrogen bonding interaction that occurred between the analyte and MIP cavity (Jalilian et al., 2021).

Meanwhile, at pH 9 (weaker basic condition), the adsorption efficiencies of MIP (MAA) of AME and NIP (MAA) of AME were 83.71 % and 49.06 %, respectively (Figure 4.33). At pH 11 (strong basic condition), the adsorption efficiencies of MIP (MAA) of AME and NIP (MAA) of AME were 79.38 % and 41.82 %, respectively. At pH 9 and above, both template molecule and the synthesized polymers were negatively charged which cause electrostatic repulsion interaction that decrease the interactions between template molecule and the synthesized polymers, hence lowering the adsorption efficiency (Uzuriaga-Sánchez et al., 2017).

Hence, this explained that the synthesized MIP (MAA) of AME was pH dependent as it required a neutral condition to obtain its highest adsorption efficiency. Overall, the synthesized MIP (MAA) of AME presenting a good imprinting effect and adsorption performance towards AME template molecule in several pH conditions as compared with NIP (MAA). The reason is MIP (MAA) of AME containing specific binding sites in its polymer cavity while NIP containing non-specific binding sites in its polymer cavity for adsorption of AME as the template molecule.

4.10.3 Effect of pH on MIP (2VP) of ATZ

Figure 4.34 displayed the comparison of adsorption efficiencies between MIP (2VP) and NIP (2VP) of ATZ at different pH conditions (Appendix 26 and Appendix 27). It was calculated that the adsorption efficiencies of MIP (2VP) of ATZ at pH 3, pH 5, pH 7, pH 9

and pH 11 were 88.48 %, 90.04 %, 91.62 %, 80.74 % and 81.68 %, respectively. Meanwhile, the adsorption efficiencies of NIP (2VP) of ATZ at pH 3, pH 5, pH 7, pH 9 and pH 11 were 24.32 %, 39.33 %, 45.68 %, 38.72 % and 31.62 %, respectively. As expected, NIP (2VP) of ATZ had much lower adsorption efficiency due to the non-specific interactions in its polymer cavity.

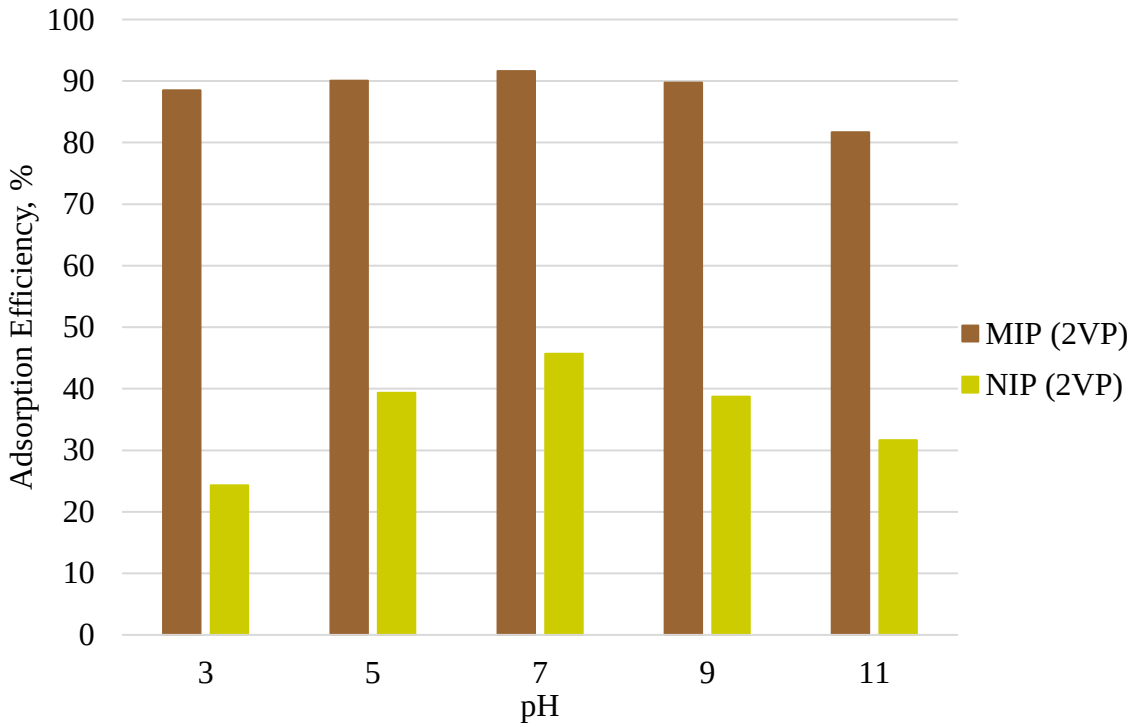


Figure 4.34: Effect of pH on MIP (2VP) and NIP (2VP) of ATZ

Overall, the adsorption efficiencies of both MIP (2VP) of ATZ and NIP (2VP) of ATZ increased steadily in acidic conditions (pH 3 and pH 5) to neutral condition (pH 7) and then decreased gradually in basic conditions (pH 9 and pH 11). This is due to the acidic and basic conditions having an influence towards the functionality of the target or template molecules and eventually the target molecule became incompatible with the MIP recognition sites (Yusof et al., 2013).

Besides that, different pH conditions can contribute to electrostatic and hydrogen bonding interactions between the target molecules and the synthesized polymers (Anirudhan et al., 2017). For instance, higher pH values of a solution lead to the potential protonation of surface functional groups which later generate electrostatic repulsion between the adsorbent and ATZ (George et al., 2023). Herrera-Garcia et al. (2019) stated that changes in solution pH can significantly impact the adsorbent performance for herbicide removal due to continuous alteration in the number of charges and characteristics of the adsorbent surface.

Based on figure 4.34, MIP (2VP) of ATZ and NIP (2VP) of ATZ had their highest adsorption efficiency in a neutral condition which indicated that pH 7 was the ideal pH condition for the maximum adsorption for MIP (2VP) of ATZ. This is due to the uncharged target or template molecules and the non-electrostatic interactions involved in the adsorption process of the synthesized polymers and the target molecules (Güzel and Sayğili, 2016).

Since the MIP imprinting process was conducted under neutral conditions, the generated polymer cavities are designed to accommodate the neutral ATZ molecule, and therefore, the acidic and basic conditions resulting in less favourable fitting of the ionic form of ATZ and the functional group of the MIP in these polymer recognition sites (Zarejousheghani et al., 2014). Zarejousheghani et al. (2014) also indicated that the optimum pH condition of ATZ solution for the MIP adsorption study was between pH 6 and pH 7. Therefore, it can be deduced that the pH of the solution is one of the critical factors that affect the adsorption efficiency of ATZ (Djozan and Ebrahimi, 2008).

4.11 Effect of Polymer Dosage

In this adsorption study, various polymer dosages (0.1 g, 0.2 g, 0.3 g, 0.4 g, 0.5 g, 0.6 g, and 0.7 g) were used to determine the effects of the amount of polymer used on the

adsorption efficiencies of MIPs of Triazine herbicides. Meanwhile, other parameters such as the CYZ concentration, pH of the solution and the contact time have remained constant.

4.11.1 Effect of Polymer Dosage of MIP (AAm) of CYZ

Based on Figure 4.35, the highest adsorption efficiency was obtained at the MIP (AAm) of CYZ dosage of 0.1g (86.39%), then the adsorption efficiencies were decreased gradually as the MIP (AAm) of CYZ dosages increased (0.2 g, 0.3 g, 0.4 g, 0.5 g, 0.6 g, and 0.7 g), whereby the lowest adsorption efficiency was recorded at MIP dosage of 0.7 g (69.31%) (Appendix 28).

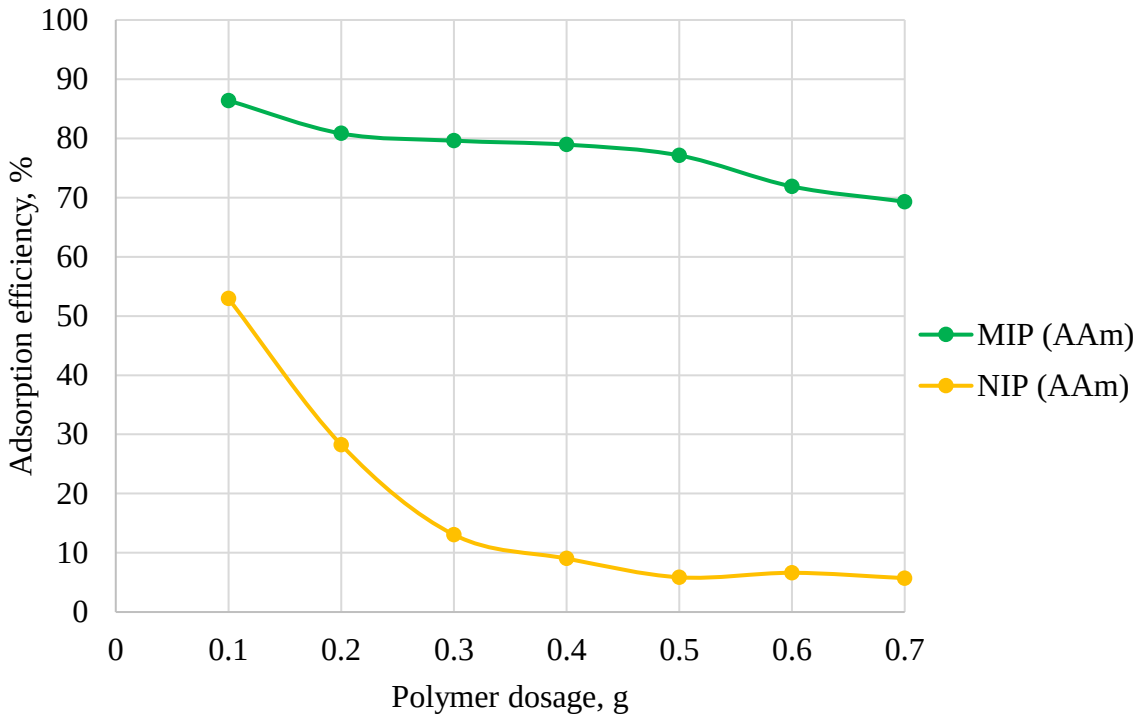


Figure 4.35: Effect of Polymer Dosage on MIP (AAm) and NIP (AAm) of CYZ

Generally, an increasing amount of polymer contributed to an increasing number of recognition sites, resulting in higher adsorption efficiency of its template compound. However, a further increase in the amount of polymer does not necessarily increase its

adsorption efficiency because the active recognition sites are hidden by the polymer particles that were clumping together. Hence, a further increase in the amount of MIP (AAm) of CYZ led to a decrease in its adsorption efficiency because an abundance amount of polymer caused overcrowding of binding sites and eventually deterred the binding of CYZ template molecule to the recognition sites in the MIP cavity. Mor et al. (2016) highlighted that further increase in polymer dosage leads to a decrease in adsorption efficiency as the excess amount of polymer leads to agglomeration of polymer particles and hence, hinders the binding process with the target molecule.

A similar trend of adsorption efficiencies can be seen on NIP (AAm) in Figure 4.35 but with much lower adsorption efficiencies (Appendix 29). Therefore, the optimum polymer dosage needed to obtain the highest binding efficiency was 0.1 g of polymer in which only a small amount of MIP (AAm) is required to efficiently remove the CYZ.

4.11.2 Effect of Polymer Dosage of MIP (MAA) of AME

Figure 4.36 described the adsorption efficiencies of MIP (MAA) of AME and NIP (MAA) of AME at various polymer dosages such as 0.1 g, 0.2 g, 0.3 g, 0.4 g, 0.5 g, 0.6 g, and 0.7 g (Appendix 30 and Appendix 31). Commonly, the increase in polymer dosage will increase the number of active binding sites and surface area for the adsorption of the target analyte (Gomes et al., 2017).

In this study, it was observed that that the increase in MIP (MAA) of AME dosage leads to gradual decrease in the adsorption efficiencies of polymer with AME as shown in Figure 4.36. The higher polymer dosage did not contribute to higher adsorption efficiency of polymer with analyte as it can cause MIP aggregation (Mor et al., 2016) that hinder

binding interactions between the analyte (template molecule) with the binding sites of the synthesized polymers.

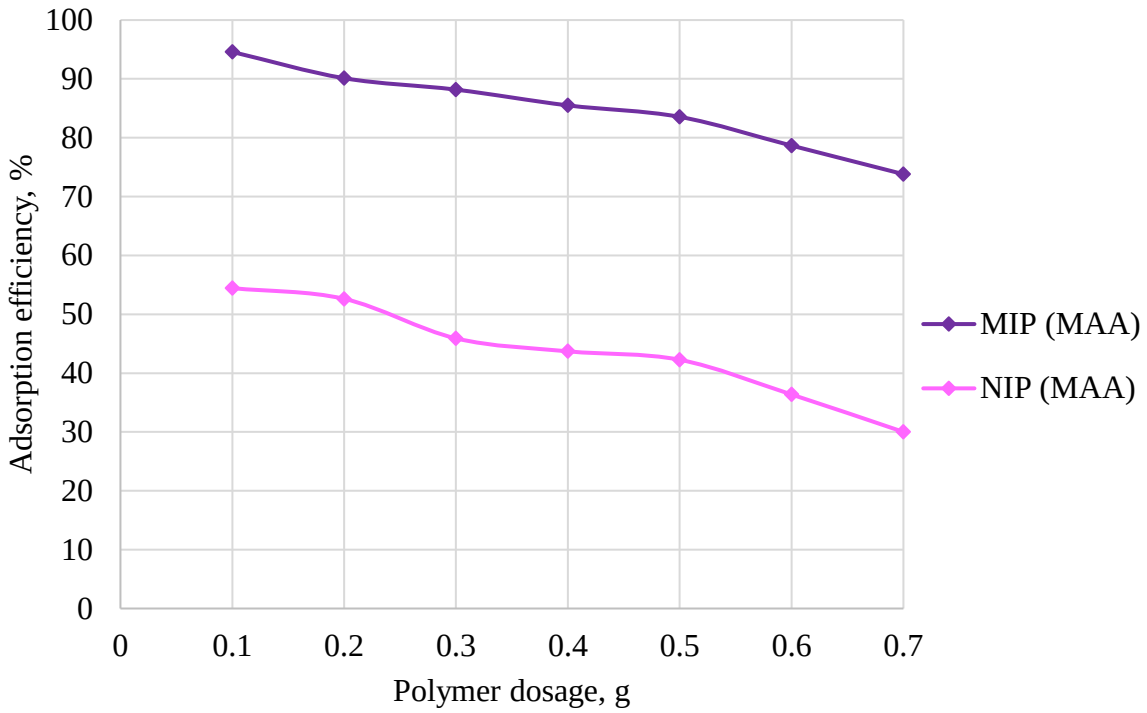


Figure 4.36: Effect of Polymer Dosage on MIP (MAA) and NIP (MAA) of AME

Correspondingly, the NIP (MAA) had similar behaviour as MIP (MAA) of AME but in much lower adsorption efficiencies. Based on Figure 4.36, 0.1 g of MIP (MAA) of AME and NIP (MAA) obtained the highest AME adsorption efficiencies of 94.58 % and 54.44 %, respectively. Meanwhile, this study was conducted until the dosage of 0.7 g of MIP (MAA) of AME and NIP (MAA) which obtained the lowest adsorption efficiencies of 73.82 % and 30.01 %, respectively. Therefore, 0.1 g of MIP (MAA) of AME is chosen as the optimum polymer dosage for the adsorption of 7 ppm AME solution.

4.11.3 Effect of Polymer Dosage of MIP (2VP) of ATZ

Figure 4.37 exhibited the comparison of ATZ adsorption efficiencies by MIP (2VP) of ATZ and NIP (2VP) of ATZ at various polymer dosages (Appendix 32 and Appendix 33). At polymer dosages of 0.1 g, 0.2 g, 0.3 g, 0.4 g, 0.5 g, 0.6 g and 0.7 g, the ATZ adsorption efficiencies by the MIP (2VP) of ATZ were 91.23 %, 92.81 %, 94.14 %, 90.33 %, 89.50 %, 87.35 % and 85.26 %, respectively. Meanwhile, the ATZ adsorption efficiencies by the NIP (2VP) of ATZ at polymer dosages of 0.1 g, 0.2 g, 0.3 g, 0.4 g, 0.5 g, 0.6 g, and 0.7 g were 44.68 %, 44.33 %, 49.06 %, 43.09 %, 40.83 %, 37.75 % and 35.33 %, respectively (Figure 4.40). As expected, MIP (2VP) of ATZ had greater adsorption efficiencies than that NIP (2VP) due to the presence of recognition sites in its polymeric matrix, resulting imprinting effect.

The adsorption efficiency of MIP (2VP) of ATZ increased with increasing the polymer dosage of less than 0.3 g as shown in Figure 4.37. The polymer dosage of more than 0.3 g showed a decrease in the adsorption efficiency of MIP (2VP) of ATZ. Increasing the polymer dosage generally leads to an increase in the adsorption capacity of MIPs. This is because a higher amount of MIP provides more recognition sites for the target or template molecule, thereby allowing a greater quantity of the target molecule to be adsorbed (Zhong et al., 2018). As the polymer dosage increases, the number of available binding sites increases, leading to higher adsorption capacity and improved efficiency in removing the target molecule from the solution. Further increase in the polymer dosage resulted in a decrease in the adsorption efficiency as an excessively amount of polymer particles causing the active recognition sites to be embedded and thus hinder the binding interaction between MIP (2VP) and ATZ.

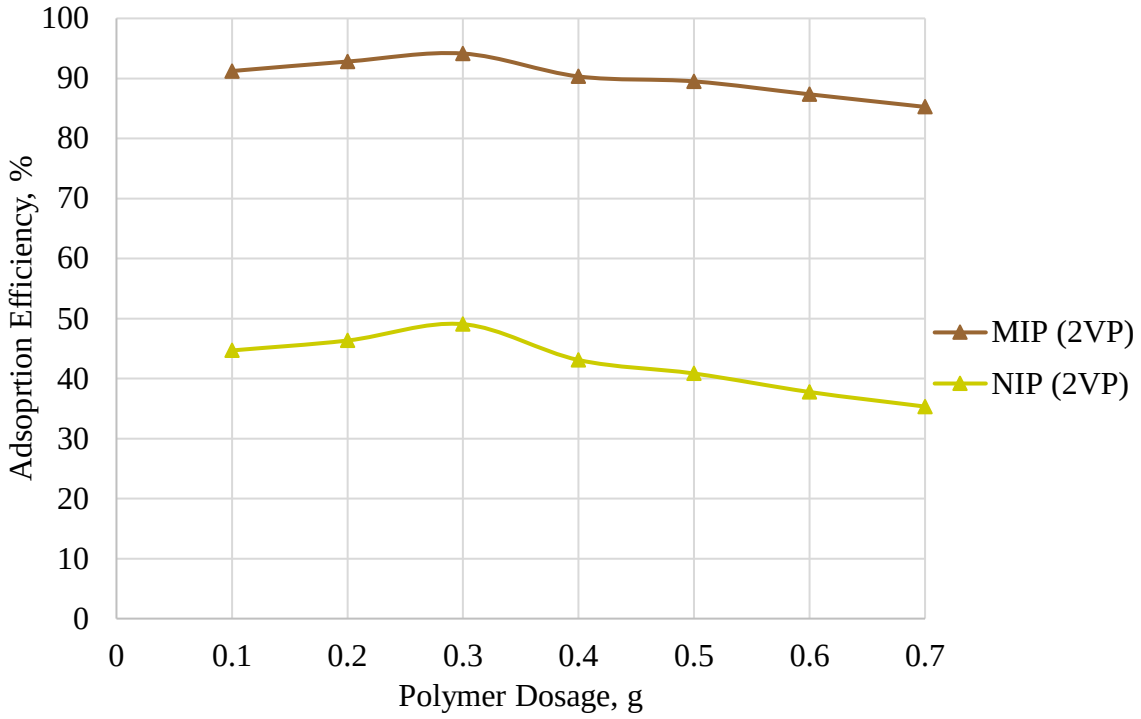


Figure 4.37: Effect of Polymer Dosage on MIP (2VP) and NIP (2VP) of ATZ

Both MIP (2VP) of ATZ and NIP (2VP) of ATZ required about 0.3 g of polymer dosage to obtain their highest ATZ adsorption efficiencies of 94.14 % and 49.06 %, respectively. This is because 0.3 g of polymers is an optimal polymer dosage that maximizes the adsorption efficiency in which the available recognition sites of polymer were sufficiently binding with the target molecule.

However, using an excessively high polymer dosage beyond its optimum polymer dosage can lead to reduced adsorption efficiency. It was observed that the usage of 0.4 g to 0.7 g of polymer dosage of both MIP (2VP) of ATZ and NIP (2VP) of ATZ leads to a gradual decrease in their adsorption efficiency towards the ATZ molecules as shown in Figure 4.37. This is due to the excess polymer dosage can result in overcrowding of binding sites, causing steric hindrance, and limiting access to the polymer binding sites. Therefore, it is essential

to determine the appropriate polymer dosage that achieves the highest adsorption efficiency without excessive use of the polymers.

4.12 Adsorption Isotherm Study

Two adsorption isotherms models namely Langmuir isotherm and Freundlich isotherm were examined to evaluate the mechanism of adsorption and extent of the Triazine herbicides absorbed on the synthesized MIPs surfaces. The Langmuir model describes the homogenous binding (Li and Husson, 2006), while the Freundlich model describes the heterogenous binding at low concentrations (Wei et al., 2005).

4.12.1 Adsorption Isotherm Study of MIP of CYZ

The Langmuir isotherm and Freundlich isotherm of MIP (AAm) of CYZ were shown in Figure 4.38 and Figure 4.39, respectively. The slopes and intercepts of the plots in Figure 4.41 and Figure 4.42 were applied for the calculations of isotherm factors such as q_{max}, K_L, R_L, n, $1/n$ and R^2 values as displayed in Table 4.8.

In this case, the Langmuir isotherm appeared to be the best-fitted adsorption isotherm model of CYZ by MIP (AAm) due to a higher correlation coefficient value ($R^2 = 0.9946$) as shown in Table 4.8. The R_L value is important to determine the type of adsorption isotherm, whether the adsorption is favourable ($0 < R_L < 1$), unfavourable ($R_L > 1$) or irreversible ($R_L = 1$) (Madikizela et al., 2018). Besides that, the R_L value was 0.1455, suggesting favourable adsorption of CYZ by MIP (AAm) as depicted in Table 4.8. Hence, it can be deduced that the adsorption of CYZ on the surface of MIP (AAm) was mono layered.

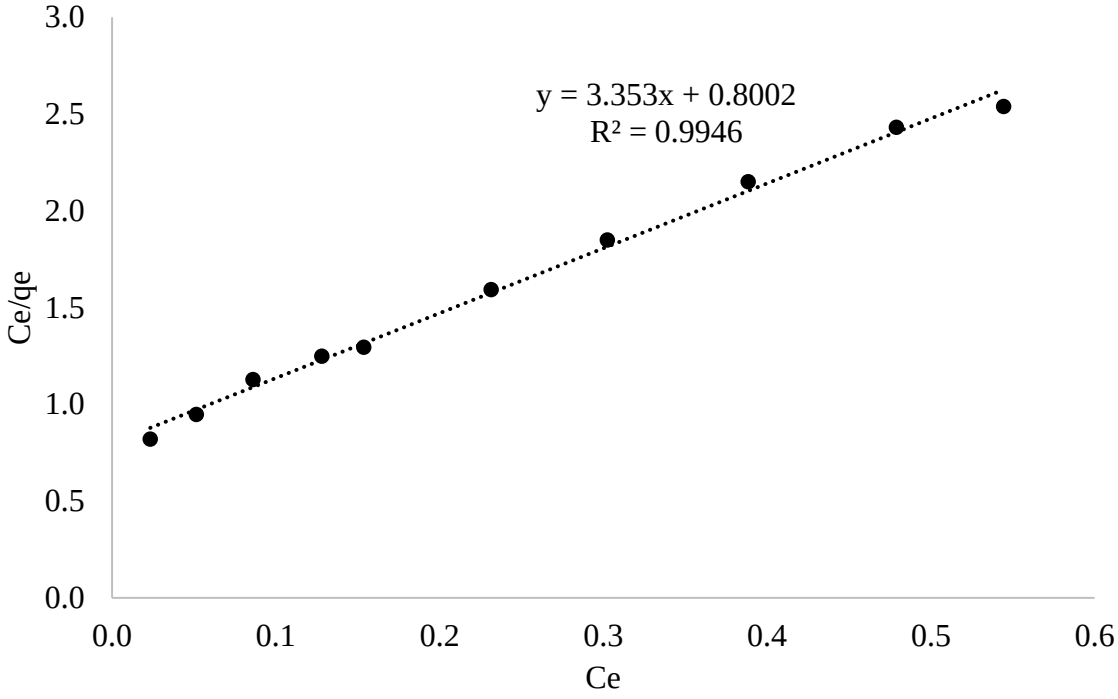


Figure 4.38: Langmuir Isotherm Model of MIP (AAm) of CYZ

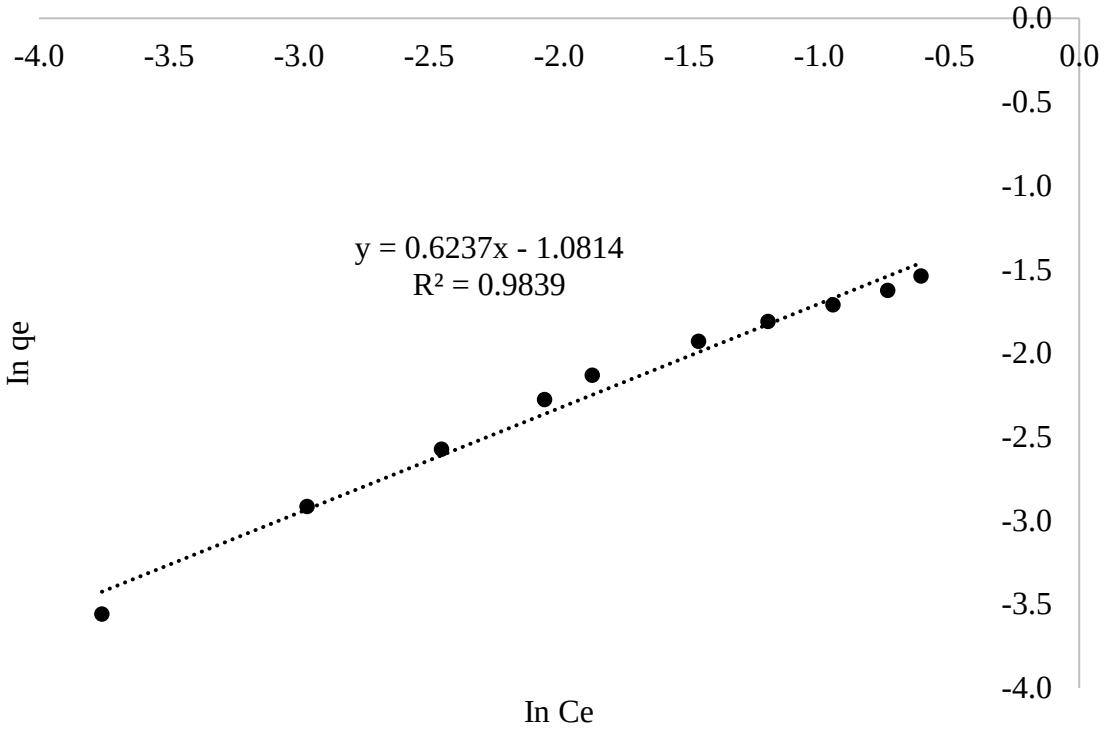


Figure 4.39: Freundlich Isotherm Model of MIP (AAm) of CYZ

Table 4.7: Adsorption Isotherm Models of MIP (AAm) of CYZ

Langmuir constants				Freundlich constants			
q_{max} (mg/g)	K_L (L/mg)	R_L	R^2	K_F (mg/g)	*n*	1/*n*	R^2
0.2982	4.1902	0.1455	0.9946	0.3391	1.6033	0.6237	0.9839

4.12.2 Adsorption Isotherm Study of MIP (MAA) of AME

Based on Figure 4.40 and Figure 4.41, it showed that the Langmuir isotherm model of MIP (MAA) of AME had a higher correlation coefficient (0.9988) than the Freundlich isotherm model (0.9606). Hence, the Langmuir isotherm model is the best to describe the chemical adsorption between AME that took place on the surface of the MIP (MAA) of AME. The Langmuir isotherm model indicates that the adsorption of absorbate was mono layer, and the adsorption sites of the absorbent were homogenous (Darwish et al., 2019).

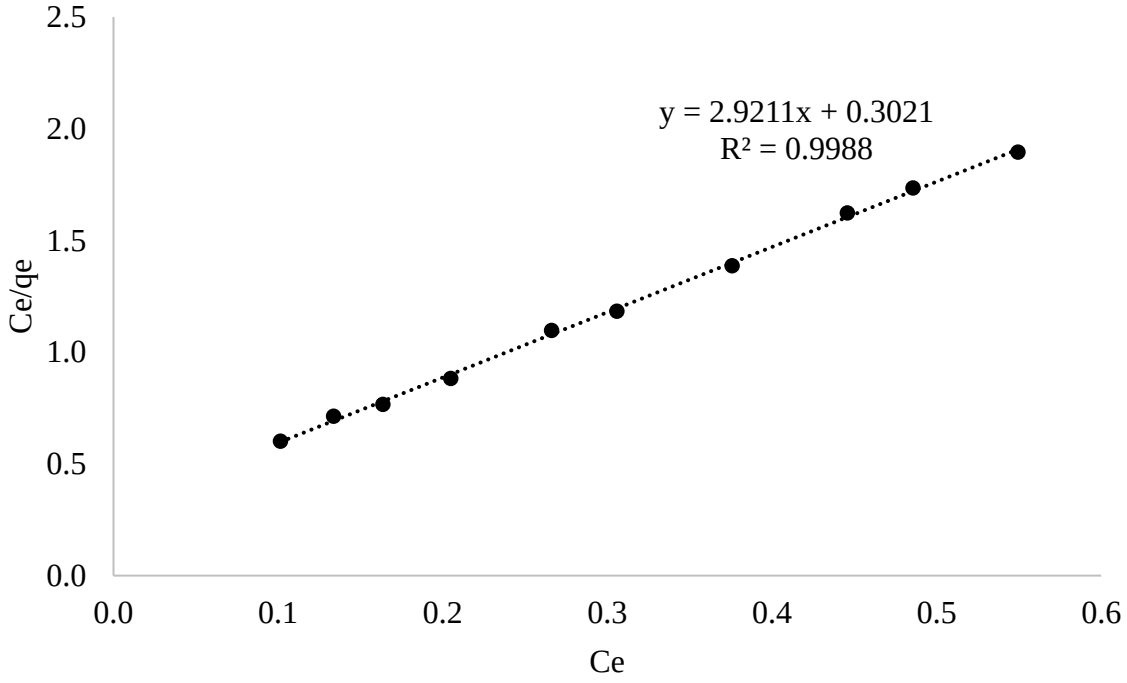


Figure 4.40: Langmuir Isotherm Model of MIP (MAA) of AME

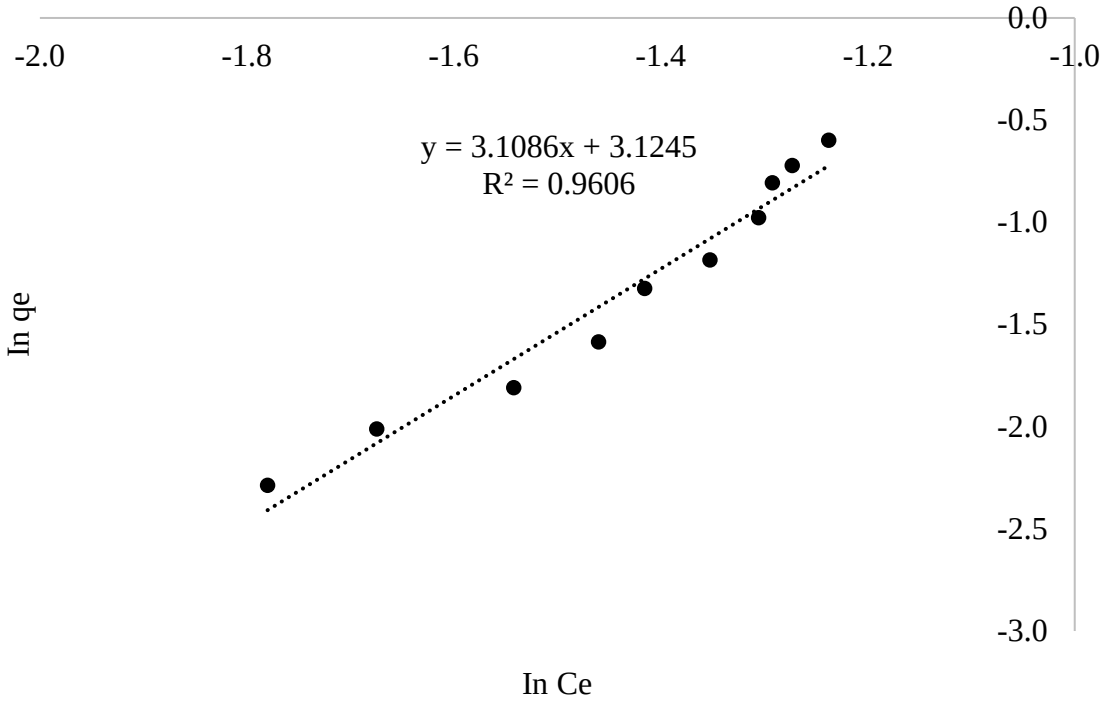


Figure 4.41: Freundlich Isotherm Model of MIP (MAA) of AME

Based on Table 4.9, the Langmuir constant of the K_L value of MIP (MAA) of AME was 9.6693 L/mg, indicating the interaction strength between AME as adsorbate and MIP (MAA) as adsorbent, as well as the equilibrium constant for the adsorption process. Due to a higher K_L value, MIP (MAA) of AME was assumed to have a stronger affinity as the adsorbent material for AME. Table 4.9 also showed that the separation factor or RL value of MIP (2VP) was 0.0803, suggesting a favourable adsorption process. This is due to the R_L value is often used to classify the adsorption process as irreversible ($R_L = 0$), favourable ($0 < R_L < 1$), linear ($R_L = 1$), or unfavourable ($R_L > 1$). Thus, MIP (MAA) of AME had a had a favourable adsorption process as it had a high affinity for the AME molecules.

Table 4.8: Adsorption Isotherm Models of MIP (MAA) of AME

Langmuir constants				**Freundlich constants**			
q_{max} (mg/g)	**K_L (L/mg)**	**R_L**	**R^2**	**K_F (mg/g)**	***n***	**1/*n***	**R^2**
0.3423	9.6693	0.0803	0.9988	22.7485	0.3217	3.1086	0.9606

4.12.3 Adsorption Isotherm Study of MIP (2VP) of ATZ

The Langmuir adsorption isotherm (Figure 4.42) and the Freundlich adsorption isotherm (Figure 4.43) of MIP (2VP) of ATZ were performed to understand the adsorption mechanisms between the MIP (2VP) as the adsorbent material and the ATZ target molecule as the adsorbates. The correlation coefficients or R^2 values of the Langmuir and the Freundlich adsorption isotherms were 0.9613 and 0.9440, respectively as shown in Table 4.10. So, the adsorption isotherm of MIP (2VP) can be explained based on the Langmuir adsorption isotherm model. The findings confirm that the binding sites for ATZ exhibit a monolayer adsorption process, where the recognition sites on the MIP surface are homogenous and all binding sites have the same affinity for the ATZ target molecules and minimal lateral interaction (Yilmaz et al., 2017).

Based on Figure 4.42 and Figure 4.43, the Langmuir constants and Freundlich constants of MIP (2VP) of ATZ were calculated as shown in Table 4.10. Since the adsorption isotherm of MIP (2VP) of ATZ is based on the Langmuir adsorption isotherm model, only Langmuir constants were further explained. The q_{max} value or the maximum amount of ATZ that can be adsorbed per unit weight or unit surface area of the MIP (2VP) of ATZ as the adsorbent was 0.3673 mg/g.

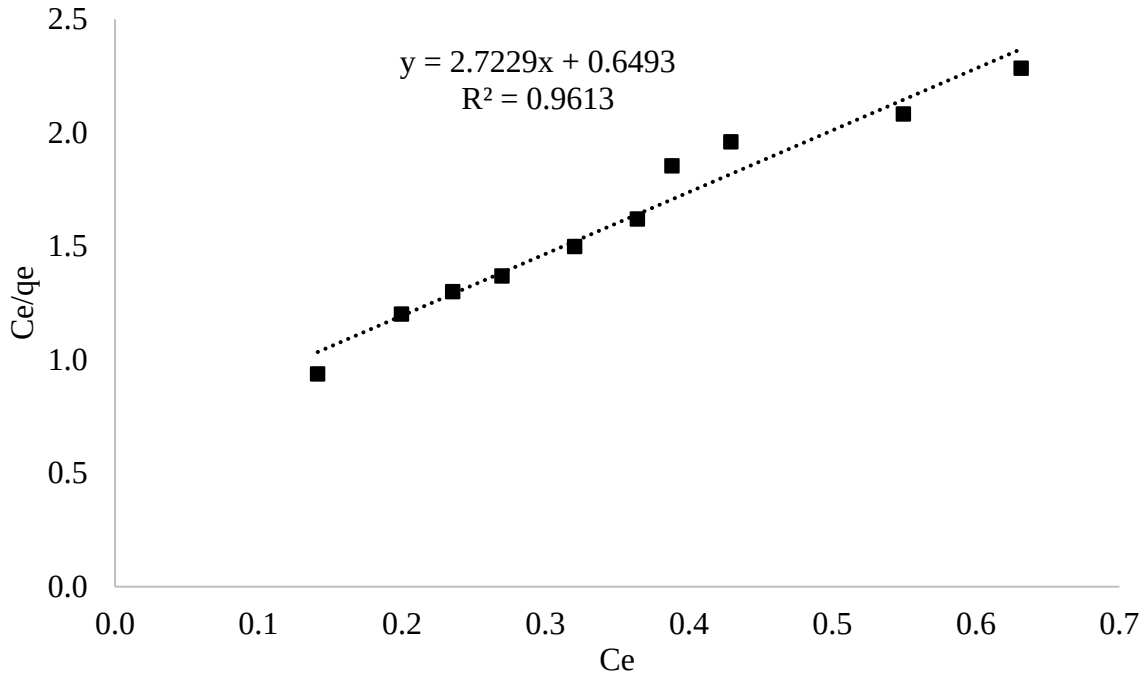


Figure 4.42: Langmuir Isotherm Model of MIP (2VP) of ATZ

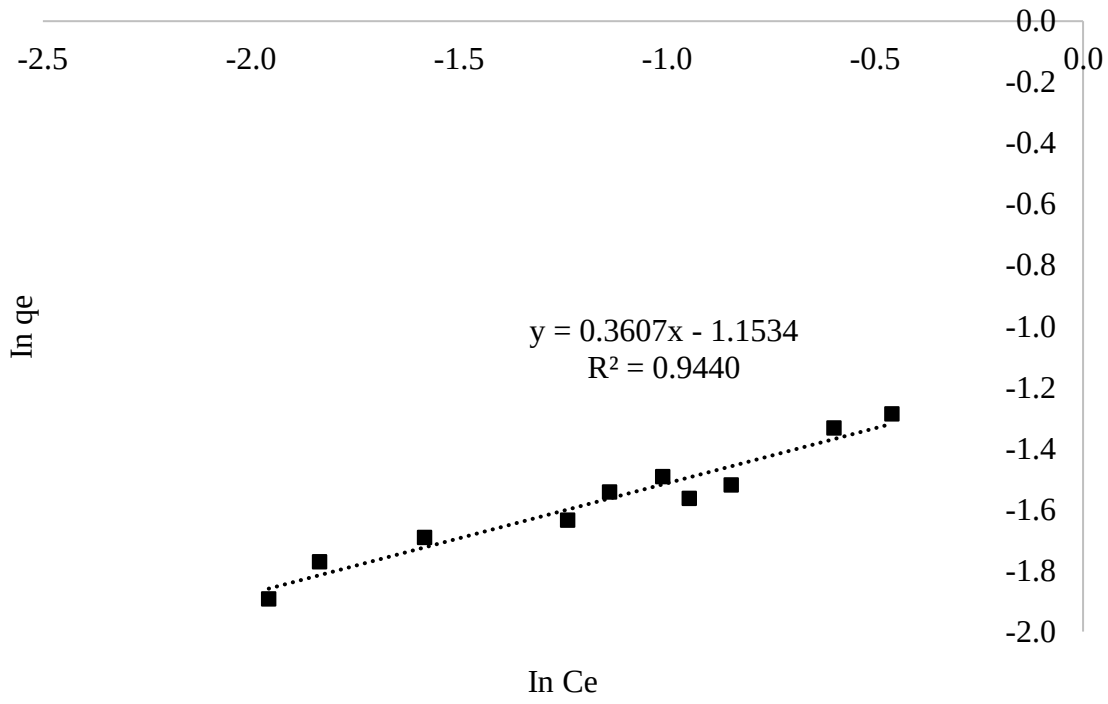


Figure 4.43: Freundlich Isotherm Model of MIP (2VP) of ATZ

The Langmuir adsorption constant or the K_L value of MIP (2VP) of ATZ was 4.1936 L/mg, which measures the strength of the ATZ adsorbate-MIP (2VP) adsorbent interactions and the equilibrium constant for the adsorption process. A higher K_L value indicated a stronger affinity of the MIP (2VP), the adsorbent material for ATZ. The separation factor or R_L value of MIP (2VP) was 0.1462, which can be applied to determine the favourability of the adsorption process. The R_L value can range from 0 to infinity and is often used to classify the adsorption process as irreversible ($R_L = 0$), favourable ($0 < R_L < 1$), linear ($R_L = 1$), or unfavourable ($R_L > 1$). An R_L value between 0 and 1 suggests a favourable adsorption process, indicating that the adsorbent material has a high affinity for adsorbate. Hence, the MIP (2VP) of ATZ had a favourable adsorption process as it had a high affinity for the ATZ molecules.

Table 4.9: Adsorption Isotherm Models of MIP (2VP) of ATZ

Langmuir constants				**Freundlich constants**			
q_{max} (mg/g)	**K_L (L/mg)**	**R_L**	**R^2**	**K_F (mg/g)**	***n***	**1/*n***	**R^2**
0.3673	4.1936	0.1462	0.9613	0.3156	0.3607	2.7724	0.9440

4.13 Selectivity Test

The selectivity test was employed to investigate the sensing property of synthesized MIPs of Triazine herbicides towards their target compound.

4.13.1 Selectivity Test of MIP (AAm) of CYZ

For the selectivity study of MIP (AAm) of CYZ, AME was selected as the competitive compound because it has an analogous chemical structure to CYZ, and is

categorised as a 1,3,5-triazine herbicide which is one of the environmental pollutants. Based on the selectivity test, the distribution ratio, K_D of MIP (AAm) of CYZ was much higher for CYZ than AME, meanwhile, the K_D of NIP (AAm) of CYZ was slightly lower for CYZ than AME, resulting in a higher selectivity coefficient, K_{sel} for CYZ than AME (Table 4.11).

Table 4.10: Selectivity Test of MIP (AAm) and NIP (AAm) of CYZ

	K_D MIP (AAm) (mg/L)	**K_D NIP (AAm) (mg/L)**	**K_{sel}**	**k'**
CYZ (Template molecule)	84.32	28.52	2.09	2.36
AME (Competitive compound)	40.37	32.19	0.89	

Hence, the calculated relative selectivity coefficient, k' was 2.36, indicating that the synthesized MIP (AAm) of CYZ was more selective towards CYZ, its own template compound than AME, the competitive compound (Appendix 34). This is because the value of the relative selectivity coefficient (k') is greater than 1 indicating that the synthesized MIP showed a good performance as molecular recognition (Yang et al., 2009).

The factor affecting the selectivity of MIP (AAm) towards CYZ than AME was the specific recognition sites in the MIP (AAm) that fit suitably with CYZ in terms of position and size because CYZ was used as the template molecule for the MIP synthesis, resulting in the imprinting effect on MIP (AAm) of CYZ. Besides that, the polymer selectivity is also depending on the shape of the binding sites and the particle size of the material (Zeng et al., 2012).

4.13.2 Selectivity Test of MIP (MAA) of AME

The selectivity test was employed to investigate the sensing property of synthesized MIP (MAA) of AME towards AME. In this study, CYZ was selected as the competitive compound which is a structural analogue of AME. The selectivity of MIP (MAA) of AME towards AME (template compound) and CYZ (competitive compound) were calculated based on the distribution ratio (K_D) selectivity coefficients (K_{sel}) and relative selectivity coefficient (k') as shown in Table 4.12 (Appendix 35). It showed that the distribution ratio of AME is much higher than the distribution ratio of CYZ, its competitive compound.

Table 4.11: Selectivity Test of MIP (MAA) and NIP (MAA) of AME

	K_D MIP (MAA) (mg/L)	**K_D NIP (MAA) (mg/L)**	**K_{sel}**	**k'**
AME (Template molecule)	94.75	31.51	2.52	2.66
CYZ (Competitive compound)	37.67	33.29	0.95	

Besides that, the selectivity coefficient of AME (template molecule) was greater than that of CYZ (competitive compound), explaining that the effect of imprinting method of MIP (MAA) of AME and its selectivity towards AME was remarkably successful. Bakhtiar et al. (2019) also emphasized that the template molecule had higher selectivity than that competitive compound because the synthesized MIP containing specific recognition sites complementary to the template molecule. The relative selectivity coefficient was 2.66, indicating that MIP (MAA) of AME has been good selectivity towards its compound of interest (AME). The value of relative selectivity coefficient greater than 1 indicated that the synthesized MIP showing a good performance as molecular recognition (Zhang et al., 2016).

Therefore, the synthesized MIP (MAA) of AME had selectively recognized the AME template molecule.

4.13.3 Selectivity Test of MIP (2VP) of ATZ

The selectivity test was conducted on MIP (2VP) of ATZ and NIP (2VP) of ATZ to evaluate their binding affinity towards the ATZ target molecule in comparison with another structural analogue compound namely AME. Based on Table 4.13, the distribution ratios or K_D values of MIP (2VP) for ATZ and AME were 95.08 mL/g and 38.11 mL/g, respectively. In contrast, the K_D values of NIP (2VP) for ATZ and AME were 29.57 mL/g and 32.87 mL/g, respectively (Appendix 36). This indicated that the K_D value of MIP (2VP) of ATZ was significantly greater for the selectivity of ATZ than AME**,** meanwhile, the K_D value of NIP (2VP) was slightly lower for the selectivity of ATZ than AME.

Table 4.12: Selectivity Test of MIP (2VP) and NIP (2VP) of ATZ

	K_D MIP (MAA) (mg/L)	**K_D NIP (MAA) (mg/L)**	**K_{sel}**	**k'**
ATZ (Template molecule)	95.08	29.57	2.50	2.77
AME (Competitive compound)	38.11	32.87	0.90	

It was calculated that the selectivity coefficient or K_{sel} value of ATZ was 2.50, much higher than the K_{sel} value of AME of 0.90, resulting in a relative selectivity coefficient (k') of 2.77. Zhang et al. (2016) stated that a relative selectivity coefficient larger than 1.00 suggested that the synthesized polymers were having good molecular recognition. This also showed that the synthesized MIP (2VP) of ATZ was more selective towards ATZ, the target

molecule as compared to AME, the competitive compound. The successful imprinting process of MIP significantly contributed to its selectivity towards ATZ, demonstrating remarkable recognition ability despite the minimal structural differences among the competitive compound, thus highlighting the combined influence of shape and size complementarity alongside analyte-functional group interactions within the three-dimensional polymer network (Chen et al., 2016).

4.14 MIP Applications in Water Samples

The synthesized MIP (AAm) of CYZ, MIP (MAA) of AME, and MIP (2VP) of ATZ were used for the application studies in water samples including DIW, tap water and river water.

4.14.1 Application of MIP (AAm) for CYZ Removal

The synthesized MIP (AAm) of CYZ was used for the removal of CYZ from water samples. Good removal efficiencies of CYZ in DIW (86.57 %), tap water (84.75 %) and river water (84.69 %) were attained by the synthesized MIP (AAm) of CYZ. Meanwhile, much lower removal efficiencies of CYZ in DIW (53.72 %), tap water (41.82 %) and river water (39.99 %) were obtained by the NIP. This showed that the synthesized MIP (AAm) of CYZ has specific binding sites complementary to CYZ as compared to the NIP (AAm) (Table 4.14). The addition of CYZ as a template molecule in the MIP (AAm) of CYZ preparation led to the imprinting effect of CYZ that generated more specific binding sites in MIP (AAm) of CYZ that were complementary to CYZ. Meanwhile, the preparation of NIP (AAm) did not involve the addition of CYZ, resulting in non-specific binding sites on its polymer structure and thus had much lower CYZ removal efficiencies in DIW, tap water and

river water. The high affinity and specificity of MIPs were influenced by the presence of the template molecule during the molecular imprinting process (Samarth et al., 2015).

Table 4.13: Removal of CYZ Using MIP (AAm) and NIP (AAm)

Samples	Amount of CYZ added (µg/mL)	Amount of CYZ found (µg/mL)	MIP (AAm) Recovery (%)	RSD	Amount of CYZ found (µg/mL)	NIP (AAm) Recovery (%)	RSD
DIW	25	21.64	86.57	0.01	13.43	53.72	0.02
Tap Water	25	21.19	84.75	0.04	10.46	41.82	0.04
River Water	25	21.17	84.69	0.01	10.00	39.99	0.11

Several other studies had been conducted for the removal of CYZ in environmental samples using adsorbents such as graphene (Wu et al., 2015), Fe3O4 (Safari et al., 2016), granular activated charcoal (Ilavaský et al., 2020), and magnetic adsorbent (Liu et al., 2023). However, MIP is the best adsorbent to extract CYZ in the environment due to its better extraction efficiency and selectivity, as well as the MIP preparation method is straightforward and inexpensive. Moreover, the terbuthylazine stir bars coated with MIP had successfully extracted various triazine herbicides including CYZ from rice samples as this MIP-coated adsorbent had improved the selectivity and removal efficiency of CYZ (Zhong et al., 2012).

4.14.2 Application of MIP (MAA) for AME Removal

Based on Table 4.15, the removal efficiency of AME from DIW, tap water and river water by using MIP (MAA) of AME were 95.01 %, 90.24 % and 88.37 %, respectively. Meanwhile, the removal efficiency of AME from DIW, tap water and river water by using NIP (MAA) were 54.97 %, 51.31 % and 49.45 %, respectively. Hence, MIP (MAA) of AME had an outstanding percentage of AME removal from different water samples than that NIP (MAA) due to the presence of specific binding sites in MIP (MAA) that are highly accessible for AME template molecule, resulting in greater imprinting effect.

Table 4.14: Removal of AME Using MIP (MAA) and NIP (MAA)

Samples	Amount of AME added (µg/mL)	Amount of AME found (µg/mL)	MIP (MAA) Recovery (%)	RSD	Amount of AME found (µg/mL)	NIP (MAA) Recovery (%)	RSD
DIW	25	23.75	95.01	0.01	13.74	54.97	0.03
Tap Water	25	22.56	90.24	0.04	12.83	51.31	0.11
River Water	25	22.09	88.37	0.01	12.36	49.45	0.01

4.14.3 Application of MIP (2VP) for ATZ Removal

Table 4.16 indicated the removal efficiency of ATZ from distilled water, tap water and river water by using the synthesized MIP (2VP) and NIP (2VP). MIP (2VP) of ATZ had successfully removed the ATZ from distilled water, tap water and river water with removal efficiencies of 95.39 %, 88.16 % and 86.75 %, respectively.

In comparison, NIP (2VP) had removed the ATZ from distilled water, tap water and river water with much lower removal efficiencies of 48.97 %, 44.04 % and 42.69 %, respectively. This proved that MIP (2VP) of ATZ had an outstanding performance as an adsorbate material to remove environmental contaminants such as ATZ in water samples. Samarth et al. (2015) exposed that the addition of a template or target molecule during MIP preparation which provides multiple interactions with the functional monomer, resulting in the MIP with greater affinity and specificity for the target molecule.

Table 4.15: Removal of ATZ Using MIP (2VP) and NIP (2VP)

Samples	Amount of ATZ added (µg/mL)	Amount of ATZ found (µg/mL)	MIP (2VP) Recovery (%)	RSD	Amount of ATZ found (µg/mL)	NIP (2VP) Recovery (%)	RSD
DIW	25	23.85	95.39	0.01	12.24	48.97	0.07
Tap Water	25	22.04	88.16	0.07	11.01	44.04	0.04
River Water	25	21.69	86.75	0.01	10.67	42.69	0.06

CHAPTER 5

CONCLUSION AND RECOMMENDATIONS

5.1 Conclusion

The MIPs of CYZ, AME and ATZ were successfully synthesized by the precipitation polymerization method with a non-covalent imprinting approach that took 6 h of polymerization reaction at temperature of 80 °C. CYZ, AME and ATZ as the template molecule, EGDMA as cross-linker, AIBN initiator, Tol and ACN as porogenic solvent, as well as different functional monomers of MAA, AAM, 2VP and 4VP. The NIP was synthesized in a similar way but without the addition of the CYZ, AME and ATZ.

The physical, chemical, and thermal properties of synthesized MIPs of CYZ, AME and ATZ were successfully analyzed by using the FTIR spectroscopy, FESEM, EDX spectroscopy, BET analyzer, and TGA. The chemical characterization of synthesized MIPs of CYZ, AME and ATZ were performed via FTIR spectrometer, whereby the presence of CYZ, AME and ATZ were detected at ~757 cm^{-1}, ~1453 cm^{-1}, and ~1390 cm^{-1}, respectively. The presence of EGDMA cross-linker can be observed at ~1135 cm^{-1} to ~1148 cm^{-1}, and ~1720 cm^{-1} to ~1725 cm^{-1}. Meanwhile, the presence of MAA, AAm, 2VP and 4VP were detected at ~1635 cm^{-1}, ~3355 cm^{-1} to ~3669 cm^{-1}, ~1051 cm^{-1} to ~1056 cm^{-1}, and ~1558 cm^{-1} to 1597 cm^{-1}, respectively. Besides that, the FESEM analysis indicated that the generated MIP (AAm) of CYZ, MIP (MAA) of AME and MIP (2VP) of ATZ were spherical in shape and the mean diameter of micro-size in range of 0.86 µm,0.52 µm, and 0.30 µm, respectively. Based on the EDX analysis, the MIP (AAm) of CYZ, MIP (MAA) of AME and MIP (2VP) of ATZ were mainly made of carbon (82.88 %, 88.52 %, and 87.87 %) and oxygen (17.12 %, 11.48 %, and 12.13 %). The BET analysis depicted that the MIP (AAm)

of CYZ were greater than its NIP (AAm) of CYZ in terms of surface area, average pore radius and total pore volume which were 21.019 m2/g, 104.900 Å, and 1.868 cm2/g, respectively. The MIP (MAA) of AME also had larger surface area, average pore radius and total pore volume of 13.6801 m2/g, 103.1369 Å, and 0.03178 cm2/g, respectively as compared to its NIP (MAA) of AME. The surface area (41.5923 m2/g), average pore radius (170.5645 Å) and total pore volume (0.1774 cm2/g) of MIP (2VP) of ATZ were also higher than its NIP (2VP) of ATZ. Moreover, the TGA analysis of MIP (AAm) of CYZ displayed a drastic weight loss was observed between ~334 °C to ~420 °C. An extreme weigh loss of MIP (MAA) of AME was also seen from ~320.51 °C to ~480 °C. For MIP (2VP) of ATZ, its drastic weight loss can be observed at ~335 °C to ~450 °C.

The binding efficiencies and adsorption parameter of MIPs of CYZ, AME and ATZ were successfully identified via UV-Vis analysis that determine the ideal contact time, initial concentration, pH, and polymer dosage to attain their highest adsorption efficiencies. MIP (AAm) of CYZ obtained its highest adsorption efficiency (86.39 %) at optimum conditions of 240 mins contact time, 6 ppm of CYZ solution at pH 7, and 0.1 g of polymer. Meanwhile, MIP (MAA) of AME attained its maximum adsorption efficiency (94.51 %) at contact time of 210 mins, 7 ppm of AME solution and o.1 g of polymer. The ideal condition for MIP (2VP) to obtain its highest adsorption efficiency (91.62 %) was at a contact time of 15 mins, 8 ppm of ATZ solution and 0.3 g of polymer.

The selectivity efficiencies of synthesized MIP (AAm) of CYZ, MIP (MAA) of AME and MIP (2VP) of ATZ were successfully determined by using RP-HPLC. Through selectivity test, MIP (AAm) of CYZ exhibited higher selectivity towards CYZ (target compound) as compared to AME (competitive compound) with a calculated relative

selectivity coefficient of 2.36. Similarly, MIP (MAA) of AME more selective towards AME as the target compound in comparison to CYZ as the competitive compound with relative selectivity coefficient of 2.66. The MIP (2VP) of ATZ also had higher selectivity towards its target compound (ATZ) as compared to its competitive compound (AME) with a relative selectivity coefficient of 2.77.

Additionally, the removal efficiency of CYZ, AME and ATZ in water samples by using synthesized MIP (AAm) of CYZ, MIP (MAA) of AME and MIP (2VP) of ATZ were successfully demonstrated. It was revealed that synthesized MIP (AAm) of CYZ had successfully removed CYZ in DIW (86.57 %), tap water (84.74 %), and river water (84.69 %). AME was also successfully removed by synthesized MIP (MAA) of AME from DIW, tap water and river water with removal efficiencies of 95.01 %, 90.24 %, and 88.37 %, respectively. The removal efficiency of ATZ in DIW, tap water and river water by using synthesized MIP (2VP) of ATZ were 95.39 %, 88.16 %, and 86.75 %, respectively. In conclusion, the advancement of MIP-based approaches for the removal of triazine herbicides plays a crucial and promising role in sustaining the environment globally.

5.2 Recommendations

MIT is a versatile approach to producing MIPs of triazine herbicides as promising adsorbent materials for the removal of environmental contaminants in water samples. Therefore, the implementation of the synthesized MIP of triazine herbicides as an adsorbent material for water treatment application in real environmental situations such as water catchment, stream and seas can be further studied.

REFERENCES

Abass, K., Pelonen, O., & Rautio, A. (2021). Chloro-s-triazines-toxicokinetic, toxicodynamic, human exposure and regulatory considerations. *Current Drug Metabolism, 22*, 645-656.

Abouzarzadeh, A., Forouzani, M., Jahanshahi, M., & Bahramifar, N. (2012). Synthesis and evaluation of uniformly sized nalidixic acid-imprinted nanospheres based on precipitation polymerization method for analytical and biomedical applications. *Journal of Molecular Recognition, 25*(7), 404-413.

Abraham, J., & Mathew, B. (2014). Grafting of molecularly imprinted polymer on multiwalled carbon nanotube for highly selective and sensitive determination of Thymine. *Scholar Research Library, 3*(3), 26-33.

Ackerman, F. (2007). The economics of atrazine. *International Journal of Occupational and Environmental Health, 13*(4), 437-445.

Ahmad, A.L., Lah, N.F.C, & Low, S.C. (2015). Molecular imprinted polymer for atrazine detection sensor: Preliminary study. *Chemical Engineering Transactions, 45,* 1483-1488.

Ahmad, A.L., Lah, N.F.C., & Low, S.C. (2018). Configuration of molecular imprinted polymer for electrochemical atrazine detection. *Journal of Polymer Research, 25,* 243.

Akhoundian, M., Alizadeh, T., Ganjali, M.R., & Rafiei, F. (2018). A new carbon paste electrode modified with MWCNTs and nano-structured molecularly imprinted polymer for ultratrace determination of trimipramine: The crucial effect of electrode components mixing on its performance. *Biosensors and Bioelectronics, 111*, 27-33.

Alamrani, N.A., & AL-Aoh, H.A. (2021). Elimination of Congo Red dye from industrial

wastewater using *Teucrium polium L.* as a low-cost local adsorbent. *Adsorption Science and Technology, 2021*, 1-12.

Ali, I., AL-Othman, Z.A., & Alwarthan, A. (2016). Green synthesis of functionalized iron nano particles and molecular liquid phase adsorption of ametryn from water. *Journal Molecular Liquid, 221*, 1168-1174.

Ali, Z., Sajid, M., Ahmed, M.M., Hanif, M., & Manzoor, S. (2023). Synthesis of green fluorescent cross-linked molecularly imprinted polymer bound with anti-cancerous drug (docetaxel) for targeted drug delivery. *Polymer Bulletin,* 1-18.

Almberg, K.S., Turyk, M.E., Jones, R.M., Rankin, K., Freels, S., & Stayner, L.T. (2018). Atrazine contamination of drinking water and adverse birth outcomes in community water systems with elevated atrazine in Ohio, 2006-2008. *International Journal of Environmental Research and Public Health, 15*(9), 1889.

Alvarez-Lorenzo, C., & Concheiro, A. (2004). Molecularly imprinted polymers for drug delivery. *Journal of Chromatography B, 804*, 231-245.

Amorim, M.S., Sales, M.G.F., & Frasco, M.F. (2022). Recent advances in virus imprinted polymers. *Biosensors and Bioelectronics: X, 10,* 100131.

Anirudhan, T.S., Christa, J., & Deepa, J.R. (2017). Extraction of melamine from milk using magnetic molecularly imprinted polymer. *Food Chemistry, 227,* 85-92.

Ansell, R.J. (2005). Molecularly imprinted polymers for the enantioseparation of chiral drugs. *Advanced Drug Delivery Reviews, 57*, 1809-1835.

Ansell, R.J., & Wang, D. (2009). Imprinted polymers for chiral resolution of (+/–)-ephedrine. Part 3: NMR predictions and HPLC results with alternative functional monomers. *Analyst, 134*(3), 564-576.

Arabzadeh, N., & Abdouss, M. (2010). Synthesis and characterization of molecularly

imprinted polymers for selective solid–phase extraction of Pseudoepherine. *Colloid Journal, 72*(4), 446-455.

Aravind, A., & Mathew, B. (2018). Electrochemical sensor based on nanostructured ion imprinted polymer for the sensing and extraction of Cr (III) ions from industrial wastewater. *Polymer International, 67*, 1595-1604.

Arshady, R., & Mosbach, K. (1981). Synthesis of substrate-selective polymers by host-guest. Polymerization. *Macromolecular Chemistry and Physics, 182*, 687-692.

Asfaram, A., Ghaedi, M., & Dashtian, K. (2017). Ultrasound assisted combined molecularly imprinted polymer for selective extraction of nicotinamide in human urine and milk samples: Spectrophotometric determination and optimization study. *Ultrasonic Sonochemistry, 34*, 640-650.

Atlabachew, M., Torto, N., Chandravanshi, B.S., Redi-Abshiro, M., Chigome, S., Mothibedi, K., & Combrinck, S. (2015). A (-)-norephedrine-based molecularly imprinted polymer for the solid phase extraction of psychoactive phenylpropylamino alkaloids from Khat (*Catha edulis Vahl. Endl*.) chewing leaves. *Biomedical Chromatography, 30*, 1007-1015.

Azizi, A., & Bottaro, C.S. (2020) A critical review of molecularly imprinted polymers for the analysis of organic pollutants in environmental water samples. *Journal of Chromatograph A, 1614*, 460603.

Bakhtiar, S., Bhawani, S.A., & Shafqat, S.R. (2019). Synthesis and characterization of molecular imprinting polymer for the removal of 2-phenylphenol from spiked blood serum and river water. *Chemical and Biological Technologies in Agriculture*, *6*(15), 1-10.

Balamurugan, K., Gokulakrishnan, K., & Prakasam, T. (2011). Preparation and evaluation of molecularly imprinted polymer liquid chromatography column for the separation of ephedrine enantiomers. *Arabian Journal of Chemistry, 9*(1), 528-536.

Baltes, L., Costiuc, L., Patachia, S., & Tierean, M. (2019). Differential scanning calorimetry-A powerful tool for the determination of morphological features of the recycled polypropylene. *Journal Thermal Analysis and Calorimetry, 138*(4), 2399-2408.

Beaulieu, M, Cabana, H., Taranu, Z., & Huot, Y. (2020). Predicting atrazine concentrations in waterbodies across the contiguous United States: The importance of land use, hydrology, and water physicochemistry. *Limnology and Oceanography, 65*, 2966-2983.

Bedin, K.C., Martins, A.C., Cazetta, A.L., Pezoti, O., & Almeida, V.C. (2016). KOH-activated carbon prepared from sucrose spherical carbon: adsorption equilibrium, kinetic and thermodynamic studies for methylene blue removal. *Chemical Engineering Journal, 286*, 476-484.

BelBruno, P.P. (2019). Molecularly Imprinted Polymers. *Chemical Reviews, 119*, 94-119.

Bergmann, N.M., & Peppas, N.A. (2008). Molecularly imprinted polymers with specific recognition for macromolecules and proteins. *Progress in Polymer Science, 33*, 271-288.

Bhaskar, S., Manoj, A., Manu, B., Sreenivasa, M.Y., & Mudipu, V. (2022). Non-ferrous fenton's oxidation of ametryn using bioleached e-waste copper as catalyst. *Journal of Sustainable Metallurgy, 8*(4), 1617-1627.

Bhawani, S.A., Bakhtiar, S., & Shafqat, S.R. (2019). Synthesis of molecularly imprinted polymers for the selective extraction/removal of 2,4,6-trichlorophenol. *The Open Chemical Engineering Journal, 13*(1), 122-133.

Bhawani, S.A., Bakhtiar, S., Roland, R.M., Shafqat, S.R., & Ibrahim, M.N.M. (2020a). Synthesis of molecularly imprinted polymers of vanillic acid and extraction of vanillic acid from spiked blood serum. *Journal of Applied Pharmaceutical Science, 10*(4), 56-62.

Bhawani, S.A., Daud, N.A.B., Bakhtiar, S., Roland, R.M., & Ibrahim, M.N.M. (2020c). Synthesis of molecularly imprinting polymers for the removal of Xylenol Orange from water. *Nature Environment and Pollution Technology, 19*(2), 825-830.

Bhawani, S.A., Juarah N.R., Bakhtiar, S., Roland, R.M., Ibrahim, M.N.M., Alotaibi, K.M., & Moheman, A. (2022). Synthesis of molecularly imprinted polymer nanoparticles for removal of Sudan III dye. *Asian Journal of Chemistry, 34*(12), 3269-3274.

Bhawani, S.A., Sen, T.S., & Ibrahim, M.N.M. (2018). Synthesis of molecular imprinting polymers for extraction of gallic acid from urine. *Chemistry Central Journal, 12*(19), 1-7.

Bhawani, S.A., Suhaili, N., Roland, R.M., Bakhtiar, S., Alotaibi, K.M., & Ibrahim, M.N.M. (2020b). Template assisted synthesis of molecularly imprinted polymer for the extraction of p-Coumaric acid. *Asian Journal of Chemistry, 34*(9), 2342-2346.

Blahová, J., Plhalová, L., Hostovský, M., Divišová, L., Dobšíková, R., Mikulíková, I., Stěpánová, S., & Svobodová, Z. (2013). Oxidative stress responses in zebrafish *Danio rerio* after subchronic exposure to atrazine. *Food and Chemical Toxicology, 61*, 82-85.

Breton, F., Euzet, P., Piletsky, S.A., Giardi, M.T., & Rouillon, R. (2006). Integration of photosynthetic biosensor with molecularly imprinted polymer-based solid phase extraction cartridge. *Analytica Chimica Acta, 569*, 50-57.

Britto, F.B., Vasco, A.N.D., Pereira, A.P.S., Júnior, A.V.M., & Nogueira, L.C. (2012). Herbicides in the upper Poxim river, Sergipe, and the risk of contamination of water sources. *Revista Ciencia Agronômica, 43*(2), 390-398.

Burkanudeen, A.R, Ahamed, M.A.R., Azarudeen, R.S., Begum, M.S., & Gurnule, W.B. (2016). Thermal degradation kinetics and antimicrobial studies of terpolymer resins. *Arabian Journal of Chemistry, 9*, 296-305.

Cavalcante, R.P., Oliveira, D.M.D., Silva, L.M.D., Giménez, J., Esplugas, S., Oliveira, S.C.D., Dantes, R.F., Sans, C., & Machulek, A. (2021). Evaluation of the main active species involved in the TiO_2 photocatalytic degradation of ametryn herbicides and its by-products. *Journal of Environmental Chemical Engineering, 9*(2), 1-13.

Ceglowski, M., Jerca, V.V., Jerca, F.A., & Hoogenboom, R. (2020). Reduction-responsive molecularly imprinted poly(2-isopropenyl-2-oxazoline) for controlled release of anticancer agents. *Pharmaceuticals, 12*, 506.

Chapuis, F., Pichon, V., Lanza, F., Sellergren, B., & Hennion, M.C (2004). Retention mechanism of analytes in the solid-phase extraction process using molecularly imprinted polymers: Application to the extraction of triazines from complex matrices. *Journal of Chromatography B, 804*, 93-101.

Chapuis, F., Pichon, V., Lanza, F., Sellerrgren, S., & Hennion, M.C. (2003). Optimization of the class-selective extraction of triazines from aqueous samples using a molecularly imprinted polymer by a comprehensive approach of the retention mechanism. *Journal of Chromatography A, 999*(1-2), 23-33.

Chen, H., Guo, J., Wang, Y., Dong, W., Zhao, Y., & Sun, L. (2022). Bio-inspired imprinting materials for biomedical applications. *Advance Science, 2022*, 2202038.

Chen, J., Bai, L., Liu, K., Liu, R., & Zhang, Y. (2014). Atrazine molecular imprinted polymers: Comparative analysis by far-infrared and ultraviolet induced polymerization. *International Journal of Molecular Sciences, 15*, 574-587.

Chen, J., Zhao, W., Tan, L., Wang, J., Li, H., & Wang, J. (2019). Separation and detection of trace atrazine from seawater using dummy template molecularly imprinted solid-phase extraction followed by high-performance liquid chromatography. *Marine Pollution Bulletin, 149,* 110502.

Chen, L., Wu, X., Wang, X., & Li, J. (2016). Molecular imprinting: Perspectives and applications. *Chemical Society Reviews, 45*, 2137-2211.

Chidya, R., Derbalah, A., Abdel-Dayem, S., Kaonga, C., & Sakugawa, H. (2021). Ecotoxicological and human health risk assessment of selected pesticides in Kurose River, Higashi-Hiroshima city (Japan). *Water Environment Research, 94*(1),1676.

Cooper, R.L. (2000). Atrazine disrupts the hypothalamic control of pituitary-ovarian function. *Toxicological Sciences, 53*, 297-307.

Cowen, T., Karim, K., & Piletsky, S. (2016). Computational approaches in the design of synthetic receptors-A review. *Analytical Chimica Acta, 936*, 62-74.

Cristallini, C., Ciardelli, G., Barbani, N., & Giusti, P. (2004). Acrylonitrile-acrylic acid copolymer membrane imprinted with uric acid for clinical uses. *Macromolecular Bioscience, 4*, 31-38.

Cui, F., Zhou, Z., & Zhou, H.S. (2020). Molecularly imprinted polymers and surface imprinted polymers based electrochemical biosensor for infectious diseases. *Sensors, 20*, 996.

Darwish, A.A.A., Rashad, M., & Al-Aoh, H.A. (2019). Methyl orange adsorption comparison and nanoparticles: isotherm, kinetics, and thermodynamic studies. *Dyes and Pigments, 160*, 563-571.

Djozan, D., & Ebrahimi, B. (2008). Preparation of new solid phase micro extraction fiber on the basis of atrazine-molecular imprinted polymer: Application for GC and GC/MS screening of triazine herbicides in water, rice, and onion. *Analytica Chimica Acta, 616*(2), 152-159.

Djozan, D., Mahkam, M., & Ebrahimi, B. (2009). Preparation and binding study of solid-phase microextraction fiber on the basis of ametryn-imprinted polymer: Application to the selective extraction of persistent triazine herbicides in tap water, rice, maize and onion. *Journal of Chromatography A, 1216,* 2211-2219.

Dong, L., Hou, C., Yang, M., Fa, H., Wu, H., Shen, C., & Huo, D. (2016). Highly sensitive colorimetric and fluorescent sensor for cyanazine based on the inner filter effect of gold nanoparticles. *Journal of Nanoparticle Research, 18*(164).

Ertück, G., & Mattiasson, B. (2017). Molecular imprinting techniques used for the preparation of biosensors. *Sensors, 17,* 288.

Esfandyari-Manesh, M., Javanbakht, M., Shahmoradi, E., Dinarvand, R., & Atyabi, F. (2013). The control of morphological and size properties of carbamazepine-imprinted microspheres and nanospheres under different synthesis conditions. *Journal of Materials Research, 28*, 2677-2686.

Fan, M., Dai, D., & Huang, B. (2012). Fourier Transform Infrared Spectroscopy for Natural Fibres. *Fourier Transform-Material Analysis*, 45-68.

Farooq, S., Wu, H., Nie, J., Ahmad, S., Muhammad, I., Zeeshan, M., Khan, R., & Asim, M. (2022). Application, advancement and green aspects of magnetic molecularly

imprinted polymers in pesticide residue detection. *Science of The Total Environment, 804*, 150293.

Fauziah, S., Gafur, A.M., Soekamto, N. H., Taba, P., & Sapar, A. (2021). Synthesis and characterization of molecularly imprinted polymers of di-(2-ethylhexyl) phthalate using the precipitation polymerization method. *Egyptian Journal of Chemistry, 64*, 2385.

Feng, M.X., Wang, G.N., Yang, K., Liu, H.Z., & Wang, J.P. (2016). Molecularly imprinted polymer-high performance liquid chromatography for the determination of tetracycline drugs in animal derived foods. *Food Control, 69*, 171-176.

Fitzhenry, L. (2011). Development of molecularly imprinted polymers for corticosteroids. Doctoral dissertation. Ireland, Waterford Institute of Technology.

Gajovic-Eichelmann, N., Athikomrattanakul, U., Dechtrirat, D., & Scheller, F.W. (2012). Molecular imprinting technique for biosensing and diagnostics. *Applications of Nanomaterials in Sensors and Diagnostics, 14*, 143-170.

Gao, B., Chen, Y., & Men, J. (2011). Constructing chiral caves and efficiently separating enantiomers of glutamic acid with novel surface-imprinting technique. *Journal of Chromatography A, 1218*, 5441-5448.

Gao, B., Liu, H., & Cui, K. (2017). Preparation and molecule-recognition characteristics of grafting type molecule-imprinted membrane and potentiometric sensor for atrazine. *Sensors and Actuators B: Chemical, 254*, 1048-1056.

Gao, S., Bie, C., Ji, Q., Ling, H., Li, C., Fu, Y., Zhao, L., & Ye, F. (2019). Preparation and characterization of cyanazine-hydroxypropyl-beta-cyclodextrin inclusion complex. *Royal Society of Chemistry Advances, 9,* 26109.

George, L., Ma, L., Zhang, W., & Yao, G. (2023). Parametric modelling and analysis to optimize adsorption of atrazine by MgO/Fe3O4-synthesized porous carbons in water environment. *Environmental Sciences Europe, 35*, 21.

Ghasemzadeh, N. (2010). Application of artificial gel antibodies for the detection and quantification of proteins in biological fluids. Doctoral thesis, Uppsala University, Sweden.

Gholivand, M.B., Sharianti-Rad, M., Karimian, N., & Torkashvand, M. (2012). A chemometrics approach for simultaneous determination of cyanazine and propazine based on a carbon paste electrode modified by a molecularly imprinted polymer. *Analyst, 137*, 1190.

Gholivand, M.B., Torkashvand, M., & Malekzadeh, G. (2012). Fabrication of an electrochemical sensor based on computationally designed molecularly imprinted polymers for detection of cyanazine in food samples. *Analytica Chimica Acta, 713,* 36-44.

Golker, K., Karlsson, B.R.C., Olsson, G.D., Rosengren, A.M., & Nicholls, I.A. (2013). *Macromolecules, 46*, 1408-1414.

Gomes, C., Sadoyan, G., Dias, R., & Costa, M.R.P.F.N. (2017). Development of molecularly imprinted polymers to target polyphenols present in plant extracts. *Processes, 5*(4), 72.

Google Maps. (n.d.). [Locality Map of Sampling Point at Kota Samarahan]. Retrieved January 7, 2024, from https://maps.app.goo.gl/txzdNg4u648WWfir6

Grillo, R., Pereira, A.D.E.S., Melo, N.F.S.D., Porto, R.M., Feitosa, L.O., Tonello, P.S., Filho, N.L.D., Rosa, A.H., Lima, R., & Fraceto, L.F. (2011). Controlled release system for ametryn using polymer microspheres: Preparation, characterization and release kinetics in water. *Journal of Hazardous Materials, 186,* 1645-1651.

Guan, G., Liu, B., Wang, Z., & Zhang, Z. (2008). Imprinting of molecular recognition sites on nanostructures and its applications in chemosensors. *Sensors, 8*, 8291-8320.

Gui, R., Jin, H., Guo, H., & Wang, Z. (2018). Recent advances and future prospects in molecularly imprinted polymers-based electrochemical biosensors. *Biosensors and Bioelectronics, 100*, 56-70.

Guo, X., Xia, Z., Wang, H., Kang, W., Lin, L., Cao, W., Zhang, H., & Zhou, W. (2017). Molecularly imprinted solid phase extraction method for simultaneous determination of seven nitroimidazoles from honey by HPLC-MS/MS. *Talanta, 166*, 101-108.

Güzel, F., & Sayğili, H. (2016). Adsorptive efficacy analysis of novel carbonaceous sorbent derived from grape industrial processing wastes towards tetracycline in aqueous solution. *Journal of the Taiwan Institute of Chemical Engineers, 60*, 236-240.

Guzzella, L., Pozzoni, F., & Baggiani, C. (2007). A cyanazine imprinted polymer for the extraction of herbicides from water samples. In A.A.M. Re, E. Capri, G. Fragoulis, & M. Trevisan (Eds.), *Environmental fate and ecological effects of pesticides* (1st ed., pp. 842-849). La Goliardica Pavese.

Han, Z., Jiang, K., Fan, Z., Diana Di Mavungu, J., Dong, M., Guo, W., Fan, K., Campbell, K., Zhao, Z., & Wu, Y. (2017). Multi-walled carbon nanotubes-based magnetic solid-phase extraction for the determination of zearalenone and its derivatives in maize by ultra-high performance liquid chromatography-tandem mass spectrometry. *Food Control, 79*, 177-184.

Harun, N. (2010). Application of molecularly imprinted solid phase extraction, enzyme-linked immunosorbent assay and liquid chromatography tandem mass spectrometry to forensic toxicology. (Doctoral thesis, University of Glasgow, Scotland). Retrieved from http://theses.gla.ac.uk/1992/1/2010harunphddf.pdf

Hasanah, A.N., Susanti, I., Marcellino, M., Maranata, G.J., Saputri, F.A., & Pratiwi, R. (2021). Microsphere molecularly imprinted solid-phase extraction for diazepam analysis using itaconic acid as monomer in propanol. *De Gruyter, 19*, 604-613.

Hashemi-Moghaddam, H., Hosseni, M., & Mohammadhonesseini, M. (2017). Preparation of molecularly imprinted polymers on the surface of optical fiber for HS-solid-phase microextraction of phenol. *Separation Science and Technology, 52*(11), 1826.

Haupt, K. (2001). Molecularly imprinted polymers in analytical chemistry. *Analyst, 126*, 749-756.

Haupt, K., & Mosbach, K. (1998). Plastic antibodies: Developments and applications. *Trends in Biotechnology, 100*(7), 2495-2504.

Haupt, K., & Mosbach, K. (2000). Molecularly imprinted polymers and their use in biometric sensors. *Chemical Reviews, 16,* 468-475.

Haupt, K., Linares, A.V., Bompart, M., & Bui, B.T.S. (2012). Molecularly imprinted polymers. *Topics in Current Chemistry, 325*, 1-28.

Haupt, K., Medina-Rangel, P.X., & Bui, B.T.S. (2020). Molecularly imprinted polymers: Antibody mimics for bioimaging and therapy. *Chemistry Reviews, 120*, 9554-9582.

Hayes, T.B., Khoury, V., Narayan, A., Nazir, M., Park, A., Brown, T., Adame, L., Chan, E., Buchholz, D., & Stueve, T. (2010). Atrazine induces complete feminization and chemical castration in male African clawed frogs (Xenopus laevis). *The Proceedings of the National Academy of Sciences USA, 107*, 4612-4617.

He, J. X., Pan, H. Y., Xu, L., & Tang, R. Y. (2021). Application of molecularly imprinted polymers for the separation and detection of aflatoxin. *Journal of Chemical Research, 45*(5-6), 400-410.

Herrera-Chacón, A., Cetó, X., del Valle, M. (2021). Molecularly imprinted polymers towards electrochemical sensors and electronic tongues. *Analytical and Bioanalytical Chemistry, 413*, 6117-6140.

Herrera-Garcia, U., Castillo, J., Patino-Ruiz, D., Solano, R., & Herrera, A. (2019). Activated carbon from yam peels modified with Fe_3O_4 for removal of 2,4-dichlorophenoxyacetic acid in aqueous solution. *Water, 11*, 19.

Ibarra, I.S., Miranda, J.M., Pérez-Silva, I., Jardinez, C., & Islas, G. (2020). Sample treatment based on molecularly imprinted polymers for the analysis of veterinary drugs in food samples: A review. *Analytical Methods, 12*, 2958-2977.

Ilavaský, J., Barloková, D., & Marton, M. (2020). Triazine herbicides removal from water with granular activated carbon. *IOP Conference Series: Earth and Environmental Science, 609*, 012088.

Iskierko, Z., Sharma, P.S., Bartold, K., Pietrzyk-Le, A., Noworyta, K., & Kutner, W. (2016). Molecularly imprinted polymers for separating and sensing of macromolecular compounds and microorganisms. *Biotechnology Advances, 34*, 30-46.

Jablonowski, N. D., Schäffer, A., & Burauel, P. (2011). Still present after all these years: Persistence plus potential toxicity raise questions about the use of atrazine. *Environmental Science and Pollution Research International, 18*(2), 328-331.

Jalilian, N., Ebrahimazadeh, H., Asgharinezhad, A.A., & Khodayari, P. (2021). Magnetic molecularly imprinted polymer for the selective dispersive micro solid phase extraction of phenolphthalein in urine samples and herbal slimming capsules prior to HPLC-PDA analysis. *Microchemical Journal, 160*, 105712.

Jawaid, S., Talpur, F.N., Sherazi, S.T.H., Nizamani, S., & Khaskheli, A.A. (2013). Rapid detection of melamine adulteration in dairy milk by SB-ATR-Fourier transform infrared spectroscopy. *Food Chemistry, 141*, 3066-3071.

Jian, Y., Chen, L., Cheng, J., Huang X., Yan, L., & Li, H. (2020). Molecularly imprinted polymers immobilized on graphene oxide film for monolithic fiber solid phase microextraction and ultrasensitive determination of triphenyl phosphate. *Analytica Chimica Acta, 1133*, 1-10.

Jin, Y., Zhang, X., Shu, L., Chen, L., Sun, L., Qian, H., Liu, W., & Fu, Z. (2010). Oxidative stress response and gene expression with atrazine exposure in adult female zebrafish (*Danio rerio*). *Chemosphere*, *78*(7), 846-852.

Jin, Y.F., Zhang, Y.J., Zhang, Y.P., Chen, J., Zhou, X.M., & Bai, L.Y. (2013). Synthesis and evaluation of molecularly imprinted polymer for the determination of the phthalate esters in the bottled beverages by HPLC. *Journal of Chemistry, 2013*, 1-9.

Jusoh, N.H.S., Mehamod, F.S., Yusof, N.F., Jani, A.M.M., Suah, F.B.M., Ariffin, M.M., & Zulkefli, N.A. (2022). Preparation and adsorption studies of molecularly imprinted polymer for selective recognition of tryptophan. *Malaysian Journal of Analytical Sciences, 26*(2),215-228.

Karimi-Maleh, H., Karimi, F., Fu, L., Sanati, A.L., Alizadeh, M., Karaman, C., & Orooji, Y. (2022). Cyanazine herbicide monitoring as hazardous substance by DNA nanostructure biosensor. *Journal of Hazardous Materials, 423*, 127058.

Karrat, A., Palacios-Santander, J.M., Amine, A., & Cubillana-Aguilera, L. (2022). A novel magnetic molecularly imprinted polymer for selective extraction and determination of quercetin in plant samples. *Analytica Chimica Acta, 1203,* 339709.

Kaur, J., Singh, K.V., Boro, R., Thampi, K.R., Raje, M., Varshney, G.C., & Suri, C.R (2007). Immunochromatographic dipstick assay format using gold nanoparticles labelled protein-hapten conjugate for the detection of atrazine. *Environmental Science and Technology, 41*(14), 5028-5036.

Khajeh, M., Heidari, Z.S., & Sanchooli, E. (2011). Synthesis, characterization and removal of lead from water samples using lead-ion imprinted polymer. *Chemical Engineering Journal, 166,* 1158-1163.

Khalifa, M.E., Ali, T.A., & Abdallah, A.B. (2020). Molecularly imprinted polymer based GCE for ultra-sensitive voltametric and potentiometric bio sensing of topiramate. *Analytical Sciences, 37*, 955-962.

Khan, S., Hussain, S., Wong, A., Foguel, M.V., Gonçalves, L.M., Gurgo, M.I.P., & Sotomayor, M.D.P.T. (2018). Synthesis and characterization of magnetic-molecularly imprinted polymers for the HPLC-UV analysis of ametryn. *Reactive and Functional Polymers, 122*, 175-182.

Konstantinou, I.K., Hela, D.G., & Albanis, T.A. (2006). The status of pesticide pollution in surface waters (rivers and lakes) of Greece. Part I. Review on occurrence and levels. *Environmental Pollution, 141*, 555-570.

Koohpaei, A.R., Shahtaheri, S.J., Ganjali, M.R., Forushani, A.R., & Golbabaei, F. (2008). Application of multivariate analysis to the screening of molecularly imprinted polymers (MIPs) for ametryn. *Talanta, 75,* 978-986.

Koohpaei, A.R., Shahtaheri, S.J., Ganjali, M.R., Forushani, A.R., & Golbabaei, F. (2009). Optimization of solid-phase extraction using developed modern sorbent for trace determination of ametryn in environmental matrices. *Journal of Hazardous Materials, 170*, 1247-1255.

Koutnik, D., Stara, A., & Velisek, J. (2015). The effect of selected triazines on fish: A review. *Slovenian Veterinary Research, 52*(3), 107-131.

Kryscio, D.R., & Peppas, N.A. (2012). Critical review and perspective of macromolecularly imprinted polymers. *Acta Biomaterialia, 8*, 461-473.

Kucka, M., Pogrmic-Majkic, K., Fa, S., Stojilkovic, S.S., & Kovacevic, R. (2012). Atrazine acts as an endocrine disrupter by inhibiting cAMP-specific phosphodiesterase-4. *Toxicology and Applied Pharmacology, 265*, 19-26.

Kuhn, R., Erni, F., Bereuter, T., & Haeusler, J. (1992). Chiral recognition and enantiomeric resolution based on host-guest complexation with crown ethers in capillary zone electrophoresis. *Analytical Chemistry, 64*, 2815-2820.

Kumar, N., Narayanan, N., & Gupta, S. (2018). Application of magnetic imprinted polymers for extraction of imidacloprid from eggplant and honey. *Food Chemistry, 255*, 81-88.

Kumar, R., & Agrawal, Y.K. (2014). Analytical strategies for characterization of molecular imprinted polymers: A current review. *International Journal of ChemTech Research, 6*(2), 1162-1167.

Kunene, P.N., & Mahlambi, P.N. (2019). Development and application of SPE-LC-PDA method for the determination of triazines in water and liquid sludge samples. *Journal of Environmental Management, 249*, 109415.

Lafarge, C., Bitar, M., El Hosry, L., Cayot, P., & Bou-Maroun, E. (2020). Comparison of molecularly imprinted polymers (MIP) and sol-gel molecularly imprinted silica (MIS) for fungicide in a hydro alcoholic solution. *Materials Today Communications, 24*(4), 101157.

Lah, N.F.C., Ahmad, A.L., Low, S.C., & Shoparwe, N.F. (2019). The role of porogen-polymer complexation in atrazine imprinted polymer to work as an electrochemical sensor in water. *Journal of Environmental Chemical Engineering, 7*(6), 103500.

Landry, M.R. (2005). Thermoporometry by differential scanning calorimetry: Experimental considerations and applications. *Thermochimica Acta, 433*(1-2), 27-50.

Lei, Y., Chen, B., You, L., He, M., & Hu, B. (2017). Polydimethylsiloxane/MIL-100(Fe) coated stir bar sorptive extraction-high performance liquid chromatography for the determination of triazines in environmental water samples. *Talanta, 175*, 158-167.

Lerch, R.N., Baffaut, C., Sadler, E.J., & Kremer, R.J. (2015). Long-term agroecosystem research in the central Mississippi River basin: Goodwater creek experimental watershed and regional herbicide water quality data. *Journal of Environmental Quality, 44*, 28-36.

Li, G., & Row, K.H. (2017). Recent applications of molecularly imprinted polymers (MIPs) on micro-extraction techniques. *Separation & Purification Reviews, 47*(1), 1-18.

Li, G., Zhang, D., Wang, M., Huang, J., & Huang, L. (2013). Preparation of activated carbons from *Iris tectorum* employing ferric nitrate as dopant for removal of tetracycline from aqueous solutions. *Ecotoxicology and Environmental Safety, 98*, 273-282.

Li, L., Li, L., Cheng, G., Wei, S., Wang, Y., Huang, Q., Wu, W., Liu, X., & Chen, G. (2022). Study of the preparation and properties of chrysin binary functional monomer molecularly imprinted polymers. *Polymers, 14*, 2771.

Li, X., & Husson, S.M. (2006). Adsorption of dansylated amino acids on molecularly imprinted surfaces: a surface plasmon resonance study. *Biosensors and Bioelectronics, 22*, 336-348.

Liang, W., Hu, H., Guo, P., Ma, Y., Li, P., Zheng, W., & Zhang, M. (2017). Combining pickering emulsion polymerization with molecular imprinting to prepare polymer microspheres for selective solid-phase extraction of malachite green. *Polymers, 9*(8), 344.

Lim, H.J., Saha, T., Tey, B.T., Tan, W.S., & Ooi, C.W. (2020). Quartz crystal microbalance-based biosensors as rapid diagnostic devices for infectious diseases. *Biosensors and Bioelectronics, 168*, 112513.

Lim, K.F., & Holdsworth, C.I. (2018). Effect of formulation on the binding efficiency and selectivity of precipitation molecularly imprinted polymers. *Molecules, 23*, 2996-3014.

Lin, Y., Liu, Y., Li, S., Rui, L., Ou, J., Wu, Q., & He, J. (2021). Template-directed preparation of three-dimensionally ordered macroporous molecularly imprinted microspheres for selective recognition and separation of quinine from cinchona extract. *Journal of Polymer Research, 28*, 1-10.

Linares, A.V., Vandevelde, F., Pantigny, J., Falcimaigne-Cordin, A., & Haupt, K. (2009). Polymer films composed of surface-bound nanofilaments with a high aspect ratio, molecularly imprinted with small molecules and proteins. *Advanced Functional Materials, 19*, 1299-1303.

Liu, G., Yang, X., Li, T., She, Y., Wang, S., Wang, J., Zhang, M., Jin, F., Jin, M., Shao, H., & Shi, M. (2015). Preparation of a magnetic molecularly imprinted polymer using g-C3N4-Fe3O4 for atrazine adsorption. *Materials Letters, 160*, 472-475.

Liu, Y., Lian, Z., Li, F., Majid, A., & Wang, J. (2021). Review on molecular imprinting technology and its application in pre-treatment and detection of marine organic pollutants. *Marine Pollution Bulletin, 169*, 112541.

Liu, Z., Wang, J., Yang, X., Wu, Q., Wang, Z., & Yan, H. (2023). Green construction of hydroxyl-functionalized magnetic porous organic framework for effective extraction of triazine herbicides from environmental water and watermelon juice samples. *Analytica Chimica Acta, 1260*, 341222.

Liu, Z., Wang, Y., Xu, F., Wei, X., Chen, J., Li, H., He, X., & Zhou, Y. (2020). A new magnetic molecularly imprinted polymer based on deep eutectic solvents as functional monomer and cross-linker for specific recognition of bovine hemoglobin. *Analytica Chimica Acta, 1129*, 45-49.

López, R., Khan, S., Torres, S.E., Wong, A., Sotomayor, M.D.P.T., & Picasso, G. (2023). Synthesis and characterization of magnetic molecularly imprinted polymer for the monitoring of amoxicillin in real samples using the chromatographic method. *Magnetochemistry, 9*(4), 92.

Lou, W., Zhu, L., Yu, C., Tang, H., Yu, H., Li, X., & Zhang, X. (2008). Synthesis of surface molecularly imprinted silica microparticles in aqueous solution and the usage for selective offline solid-phase extraction of 2,4-dinitrophenol from water matrixes. *Analytica Chimica Acta, 618*(2), 147-156.

Lu, H., Tian, H., Wang, C., & Xu, S. (2020). Designing and controlling the morphology of spherical molecularly imprinted polymers. *Materials Advances, 1,* 2184-2201.

Luo, X., Zhong, W., Luo, J., Yang, L., Long, J., Guo, B., & Luo, S. (2017). Lithium ion-imprinted polymers with hydrophilic PHEMA polymer brushes: The role of grafting density in anti-interference and anti-blockage in wastewater. *Journal of Colloid and Interface Science, 492*, 146-156.

Lusina, A., & Ceglowski, M. (2022). Molecularly imprinted polymers as state-of-the-art drug carriers in hydrogel transdermal drug delivery applications. *Polymers, 14*, 640.

Lv, Y., Lin, Z., Feng, W., & Tan, T. (2007). Evaluation of the polymerization and recognition mechanism for phenol imprinting SPE. *Chromatographia, 66*(5-6), 339-347.

Ma, W., An, Y., & Row, K.H. (2019). Preparation and evaluation of a green solvent-based molecularly imprinted monolithic column for the recognition of proteins by high-performance liquid chromatography. *Analyst, 144*, 6327.

Madikizela, L.M., Nomngongo, P.N., & Pakade, V.E. (2022). Synthesis of molecularly imprinted polymers for extraction of fluoroquinolones in environmental, food and biological samples. *Journal of Pharmaceutical and Biomedical Analysis, 208*, 114447.

Madikizela, L.M., Zunngu, S.S., Mlunguza, N.Y., Tavengwa, N.T., Mdluli, P.S., & Chimuka, L. (2018). Application of molecularly imprinted polymer designed for the selective extraction of ketoprofen from wastewater. *Water SA, 44*(3), 406-418.

Mafu, L.D., Msagati, T.A.M., & Mamba, B.B. (2013). Ion-imprinted polymers for the environmental monitoring of inorganic pollutants: Synthesis, characterization, and application. *Environmental Science and Pollution Research, 20*, 790-802.

Magesh, N., Renita, A.A., Siva, R., Harirajan, N., & Santhosh, A. (2022). Adsorption behavior of fuoroquinolone (ciprofoxacin) using zinc oxide impregnated activated carbon prepared from jack fruit peel: Kinetics and isotherm studies. *Chemosphere, 290*, 133227.

Mahesh, G.B., & Manu, B. (2019). Removal of ametryn and organic matter from wastewater using sequential anaerobic-aerobic batch reactor: A performance evaluation study. *Journal of Environmental Management, 249*, 1-9.

Mahony, J.O., Nolan, K., Smyth, M.R., & Mizaikoff, B. (2004). Molecularly imprinted polymer: Potential and challenges in analytical chemistry. *Analytica Chimica Acta*, *534,* 31-39.

Maranata, G.J., Surya, N.O., & Hasanah, A.N. (2021). Optimising factors affecting solid phase extraction performances of molecular imprinted polymer as recent sample preparation technique. *Heliyon*, *7*, e05934.

Marchyk, N., Maximilien, J., Beyazit, S., Haupt, K., & Bui, B.T.S. (2014). One-pot synthesis of iniferter-bound polystyrene core nanoparticles for the controlled grafting of multilayer shells. *Nanoscale, 6*, 2872-2878.

Masumoto, S., Nakamura, Y., & Haginaka, J. (2021). Molecularly imprinted polymers for arbutin and rutin by modified precipitation polymerization and their application for selective extraction of rutin in nutritional supplements. *Journal of Pharmaceutical and Biomedical Analysis, 205,* 114294.

Mehamod, F.S., Jusih, N., Yusof, N.F., Kadir, M.A., & Suah, F.B. (2018). Synthesis and adsorption studies for newly prepared Ni^{2+}-imprinted polymer co-functionalized with picolinic acid. *ASM Science Journal, 2018*(1), 114-123.

Men, H., Liu, H., Zhang, Z., Huang, J., Zhang, J., Zhai Y., & Li, L. (2012). Synthesis properties and application research of atrazine $Fe_3O_4SiO_2$ magnetic molecularly imprinted polymer. *Environmental Science and Pollution Research, 19*, 2271-2280.

Mesnage, R., Szekacs, A., & Zaller, J.G. (2021). Herbicides: Brief history, agricultural use, and potential alternatives for weed control. In R., Mesnage, & J.G. Zaller (Eds.), *Herbicides: Chemistry, efficacy, toxicology, and environmental impacts emerging issues in analytical chemistry* (1st ed., pp. 1-20). Elsevier.

Mirata, F., & Resmini, M. (2015). Molecularly imprinted polymers for catalysis and synthesis. *Advances in Biochemical Engineering/Biotechnology, 150,* 107-129.

Mohebali, A., Abdouss, M., & Zahedi, P. (2018). Isosorbide dinitrate template-based molecularly imprinted poly (methacrylic acid) nanoparticles: Effect of initiator concentration on morphology and physiochemical properties. *Chemical Papers, 72*(12), 3005-3016.

Montgomery, M.P., Kamel, F., Saldana, T.M., Alavanja, M.C., & Sandler, D.P. (2008). Incident diabetes and pesticide exposure among licensed pesticide applicators: Agricultural health study, 1993-2003. *American Journal of Epidemiology, 167*(10), 1235-1246.

Mor, S., Chhoden, K., & Ravindra, K. (2016). Application of agro-waste rice husk ash for the removal of phosphate from the wastewater. *Journal of Cleaner Production, 129,* 673-680.

Mosbach, K., & Ramström, O. (1996). The emerging technique of molecular imprinting and its future impact on biotechnology. *Nature Biotechnology, 14*, 163-170.

Munajad, A., Subroto, C., & Suwarno. (2018). Fourier transform infrared (FTIR) spectroscopy analysis of transformer paper in mineral oil-paper composite insulation under accelerated thermal aging. *Energies, 11,* 364.

Murdaya, N., Triadenda, A.L., Rahayu, D., & Hasanah, A.N. (2022). A review: Using multiple templates for molecular imprinted polymer-Is it good? *Polymers, 14*, 4441.

Nabavi, S.A., Vladisavljevic, G.T., Wicaksono, A., Georgiadou, S., & Manovic, V. (2017). Production of molecularly imprinted polymer particles with amide-decorated cavities for CO_2 capture using membrane emulsification/suspension polymerisation. *Colloids and Surfaces A: Physicochemical and Engineering Aspects, 531,* 231-238.

Nandiyanto, A.B.D., Oktiani, R., & Ragadhita, R. (2019). How to read and interpret FTIR spectroscope of organic material. *Indonesian Journal of Science & Technology, 4*(1), 97-118.

Nguyen, H.T., Bui, N.V., Kanhounnon, W.G., Huynh, K.V., Nguyen, T.V.A., Nguyen, H.M., Do, M.H., Badawi, M., & Thach, U. D. (2021). Co-precipitation polymerization of dual functional monomers and polystyrene-co-divinylbenzene for ciprofloxacin imprinted polymer preparation. *Royal Society of Chemistry Advances, 11*, 34281-34290.

Nikoleli, G.P., Nikolelis, D.P., Siontorou, C.G., Karapetis, S., Varzakas, T. (2018). Novel biosensors for the rapid detection of toxicants in foods. *Advances in Food and Nutrition Research, 84*, 57-102.

Nishchaya, K., Rai, V.K., & Bansode, H. (2023). Methacrylic acid as potential monomer for molecular imprinting: A review of recent advances. *Results in Materials, 18*, 100379.

Norell, M.C., Andersson, H.S., & Nicholls, I.A. (1998). Theophylline molecularly imprinted polymer dissociation kinetics: A novel sustained release drug dosage mechanism. *Journal of Molecular Recognition, 11*, 98-102.

Nsibande, S.A., & Forbes, P.B.C. (2019). Development of a quantum dot molecularly imprinted polymer sensor for fluorescence detection of atrazine. *Luminescence, 34*(5), 480-488.

Oxelbark, J., Legido-Quigley, C., Aureliano, C.S.A., Titirici, M.M., Schillinger, E., Sellergren, B., Courtois, J., Irgum, K., Dambies, L., Cormack, P.A.G., Sherrington, D.C., & De Lorenzi, E. (2007). Chromatographic comparison of bupivacaine imprinted polymers prepared in crushed monolith, microsphere, silica-based composite and capillary monolith formats. *Journal of Chromatography A, 1160*, 215-226.

Ozcelikay, G., Kaya, S.I., Ozkan, E., Cetinkaya, A., Nemutlu, E., Kır, S., & Ozkan, S.A. (2022). Sensor-based MIP technologies for targeted metabolomics analysis. *Trends in Analytical Chemistry, 146*, 116487.

Pap, T., Horvath, V., Tolokan, A., Horvai, G., & Sellergren, B. (2002). Effect of solvents on the selectivity of terbutylazine imprinted polymer sorbents used in solid-phase extraction. *Journal of Chromatography A, 973*(1-2), 1-12.

Pareek, K., Rohana, R., & Cheng, H. (2015). Polymeric organo-magnesium complex for room temperature hydrogen physisorption. *Royal Society of Chemistry Advances, 5*, 10886-10891.

Peñalver, R., Arroyo-Manzanares, N., López-García, I., & Hernández-Córdoba, M. (2020). An overview of microplastics characterization by thermal analysis. *Chemosphere, 242*, 125170.

Pengkamta, T., Mala, M., Klakasikit, C., Kanawuttikorn, P., Boonkorn, P., Chuaejedton, A., & Karuehanon, W. (2020). Synthesis and evaluation of molecularly imprinted polymer as a selective material for vanillin. *Suan Sunandha Science and Technology Journal, 7*, 1-6.

Prasad, B. B., & Pathak, P. K. (2017). Development of surface imprinted nanospheres using the inverse suspension polymerization method for electrochemical ultra sensing of dacarbazine. *Analytica Chimica Acta, 974*, 75-86.

Prati, S., Joseph, E., Sciutto, G., & Mazzeo, R. (2010). New advances in the application of FTIR microscopy and spectroscopy for the characterization of artistic materials. *Accounts of Chemical Research, 43*(6), 782-801.

Pratiwi, R., Megantara, S., Rahayu, D., Pitaloka, I., & Hasanah, A.N. (2018). Comparison of bulk and precipitation polymerization method of synthesis molecular imprinted

solid phase extraction for atenolol using methacrylic acid. *Journal of Young Pharmacists, 11*, 12-16.

Qi, P.P., Wang, J.C., Wang, L.D., Li, Y., Jin, J., Su, F., Tian, Y.Z., & Chen, J.P. (2010). Molecularly imprinted polymers synthesized via semi-covalent imprinting with sacrificial spacer for imprinting phenols. *Polymer, 51*, 5417-5423.

Qiao, F.X., Row, K.H., Wang, & M.G. (2014). Water-compatible magnetic imprinted microspheres for rapid separation and determination of triazine herbicides in environmental water. *Journal of Chromatography B, 957*, 84-89.

Quinto, M.L., Khan, S., Picasso, G., & Sotomayor, M.D.P.T. (2020). Synthesis, characterization, and evaluation of a selective molecularly imprinted polymer for quantification of the textile dye acid violet 19 in real water samples. *Journal of Hazardous Materials, 384*, 121374.

Rao, V.S. (2000). Principles of Weed Science, 2nd ed., California: CRC Press.

Raof, S.F.A. (2014). Synthesis, characterization and adsorption properties of molecularly imprinted silica gel for the removal of 2-hydroxybenzoic acid (2-HA) from aqueous solution. Master thesis, University of Malaya, Malaysia. Retrieved from http://studentsrepo.um.edu.my/4784/1/Thesis_SITI_FARHANA_SGR_100106.pdf

Refaat, D., Aggour, M.G., Farghali, A.A., Mahajan, R., Wiklander, J.G., Nicholls, I.A., & Piletsky, S.A. (2019). Strategies for molecular imprinting and the evolution of MIP nanoparticles as plastic antibodies-Synthesis and applications. *International Journal of Molecular Sciences, 20*, 6304.

Reimhult, K., Yoshimatsu, K., Risveden, K., Chen, S., Ye, L., & Krozer, A. (2008). Characterization of QCM sensor surfaces coated with molecularly imprinted nanoparticles. *Biosensors and Bioelectronics, 23*, 1908-1914.

Rohr, J.R., & McCoy, K.A. (2010). A qualitative meta-analysis reveals consistent effects of atrazine on freshwater fish and amphibians. *Environmental Health Perspectives, 118*(1), 20-32.

Royani, I., Widayani, Abdullah, M., & Khairurrijal. (2014). An atrazine molecularly imprinted polymer synthesized using a cooling-heating method with repeated washing: Its physicochemical characteristics and enhanced cavities. *International Journal of Electrochemical Science, 9,* 5651-5662.

Saavedra, L.N.M., Penindo, R.G., Santos, L.A., Ramalho, T.C., Baeta, B.E.L., Pereira, M.C., & Silva, A.C. (2018). Molecularly imprinted polymers for selective adsorption of quinoline: Theoretical and experimental studies. *Royal Society of Chemistry Advances, 2018*(8), 28775-28786.

Sadia, M., Ahmad, I., Ali, F., Zahoor, M., Ullah, R., Ali, F.E.A., & Sohail, A. (2022). Selective removal of the emerging dye Basic Blue 3 via molecularly imprinting technique. *Molecules, 27,* 3276.

Safari, M., Yamini, Y., Tahmasebi, E., & Ebrahimpour, B. (2016). Magnetic nanoparticles assisted supramolecular solvent extraction of triazine herbicides prior to their determination by HPLC with UV detection. *Microchimica Acta, 183*, 203-210.

Sajini, T., & Mathew, B. (2021). A brief overview of molecularly imprinted polymers: Highlighting computational design, nano and photo-responsive imprinting. *Talanta Open, 4,* 100072.

Saka, M., Tada, N., & Kamata, Y. (2018). Chronic toxicity of 1,35-triazine herbicides in the postembryonic development of the western clawed frog *Silurana tropicalis*. *Ecotoxicology and Environmental Safety, 147,* 373-381.

Salahshoor, Z., Ho, K.V., Hsu, S.Y., Lin, C.H., & Cortalezzi, M.F.D. (2022). Detection of atrazine and its metabolites by photonic molecularly imprinted polymers in aqueous solutions. *Chemical Engineering Journal Advances, 12*, 100368.

Sallacan, N., Zayats, M., Bourenko, T., Kharitonov, A.B., & Willner, I. (2002). Imprinting of nucleotide and monosaccharide recognition sites in acrylamidephenylboronic acid-acrylamide copolymer membranes associated with electronic transducers. *Analytical Chemistry, 74*, 702-712.

Samarth, N.B., Kamble, V., Mahanwar, P. A., Rane, A.V., & Abitha, V.K. (2015). A historical perspective and the development of molecular imprinting polymer-A review. *Chemistry International, 1*(4), 202-210.

Sanagi, M.M., Salleh, S., Ibrahim, W.A.W., Naim, A.A., Hermawan, D., Miskam, M., Hussain, I., & Aboul-Enein, H.Y. (2013). Molecularly imprinted polymer solid-phase extraction for the analysis of organophosphorus pesticides in fruit samples. *Journal of Food Composition and Analysis, 32*, 155-161.

Sanchez-Domene, D., Silva, F.R., Provete, D.B., Navarro-Lozano, A., Acayaba, R.D., Montagner, C.C., Rossa-Feres, D.C., Lopez-Iborra, G.M., & Almeida, E.A. (2022). Combined effects of landscape composition and agrochemicals on frog communities amid sugarcane-dominated agroecosystems. *Ecological Applications, 33*(2), 2781.

Sánchez-González, J., Peña-Gallego, Á., Sanmartín, J., Bermejo, A.M., Bermejo-Barrera, P., & Moreda-Piñeiro, A. (2019). NMR spectroscopy for assessing cocaine-functional monomer interactions when preparing molecularly imprinted polymers. *Microchemical Journal, 147*, 813-817.

Scheel, G.L., & Tarley, C.R.T. (2017). Feasibility of supramolecular solvent-based microextraction for simultaneous preconcentration of herbicides from natural waters with posterior determination by HPLC-DAD. *Microchemical Journal, 133*, 650-657.

Schindler, A., Doedt, M., Gezgin, Ş., Menzel, J., & Schmölzer, S. (2017). Identification of polymers by means of DSC, TG, STA and computer-assisted database search. *Journal Thermal Analysis and Calorimetry, 129*(2), 833-842.

Schirhagl, R. (2013). Bioapplications for molecularly imprinted polymers. *Analytical Chemistry, 86*(1), 250-261.

Sellergren, B., & Allender, C.J. (2005). Molecularly imprinted polymers: A bridge to advanced drug delivery. *Advanced Drug Delivery Reviews, 57*, 1733-1741.

Shabaka, S.M., Marey, R.S., Ghobashy, M., Abushady, A.M., Ismail, G.A., & Khairy, H.M. (2020). Thermal analysis and enhanced visual technique for assessment of microplastics in fish from an Urban Harbor, Mediterranean Coast of Egypt. *Marine Pollution Bulletin, 159*, 111465.

Shadabfar, M., Abdouss, M., & Khonakdar, H.A. (2020). Synthesis, characterization, and evaluation of a magnetic molecular imprinted polymer for 5-fluorouracil as an intelligent drug delivery system for breast cancer treatment. *Journal of Materials Science, 55*, 12287-12304.

Shafqat, S.R., Bhawani, S.A., Bakhtiar, S., & Ibrahim, M.N.M. (2020). Synthesis of molecularly imprinted polymer for removal of Congo red. *BioMed Central Chemistry, 14*(27), 1-15.

Shafqat, S.R., Bhawani, S.A., Bakhtiar, S., Ibrahim, M.N.M., & Shafqat, S.S. (2023). Template-assisted synthesis of molecularly imprinted polymers for the removal of methyl red from aqueous media. *BioMed Central Chemistry, 17*, 46.

Shah, M., Haneef, M., Park, J., & Ul-Islam, M. (2012). A brief overview of molecularly imprinted polymers: From basics to applications. *Journal of Pharmacy and Pharmaceutical Research, 5*, 3309-3317.

Shah, S.A.H., Ramachandran, M.R., Mansur, S.A., Saleh, N.M., & Asman, S. (2023). Selective recognition of bisphenol a using molecularly imprinted polymer based on choline chloride-methacrylic acid deep eutectic solvent monomer: Synthesis characterization and adsorption study. *Polymer, 283*, 126279.

Shea, K.J., & Sasaki, D.Y. (1991). An analysis of small-molecule binding to functionalized synthetic polymers by 13C CP/MAS NMR and FT-IR spectroscopy. *Journal of the American Chemical Society, 113,* 4109-4120.

Shen, F., & Ren, X. (2014). Covalent molecular imprinting made easy-A case study of mannose imprinted polymer. *The Royal Society of Chemistry Advances, 4*(25), 13123-13125.

Sooraj, M.P., Archana, S.N., Mathew, B., & Thomas, S. (2020). *Molecularly Imprinted Polymer Composites: Synthesis, Characterisation and Applications*, Cambridge: Woodhead Publishing.

Spivak, D.A., & Shea, K.J. (2001). Investigation into the scope and limitations of molecular imprinting with DNA molecules. *Analytica Chimica Acta, 435*, 65-74.

Stayner, L.T., Almberg, K., Jones, R., Graber, J., Pedersen, M., & Turyk, M., (2017). Atrazine and nitrate in drinking water and the risk of preterm delivery and low birth weight in four midwestern states. *Environmental Research, 152*, 294-303.

Strikovsky, A., Hradil, J., & Wulff, G. (2003). Catalytically active, molecularly imprinted polymers in bead form. *Reactive and Functional Polymers, 54*, 49-61.

Su, W., Rick, J., & Chou, T. (2009). Selective recognition of ovalbumin using a molecularly imprinted polymer. *Microchemical Journal, 92*(2), 123-128.

Suedee, R., Srichana, T., Chotivatesin, R., & Martin, G.P. (2002). Stereoselective release behaviors of imprinted bead matrices. *Drug Development and Industrial Pharmacy, 28*, 545-554.

Sun, Y., Ren, T., Deng, Z., Yang, Y., & Zhong, S. (2018). Molecularly imprinted polymers fabricated using Janus particle-stabilized Pickering emulsion and charged monomer polymerization. *New Journal of Chemistry*, *9*(42),7355-7363.

Tang, Q., Meng, X., Jiang, H., Zhou, T., Gong, C., Fu, X., & Shi, S. (2010). Synthesis and characterization of photo-and pH-responsive nanoparticles containing amino-substituted azobenzene. *Journal of Materials Chemistry, 20*(41), 9133-9139.

Tian, Y., Wang, Y., Wu, S., Sun, W., & Gong, B. (2018). Preparation of ampicillin surface molecularly imprinted polymers for its selective recognition of ampicillin in egg samples. *International Journal of Analytical Chemistry, 2018*, 1-11.

Tóth, B. (2010). Chromatographic properties of molecularly imprinted polymers (Unpublished doctoral thesis). Semmelweis University, Hungary.

Turiel, E., & Esteban, A.M. (2020). Molecularly imprinted polymers. In C.F. Poole (Ed.), *Solid-phase extraction* (1st ed., pp. 215-233). Elsevier.

Turkewitsch, P., Massé, R., & Powell, W.S. (2005). Molecular imprinting. *Advanced Concepts in Fluorescence Sensing, 10*, 157-209.

Urriza-Arsuaga, I., Guadaño-Sánchez, M., & Urraca, J.L. (2023). Current trends in molecular imprinting: Strategies, applications and determination of target molecules in Spain. *International Journal of Molecular Science, 24*, 1915.

Uzuriaga-Sánchez, R.J., Wong, A., Khan, S., Picasso, P.G., & Sotomayor, M.D.P.T. (2017). Synthesis of a new magnetic-MIP for the selective detection of 1-chloro-2,4-dinitrobenzene, a highly allergenic compound. *Materials Science and Engineering C, 74*, 365-373.

Vaihinger, D., Landfester, K., Kräuter, I., Brunner, H., & Tovar, G.E. (2002). Molecularly imprinted polymer nanospheres as synthetic affinity receptors obtained by miniemulsion polymerisation. *Macromolecular Chemistry and Physics, 203*, 1965-1973.

Valcin, M., Henneberger, P.K., Kullman, G.J., Umbach, D.M., London, S.J., Alavanja, M.C., Sandler, D.P., & Hoppin, J.A. (2007). Chronic bronchitis among nonsmoking farm women in the agricultural health study. *Journal of Occupational and Environmental Medicine, 49*(5), 574-583.

Vasapollo, G., Sole, R.D., Mergola, L., Lazzoi, M.R., Scardino, A., Scorrano, S., & Mele, G. (2011). Molecularly imprinted polymers: Present and future prospective. *International Journal of Molecular Sciences, 12*, 5908-5945.

Viveiros, R., Pinto, J.J., Costa, N., Heggie, W., & Casimiro, T. (2023). Development of affinity polymeric particles for the removal of 4-dimethhylaminopyridine (DMAP) from active pharmaceutical ingredients crude stream using a green technology. *The Journal of Supercritical Fluids, 194*, 105853.

Vlatakis, G., Andersson, L.I., Miller, R., & Mosbach, K. (1993). Drug assay using antibody mimics made by molecular imprinting. *Nature, 361*, 645-647.

Vryzas, Z., Vassiliou, G., Alexoudis, C., Papadopoulou-Mourkidou, E. (2009). Spatial and temporal distribution of pesticide residues in surface waters in northeastern Greece. *Water Research, 43*, 1-10.

Wackerlig, J., & Schirhagl, R. (2016). Applications of molecularly imprinted polymer nanoparticles and their advances towards industrial use: A review. *Analytical Chemistry, 88*(1), 250-261.

Wadie, M., Marzouk, H.M., Rezk, M.R., Abdel-Moety, E.M., & Tantawy, M.A. (2022). A sensing platform of molecular imprinted polymer-based polyaniline/carbon paste electrodes for simultaneous potentiometric determination of alfuzosin and solifenacin in binary co-formulation and spiked plasma. *Analytica Chimica Acta, 1200,* 339599.

Wang, F., Yang, B., Wang, H., Song, Q., Tan, F., & Cao, Y. (2016). Removal of ciprofloxacin from aqueous solution by a magnetic chitosan grafted graphene oxide composite. *Journal of Molecular Liquids, 222,* 188-194.

Wang, M., & Kan, X. (2020). Imprinted polymer/Fe_3O_4 micro-particles decorated multi-layer graphite paper: Electrochemical and colorimetric dual-modal sensing interface for aloe-emodin assay. *Sensors and Actuators B: Chemical, 323,* 128672.

Wang, X., Huang, P., Ma, X., Du, X., & Lu, X. (2019). Enhanced in-out-tube solid-phase microextraction by molecularly imprinted polymers-coated capillary followed by HPLC for endocrine disrupting chemicals analysis. *Talanta, 194,* 7-13.

Wang, X., Jia, R., Song, Y., Wang, M., Zhao, Q., & Sun, S. (2019). Determination of pesticides and their degradation products in water samples by solid-phase extraction coupled with liquid chromatography-mass spectrometry. *Microchemical Journal, 149,* 104013.

Wang, Z., Qiu, T., Guo, L., Ye, J., He, L., & Li, X. (2018). Polymerization induced shaping of Pickering emulsion droplets: From simple hollow microspheres to molecularly imprinted multicore microrattles. *Chemical Engineering Journal, 332,* 409-418.

Wang, Z., Qiu, T., Guo, L., Ye, J., He, L., & Li, X. (2018). The synthesis of molecular recognition polymer particles via miniemulsion polymerization. *Reactive and Functional Polymers, 126,* 1-8.

Weetall, H.H., & Rogers, K.R. (2004). Preparation and characterization of molecularly imprinted electropolymerized carbon electrodes. *Talanta, 62,* 329-335.

Wei, X., Samadi, A., & Husson, S.M. (2005). Synthesis and characterization of molecularly imprinted polymers for chromatographic separations. *Separation Science and Technology, 40,* 109-129.

Weselak, M., Arbuckle, T.E., Wigle, D.T., Walker, M.C., & Krewski, D. (2008). Pre- and post-conception pesticide exposure and the risk of birth defects in an Ontario farm population. *Reproductive Toxicology, 25*(4), 472-480.

Whitcombe, M.J., Rodriguez, M.E., Villar, P., & Vulfson, E.N. (1995). A new method for the introduction of recognition site functionality into polymers prepared by molecular imprinting: Synthesis and characterization of polymeric receptors for cholesterol. *Journal of the American Chemical Society, 117,* 7105-7111.

Wloch, M., & Datta, J. (2019). Synthesis and polymerisation techniques of molecularly imprinted polymers. *Comprehensive Analytical Chemistry, 86,* 17-40.

Wu, H., Tian, Q., Zheng, W., Jiang, Y., Xu, J., Li, X., Zhang, W., & Qiu, F. (2019). Non-enzymatic glucose sensor based on molecularly imprinted polymer: A theoretical, strategy fabrication and application. *Journal of Solid State Electrochemical, 23,* 1379-1388.

Wu, X., Shen, S., Yan, H., & Yuan, Y. (2021). Efficient enrichment and analysis of atrazine and its degradation products in Chinese yam using accelerated solvent extraction and

pipette tip solid-phase extraction followed by UPLC-DAD. *Food Chemistry, 337*, 127752.

Wu, X.L., Meng, L., Wu, Y., Luk, Y.Y., Ma, Y., & Du, Y. (2015). Evaluation of graphene for dispersive solid-phase extraction of triazine and neonicotine pesticides from environmental water. *Journal of the Brazilian Chemical Society, 26*, 131-139.

Wulff, G. (2002). Enzyme-like catalysis by molecularly imprinted polymers. *Chemical Reviews, 102*, 1-28.

Wulff, G. Vesper, W., Grobe-Einsler, R., & Sarhan, A. (1977). Enzyme-analogue built polymers, 4. On the synthesis of polymers containing chiral cavities and their use for the resolution of racemates. *Die Makromolekulare Chemie, 178*(10), 2799-2816.

Wulff, G., & Sarhan, A. (1972). Use of polymers with enzyme-analogous structures for the resolution of racemates. *Angewandte Chemie International Edition, 11*, 341-342.

Wulff, G., & Vietmeier, J. (1989). Enzyme-analogue built polymers, XXVI. Enantioselective synthesis of amino-acids using polymers possessing chiral cavities obtained by an imprinting procedure with template molecules. *Macromolecular Chemistry and Physics, 190*, 1727-1735.

Wypych, G. (2019). *Handbook of Curatives and Crosslinkers*, Toronto: ChemTech Publishing.

Xia, Q., Yun, Y., Li, Q., Huang, Z., & Liang, Z. (2017). Preparation and characterization of monodisperse molecularly imprinted polymer microspheres by precipitation polymerization for kaempferol. *Designed Monomers and Polymers, 21*(1), 201-209.

Xiao, D., Jiang, Y., & Bi, Y. (2018). Molecularly imprinted polymers for the detection of illegal drugs and additives-A review. *Microchimica Acta, 185*, 247.

Xie, L., Xiao, N., Li, L., Xie, X., & Li, Y. (2019). An investigation of the intermolecular interactions and recognition properties of molecular imprinted polymers for deltamethrin through computational strategies. *Polymers, 11*, 1872.

Xu, S., Li, J., & Chen, L. (2011). Molecularly imprinted polymers by reversible addition-fragmentation chain transfer precipitation polymerization for preconcentration of atrazine in food matrices. *Talanta, 85*, 282-289.

Xu, S., Lu, H., Zheng, X., & Chen, L. (2013). Stimuli-responsive molecularly imprinted polymers: Versatile functional materials. *Journal of Material Chemistry C, 1*, 4406-4422.

Xu, X., & Liang, S. (2019). Molecularly imprinted solid-phase extraction method for the gas chromatographic analysis of organochlorine fungicides in ginseng. *Journal of Separation Science, 42*(7), 1393-1403.

Xue, M., Wang, Y., Meng, Z., Zhang, W., Wu, Y., & Jiang, S. (2013). Extraction of shikimic acid from Chinese star anise using flash column chromatography on a molecularly imprinted polymer column. *Journal of Liquid Chromatography & Related Technologies*, *36*(19), 2677-2686.

Yan, H., & Row, K.H. (2006). Characteristic and synthetic approach of molecularly imprinted polymer. *International Journal of Molecular Sciences, 7*, 155-178.

Yang, F., Wang, R., Na, G., Yan, Q., Lin, Z., & Zhang, Z. (2018). Preparation and application of a molecularly imprinted monolith for specific recognition of domoic acid. *Analytical and Bioanalytical Chemistry, 410*, 1845-1854.

Yang, H.H., Zhou, W.H., Guo, X.C., Chen, H.Q., & Zhao, H.Q. (2009). Molecularly imprinted polymer as SPE sorbent for selective extraction of melamine in dairy products. *Talanta, 80*, 821-825.

Yang, Y., Meng, X., & Xiao, Z. (2018). Synthesis of a surface molecular imprinting polymer based on silica and its application in the identification of nitrocellulose. *Royal Society Chemistry Advances, 8*, 9802-9811.

Yanti, Nurhayati, T., Royani, I., Widayani, & Khairurrijal. (2016). Synthesis and characterization of MAA-based molecularly imprinted polymer (MIP) with D-glucose template. *Journal of Physics, 739* (1), 1-7.

Ye, L. (2016). Molecularly imprinted polymers with multi-functionality. *Analytical and Bioanalytical Chemistry*, *408*(7), 1727-1733.

Ye, L., & Mosbach, K. (2001). Molecularly imprinted microspheres as antibody binding mimics. *Reactive and Functional Polymers, 48*, 149-157.

Yemis, F., Alkan, P., Yenigül, B., & Yenigül, M. (2013). Molecularly imprinted polymers and their synthesis by different methods. *Polymers and Polymer Composites, 21*(3), 145-150.

Yeow, J., Chapman, R., Gormley A.J., & Boyer, C. (2018). Oxygen tolerance in controlled/living radical polymerisation. *Chemical Society Reviews, 47*(12), 4357-4387.

Yilmaz, E., Özgür, E., Bereli, N., Türkmen D., & Denizli, A. (2017). Plastic antibody based surface plasmon resonance nanosensors for selective atrazine detection. *Materials Science and Engineering C, 73*, 603-610.

Yin, R., Gao, L., Qin, D., Chen, L., & Niu, N. (2022). Preparation of porous carbon-based molecularly imprinted polymers for separation of triazine herbicides in corn. *Microchimica Acta, 189*, 23.

Yu, H., Shao, P., Fang, L., Pei, J., Ding, L., Pavlostathis, S.G., & Luo, X. (2018). Palladium ion-imprinted polymers with PHEMA polymer brushes-Role of grafting

polymerization degree in anti-interference. *Chemical Engineering Journal, 359*(1), 176-185.

Yu, X., Zhang, R., Liu, H., Zhang, Z., Shi, X., Sun, A., & Chen, J. (2021). Highly-selective complex matrices removal via a modified QuEChERS for determination of triazine herbicide residues and risk assessment in bivalves. *Food Chemistry, 347*, 129030.

Yusof, N.A., Beyan, A., & Ibrahim, N.A. (2010). Synthesis characterization of a molecularly imprinted polymer for Pb2+ uptake using 2-vinylpyridine as the complexing monomer. *Sains Malaysiana, 39*(5), 829-835.

Yusof, N.A., Rahman, S.K.A., Hussien, M.Z., & Ibrahim, N.A. (2013). Preparation and characterization of molecularly imprinted polymer as SPE Sorbent for melamine isolation. *Polymers, 5*, 1215-1228.

Yusof, N.F., Mehamod, F.S., Jusoh, N., Amin, K.A.M., & Suah, F.B.M. (2017). Ion-imprinted polymer-based on picolinic acid as a co-functional monomer for highly selective sorption of Cu (II) ions in an aqueous solution. *AIP Conference Proceedings, 1885*, 020017.

Zadaka, D., Nir, S., Radian, A., & Mishael, Y.G. (2009). Atrazine removal from water by polycation-clay composites: effect of dissolved organic matter and comparison to activated carbon. *Water Research, 43*, 677-683.

Zaidi, S.A. (2016). Molecularly imprinted polymers as drug delivery vehicles. *Drug Delivery, 23*, 2262-2271.

Zajíčeka, P., Koláře, M., Pruceka, R, Ranca, V., Bednářb, P., Varmac, R.S., Sharmad, V.K., & Zbořila, R. (2015). Oxidative degradation of triazine- and sulfonylurea-based herbicides using Fe (VI): The case study of atrazine and iodosulfuron with kinetics and degradation products. *Separation and Purification Technology, 156*, 1041-1046.

Zare, E.N., Fallah, Z., Le, V.T., Doan V., Mudhoo, A., Joo, S., Vasseghian, Y., Tajbakhsh, M., Moradi, O., Sillanpää, M., & Varma, R.S. (2022). Remediation of pharmaceuticals from contaminated water by molecularly imprinted polymers: A review. *Environmental Chemistry Letters, 20,* 2629-2664.

Zarejousheghani, M., Fiedler, P., Moder, M., & Borsdorf, H. (2014). Selective mixed-bed solid phase extraction of atrazine herbicide from environmental water samples using molecularly imprinted polymer. *Talanta, 129,* 132-138.

Zeng, H., Wang, Y., Liu, X., Kong, J., & Nie, C. (2012). Preparation of molecular imprinted polymers using bi-functional monomer and bi-crosslinker for solid-phase extraction of rutin. *Talanta, 93,* 172-181.

Zhan, Y., Luo, X., Nie, S., Huang, Y., Tu, X., & Luo, S. (2011). Selective separation of Cu (II) from aqueous solution with a novel Cu (II) surface magnetic ion-imprinted polymer. *Industrial & Engineering Chemistry Research, 50,* 6355-6361.

Zhang, J., Guo, X.T., Zhou, J.P., Liu, G.Z., & Zhang, S.Y. (2018). Electrochemical preparation of surface molecularly imprinted poly (3-aminophenylboronic acid)/MWCNTs nanocompvdvdosite for sensitive sensing of epinephrine. *Materials Science and Engineering: C, 91,* 696-704.

Zhang, L., Zhang, H., Li, L., Zuo, P., Zhao, F., Liu, M., Ye, B.C., & Li, Y. (2016). Pneumocandin B0-imprinted polymer using surface-imprinting technique for efficient purification of crude product. *Analytical Sciences, 32,* 923-930.

Zhang, R., Gao, R., Gou, Q., Lai, J., & Li, X. (2022). Precipitation polymerization: A powerful tool for preparation of uniform polymer particles. *Polymers, 14,* 1851.

Zhang, Y., Qin, B., Zhang, B., Ma, J., Hu, Y., Han, L., He, M., & Liu, C. (2020). Specific enrichment of caffeic acid from *Taraxacum mon-golicum* Hand. -Mazz. by pH and

magnetic dual-responsive molecularly imprinted polymers. *Analytica Chimica Acta, 1096,* 193-202.

Zhang, Y., Song, D., Lanni, L.M., & Shimizu, K. D. (2010). Importance of functional monomer dimerization in the molecular imprinting process. *Macromolecules, 43,* 6284-6294.

Zhao, B., Feng, S., Hu, Y., Wang, S., & Lu, X. (2019). Rapid determination of atrazine in apple juice using molecularly imprinted polymers coupled with gold nanoparticles-colorimetric/SERS dual chemosensor. *Food Chemistry, 276,* 366-375.

Zhao, G., Liu, J., Liu, M., Han, X., Peng, Y., Tian, X., Liu, J., & Zhang, S. (2020). Synthesis of molecularly imprinted polymer via emulsion polymerization for application in solanesol separation. *Applied Sciences, 10,* 2868.

Zhong, M., Wang, Y.H., Wang, L., Long, R.Q., & Chen, C.L. (2018). Preparation and application of magnetic molecularly imprinted polymers for the isolation of chelerythrine from Macleaya cordata. *Journal of Separation Science, 41,* 3318-3327.

Zhong, Q., Hu, Y., Hu, Y., & Li, G. (2012). Online desorption of molecularly imprinted stir bar sorptive extraction coupled to high performance liquid chromatography for the trace analysis of triazines in rice. *Journal of Separation Science, 35,* 3396-3402.

Zhou, T., Ding, J., He, Z., Li, J., Liang, Z., Li, C., Li, Y, Chen, Y., & Ding, L. (2018). Preparation of magnetic superhydrophilic molecularly imprinted composite resin based on multi-walled carbon nanotubes to detect triazines in environmental water. *Chemical Engineering Journal, 334,* 2293-2302.

APPENDICES

Appendix 1: FESEM Analysis of MIPs and NIP of CYZ

Polymer	Reading	Diameter, µm	Mean diameter, µm
MIP (MAA) of CYZ	Reading 1	0.60	0.64
	Reading 2	0.66	
	Reading 3	0.66	
MIP (AAm) of CYZ	Reading 1	0.88	0.86
	Reading 2	0.84	
	Reading 3	0.86	
NIP (AAm) of CYZ	Reading 1	1.00	0.98
	Reading 2	0.96	
	Reading 3	0.98	
MIP (4VP) of CYZ	Reading 1	1.02	1.05
	Reading 2	1.08	
	Reading 3	1.06	

Appendix 2: FESEM Analysis of MIPs and NIP of AME

Polymer	Reading	Diameter, µm	Mean diameter, µm
MIP (MAA) of AME	Reading 1	0.54	0.52
	Reading 2	0.49	
	Reading 3	0.52	
NIP (MAA) of AME	Reading 1	0.82	0.80
	Reading 2	0.79	
	Reading 3	0.80	
MIP (AAm) of AME	Reading 1	1.26	1.23
	Reading 2	1.32	
	Reading 3	1.11	
MIP (2VP) of AME	Reading 1	0.32	0.36
	Reading 2	0.37	
	Reading 3	0.38	

Appendix 3: FESEM Analysis of MIPs and NIP of ATZ

Polymer	Reading	Diameter, µm	Mean diameter, µm
MIP (MAA) of ATZ	Reading 1	1.05	1.04
	Reading 2	1.04	
	Reading 3	1.03	
MIP (AAm) of ATZ	Reading 1	1.28	1.20
	Reading 2	1.19	
	Reading 3	1.14	
MIP (2VP) of ATZ	Reading 1	0.30	0.30
	Reading 2	0.29	
	Reading 3	0.32	
NIP (2VP) of ATZ	Reading 1	0.46	0.40
	Reading 2	0.35	
	Reading 3	0.38	

Appendix 4: Batch Binding of MIP (MAA) of CYZ

Duration	Ci	Cf	(Ci - Cf)	(Ci - Cf)/Ci	Binding efficiency, %	Mean, %	Standard deviation, σ	RSD
5 mins	1.5804	1.1071	0.4733	0.2995	29.95	28.91	0.7319	2.5314
	1.5474	1.1079	0.4395	0.2840	28.40			
	1.5471	1.1079	0.4392	0.2839	28.39			
10 mins	1.5804	1.0726	0.5078	0.3213	32.13	31.12	0.7259	2.3324
	1.5474	1.0762	0.4712	0.3045	30.45			
	1.5471	1.0708	0.4763	0.3079	30.79			
15 mins	1.5804	0.9901	0.5903	0.3735	37.35	36.08	0.8994	2.4926
	1.5474	0.9979	0.5495	0.3551	35.51			
	1.5471	0.9997	0.5474	0.3538	35.38			
20 mins	1.5804	0.9788	0.6016	0.3807	38.07	37.31	0.5376	1.4410
	1.5474	0.9764	0.5710	0.3690	36.90			
	1.5471	0.9754	0.5717	0.3695	36.95			

Appendix 4 continued

25 mins	1.5804	0.9686	0.6118	0.3871	38.71	38.03	0.5213	1.3707
	1.5474	0.9680	0.5794	0.3744	37.44			
	1.5471	0.9600	0.5871	0.3795	37.95			
30 mins	1.5804	0.9482	0.6322	0.4000	40.00	39.19	0.5772	1.4729
	1.5474	0.9471	0.6003	0.3879	38.79			
	1.5471	0.9474	0.5997	0.3876	38.76			
60 mins	1.5804	0.9228	0.6576	0.4161	41.61	40.71	0.6451	1.5846
	1.5474	0.9265	0.6209	0.4013	40.13			
	1.5471	0.9221	0.6250	0.4040	40.40			
90 mins	1.5804	0.9012	0.6792	0.4298	42.98	42.08	0.6338	1.5062
	1.5474	0.9023	0.6451	0.4169	41.69			
	1.5471	0.9038	0.6433	0.4158	41.58			
120 mins	1.5804	0.8824	0.6980	0.4417	44.17	43.27	0.6749	1.5597
	1.5474	0.8892	0.6582	0.4254	42.54			
	1.5471	0.8801	0.6670	0.4311	43.11			

Appendix 4 continued

150 mins	1.5804	0.8562	0.7242	0.4582	45.82	45.03	0.5596	1.2426
	1.5474	0.8564	0.6910	0.4466	44.66			
	1.5471	0.8568	0.6903	0.4462	44.62			
180 mins	1.5804	0.8090	0.7714	0.4881	48.81	48.05	0.5354	1.1141
	1.5474	0.8095	0.7379	0.4769	47.69			
	1.5471	0.8097	0.7374	0.4766	47.66			
210 mins	1.5804	0.7756	0.8048	0.5092	50.92	50.24	0.4805	0.9564
	1.5474	0.7750	0.7724	0.4992	49.92			
	1.5471	0.7752	0.7719	0.4989	49.89			
240 mins	1.5804	0.7187	0.8617	0.5452	54.52	53.87	0.4640	0.8614
	1.5474	0.7187	0.8287	0.5355	53.55			
	1.5471	0.7190	0.8281	0.5353	53.53			
270 mins	1.5804	0.7699	0.8105	0.5128	51.28	50.61	0.4784	0.9453
	1.5474	0.7697	0.7777	0.5026	50.26			
	1.5471	0.7692	0.7779	0.5028	50.28			

Appendix 4 continued

300 mins	1.5804	0.7938	0.7866	0.4977	49.77	49.08	0.4907	0.9998
	1.5474	0.7931	0.7543	0.4875	48.75			
	1.5471	0.7934	0.7537	0.4872	48.72			

Appendix 5: Batch Binding of MIP (AAm) of CYZ

Duration	Ci	Cf	(Ci - Cf)	(Ci - Cf)/Ci	Binding efficiency, %	Mean, %	Standard deviation, σ	RSD
5 mins	1.3390	0.7966	0.5424	0.4051	40.51	40.50	0.0177	0.0438
	1.3402	0.7971	0.5431	0.4052	40.52			
	1.3394	0.7972	0.5422	0.4048	40.48			
10 mins	1.3390	0.7666	0.5724	0.4275	42.75	42.77	0.0292	0.0683
	1.3402	0.7664	0.5738	0.4281	42.81			
	1.3394	0.7667	0.5727	0.4276	42.76			
15 mins	1.3390	0.6967	0.6423	0.4797	47.97	47.99	0.0273	0.0569
	1.3402	0.6965	0.6437	0.4803	48.03			
	1.3394	0.6968	0.6426	0.4798	47.98			
20 mins	1.3390	0.6471	0.6919	0.5167	51.67	51.71	0.0299	0.0577
	1.3402	0.6467	0.6935	0.5175	51.75			
	1.3394	0.6468	0.6926	0.5171	51.71			

Appendix 5 continued

25 mins	1.3390	0.5559	0.7831	0.5848	58.48	58.34	0.1238	0.2122
	1.3402	0.5580	0.7822	0.5836	58.36			
	1.3394	0.5601	0.7793	0.5818	58.18			
30 mins	1.3390	0.5100	0.8290	0.6191	61.91	60.66	0.9877	1.6284
	1.3402	0.5428	0.7974	0.5950	59.50			
	1.3394	0.5283	0.8111	0.6056	60.56			
60 mins	1.3390	0.4568	0.8822	0.6588	65.88	65.90	0.0161	0.0244
	1.3402	0.4567	0.8835	0.6592	65.92			
	1.3394	0.4568	0.8826	0.6590	65.90			
90 mins	1.3390	0.3966	0.9424	0.7038	70.38	70.37	0.0151	0.0214
	1.3402	0.3971	0.9431	0.7037	70.37			
	1.3394	0.3972	0.9422	0.7034	70.34			
120 mins	1.3390	0.3662	0.9728	0.7265	72.65	72.65	0.0062	0.0086
	1.3402	0.3667	0.9735	0.7264	72.64			
	1.3394	0.3663	0.9731	0.7265	72.65			

Appendix 5 continued

150 mins	1.3390	0.3218	1.0172	0.7597	75.97	76.59	0.4939	0.6449
	1.3402	0.3059	1.0343	0.7718	77.18			
	1.3394	0.3130	1.0264	0.7663	76.63			
180 mins	1.3390	0.3081	1.0309	0.7699	76.99	77.00	0.0115	0.0149
	1.3402	0.3080	1.0322	0.7702	77.02			
	1.3394	0.3080	1.0314	0.7700	77.00			
210 mins	1.3390	0.2845	1.0545	0.7875	78.75	78.73	0.0244	0.0310
	1.3402	0.2848	1.0554	0.7875	78.75			
	1.3394	0.2853	1.0541	0.7870	78.70			
240 mins	1.3390	0.2734	1.0656	0.7958	79.58	79.57	0.0174	0.0218
	1.3402	0.2737	1.0665	0.7958	79.58			
	1.3394	0.2740	1.0654	0.7954	79.54			
270 mins	1.3390	0.3126	1.0264	0.7665	76.65	76.62	0.0235	0.0307
	1.3402	0.3135	1.0267	0.7661	76.61			
	1.3394	0.3134	1.0260	0.7660	76.60			

Appendix 5 continued

300 mins	1.3390	0.3438	0.9952	0.7432	74.32	74.38	0.0434	0.0583
	1.3402	0.3432	0.9970	0.7439	74.39			
	1.3394	0.3425	0.9969	0.7443	74.43			

Appendix 6: Batch Binding of MIP (4VP) of CYZ

Duration	Ci	Cf	(Ci - Cf)	(Ci - Cf)/Ci	Binding efficiency, %	Mean, %	Standard deviation, σ	RSD
5 mins	1.3852	0.9034	0.4818	0.3478	34.78	34.71	0.0551	0.1587
	1.3845	0.9041	0.4804	0.3470	34.70			
	1.3839	0.9044	0.4795	0.3465	34.65			
10 mins	1.3852	0.8468	0.5384	0.3887	38.87	38.85	0.0252	0.0648
	1.3845	0.8465	0.5380	0.3886	38.86			
	1.3839	0.8468	0.5371	0.3881	38.81			
15 mins	1.3852	0.8062	0.5790	0.4180	41.80	41.77	0.0225	0.0537
	1.3845	0.8061	0.5784	0.4178	41.78			
	1.3839	0.8062	0.5777	0.4174	41.74			
20 mins	1.3852	0.7559	0.6293	0.4543	45.43	45.41	0.0180	0.0396
	1.3845	0.7558	0.6287	0.4541	45.41			
	1.3839	0.7558	0.6281	0.4539	45.39			

Appendix 6 continued

25 mins	1.3852	0.7346	0.6506	0.4697	46.97	46.96	0.0162	0.0346
	1.3845	0.7347	0.6498	0.4693	46.93			
	1.3839	0.7339	0.6500	0.4697	46.97			
30 mins	1.3852	0.7236	0.6616	0.4776	47.76	47.74	0.0146	0.0306
	1.3845	0.7237	0.6608	0.4773	47.73			
	1.3839	0.7233	0.6606	0.4773	47.73			
60 mins	1.3852	0.7099	0.6753	0.4875	48.75	48.75	0.0327	0.0670
	1.3845	0.7090	0.6755	0.4879	48.79			
	1.3839	0.7098	0.6741	0.4871	48.71			
90 mins	1.3852	0.6994	0.6858	0.4951	49.51	49.50	0.0087	0.0175
	1.3845	0.6993	0.6852	0.4949	49.49			
	1.3839	0.6990	0.6849	0.4949	49.49			
120 mins	1.3852	0.6796	0.7056	0.5094	50.94	50.92	0.0131	0.0257
	1.3845	0.6797	0.7048	0.5091	50.91			
	1.3839	0.6792	0.7047	0.5092	50.92			

Appendix 6 continued

150 mins	1.3852	0.6453	0.7399	0.5341	53.41	53.39	0.0216	0.0405
	1.3845	0.6455	0.7390	0.5338	53.38			
	1.3839	0.6454	0.7385	0.5336	53.36			
180 mins	1.3852	0.6340	0.7512	0.5423	54.23	54.20	0.0246	0.0455
	1.3845	0.6343	0.7502	0.5419	54.19			
	1.3839	0.6342	0.7497	0.5417	54.17			
210 mins	1.3852	0.6011	0.7841	0.5661	56.61	56.59	0.0266	0.0470
	1.3845	0.6006	0.7839	0.5662	56.62			
	1.3839	0.6012	0.7827	0.5656	56.56			
240 mins	1.3852	0.5519	0.8333	0.6016	60.16	60.14	0.0124	0.0206
	1.3845	0.5518	0.8327	0.6014	60.14			
	1.3839	0.5518	0.8321	0.6013	60.13			
270 mins	1.3852	0.6045	0.7807	0.5636	56.36	56.36	0.0031	0.0056
	1.3845	0.6043	0.7802	0.5635	56.35			
	1.3839	0.6040	0.7799	0.5636	56.36			

Appendix 6 continued

300 mins	1.3852	0.6186	0.7666	0.5534	55.34	55.33	0.0180	0.0326
	1.3845	0.6182	0.7663	0.5535	55.35			
	1.3839	0.6185	0.7654	0.5531	55.31			

Appendix 7: Batch Binding of NIP (AAm) of CYZ

Duration	Ci	Cf	(Ci - Cf)	(Ci - Cf)/Ci	Binding efficiency, %	Mean, %	Standard deviation, σ	RSD
5 mins	1.3307	0.8538	0.4769	0.3584	35.84	35.10	1.0611	3.0230
	1.3305	0.8533	0.4772	0.3587	35.87			
	1.3306	0.8835	0.4471	0.3360	33.60			
10 mins	1.3307	0.8218	0.5089	0.3824	38.24	38.86	0.4850	1.2482
	1.3305	0.8059	0.5246	0.3943	39.43			
	1.3306	0.8130	0.5176	0.3890	38.90			
15 mins	1.3307	0.7661	0.5646	0.4243	42.43	42.46	0.0391	0.0920
	1.3305	0.7659	0.5646	0.4244	42.44			
	1.3306	0.7649	0.5657	0.4251	42.51			
20 mins	1.3307	0.7194	0.6113	0.4594	45.94	45.87	0.0555	0.1210
	1.3305	0.7211	0.6094	0.4580	45.80			
	1.3306	0.7203	0.6103	0.4587	45.87			

Appendix 7 continued

25 mins	1.3307	0.6970	0.6337	0.4762	47.62	47.62	0.0231	0.0485
	1.3305	0.6966	0.6339	0.4764	47.64			
	1.3306	0.6974	0.6332	0.4759	47.59			
30 mins	1.3307	0.6856	0.6451	0.4848	48.48	48.51	0.0245	0.0505
	1.3305	0.6847	0.6458	0.4854	48.54			
	1.3306	0.6852	0.6454	0.4850	48.50			
60 mins	1.3307	0.6675	0.6632	0.4984	49.84	49.88	0.0295	0.0591
	1.3305	0.6668	0.6637	0.4988	49.88			
	1.3306	0.6665	0.6641	0.4991	49.91			
90 mins	1.3307	0.6462	0.6845	0.5144	51.44	51.40	0.0337	0.0655
	1.3305	0.6472	0.6833	0.5136	51.36			
	1.3306	0.6467	0.6839	0.5140	51.40			
120 mins	1.3307	0.6437	0.6870	0.5163	51.63	51.61	0.0140	0.0271
	1.3305	0.6439	0.6866	0.5160	51.60			
	1.3306	0.6441	0.6865	0.5159	51.59			

Appendix 7 continued

150 mins	1.3307	0.6437	0.6870	0.5163	51.63	51.62	0.0063	0.0122
	1.3305	0.6438	0.6867	0.5161	51.61			
	1.3306	0.6437	0.6869	0.5162	51.62			
180 mins	1.3307	0.6407	0.6900	0.5185	51.85	51.84	0.0123	0.0237
	1.3305	0.6410	0.6895	0.5182	51.82			
	1.3306	0.6408	0.6898	0.5184	51.84			
210 mins	1.3307	0.6160	0.7147	0.5371	53.71	53.67	0.0294	0.0547
	1.3305	0.6168	0.7137	0.5364	53.64			
	1.3306	0.6167	0.7139	0.5365	53.65			
240 mins	1.3307	0.5832	0.7475	0.5617	56.17	56.17	0.0018	0.0032
	1.3305	0.5831	0.7474	0.5617	56.17			
	1.3306	0.5832	0.7474	0.5617	56.17			
270 mins	1.3307	0.5895	0.7412	0.5570	55.70	55.70	0.0079	0.0141
	1.3305	0.5896	0.7409	0.5569	55.69			
	1.3306	0.5894	0.7412	0.5570	55.70			

Appendix 7 continued

300 mins	1.3307	0.6032	0.7275	0.5467	54.67	54.74	0.0508	0.0927
	1.3305	0.6017	0.7288	0.5478	54.78			
	1.3306	0.6017	0.7289	0.5478	54.78			

Appendix 8: Batch Binding of MIP (MAA) of AME

Duration	Ci	Cf	(Ci - Cf)	(Ci - Cf)/Ci	Binding efficiency, %	Mean, %	Standard deviation, σ	RSD
5 mins	1.3519	0.2465	1.1054	0.8177	81.77	81.82	0.0390	0.0476
	1.3510	0.2451	1.1059	0.8186	81.86			
	1.3510	0.2454	1.1056	0.8184	81.84			
10 mins	1.3519	0.2150	1.1369	0.8410	84.10	84.08	0.0137	0.0163
	1.3510	0.2150	1.1360	0.8409	84.09			
	1.3510	0.2153	1.1357	0.8406	84.06			
15 mins	1.3519	0.1981	1.1538	0.8535	85.35	85.29	0.0413	0.0484
	1.3510	0.1993	1.1517	0.8525	85.25			
	1.3510	0.1989	1.1521	0.8528	85.28			
20 mins	1.3519	0.1962	1.1557	0.8549	85.49	85.45	0.0345	0.0404
	1.3510	0.1965	1.1545	0.8546	85.46			
	1.3510	0.1972	1.1538	0.8540	85.40			

Appendix 8 continued

25 mins	1.3519	0.1132	1.2387	0.9163	91.63	91.64	0.0099	0.0108
	1.3510	0.1128	1.2382	0.9165	91.65			
	1.3510	0.1130	1.2380	0.9164	91.64			
30 mins	1.3519	0.0963	1.2556	0.9288	92.88	92.91	0.0294	0.0317
	1.3510	0.0953	1.2557	0.9295	92.95			
	1.3510	0.0960	1.2550	0.9289	92.89			
60 mins	1.3519	0.0942	1.2577	0.9303	93.03	93.03	0.0050	0.0053
	1.3510	0.0943	1.2567	0.9302	93.02			
	1.3510	0.0942	1.2568	0.9303	93.03			
90 mins	1.3519	0.0923	1.2596	0.9317	93.17	93.16	0.0203	0.0218
	1.3510	0.0922	1.2588	0.9318	93.18			
	1.3510	0.0928	1.2582	0.9313	93.13			
120 mins	1.3519	0.0925	1.2594	0.9316	93.16	93.17	0.0269	0.0289
	1.3510	0.0925	1.2585	0.9315	93.15			
	1.3510	0.0917	1.2593	0.9321	93.21			

Appendix 8 continued

150 mins	1.3519	0.0915	1.2604	0.9323	93.23	93.21	0.0140	0.0150
	1.3510	0.0919	1.2591	0.9320	93.20			
	1.3510	0.0917	1.2593	0.9321	93.21			
180 mins	1.3519	0.0850	1.2669	0.9371	93.71	93.65	0.0536	0.0573
	1.3510	0.0856	1.2654	0.9366	93.66			
	1.3510	0.0867	1.2643	0.9358	93.58			
210 mins	1.3519	0.0836	1.2683	0.9382	93.82	93.73	0.1094	0.1167
	1.3510	0.0838	1.2672	0.9380	93.80			
	1.3510	0.0868	1.2642	0.9358	93.58			
240 mins	1.3519	0.0852	1.2667	0.9370	93.70	93.70	0.0050	0.0053
	1.3510	0.0850	1.2660	0.9371	93.71			
	1.3510	0.0850	1.2660	0.9371	93.71			
270 mins	1.3519	0.0951	1.2568	0.9297	92.97	92.94	0.0267	0.0288
	1.3510	0.0959	1.2551	0.9290	92.90			
	1.3510	0.0953	1.2557	0.9295	92.95			

Appendix 8 continued

	1.3519	0.1070	1.2449	0.9209	92.09			
300 mins	1.3510	0.1067	1.2443	0.9210	92.10	92.09	0.0069	0.0075
	1.3510	0.1068	1.2442	0.9209	92.09			

Appendix 9: Batch Binding of MIP (AAm) of AME

Duration	Ci	Cf	(Ci - Cf)	(Ci - Cf)/Ci	Binding efficiency, %	Mean, %	Standard deviation, σ	RSD
5 mins	1.4024	0.4556	0.9468	0.6751	67.51	67.59	0.0577	0.0854
	1.4023	0.4542	0.9481	0.6761	67.61			
	1.4031	0.4539	0.9492	0.6765	67.65			
10 mins	1.4024	0.3659	1.0365	0.7391	73.91	73.93	0.0251	0.0340
	1.4023	0.3658	1.0365	0.7391	73.91			
	1.4031	0.3653	1.0378	0.7396	73.96			
15 mins	1.4024	0.3117	1.0907	0.7777	77.77	77.79	0.0162	0.0208
	1.4023	0.3114	1.0909	0.7779	77.79			
	1.4031	0.3113	1.0918	0.7781	77.81			
20 mins	1.4024	0.2913	1.1111	0.7923	79.23	79.21	0.0182	0.0229
	1.4023	0.2919	1.1104	0.7918	79.18			
	1.4031	0.2917	1.1114	0.7921	79.21			

Appendix 9 continued

25 mins	1.4024	0.2801	1.1223	0.8003	80.03	80.00	0.0210	0.0262
	1.4023	0.2808	1.1215	0.7998	79.98			
	1.4031	0.2806	1.1225	0.8000	80.00			
30 mins	1.4024	0.2763	1.1261	0.8030	80.30	80.31	0.0169	0.0210
	1.4023	0.2762	1.1261	0.8030	80.30			
	1.4031	0.2759	1.1272	0.8034	80.34			
60 mins	1.4024	0.2652	1.1372	0.8109	81.09	81.14	0.0402	0.0495
	1.4023	0.2642	1.1381	0.8116	81.16			
	1.4031	0.2640	1.1391	0.8118	81.18			
90 mins	1.4024	0.2499	1.1525	0.8218	82.18	82.20	0.0183	0.0223
	1.4023	0.2495	1.1528	0.8221	82.21			
	1.4031	0.2494	1.1537	0.8223	82.23			
120 mins	1.4024	0.2323	1.1701	0.8344	83.44	83.47	0.0338	0.0404
	1.4023	0.2320	1.1703	0.8346	83.46			
	1.4031	0.2313	1.1718	0.8352	83.52			

Appendix 9 continued

150 mins	1.4024	0.2210	1.1814	0.8424	84.24	84.24	0.0097	0.0115
	1.4023	0.2212	1.1811	0.8423	84.23			
	1.4031	0.2210	1.1821	0.8425	84.25			
180 mins	1.4024	0.2191	1.1833	0.8438	84.38	84.38	0.0051	0.0060
	1.4023	0.2190	1.1833	0.8438	84.38			
	1.4031	0.2193	1.1838	0.8437	84.37			
210 mins	1.4024	0.2021	1.2003	0.8559	85.59	85.61	0.0184	0.0215
	1.4023	0.2015	1.2008	0.8563	85.63			
	1.4031	0.2017	1.2014	0.8562	85.62			
240 mins	1.4024	0.2180	1.1844	0.8446	84.46	84.42	0.0267	0.0316
	1.4023	0.2189	1.1834	0.8439	84.39			
	1.4031	0.2186	1.1845	0.8442	84.42			
270 mins	1.4024	0.2202	1.1822	0.8430	84.30	84.29	0.0175	0.0208
	1.4023	0.2207	1.1816	0.8426	84.26			
	1.4031	0.2203	1.1828	0.8430	84.30			

Appendix 9 continued

300 mins	1.4024	0.2259	1.1765	0.8389	83.89	83.89	0.0041	0.0049
	1.4023	0.2260	1.1763	0.8388	83.88			
	1.4031	0.2260	1.1771	0.8389	83.89			

Appendix 10: Batch Binding of MIP (2VP) of AME

Duration	Ci	Cf	(Ci - Cf)	(Ci - Cf)/Ci	Binding efficiency, %	Mean, %	Standard deviation, σ	RSD
5 mins	1.3804	0.6792	0.7012	0.5080	50.80	50.71	0.0594	0.1172
	1.3759	0.6789	0.6970	0.5066	50.66			
	1.3762	0.6786	0.6976	0.5069	50.69			
10 mins	1.3804	0.6552	0.7252	0.5254	52.54	52.44	0.0715	0.1363
	1.3759	0.6553	0.7206	0.5237	52.37			
	1.3762	0.6551	0.7211	0.5240	52.40			
15 mins	1.3804	0.6479	0.7325	0.5306	53.06	52.98	0.0618	0.1166
	1.3759	0.6477	0.7282	0.5293	52.93			
	1.3762	0.6476	0.7286	0.5294	52.94			
20 mins	1.3804	0.6385	0.7419	0.5375	53.75	53.66	0.0651	0.1213
	1.3759	0.6385	0.7374	0.5359	53.59			
	1.3762	0.6382	0.7380	0.5363	53.63			

Appendix 10 continued

25 mins	1.3804	0.6281	0.7523	0.5450	54.50	54.48	0.0940	0.1725
	1.3759	0.6280	0.7479	0.5436	54.36			
	1.3762	0.6250	0.7512	0.5459	54.59			
30 mins	1.3804	0.6107	0.7697	0.5576	55.76	55.67	0.0612	0.1099
	1.3759	0.6106	0.7653	0.5562	55.62			
	1.3762	0.6105	0.7657	0.5564	55.64			
60 mins	1.3804	0.5751	0.8053	0.5834	58.34	58.24	0.0696	0.1195
	1.3759	0.5754	0.8005	0.5818	58.18			
	1.3762	0.5752	0.8010	0.5820	58.20			
90 mins	1.3804	0.5302	0.8502	0.6159	61.59	61.52	0.0525	0.0853
	1.3759	0.5301	0.8458	0.6147	61.47			
	1.3762	0.5300	0.8462	0.6149	61.49			
120 mins	1.3804	0.5005	0.8799	0.6374	63.74	63.68	0.0459	0.0721
	1.3759	0.5003	0.8756	0.6364	63.64			
	1.3762	0.5002	0.8760	0.6365	63.65			

Appendix 10 continued

150 mins	1.3804	0.4606	0.9198	0.6663	66.63	66.57	0.0428	0.0643
	1.3759	0.4605	0.9154	0.6653	66.53			
	1.3762	0.4602	0.9160	0.6656	66.56			
180 mins	1.3804	0.4327	0.9477	0.6865	68.65	68.60	0.0420	0.0612
	1.3759	0.4326	0.9433	0.6856	68.56			
	1.3762	0.4325	0.9437	0.6857	68.57			
210 mins	1.3804	0.3671	1.0133	0.7341	73.41	73.39	0.0221	0.0302
	1.3759	0.3666	1.0093	0.7336	73.36			
	1.3762	0.3661	1.0101	0.7340	73.40			
240 mins	1.3804	0.3734	1.0070	0.7295	72.95	72.87	0.0587	0.0805
	1.3759	0.3735	1.0024	0.7285	72.85			
	1.3762	0.3742	1.0020	0.7281	72.81			
270 mins	1.3804	0.3771	1.0033	0.7268	72.68	72.62	0.0443	0.0610
	1.3759	0.3771	0.9988	0.7259	72.59			
	1.3762	0.3773	0.9989	0.7258	72.58			

Appendix 10 continued

300 mins	1.3804	0.3860	0.9944	0.7204	72.04	71.97	0.0505	0.0702
	1.3759	0.3863	0.9896	0.7192	71.92			
	1.3762	0.3862	0.9900	0.7194	71.94			

Appendix 11: Batch Binding of NIP (MAA) of AME

Duration	Ci	Cf	(Ci - Cf)	(Ci - Cf)/Ci	Binding efficiency, %	Mean, %	Standard deviation, σ	RSD
5 mins	1.3364	0.5548	0.7816	0.5849	58.49	58.45	0.0394	0.0673
	1.3360	0.5549	0.7811	0.5847	58.47			
	1.3361	0.5559	0.7802	0.5839	58.39			
10 mins	1.3364	0.5487	0.7877	0.5894	58.94	59.00	0.0557	0.0944
	1.3360	0.5480	0.7880	0.5898	58.98			
	1.3361	0.5468	0.7893	0.5907	59.07			
15 mins	1.3364	0.5386	0.7978	0.5970	59.70	59.68	0.0194	0.0326
	1.3360	0.5390	0.7970	0.5966	59.66			
	1.3361	0.5385	0.7976	0.5970	59.70			
20 mins	1.3364	0.5294	0.8070	0.6039	60.39	60.38	0.0069	0.0115
	1.3360	0.5293	0.8067	0.6038	60.38			
	1.3361	0.5295	0.8066	0.6037	60.37			

Appendix 11 continued

25 mins	1.3364	0.5289	0.8075	0.6042	60.42	60.45	0.0211	0.0349
	1.3360	0.5283	0.8077	0.6046	60.46			
	1.3361	0.5281	0.8080	0.6047	60.47			
30 mins	1.3364	0.5268	0.8096	0.6058	60.58	60.54	0.0270	0.0447
	1.3360	0.5275	0.8085	0.6052	60.52			
	1.3361	0.5273	0.8088	0.6053	60.53			
60 mins	1.3364	0.5256	0.8108	0.6067	60.67	60.60	0.0535	0.0883
	1.3360	0.5271	0.8089	0.6055	60.55			
	1.3361	0.5268	0.8093	0.6057	60.57			
90 mins	1.3364	0.5221	0.8143	0.6093	60.93	60.93	0.0233	0.0382
	1.3360	0.5216	0.8144	0.6096	60.96			
	1.3361	0.5224	0.8137	0.6090	60.90			
120 mins	1.3364	0.5193	0.8171	0.6114	61.14	61.13	0.0123	0.0201
	1.3360	0.5195	0.8165	0.6112	61.12			
	1.3361	0.5192	0.8169	0.6114	61.14			

Appendix 11 continued

150 mins	1.3364	0.5142	0.8222	0.6152	61.52	61.49	0.0231	0.0375
	1.3360	0.5148	0.8212	0.6147	61.47			
	1.3361	0.5145	0.8216	0.6149	61.49			
180 mins	1.3364	0.5120	0.8244	0.6169	61.69	61.73	0.0288	0.0467
	1.3360	0.5110	0.8250	0.6175	61.75			
	1.3361	0.5111	0.8250	0.6175	61.75			
210 mins	1.3364	0.4981	0.8383	0.6273	62.73	62.74	0.0182	0.0289
	1.3360	0.4980	0.8380	0.6272	62.72			
	1.3361	0.4975	0.8386	0.6276	62.76			
240 mins	1.3364	0.4977	0.8387	0.6276	62.76	62.70	0.0402	0.0641
	1.3360	0.4986	0.8374	0.6268	62.68			
	1.3361	0.4988	0.8373	0.6267	62.67			
270 mins	1.3364	0.5047	0.8317	0.6223	62.23	62.20	0.0578	0.0929
	1.3360	0.5045	0.8315	0.6224	62.24			
	1.3361	0.5062	0.8299	0.6211	62.11			

Appendix 11 continued

300 mins	1.3364	0.5074	0.8290	0.6203	62.03	62.00	0.0527	0.0850
	1.3360	0.5071	0.8289	0.6204	62.04			
	1.3361	0.5087	0.8274	0.6193	61.93			

Appendix 12: Batch Binding of MIP (MAA) of ATZ

Duration	Ci	Cf	(Ci - Cf)	(Ci - Cf)/Ci	Binding efficiency, %	Mean, %	Standard deviation, σ	RSD
5 mins	0.9588	0.2157	0.7431	0.7750	77.50	77.48	0.0309	0.0399
	0.9587	0.2158	0.7429	0.7749	77.49			
	0.9580	0.2162	0.7418	0.7743	77.43			
10 mins	0.9588	0.1956	0.7632	0.7960	79.60	79.54	0.0394	0.0496
	0.9587	0.1963	0.7624	0.7952	79.52			
	0.9580	0.1963	0.7617	0.7951	79.51			
15 mins	0.9588	0.1856	0.7732	0.8064	80.64	80.63	0.0069	0.0086
	0.9587	0.1857	0.7730	0.8063	80.63			
	0.9580	0.1856	0.7724	0.8063	80.63			
20 mins	0.9588	0.1892	0.7696	0.8027	80.27	80.24	0.0417	0.0520
	0.9587	0.1892	0.7695	0.8026	80.26			
	0.9580	0.1899	0.7681	0.8018	80.18			

Appendix 12 continued

25 mins	0.9588	0.1999	0.7589	0.7915	79.15	79.17	0.0211	0.0266
	0.9587	0.1994	0.7593	0.7920	79.20			
	0.9580	0.1996	0.7584	0.7916	79.16			
30 mins	0.9588	0.2015	0.7573	0.7898	78.98	78.98	0.0108	0.0136
	0.9587	0.2014	0.7573	0.7899	78.99			
	0.9580	0.2015	0.7565	0.7897	78.97			
60 mins	0.9588	0.2083	0.7505	0.7827	78.27	78.23	0.0295	0.0377
	0.9587	0.2089	0.7498	0.7821	78.21			
	0.9580	0.2087	0.7493	0.7822	78.22			
90 mins	0.9588	0.2112	0.7476	0.7797	77.97	77.93	0.0332	0.0426
	0.9587	0.2115	0.7472	0.7794	77.94			
	0.9580	0.2118	0.7462	0.7789	77.89			
120 mins	0.9588	0.2178	0.7410	0.7728	77.28	77.40	0.0818	0.1057
	0.9587	0.2160	0.7427	0.7747	77.47			
	0.9580	0.2161	0.7419	0.7744	77.44			

Appendix 12 continued

150 mins	0.9588	0.2196	0.7392	0.7710	77.10	77.11	0.0373	0.0484
	0.9587	0.2190	0.7397	0.7716	77.16			
	0.9580	0.2197	0.7383	0.7707	77.07			
180 mins	0.9588	0.2209	0.7379	0.7696	76.96	76.94	0.0215	0.0279
	0.9587	0.2210	0.7377	0.7695	76.95			
	0.9580	0.2212	0.7368	0.7691	76.91			
210 mins	0.9588	0.2305	0.7283	0.7596	75.96	75.93	0.0253	0.0333
	0.9587	0.2308	0.7279	0.7593	75.93			
	0.9580	0.2309	0.7271	0.7590	75.90			
240 mins	0.9588	0.2389	0.7199	0.7508	75.08	75.12	0.0266	0.0355
	0.9587	0.2383	0.7204	0.7514	75.14			
	0.9580	0.2382	0.7198	0.7514	75.14			
270 mins	0.9588	0.2511	0.7077	0.7381	73.81	73.78	0.0260	0.0352
	0.9587	0.2514	0.7073	0.7378	73.78			
	0.9580	0.2515	0.7065	0.7375	73.75			

Appendix 12 continued

300 mins	0.9588	0.2694	0.6894	0.7190	71.90	71.89	0.0139	0.0194
	0.9587	0.2695	0.6892	0.7189	71.89			
	0.9580	0.2695	0.6885	0.7187	71.87			

Appendix 13: Batch Binding of MIP (AAm) of ATZ

Duration	Ci	Cf	(Ci - Cf)	(Ci - Cf)/Ci	Binding efficiency, %	Mean, %	Standard deviation, σ	RSD
5 mins	0.9144	0.2839	0.6305	0.6895	68.95	68.90	0.0366	0.0531
	0.9152	0.2847	0.6305	0.6889	68.89			
	0.9144	0.2847	0.6297	0.6886	68.86			
10 mins	0.9144	0.2395	0.6749	0.7381	73.81	73.87	0.0475	0.0644
	0.9152	0.2387	0.6765	0.7392	73.92			
	0.9144	0.2387	0.6757	0.7390	73.90			
15 mins	0.9144	0.2314	0.6830	0.7469	74.69	74.71	0.0288	0.0386
	0.9152	0.2311	0.6841	0.7475	74.75			
	0.9144	0.2315	0.6829	0.7468	74.68			
20 mins	0.9144	0.2398	0.6746	0.7378	73.78	73.80	0.0189	0.0256
	0.9152	0.2396	0.6756	0.7382	73.82			
	0.9144	0.2395	0.6749	0.7381	73.81			

Appendix 13 continued

25 mins	0.9144	0.2419	0.6725	0.7355	73.55	73.56	0.0192	0.0260
	0.9152	0.2417	0.6735	0.7359	73.59			
	0.9144	0.2418	0.6726	0.7356	73.56			
30 mins	0.9144	0.2436	0.6708	0.7336	73.36	73.37	0.0213	0.0290
	0.9152	0.2434	0.6718	0.7340	73.40			
	0.9144	0.2436	0.6708	0.7336	73.36			
60 mins	0.9144	0.2441	0.6703	0.7330	73.30	73.29	0.0188	0.0256
	0.9152	0.2444	0.6708	0.7330	73.30			
	0.9144	0.2445	0.6699	0.7326	73.26			
90 mins	0.9144	0.2492	0.6652	0.7275	72.75	72.76	0.0195	0.0268
	0.9152	0.2491	0.6661	0.7278	72.78			
	0.9144	0.2493	0.6651	0.7274	72.74			
120 mins	0.9144	0.2521	0.6623	0.7243	72.43	72.41	0.0298	0.0412
	0.9152	0.2529	0.6623	0.7237	72.37			
	0.9144	0.2521	0.6623	0.7243	72.43			

Appendix 13 continued

150 mins	0.9144	0.2558	0.6586	0.7203	72.03	72.03	0.0064	0.0089
	0.9152	0.2559	0.6593	0.7204	72.04			
	0.9144	0.2558	0.6586	0.7203	72.03			
180 mins	0.9144	0.2611	0.6533	0.7145	71.45	71.43	0.0214	0.0299
	0.9152	0.2613	0.6539	0.7145	71.45			
	0.9144	0.2615	0.6529	0.7140	71.40			
210 mins	0.9144	0.2797	0.6347	0.6941	69.41	69.41	0.0066	0.0095
	0.9152	0.2799	0.6353	0.6942	69.42			
	0.9144	0.2798	0.6346	0.6940	69.40			
240 mins	0.9144	0.2829	0.6315	0.6906	69.06	69.10	0.0269	0.0389
	0.9152	0.2828	0.6324	0.6910	69.10			
	0.9144	0.2823	0.6321	0.6913	69.13			
270 mins	0.9144	0.2990	0.6154	0.6730	67.30	67.26	0.0367	0.0545
	0.9152	0.2995	0.6157	0.6727	67.27			
	0.9144	0.2998	0.6146	0.6721	67.21			

Appendix 13 continued

300 mins	0.9144	0.3047	0.6097	0.6668	66.68	66.76	0.0558	0.0837
	0.9152	0.3039	0.6113	0.6679	66.79			
	0.9144	0.3036	0.6108	0.6680	66.80			

Appendix 14: Batch Binding of MIP (2VP) of ATZ

Duration	Ci	Cf	(Ci - Cf)	(Ci - Cf)/Ci	Binding efficiency, %	Mean, %	Standard deviation, σ	RSD
5 mins	0.9210	0.1215	0.7995	0.8681	86.81	86.80	0.0089	0.0102
	0.9210	0.1217	0.7993	0.8679	86.79			
	0.9210	0.1216	0.7994	0.8680	86.80			
10 mins	0.9210	0.1137	0.8073	0.8765	87.65	87.66	0.0135	0.0154
	0.9210	0.1135	0.8075	0.8768	87.68			
	0.9210	0.1138	0.8072	0.8764	87.64			
15 mins	0.9210	0.1065	0.8145	0.8844	88.44	88.44	0.0000	0.0000
	0.9210	0.1065	0.8145	0.8844	88.44			
	0.9210	0.1065	0.8145	0.8844	88.44			
20 mins	0.9210	0.1122	0.8088	0.8782	87.82	87.83	0.0089	0.0101
	0.9210	0.1120	0.8090	0.8784	87.84			
	0.9210	0.1121	0.8089	0.8783	87.83			

Appendix 14 continued

25 mins	0.9210	0.1191	0.8019	0.8707	87.07	87.03	0.0285	0.0327
	0.9210	0.1197	0.8013	0.8700	87.00			
	0.9210	0.1196	0.8014	0.8701	87.01			
30 mins	0.9210	0.1207	0.8003	0.8689	86.89	86.89	0.0051	0.0059
	0.9210	0.1208	0.8002	0.8688	86.88			
	0.9210	0.1207	0.8003	0.8689	86.89			
60 mins	0.9210	0.1288	0.7922	0.8602	86.02	86.06	0.0320	0.0371
	0.9210	0.1281	0.7929	0.8609	86.09			
	0.9210	0.1283	0.7927	0.8607	86.07			
90 mins	0.9210	0.1328	0.7882	0.8558	85.58	85.58	0.0051	0.0060
	0.9210	0.1327	0.7883	0.8559	85.59			
	0.9210	0.1328	0.7882	0.8558	85.58			
120 mins	0.9210	0.1387	0.7823	0.8494	84.94	84.94	0.0135	0.0159
	0.9210	0.1388	0.7822	0.8493	84.93			
	0.9210	0.1385	0.7825	0.8496	84.96			

Appendix 14 continued

150 mins	0.9210	0.1494	0.7716	0.8378	83.78	83.78	0.0089	0.0106
	0.9210	0.1493	0.7717	0.8379	83.79			
	0.9210	0.1495	0.7715	0.8377	83.77			
180 mins	0.9210	0.1534	0.7676	0.8334	83.34	83.33	0.0089	0.0106
	0.9210	0.1535	0.7675	0.8333	83.33			
	0.9210	0.1536	0.7674	0.8332	83.32			
210 mins	0.9210	0.1681	0.7529	0.8175	81.75	81.78	0.0266	0.0325
	0.9210	0.1678	0.7532	0.8178	81.78			
	0.9210	0.1675	0.7535	0.8181	81.81			
240 mins	0.9210	0.1781	0.7429	0.8066	80.66	80.65	0.0154	0.0190
	0.9210	0.1784	0.7426	0.8063	80.63			
	0.9210	0.1781	0.7429	0.8066	80.66			
270 mins	0.9210	0.1828	0.7382	0.8015	80.15	80.14	0.0102	0.0128
	0.9210	0.1830	0.7380	0.8013	80.13			
	0.9210	0.1830	0.7380	0.8013	80.13			

Appendix 14 continued

300 mins	0.9210	0.1918	0.7292	0.7917	79.17	79.16	0.0185	0.0233
	0.9210	0.1919	0.7291	0.7916	79.16			
	0.9210	0.1922	0.7288	0.7913	79.13			

Appendix 15: Batch Binding of NIP (2VP) of ATZ

Duration	Ci	Cf	(Ci - Cf)	(Ci - Cf)/Ci	Binding efficiency, %	Mean, %	Standard deviation, σ	RSD
5 mins	0.9209	0.4700	0.4509	0.4896	48.96	48.95	0.0092	0.0189
	0.9208	0.4701	0.4507	0.4895	48.95			
	0.9209	0.4702	0.4507	0.4894	48.94			
10 mins	0.9209	0.4704	0.4505	0.4892	48.92	49.93	1.5423	3.0892
	0.9208	0.4410	0.4798	0.5211	52.11			
	0.9209	0.4719	0.4490	0.4876	48.76			
15 mins	0.9209	0.4450	0.4759	0.5168	51.68	51.04	0.4496	0.8809
	0.9208	0.4535	0.4673	0.5075	50.75			
	0.9209	0.4540	0.4669	0.5070	50.70			
20 mins	0.9209	0.4546	0.4663	0.5064	50.64	50.68	0.0339	0.0669
	0.9208	0.4538	0.4670	0.5072	50.72			
	0.9209	0.4541	0.4668	0.5069	50.69			

Appendix 15 continued

25 mins	0.9209	0.4716	0.4493	0.4879	48.79	48.77	0.0480	0.0984
	0.9208	0.4723	0.4485	0.4871	48.71			
	0.9209	0.4713	0.4496	0.4882	48.82			
30 mins	0.9209	0.4720	0.4489	0.4875	48.75	48.75	0.0156	0.0320
	0.9208	0.4721	0.4487	0.4873	48.73			
	0.9209	0.4718	0.4491	0.4877	48.77			
60 mins	0.9209	0.5017	0.4192	0.4552	45.52	45.48	0.0340	0.0748
	0.9208	0.5024	0.4184	0.4544	45.44			
	0.9209	0.5022	0.4187	0.4547	45.47			
90 mins	0.9209	0.5214	0.3995	0.4338	43.38	43.33	0.0532	0.1228
	0.9208	0.5225	0.3983	0.4326	43.26			
	0.9209	0.5217	0.3992	0.4335	43.35			
120 mins	0.9209	0.5234	0.3975	0.4316	43.16	43.24	0.0621	0.1437
	0.9208	0.5227	0.3981	0.4323	43.23			
	0.9209	0.5220	0.3989	0.4332	43.32			

Appendix 15 continued

150 mins	0.9209	0.5287	0.3922	0.4259	42.59	42.64	0.0376	0.0881
	0.9208	0.5280	0.3928	0.4266	42.66			
	0.9209	0.5279	0.3930	0.4268	42.68			
180 mins	0.9209	0.5328	0.3881	0.4214	42.14	42.16	0.0355	0.0841
	0.9208	0.5329	0.3879	0.4213	42.13			
	0.9209	0.5322	0.3887	0.4221	42.21			
210 mins	0.9209	0.5450	0.3759	0.4082	40.82	40.81	0.0251	0.0616
	0.9208	0.5453	0.3755	0.4078	40.78			
	0.9209	0.5448	0.3761	0.4084	40.84			
240 mins	0.9209	0.5478	0.3731	0.4051	40.51	40.46	0.0430	0.1062
	0.9208	0.5487	0.3721	0.4041	40.41			
	0.9209	0.5484	0.3725	0.4045	40.45			
270 mins	0.9209	0.5737	0.3472	0.3770	37.70	37.58	0.0837	0.2228
	0.9208	0.5752	0.3456	0.3753	37.53			
	0.9209	0.5754	0.3455	0.3752	37.52			

Appendix 15 continued

300 mins	0.9209	0.5761	0.3448	0.3744	37.44	37.41	0.0394	0.1054
	0.9208	0.5761	0.3447	0.3743	37.43			
	0.9209	0.5769	0.3440	0.3735	37.35			

Appendix 16: Effect of Initial Concentration on MIP (AAm) of CYZ

Concentration	Ci	Cf	(Ci - Cf)	(Ci - Cf)/Ci	Binding efficiency, %	Mean, %	Standard deviation, σ	RSD
1 ppm	0.3080	0.2294	0.0786	0.2552	25.52	25.51	0.1053	0.4129
	0.3086	0.2295	0.0791	0.2563	25.63			
	0.3070	0.2291	0.0779	0.2537	25.37			
2 ppm	0.5931	0.3423	0.2508	0.4229	42.29	42.43	0.3865	0.9109
	0.5929	0.3382	0.2547	0.4296	42.96			
	0.5927	0.3435	0.2492	0.4204	42.04			
3 ppm	0.8487	0.2891	0.5596	0.6594	65.94	66.29	0.4308	0.6498
	0.8489	0.2810	0.5679	0.6690	66.90			
	0.8487	0.2882	0.5605	0.6604	66.04			
4 ppm	1.1515	0.3084	0.8431	0.7322	73.22	73.27	0.0398	0.0543
	1.1526	0.3078	0.8448	0.7330	73.30			
	1.1535	0.3079	0.8456	0.7331	73.31			

Appendix 16 continued

5 ppm	1.3390	0.2734	1.0656	0.7958	79.58	79.57	0.0174	0.0218
	1.3402	0.2737	1.0665	0.7958	79.58			
	1.3394	0.2740	1.0654	0.7954	79.54			
6 ppm	1.6837	0.2314	1.4523	0.8626	86.26	86.26	0.0053	0.0061
	1.6839	0.2315	1.4524	0.8625	86.25			
	1.6840	0.2313	1.4527	0.8626	86.26			
7 ppm	1.9376	0.3422	1.5954	0.8234	82.34	82.32	0.0120	0.0146
	1.9367	0.3426	1.5941	0.8231	82.31			
	1.9372	0.3425	1.5947	0.8232	82.32			
8 ppm	2.1937	0.4192	1.7745	0.8089	80.89	80.93	0.0259	0.0320
	2.1930	0.4178	1.7752	0.8095	80.95			
	2.1928	0.4179	1.7749	0.8094	80.94			
9 ppm	2.4478	0.5080	1.9398	0.7925	79.25	79.21	0.0261	0.0330
	2.4478	0.5088	1.9390	0.7921	79.21			
	2.4494	0.5099	1.9395	0.7918	79.18			

Appendix 16 continued

10 ppm	2.6871	0.5765	2.1106	0.7855	78.55	78.63	0.0677	0.0861
	2.6878	0.5744	2.1134	0.7863	78.63			
	2.6883	0.5723	2.1160	0.7871	78.71			

Appendix 17: Effect of Initial Concentration on NIP (AAm) of CYZ

Concentration	Ci	Cf	(Ci - Cf)	(Ci - Cf)/Ci	Binding efficiency, %	Mean, %	Standard deviation, σ	RSD
1 ppm	0.2977	0.2459	0.0518	0.1740	17.40	17.42	0.0426	0.2444
	0.2973	0.2456	0.0517	0.1739	17.39			
	0.2974	0.2454	0.0520	0.1748	17.48			
2 ppm	0.5888	0.4463	0.1425	0.2420	24.20	24.22	0.0496	0.2047
	0.5889	0.4466	0.1423	0.2416	24.16			
	0.5889	0.4459	0.1430	0.2428	24.28			
3 ppm	0.8572	0.5925	0.2647	0.3088	30.88	30.87	0.0314	0.1017
	0.8574	0.5931	0.2643	0.3083	30.83			
	0.8576	0.5926	0.2650	0.3090	30.90			
4 ppm	1.1488	0.7541	0.3947	0.3436	34.36	34.34	0.0154	0.0450
	1.1489	0.7546	0.3943	0.3432	34.32			
	1.1491	0.7545	0.3946	0.3434	34.34			

Appendix 17 continued

5 ppm	1.3307	0.7832	0.5475	0.4114	41.14	41.14	0.0019	0.0045
	1.3305	0.7831	0.5474	0.4114	41.14			
	1.3306	0.7832	0.5474	0.4114	41.14			
6 ppm	1.6810	0.8401	0.8409	0.5002	50.02	50.03	0.0037	0.0074
	1.6815	0.8402	0.8413	0.5003	50.03			
	1.6812	0.8401	0.8411	0.5003	50.03			
7 ppm	1.9375	1.0422	0.8953	0.4621	46.21	46.19	0.0270	0.0586
	1.9377	1.0435	0.8942	0.4615	46.15			
	1.9379	1.0426	0.8953	0.4620	46.20			
8 ppm	2.2054	1.3027	0.9027	0.4093	40.93	40.99	0.0469	0.1145
	2.2045	1.3007	0.9038	0.4100	41.00			
	2.2051	1.3000	0.9051	0.4105	41.05			
9 ppm	2.4435	1.5163	0.9272	0.3795	37.95	38.00	0.0517	0.1361
	2.4436	1.5134	0.9302	0.3807	38.07			
	2.4427	1.5151	0.9276	0.3797	37.97			

Appendix 17 continued

10 ppm	2.6773	1.6771	1.0002	0.3736	37.36	37.40	0.0305	0.0816
	2.6766	1.6756	1.0010	0.3740	37.40			
	2.6757	1.6741	1.0016	0.3743	37.43			

Appendix 18: Effect of Initial Concentration on MIP (MAA) of AME

Concentration	Ci	Cf	(Ci - Cf)	(Ci - Cf)/Ci	Binding efficiency, %	Mean, %	Standard deviation, σ	RSD
1 ppm	0.2661	0.0933	0.1728	0.6494	64.94	65.01	0.0950	0.1461
	0.2631	0.0922	0.1709	0.6496	64.96			
	0.2634	0.0918	0.1716	0.6515	65.15			
2 ppm	0.5514	0.0823	0.4691	0.8507	85.07	85.07	0.0053	0.0062
	0.5511	0.0823	0.4688	0.8507	85.07			
	0.5509	0.0822	0.4687	0.8508	85.08			
3 ppm	0.7834	0.0806	0.7028	0.8971	89.71	89.70	0.0174	0.0194
	0.7835	0.0809	0.7026	0.8967	89.67			
	0.7834	0.0806	0.7028	0.8971	89.71			
4 ppm	1.0729	0.0974	0.9755	0.9092	90.92	90.95	0.0194	0.0213
	1.0743	0.0971	0.9772	0.9096	90.96			
	1.0746	0.0971	0.9775	0.9096	90.96			

Appendix 18 continued

5 ppm	1.2441	0.0996	1.1445	0.9199	91.99	91.98	0.0073	0.0079
	1.2443	0.0998	1.1445	0.9198	91.98			
	1.2441	0.0998	1.1443	0.9198	91.98			
6 ppm	1.5470	0.1009	1.4461	0.9348	93.48	93.48	0.0084	0.0090
	1.5467	0.1009	1.4458	0.9348	93.48			
	1.5480	0.1007	1.4473	0.9349	93.49			
7 ppm	1.7889	0.1016	1.6873	0.9432	94.32	94.32	0.0072	0.0076
	1.7875	0.1013	1.6862	0.9433	94.33			
	1.7874	0.1016	1.6858	0.9432	94.32			
8 ppm	2.0074	0.1343	1.8731	0.9331	93.31	93.34	0.0210	0.0225
	2.0083	0.1334	1.8749	0.9336	93.36			
	2.0075	0.1335	1.8740	0.9335	93.35			
9 ppm	2.3029	0.1635	2.1394	0.9290	92.90	92.89	0.0071	0.0076
	2.3029	0.1638	2.1391	0.9289	92.89			
	2.3032	0.1639	2.1393	0.9288	92.88			

Appendix 18 continued

10 ppm	2.5274	0.2050	2.3224	0.9189	91.89	91.89	0.0065	0.0071
	2.5281	0.2047	2.3234	0.9190	91.90			
	2.5251	0.2048	2.3203	0.9189	91.89			

Appendix 19: Effect of Initial Concentration on NIP (MAA) of AME

Concentration	Ci	Cf	(Ci - Cf)	(Ci - Cf)/Ci	Binding efficiency, %	Mean, %	Standard deviation, σ	RSD
1 ppm	0.2627	0.2234	0.0393	0.1496	14.96	15.04	0.0686	0.4560
	0.2631	0.2233	0.0398	0.1513	15.13			
	0.2628	0.2233	0.0395	0.1503	15.03			
2 ppm	0.5510	0.3453	0.2057	0.3733	37.33	37.26	0.0533	0.1431
	0.5509	0.3459	0.2050	0.3721	37.21			
	0.5512	0.3460	0.2052	0.3723	37.23			
3 ppm	0.7842	0.4230	0.3612	0.4606	46.06	46.04	0.0521	0.1131
	0.7857	0.4235	0.3622	0.4610	46.10			
	0.7837	0.4234	0.3603	0.4597	45.97			
4 ppm	1.0729	0.5631	0.5098	0.4752	47.52	47.45	0.0602	0.1269
	1.0722	0.5643	0.5079	0.4737	47.37			
	1.0727	0.5636	0.5091	0.4746	47.46			

Appendix 19 continued

5 ppm	1.2441	0.6281	0.6160	0.4951	49.51	49.51	0.0201	0.0406
	1.2443	0.6280	0.6163	0.4953	49.53			
	1.2441	0.6285	0.6156	0.4948	49.48			
6 ppm	1.5472	0.7540	0.7932	0.5127	51.27	51.25	0.0184	0.0358
	1.5472	0.7541	0.7931	0.5126	51.26			
	1.5469	0.7545	0.7924	0.5123	51.23			
7 ppm	1.7880	0.8459	0.9421	0.5269	52.69	52.69	0.0102	0.0194
	1.7882	0.8462	0.9420	0.5268	52.68			
	1.7883	0.8458	0.9425	0.5270	52.70			
8 ppm	2.0084	0.9593	1.0491	0.5224	52.24	52.20	0.0241	0.0462
	2.0066	0.9592	1.0474	0.5220	52.20			
	2.0070	0.9598	1.0472	0.5218	52.18			
9 ppm	2.3020	1.1054	1.1966	0.5198	51.98	52.00	0.0118	0.0228
	2.3032	1.1054	1.1978	0.5201	52.01			
	2.3030	1.1053	1.1977	0.5201	52.01			

Appendix 19 continued

10 ppm	2.5283	1.2331	1.2952	0.5123	51.23	51.24	0.0086	0.0168
	2.5289	1.2333	1.2956	0.5123	51.23			
	2.5283	1.2326	1.2957	0.5125	51.25			

Appendix 20: Effect of Initial Concentration on MIP (2VP) of ATZ

Concentration	Ci	Cf	(Ci - Cf)	(Ci - Cf)/Ci	Binding efficiency, %	Mean, %	Standard deviation, σ	RSD
1 ppm	0.2736	0.0826	0.1910	0.6981	69.81	69.89	0.0573	0.0820
	0.2732	0.0821	0.1911	0.6995	69.95			
	0.2734	0.0823	0.1911	0.6990	69.90			
2 ppm	0.4580	0.0909	0.3671	0.8015	80.15	80.18	0.0196	0.0245
	0.4584	0.0908	0.3676	0.8019	80.19			
	0.4580	0.0907	0.3673	0.8020	80.20			
3 ppm	0.6440	0.0908	0.5532	0.8590	85.90	85.88	0.0145	0.0169
	0.6438	0.0909	0.5529	0.8588	85.88			
	0.6438	0.0910	0.5528	0.8587	85.87			
4 ppm	0.8393	0.1075	0.7318	0.8719	87.19	87.18	0.0105	0.0121
	0.8394	0.1077	0.7317	0.8717	87.17			
	0.8394	0.1077	0.7317	0.8717	87.17			

Appendix 20 continued

5 ppm	1.0701	0.1268	0.9433	0.8815	88.15	88.16	0.0033	0.0037
	1.0708	0.1268	0.9440	0.8816	88.16			
	1.0706	0.1268	0.9438	0.8816	88.16			
6 ppm	1.2225	0.1376	1.0849	0.8874	88.74	88.75	0.0035	0.0039
	1.2225	0.1375	1.0850	0.8875	88.75			
	1.2223	0.1375	1.0848	0.8875	88.75			
7 ppm	1.4540	0.1350	1.3190	0.9072	90.72	90.71	0.0064	0.0070
	1.4539	0.1352	1.3187	0.9070	90.70			
	1.4542	0.1352	1.3190	0.9070	90.70			
8 ppm	1.6480	0.1414	1.5066	0.9142	91.42	91.43	0.0088	0.0096
	1.6485	0.1413	1.5072	0.9143	91.43			
	1.6486	0.1411	1.5075	0.9144	91.44			
9 ppm	1.8625	0.1997	1.6628	0.8928	89.28	89.28	0.0062	0.0069
	1.8621	0.1996	1.6625	0.8928	89.28			
	1.8622	0.1994	1.6628	0.8929	89.29			

Appendix 20 continued

10 ppm	2.0480	0.2366	1.8114	0.8845	88.45	88.50	0.0953	0.1077
	2.0480	0.2327	1.8153	0.8864	88.64			
	2.0476	0.2370	1.8106	0.8843	88.43			

Appendix 21: Effect of Initial Concentration on NIP (2VP) of ATZ

Concentration	Ci	Cf	(Ci - Cf)	(Ci - Cf)/Ci	Binding efficiency, %	Mean, %	Standard deviation, σ	RSD
1 ppm	0.2733	0.2109	0.0624	0.2283	22.83	22.89	0.0456	0.1993
	0.2733	0.2107	0.0626	0.2291	22.91			
	0.2733	0.2106	0.0627	0.2294	22.94			
2 ppm	0.4581	0.2909	0.1672	0.3650	36.50	36.52	0.0179	0.0489
	0.4581	0.2907	0.1674	0.3654	36.54			
	0.4578	0.2906	0.1672	0.3652	36.52			
3 ppm	0.6436	0.3710	0.2726	0.4236	42.36	42.36	0.0165	0.0389
	0.6429	0.3707	0.2722	0.4234	42.34			
	0.6430	0.3705	0.2725	0.4238	42.38			
4 ppm	0.8398	0.4521	0.3877	0.4617	46.17	46.14	0.0187	0.0405
	0.8397	0.4524	0.3873	0.4612	46.12			
	0.8396	0.4523	0.3873	0.4613	46.13			

Appendix 21 continued

5 ppm	1.0702	0.5647	0.5055	0.4723	47.23	47.27	0.0246	0.0521
	1.0704	0.5643	0.5061	0.4728	47.28			
	1.0702	0.5641	0.5061	0.4729	47.29			
6 ppm	1.2223	0.6375	0.5848	0.4784	47.84	47.85	0.0180	0.0376
	1.2227	0.6373	0.5854	0.4788	47.88			
	1.2223	0.6376	0.5847	0.4784	47.84			
7 ppm	1.4545	0.7386	0.7159	0.4922	49.22	49.21	0.0085	0.0172
	1.4543	0.7388	0.7155	0.4920	49.20			
	1.4544	0.7387	0.7157	0.4921	49.21			
8 ppm	1.6488	0.8071	0.8417	0.5105	51.05	51.04	0.0065	0.0128
	1.6487	0.8073	0.8414	0.5103	51.03			
	1.6486	0.8072	0.8414	0.5104	51.04			
9 ppm	1.8623	0.9362	0.9261	0.4973	49.73	49.73	0.0058	0.0116
	1.8625	0.9365	0.9260	0.4972	49.72			
	1.8624	0.9362	0.9262	0.4973	49.73			

Appendix 21 continued

10 ppm	2.0481	1.0502	0.9979	0.4872	48.72	48.70	0.0145	0.0298
	2.0481	1.0508	0.9973	0.4869	48.69			
	2.0476	1.0506	0.9970	0.4869	48.69			

Appendix 22: Effect of pH on MIP (AAm) of CYZ

pH	Ci	Cf	(Ci - Cf)	(Ci - Cf)/Ci	Binding efficiency, %	Mean, %	Standard deviation, σ	RSD
3	1.4322	0.4516	0.9806	0.6847	68.47	68.60	0.0965	0.1407
	1.4419	0.4518	0.9901	0.6867	68.67			
	1.4421	0.4517	0.9904	0.6868	68.68			
5	1.6081	0.3620	1.2461	0.7749	77.49	77.48	0.0097	0.0125
	1.6078	0.3623	1.2455	0.7747	77.47			
	1.6078	0.3622	1.2456	0.7747	77.47			
7	1.6837	0.2290	1.4547	0.8640	86.40	86.39	0.0125	0.0145
	1.6839	0.2295	1.4544	0.8637	86.37			
	1.6840	0.2291	1.4549	0.8640	86.40			
9	2.7444	2.0201	0.7243	0.2639	26.39	26.35	0.0559	0.2122
	2.7395	2.0197	0.7198	0.2627	26.27			
	2.7437	2.0195	0.7242	0.2640	26.40			

Appendix 22 continued

11	3.5320	3.0364	0.4956	0.1403	14.03	14.41	0.2710	1.8798
	3.5320	3.0159	0.5161	0.1461	14.61			
	3.5505	3.0321	0.5184	0.1460	14.60			

Appendix 23: Effect of pH on NIP (AAm) of CYZ

pH	Ci	Cf	(Ci - Cf)	(Ci - Cf)/Ci	Binding efficiency, %	Mean, %	Standard deviation, σ	RSD
3	3.4471	2.1151	1.3320	0.3864	38.64	38.76	0.1469	0.3790
	3.4476	2.1144	1.3332	0.3867	38.67			
	3.4617	2.1128	1.3489	0.3897	38.97			
5	3.2214	1.6280	1.5934	0.4946	49.46	49.44	0.0278	0.0561
	3.2211	1.6278	1.5933	0.4946	49.46			
	3.2177	1.6280	1.5897	0.4940	49.40			
7	1.681	0.7789	0.9021	0.5366	53.66	53.70	0.0282	0.0525
	1.6815	0.7780	0.9035	0.5373	53.73			
	1.6812	0.7782	0.9030	0.5371	53.71			
9	2.0874	1.7915	0.2959	0.1418	14.18	14.05	0.0889	0.6331
	2.0839	1.7924	0.2915	0.1399	13.99			
	2.0843	1.7928	0.2915	0.1399	13.99			

Appendix 23 continued

11	3.5237	3.3278	0.1959	0.0556	5.56	5.91	0.2517	4.2630
	3.5343	3.3169	0.2174	0.0615	6.15			
	3.5482	3.3351	0.2131	0.0601	6.01			

Appendix 24: Effect of pH on MIP (MAA) of AME

pH	Ci	Cf	(Ci - Cf)	(Ci - Cf)/Ci	Binding efficiency, %	Mean, %	Standard deviation, σ	RSD
3	1.5816	0.3081	1.2735	0.8052	80.52	80.56	0.0279	0.0346
	1.5822	0.3073	1.2749	0.8058	80.58			
	1.5829	0.3074	1.2755	0.8058	80.58			
5	1.8264	0.2476	1.5788	0.8644	86.44	86.44	0.0013	0.0015
	1.8269	0.2477	1.5792	0.8644	86.44			
	1.8267	0.2477	1.5790	0.8644	86.44			
7	1.9282	0.1061	1.8221	0.9450	94.50	94.51	0.0074	0.0078
	1.9285	0.1058	1.8227	0.9451	94.51			
	1.9297	0.1059	1.8238	0.9451	94.51			
9	2.1128	0.3442	1.7686	0.8371	83.71	83.71	0.0052	0.0062
	2.1139	0.3443	1.7696	0.8371	83.71			
	2.1129	0.3444	1.7685	0.8370	83.70			

Appendix 24 continued

11	2.6142	0.5392	2.0750	0.7937	79.37	79.38	0.0077	0.0098
	2.6156	0.5390	2.0766	0.7939	79.39			
	2.6160	0.5394	2.0766	0.7938	79.38			

Appendix 25: Effect of pH on NIP (MAA) of AME

pH	Ci	Cf	(Ci - Cf)	(Ci - Cf)/Ci	Binding efficiency, %	Mean, %	Standard deviation, σ	RSD
3	1.5833	0.9177	0.6656	0.4204	42.04	42.06	0.0164	0.0390
	1.5831	0.9172	0.6659	0.4206	42.06			
	1.5837	0.9173	0.6664	0.4208	42.08			
5	1.8267	0.9163	0.9104	0.4984	49.84	49.83	0.0047	0.0094
	1.8268	0.9164	0.9104	0.4984	49.84			
	1.8261	0.9162	0.9099	0.4983	49.83			
7	1.9314	0.9005	1.0309	0.5338	53.38	53.21	0.2168	0.4074
	1.9320	0.9099	1.0221	0.5290	52.90			
	1.9312	0.9009	1.0303	0.5335	53.35			
9	2.1133	1.0766	1.0367	0.4906	49.06	49.06	0.0077	0.0158
	2.1128	1.0761	1.0367	0.4907	49.07			
	2.1132	1.0767	1.0365	0.4905	49.05			

Appendix 25 continued

11	2.6158	1.4552	1.1606	0.4437	44.37	41.82	1.7994	4.3021
	2.6187	1.5553	1.0634	0.4061	40.61			
	2.6142	1.5555	1.0587	0.4050	40.50			

Appendix 26: Effect of pH on MIP (2VP) of ATZ

pH	Ci	Cf	(Ci - Cf)	(Ci - Cf)/Ci	Binding efficiency, %	Mean, %	Standard deviation, σ	RSD
3	2.1803	0.2514	1.9289	0.8847	88.47	88.48	0.0459	0.0519
	2.1811	0.2522	1.9289	0.8844	88.44			
	2.1810	0.2498	1.9312	0.8855	88.55			
5	2.2060	0.2145	1.9915	0.9028	90.28	90.04	0.3344	0.3714
	2.2060	0.2145	1.9915	0.9028	90.28			
	2.0560	0.2145	1.8415	0.8957	89.57			
7	2.2406	0.1876	2.0530	0.9163	91.63	91.62	0.0075	0.0082
	2.2396	0.1879	2.0517	0.9161	91.61			
	2.2404	0.1879	2.0525	0.9161	91.61			
9	2.2260	0.2280	1.9980	0.8976	89.76	89.74	0.0121	0.0134
	2.2303	0.2290	2.0013	0.8973	89.73			
	2.2301	0.2290	2.0011	0.8973	89.73			

Appendix 26 continued

11	2.2706	0.4161	1.8545	0.8167	81.67	81.68	0.0085	0.0104
	2.2722	0.4160	1.8562	0.8169	81.69			
	2.2699	0.4160	1.8539	0.8167	81.67			

Appendix 27: Effect of pH on NIP (2VP) of ATZ

pH	Ci	Cf	(Ci - Cf)	(Ci - Cf)/Ci	Binding efficiency, %	Mean, %	Standard deviation, σ	RSD
3	2.1816	1.6512	0.5304	0.2431	24.31	24.32	0.0084	0.0344
	2.1819	1.6510	0.5309	0.2433	24.33			
	2.1812	1.6508	0.5304	0.2432	24.32			
5	2.2071	1.3382	0.8689	0.3937	39.37	39.33	0.0245	0.0623
	2.2062	1.3387	0.8675	0.3932	39.32			
	2.2059	1.3387	0.8672	0.3931	39.31			
7	2.2399	1.2172	1.0227	0.4566	45.66	45.68	0.0154	0.0336
	2.2390	1.2161	1.0229	0.4569	45.69			
	2.2401	1.2165	1.0236	0.4569	45.69			
9	2.2295	1.3653	0.8642	0.3876	38.76	38.72	0.0303	0.0782
	2.2280	1.3659	0.8621	0.3869	38.69			
	2.2275	1.3654	0.8621	0.3870	38.70			

Appendix 27 continued

11	2.2710	1.5541	0.7169	0.3157	31.57	31.62	0.0357	0.1128
	2.2711	1.5524	0.7187	0.3165	31.65			
	2.2708	1.5523	0.7185	0.3164	31.64			

Appendix 28: Effect of Polymer Dosage on MIP (AAm) of CYZ

Polymer dosage, g	Ci	Cf	(Ci - Cf)	(Ci - Cf)/Ci	Binding efficiency, %	Mean, %	Standard deviation, σ	RSD
0.1	1.6837	0.2284	1.4553	0.8643	86.43	86.39	0.0358	0.0414
	1.6839	0.2299	1.4540	0.8635	86.35			
	1.6840	0.2291	1.4549	0.8640	86.40			
0.2	1.7907	0.3435	1.4472	0.8082	80.82	80.83	0.0085	0.0105
	1.7904	0.3431	1.4473	0.8084	80.84			
	1.7907	0.3432	1.4475	0.8083	80.83			
0.3	1.7907	0.3716	1.4191	0.7925	79.25	79.16	0.0618	0.0781
	1.7904	0.3735	1.4169	0.7914	79.14			
	1.7907	0.3742	1.4165	0.7910	79.10			
0.4	1.7907	0.3772	1.4135	0.7894	78.94	78.94	0.0141	0.0178
	1.7904	0.3772	1.4132	0.7893	78.93			
	1.7907	0.3767	1.4140	0.7896	78.96			

Appendix 28 continued

0.5	1.7907	0.4098	1.3809	0.7712	77.12	77.12	0.0053	0.0069
	1.7904	0.4095	1.3809	0.7713	77.13			
	1.7907	0.4097	1.3810	0.7712	77.12			
0.6	1.7907	0.504	1.2867	0.7185	71.85	71.88	0.0149	0.0208
	1.7904	0.5033	1.2871	0.7189	71.89			
	1.7907	0.5035	1.2872	0.7188	71.88			
0.7	1.7907	0.5484	1.2423	0.6938	69.38	69.31	0.0682	0.0983
	1.7904	0.5488	1.2416	0.6935	69.35			
	1.7907	0.5512	1.2395	0.6922	69.22			

Appendix 29: Effect of Polymer Dosage on NIP (AAm) of CYZ

Polymer dosage, g	Ci	Cf	(Ci - Cf)	(Ci - Cf)/Ci	Binding efficiency, %	Mean, %	Standard deviation, σ	RSD
0.1	1.6810	0.7909	0.8901	0.5295	52.95	52.95	0.0083	0.0158
	1.6815	0.7910	0.8905	0.5296	52.96			
	1.6812	0.7912	0.8900	0.5294	52.94			
0.2	1.7879	1.2910	0.4969	0.2779	27.79	28.26	0.3324	1.1760
	1.7881	1.2791	0.5090	0.2847	28.47			
	1.7893	1.2789	0.5104	0.2853	28.53			
0.3	1.7879	1.5658	0.2221	0.1242	12.42	13.06	0.6504	4.9789
	1.7881	1.5590	0.2291	0.1281	12.81			
	1.7893	1.5396	0.2497	0.1396	13.96			
0.4	1.7879	1.6287	0.1592	0.0890	8.90	9.03	0.9173	10.1544
	1.7881	1.6454	0.1427	0.0798	7.98			
	1.7893	1.6065	0.1828	0.1022	10.22			

Appendix 29 continued

0.5	1.7879	1.6664	0.1215	0.0680	6.80	5.86	0.8080	13.7975
	1.7881	1.6817	0.1064	0.0595	5.95			
	1.7893	1.703	0.0863	0.0482	4.82			
0.6	1.7879	1.6632	0.1247	0.0697	6.97	6.62	0.7260	10.9624
	1.7881	1.6579	0.1302	0.0728	7.28			
	1.7893	1.6889	0.1004	0.0561	5.61			
0.7	1.7879	1.6821	0.1058	0.0592	5.92	5.72	1.1076	19.3705
	1.7881	1.7117	0.0764	0.0427	4.27			
	1.7893	1.6647	0.1246	0.0696	6.96			

Appendix 30: Effect of Polymer Dosage on MIP (MAA) of AME

Polymer dosage, g	Ci	Cf	(Ci - Cf)	(Ci - Cf)/Ci	Binding efficiency, %	Mean, %	Standard deviation, σ	RSD
0.1	1.8573	0.1004	1.7569	0.9459	94.59	94.58	0.0071	0.0075
	1.8570	0.1006	1.7564	0.9458	94.58			
	1.8570	0.1007	1.7563	0.9458	94.58			
0.2	1.8573	0.1836	1.6737	0.9011	90.11	90.12	0.0060	0.0067
	1.8570	0.1833	1.6737	0.9013	90.13			
	1.8570	0.1834	1.6736	0.9012	90.12			
0.3	1.8573	0.2193	1.6380	0.8819	88.19	88.18	0.0118	0.0134
	1.8570	0.2198	1.6372	0.8816	88.16			
	1.8570	0.2195	1.6375	0.8818	88.18			
0.4	1.8573	0.2695	1.5878	0.8549	85.49	85.50	0.0057	0.0066
	1.8570	0.2693	1.5877	0.8550	85.50			
	1.8570	0.2692	1.5878	0.8550	85.50			

Appendix 30 continued

0.5	1.8573	0.3058	1.5515	0.8354	83.54	83.55	0.0150	0.0179
	1.8570	0.3056	1.5514	0.8354	83.54			
	1.8570	0.3051	1.5519	0.8357	83.57			
0.6	1.8573	0.3961	1.4612	0.7867	78.67	78.67	0.0123	0.0156
	1.8570	0.3960	1.4610	0.7868	78.68			
	1.8570	0.3965	1.4605	0.7865	78.65			
0.7	1.8573	0.4861	1.3712	0.7383	73.83	73.82	0.0138	0.0187
	1.8570	0.4866	1.3704	0.7380	73.80			
	1.8570	0.4861	1.3709	0.7382	73.82			

Appendix 31: Effect of Polymer Dosage on NIP (MAA) of AME

Polymer dosage, g	Ci	Cf	(Ci - Cf)	(Ci - Cf)/Ci	Binding efficiency, %	Mean, %	Standard deviation, σ	RSD
0.1	1.8571	0.8459	1.0112	0.5445	54.45	54.44	0.0095	0.0174
	1.8569	0.8462	1.0107	0.5443	54.43			
	1.8568	0.8458	1.0110	0.5445	54.45			
0.2	1.8571	0.8795	0.9776	0.5264	52.64	52.62	0.0119	0.0227
	1.8569	0.8799	0.9770	0.5261	52.61			
	1.8568	0.8798	0.9770	0.5262	52.62			
0.3	1.8571	1.0044	0.8527	0.4592	45.92	45.91	0.0122	0.0265
	1.8569	1.0048	0.8521	0.4589	45.89			
	1.8568	1.0043	0.8525	0.4591	45.91			
0.4	1.8571	1.0451	0.8120	0.4372	43.72	43.71	0.0105	0.0240
	1.8569	1.0453	0.8116	0.4371	43.71			
	1.8568	1.0454	0.8114	0.4370	43.70			

Appendix 31 continued

0.5	1.8571	1.0724	0.7847	0.4225	42.25	42.27	0.0091	0.0216
	1.8569	1.0719	0.7850	0.4227	42.27			
	1.8568	1.0719	0.7849	0.4227	42.27			
0.6	1.8571	1.1819	0.6752	0.3636	36.36	36.37	0.0082	0.0226
	1.8569	1.1814	0.6755	0.3638	36.38			
	1.8568	1.1815	0.6753	0.3637	36.37			
0.7	1.8571	1.2997	0.5574	0.3001	30.01	30.01	0.0118	0.0393
	1.8569	1.2999	0.5570	0.3000	30.00			
	1.8568	1.2993	0.5575	0.3002	30.02			

Appendix 32: Effect of Polymer Dosage on MIP (2VP) of ATZ

Polymer dosage, g	Ci	Cf	(Ci - Cf)	(Ci - Cf)/Ci	Binding efficiency, %	Mean, %	Standard deviation, σ	RSD
0.1	2.2933	0.2010	2.0923	0.9124	91.24	91.23	0.0060	0.0066
	2.2926	0.2012	2.0914	0.9122	91.22			
	2.2920	0.2012	2.0908	0.9122	91.22			
0.2	2.2933	0.1647	2.1286	0.9282	92.82	92.81	0.0047	0.0050
	2.2926	0.1649	2.1277	0.9281	92.81			
	2.2920	0.1648	2.1272	0.9281	92.81			
0.3	2.2933	0.1347	2.1586	0.9413	94.13	94.14	0.0122	0.0130
	2.2926	0.1341	2.1585	0.9415	94.15			
	2.2920	0.1340	2.1580	0.9415	94.15			
0.4	2.2933	0.2217	2.0716	0.9033	90.33	90.33	0.0048	0.0053
	2.2926	0.2219	2.0707	0.9032	90.32			
	2.2920	0.2217	2.0703	0.9033	90.33			

Appendix 32 continued

0.5	2.2933	0.2406	2.0527	0.8951	89.51	89.50	0.0043	0.0048
	2.2926	0.2406	2.0520	0.8951	89.51			
	2.2920	0.2407	2.0513	0.8950	89.50			
0.6	2.2933	0.2902	2.0031	0.8735	87.35	87.35	0.0032	0.0036
	2.2926	0.2900	2.0026	0.8735	87.35			
	2.2920	0.2901	2.0019	0.8734	87.34			
0.7	2.2933	0.3378	1.9555	0.8527	85.27	85.26	0.0093	0.0109
	2.2926	0.3381	1.9545	0.8525	85.25			
	2.2920	0.3381	1.9539	0.8525	85.25			

Appendix 33: Effect of Polymer Dosage on NIP (2VP) of ATZ

Polymer dosage, g	Ci	Cf	(Ci - Cf)	(Ci - Cf)/Ci	Binding efficiency, %	Mean, %	Standard deviation, σ	RSD
0.1	2.2928	1.2696	1.0232	0.4463	44.63	44.68	0.0452	0.1013
	2.2927	1.2687	1.0240	0.4466	44.66			
	2.2937	1.2676	1.0261	0.4474	44.74			
0.2	2.2928	1.2308	1.0620	0.4632	46.32	46.33	0.0136	0.0293
	2.2927	1.2307	1.0620	0.4632	46.32			
	2.2937	1.2306	1.0631	0.4635	46.35			
0.3	2.2928	1.1683	1.1245	0.4904	49.04	49.06	0.0131	0.0266
	2.2927	1.1682	1.1245	0.4905	49.05			
	2.2937	1.1681	1.1256	0.4907	49.07			
0.4	2.2928	1.3060	0.9868	0.4304	43.04	43.09	0.0459	0.1066
	2.2927	1.3052	0.9875	0.4307	43.07			
	2.2937	1.3040	0.9897	0.4315	43.15			

Appendix 33 continued

0.5	2.2928	1.3567	0.9361	0.4083	40.83	40.83	0.0358	0.0876
	2.2927	1.3574	0.9353	0.4079	40.79			
	2.2937	1.3560	0.9377	0.4088	40.88			
0.6	2.2928	1.4276	0.8652	0.3774	37.74	37.75	0.0131	0.0348
	2.2927	1.4268	0.8659	0.3777	37.77			
	2.2937	1.4278	0.8659	0.3775	37.75			
0.7	2.2928	1.4836	0.8092	0.3529	35.29	35.33	0.0251	0.0711
	2.2927	1.4826	0.8101	0.3533	35.33			
	2.2937	1.4828	0.8109	0.3535	35.35			

Appendix 34: Selectivity Test of MIP (AAm) and NIP (AAm) of CYZ

Compound	**Cyanazine**		**Ametryn**	
Polymer	**MIP (AAm)**	**NIP (AAm)**	**MIP (AAm)**	**NIP (AAm)**
Ci	22917	22917	21771	21771
Cf	3593	16382	12981	14763
Ci - Cf	19324	6535	8790	7008
V	10	10	10	10
(Ci - Cf) V	193240	65350	87900	70080
m	0.1	0.1	0.1	0.1
Ci*m*	2291.7	2291.7	2177.1	2177.1
KD	84.32	28.52	40.37	32.19

Appendix 35: Selectivity Test of MIP (MAA) and NIP (MAA) of AME

Compound	**Ametryn**		**Cyanazine**	
Polymer	**MIP (MAA)**	**NIP (MAA)**	**MIP (MAA)**	**NIP (MAA)**
Ci	56528	56528	56528	56528
Cf	2966	38718	2966	38718
Ci - Cf	53562	17810	53562	17810
V	10	10	10	10
(Ci - Cf) V	535620	178100	535620	178100
m	0.1	0.1	0.1	0.1
Ci*m*	5652.8	5652.8	5652.8	5652.8
KD	94.75	31.51	94.75	31.51

Appendix 36: Selectivity Test of MIP (2VP) and NIP (2VP) of ATZ

Compound	**Atrazine**		**Ametryn**	
Polymer	**MIP (2VP)**	**NIP (2VP)**	**MIP (2VP)**	**NIP (2VP)**
Ci	66898	66898	66898	66898
Cf	3290	47117	3290	47117
Ci - Cf	63608	19781	63608	19781
V	10	10	10	10
(Ci - Cf) V	636080	197810	636080	197810
m	0.1	0.1	0.1	0.1
Ci*m*	6689.8	6689.8	6689.8	6689.8
KD	95.08	29.57	95.08	29.57